Thiol-ene miniemulsion and emulsion photopolymerization : seizing new light opportunities

Cuong Minh Quoc Le

Année 2022 N° d'ordre : (attribué par le SCD)

UNIVERSITÉ DE HAUTE-ALSACE
UNIVERSITÉ DE STRASBOURG

THESE

Pour l'obtention du grade de

DOCTEUR DE L'UNIVERSITÉ DE HAUTE-ALSACE

L'Ecole Doctorale de Physique et Chimie Physique (ED 182)

Discipline : Chimie des Polymères

Présentée et soutenue publiquement

Par

Cuong Minh Quoc LE
Le 11/01/2022

THIOL-ENE MINIEMULSION AND EMULSION PHOTOPOLYMERIZATION: SEIZING NEW LIGHT OPPORTUNITIES

Sous la direction du Dr. Abraham CHEMTOB

Jury : Dr. Emmanuel LACÔTE,---------Université Claude Bernard Lyon 1 ---------- (Rapporteur)

Dr. Maud SAVE, ----------Université de Pau et des Pays de l'Adour ------ (Rapporteure)

Dr. Madeline VAUTHIER, ------Université de Strasbourg ---------- (Examinatrice)

Dr. Michaël WÖRNER, ---------Institut Technologique de Karlsruhe ---------- (Examinateur)

Dr. Abraham CHEMTOB, ------Université de Haute Alsace ---------- (Directeur de thèse)

Acknowledgements

I am grateful to have been awarded a Marie Skłodowska-Curie PhD fellowship for the research and training project *Photo-Emulsion*. This Innovative Training Network (ITN) project was funded by the European Union's Horizon 2020 research and innovation program.

I would like to give my thanks and deepest appreciation to my supervisor, Dr. Abraham CHEMTOB, for endless support, insightful advice, and guiding me through my PhD study. He has always been open, supportive, and kind-hearted. It has been truly a pleasure for me to work under his leadership. I would not be where I am today without him.

I also would like to express my warmest gratitude to Dr. Mariusz GALEK and Dr. Joana ORTYL at Photo High Technologies Company (Poland) for their scientific guidance, enthusiasm, and immense knowledge in organic synthesis shared during and after my industrial secondment.

I would like also to thank my academic co-supervisor Dr. Héloïse THERIEN-AUBIN (Max Planck Institute for Polymer Research, Mainz, Germany) for her scientific comments and career guidance through a number of meetings. In addition, I would like also to thank Prof. Günter REITER, who gave me the opportunity to conduct an academic secondment at the Institute of Physics (University of Freiburg). This allowed me to collaborate with another doctoral student of the European project, Brahim BESSIF, on the crystallization characterization of poly(thioether)s.

I would like to thank Prof. Christophe A. SERRA and Eirini SKOUFA who made efforts to set a collaboration between our lab and Institut Charles Sadron (ICS – Strasbourg) to measure monomer miniemulsion size by cryo-TEM. I would like to express my appreciation to Dr. Marc Schmutz at ICS for a number of cryo-TEM measurements.

I would like to express my warmest gratitude to the analytical platform at IS2M for the hundreds of measurements and fruitful discussion: Dr. Loïc VIDAL (electron microscopy), Gautier SCHRODJ (thermal analysis), Dr. Cyril VAULOT (NMR spectroscopy), Dr. Fabrice MORLET-SAVARY (electron paramagnetic resonance) and the group members for their support in the lab about scientific and non-scientific topics. Finally, I also would like to

acknowledge the help from staff members in IS2M for preparation of administrative documents during my Ph.D.

Last but not least, I would like to thank my parents and my sisters who love me unconditionally and support me constantly.

Table of Contents

List of Figures

List of Tables

List of Abbreviations

AA	Acrylic acid
AIBN	Azobisisobutyronitrile
APOENPES	Ammonium poly(oxyethylene)$_{10}$-p-nonyl phenyl ether sulfate
AUBDMAB	11-(acryloyloxy)undecyl–butyl dimethylammonium bromide
BA	Butyl acrylate
BAPO	Bis(2,4,6-trimethylbenzoyl)phenylphosphine oxide (Irgacure 819)
BDHQ	2,5-di-tert-butylhydroquinone
BMA	Benzyl methacrylate
BuMA	Butyl methacrylate
CHDM	1,4-bis[(vinyloxy)methyl]cyclohexane
CLRP	Controlled/living radical polymerization
CM	g-CN derived from the cyanuric acid/melamine complex
CMC	Critical micelle concentration
CMD	1-Decene grafted CM
$CMSO_3$	AHPA modified CM
CTA	Chain transfer agent
CTAB	cetyl trimethyl ammonium bromide
Đ	Molecular weight dispersity
DAA	Diallyl adipate
DAIP	Diallyl isophthalate
DAP	Diallyl phthalate
DATP	Diallyl terephthalate
DLS	Dynamic light scattering
DMSO	Dimethyl sulfoxide
DOTAP	1,2-Dioleoyl-3-trimethylammonium-propane (Chloride Salt) (DOTAP)
DSC	Differential scanning calorimetry
DTBA	*p*-(4-Diethylthiocarbamoylsulfanylmethyl) benzoic acid
DVE	Di(ethylene glycol) divinyl ether
EPR	Electron paramagnetic resonance
FT-NIR	Fourier transform – near-infrared spectroscopy
HD	Hexadecane
HDDA	Hexanediol diacrylate
HEMA	2-Hydroxyethyl methacrylate
ITX	2-Isopropylthioxanthone
LEDs	Light-emitting-diodes
MAH	Molecule-assisted homolysis

MMA	Methyl methacrylate
PBN	*N*-tert-butyl-α-phenylnitrone
PDI	Polydispersity index
PhCMp	g-CN derived a phenyl group modified cyanuric acid/melamine complex
POENPE	Poly(oxyethylene)$_{20}$-*p*-nonyl phenyl ether
ROMP	Ring-opening metathesis photopolymerization
SDS	Sodium dodecyl sulfate
SEC	Size Exclusion Chromatography
tBuMA	*tert*-Butyl methacrylate
TEM	Transmission electron microscopy
T_g	Glass transition temperature
THF	Tetrahydrofuran
TOCO	Thiol−olefin cooxidation
TPO	Diphenyl(2,4,6-trimethylbenzoyl)phosphine oxide
TPO-Li	Lithium phenyl(2,4,6-trimethylbenzoyl)phosphinate
vTA-CMp	vTA grafted PhCMp
XRD	X-ray diffraction

GENERAL INTRODUCTION

1 BACKGROUND OVERVIEWS

Synthetic polymers can be regarded as the materials of the twentieth century since they have penetrated almost every aspect of human life from daily tasks to the most technical needs.[1,2] The exponential growth of synthetic polymers is driven by their unique, broad, and customized properties. Nowadays, the polymer industry is facing significant challenges such as natural resources limitations, current and future environmental regulations, and increasing customer awareness about environmental issues. In this context, the development of monomer formulations with low or no VOCs, less energy-intensive polymerization processes, and minimal waste production have become priority directions.[3] Up to now, two technologies namely *polymerization in dispersed medi*a and *photopolymerization* are compliant with the needs of eco-efficient processes and zero-volatile-organic-compounds (zero-VOCs) polymer products.[4] Firstly, polymerizations in dispersed media, in particular water-based emulsion and suspension polymerizations, offer a range of synthetic routes to polymer particles of variable sizes from nano- to micrometer range. These processes have resulted in high tonnage industrial applications including coatings, non-woven textiles, inks, as well as niche applications in drug delivery and immunoassay.[5,6] Currently, the approach for conducting an emulsion polymerization process relies almost exclusively on chain-growth radical polymerization using thermal or redox radical initiators.[7] Secondly, photopolymerization is another major zero-VOC and energy-saving polymerization process used industrially. It is well suited for surface and other thin-layer applications such as inks, varnishes, industrial coatings, and more recently, for additive manufacturing (stereolithography).[8–10] Most of these applications involve a crosslinking of a solvent-free mixture made up of monomers and reactive oligomers. In this process, active species (mostly radicals) are produced by ultraviolet (UV) and visible-light irradiation of a reaction system.

Of interest is a hybridization of these two individual polymerization technologies with the potential to promote the transition to a smarter and greener economy. Research into photopolymerization in dispersed media began as early as the 1980s,[11] but it has remained difficult to establish itself as a practical alternative to conventional emulsion polymerization. The reason for the slow progress is that radiation penetration in these turbid (backscattering) dispersed systems remains generally a critical problem. This also explains why photopolymerization is limited only in surface and thin film crosslinking applications.[12] Other

aspects that hinder the progress of photopolymerization in dispersed media relate to the lack of appropriate polymerization process, photoreactor, lamp, and photoinitiator.[4] There is a need to go beyond the current state-of-the-art emulsion polymerization technology, to make it more efficient and environmentally friendly, and expand the range of products and their properties.

2 AIM AND OUTLINES

This Ph.D. project aims to achieve these goals using *thiol-ene step photopolymerization in dispersed media.* The radical-mediated thiol-ene addition reaction has been known for more than a century[13,14] and the major application of this reaction is in polymerization.[15] Generally, a thiol-ene step polymerization involves a bulk mixture of multifunctional thiol/ene monomers and radical initiator to yield poly(thioether) cross-linked structures. The polymer growth mechanism involves a series of H-transfer and addition reactions (**Scheme I-1**). This step polymerization has been proposed as an alternative to conventional chain-growth radical polymerization since it can overcome some limitations such as oxygen inhibition, residual stresses and heterogeneous network.[16] However it has been rarely used in dispersed systems to produce polymer particles.[17–19]

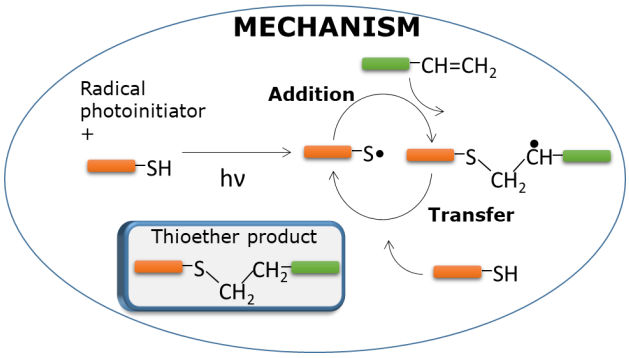

Scheme I-1 General mechanism of thiol-ene polymerization

Central to this PhD project is the development of *thiol-ene step photopolymerization processes in dispersed media*. The main approach starts with highly reactive dithiol-diene monomer emulsions or miniemulsions (nanoemulsions), which are later converted into water-based poly(thioether) latexes by a short exposure to light in a photoreactor. Such "hybrid" process is particularly interesting and potentially innovative. Firstly, it is relevant in terms of particle size control, absence of oxygen inhibition, safety due to its ability to be

controlled temporally, and low energy consumption due to the LED photoreactor. Secondly, a step growth thiol-ene polymerization mechanism offers several advantages: latexes with low residual monomer content due to an early monomer consumption, functionalized polymer particles by means of non-stoichiometric polymerization,[18] access to highly regular linear polymer chains prone to crystallization due to the absence of chain transfer reactions and side reactions.[20,21] This manuscript focuses on the development of thiol-ene step photopolymerization processes in miniemulsion and emulsion.

As shown in **Scheme I-2**, this dissertation is divided into five chapters, including a bibliographic section and four experimental sections that address the main challenges of thiol-ene photopolymerization in dispersed media: controlling/understanding the spontaneous polymerization of thiol-ene monomer mixtures (**2**), developing of miniemulsion (**3**) and emulsion (**4**) photoinitiated processes with emphasis on particle formation and particle size control, and finally, expanding these latter processes through the use of visible-light photocatalysis and photochemical reactor (**5**).

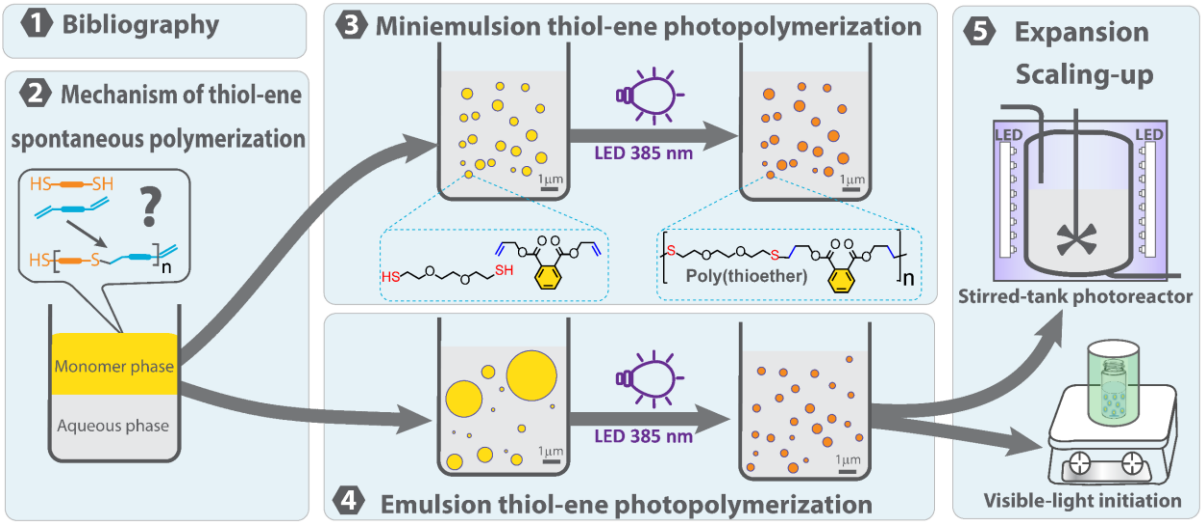

Scheme I-2. Process development of thiol-ene photopolymerization in emulsion and miniemulsion

In **Chapter 1**, a bibliographical study is presented, describing historical aspects of radical mediated thiol-ene polymerization, basic kinetics as well as advantages and challenges. A second part provides basic knowledge on photopolymerization and its implementation in emulsion and miniemulsion using mostly a chain radical polymerization mechanism.

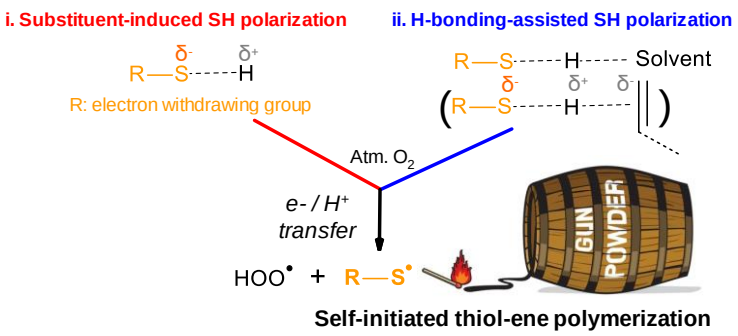

Chapter 2 is dedicated to the investigation of **spontaneous thiol-ene polymerization**.[22] Lack of chemical stability has been reported for a broad range of thiol-ene monomers in bulk condition[23–25] and represents one of the most important and unresolved issues in thiol-ene chemistry. Premature polymerization leads to a lot of consequent problems including shelf-life storage and shipment, and irreproducible polymerizations.[26] These drawbacks prevent the implementation of thiol-ene polymerization in dispersed media involving the preparation of a photolatent bicomponent thiol-ene monomer miniemulsion or emulsion before irradiation. Understanding and managing this issue are required for further development of a photopolymerization reaction in dispersed system. In our search for a consistent mechanism accounting for the self-initiation of thiol-ene polymerization, we highlight the role of thiyl initiating radicals generated by air oxidation of thiols.

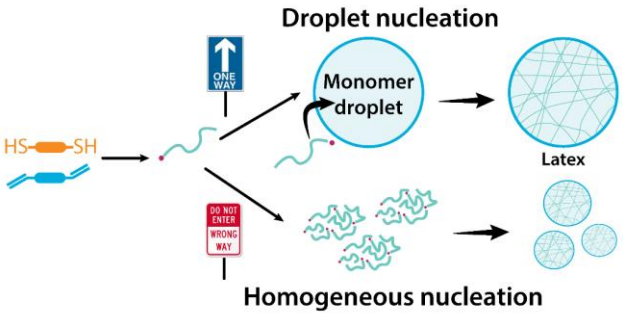

Chapter 3 describes the formation of colloidally stable poly(thioether) latexes by **miniemulsion thiol-ene photopolymerization**. An in-depth study of the thiol-ene miniemulsion photopolymerization process based on diallyl phthalate (**DAP**) and 2,2-(ethylenedioxy)diethanedithiol (**EDDT**) was carried out. We have studied the effects of radical inhibitor concentration on the photolatency of monomer miniemulsion and its droplet stability, polymerization kinetics and molecular weight progress, and the colloidal properties of the polymer particles. Reaction parameters which are important in favoring droplet nucleation in a miniemulsion thiol-ene step polymerization are reviewed, droplet size, initiator solubility and monomer solubility.

Chapter 4 reports an unprecedented approach to obtain poly(thioether) latexes **by emulsion thiol-ene photopolymerization**. First, the reaction kinetic, particle size evolution, and molecular weight progress were conducted with the same model couple of thiol-ene monomers **DAP-EDDT** using a water-soluble photoinitiator activable under UV radiation. Furthermore, the influence of monomer polarity on particle formation and particle number in thiol-ene emulsion step photopolymerization was also systematically addressed.

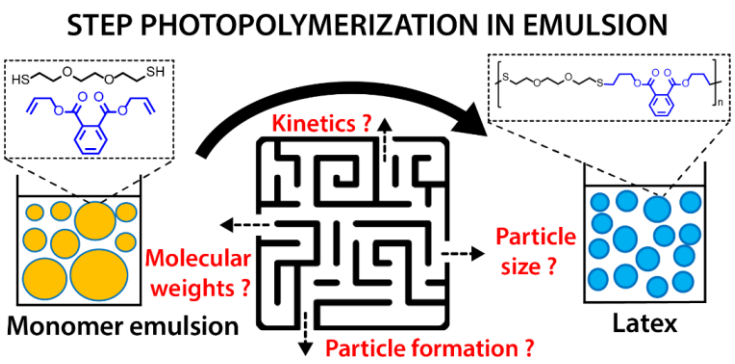

Chapter 5 describes **how to expand thiol-ene emulsion photopolymerization** in two directions: the shift from UV to visible-light irradiation and the process scaling-up through the use of a LED stirred-tank photoreactor. In the first part, a photocatalytic thiol-ene aqueous emulsion polymerization was developed to prepare linear semi-crystalline latexes using eosin-Y disodium (EY^{2-}) as photocatalyst under green light irradiation. The process development was accompanied by a detailed mechanistic investigation of the reaction. The feasibility of the process is finally demonstrated by the preparation of different latexes exhibiting semi-crystalline properties. In the second part of this chapter, we also demonstrate the potentialities of process scaling-up in a stirred-tank photoreactor either in batch or semi-batch operation.

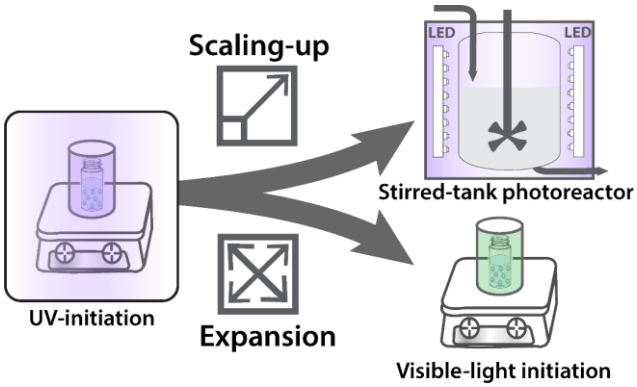

CHAPTER I. BIBLIOGRAPHY

1 RADICAL MEDIATED THIOL-ENE STEP POLYMERIZATION

1.1 Introduction

Thiol-X chemistries cover all reactions involving thiols with other functional groups X, where X may be an alkene, an alkyne, an epoxy, an isocyanate, or another functional group.[27] The radical-mediated and base-mediated (thiol-Michael) thiol-ene reactions are among the most commonly known thiol-X reactions. These latter have gained a central role in organic synthesis, functionalization reaction, as well as polymerization[28] because of many advantages such as high yield, no by-products, selectivity and mild reaction conditions. This thesis will focus on the *radical-mediated thiol-ene polymerization*. More specifically, we aim to develop photochemically initiated thiol-ene polymerizations in dispersed media. The primary goal of this chapter is to introduce the reader about some fundamental topics of radical mediated thiol-ene polymerization: genesis, basic kinetics and its implementation in mini(emulsion) photopolymerization.

1.2 Historical perspective

The thiol-ene reaction was originally reported in 1905 by the German chemist Posner.[29] The first thiol-ene polymerization reaction was discovered in 1926 and its radical mediated mechanism proposed by Kharasch and his coworkers in 1938 is still the authoritative mechanism until today.[30] They found that thiol oxidation by atmospheric molecular oxygen led to the formation of thiyl radicals which could subsequently play a role in initiating thiol-ene reactions. In 1944, Drake et al. described in a patent, perhaps the first thiol-ene photopolymerization.[31] He discovered that stoichiometric mixtures of dienes and dithiols yielded liquid poly(thioether) products either upon heating or under the irradiation of a mercury arc lamp. Since these pioneering studies, thiol-ene reaction has grown exponentially in polymer and organic chemistry, especially since the advent of “click” reaction in the early 2000s.[15] A large number of excellent reviews in this field have been published covering a broad range of research areas.[27,32–35]

1.3 Basic kinetics

The radical-mediated thiol-ene polymerization proceeds via a step-growth addition mechanism that includes three typical steps: initiation, propagation, and termination. At first,

reaction starts via H-abstraction from the thiol by one of the primary free radicals often generated from a radical initiator. Almost any type of radical initiators can be used to generate primary radicals in the initiation step including thermal, redox, and photochemical initiators. The resulting thiyl radical then reversibly adds to carbon-carbon double bonds yielding a carbon-centered radical. Then, this latter radical undergoes a radical-chain transfer to another thiol group to form thiol-ene adduct with *anti*-Markovnikov configuration. The reaction then continues until thiol and ene groups are all consumed. Finally, termination involves a set of bimolecular recombination reactions **(Figure I-1)**.

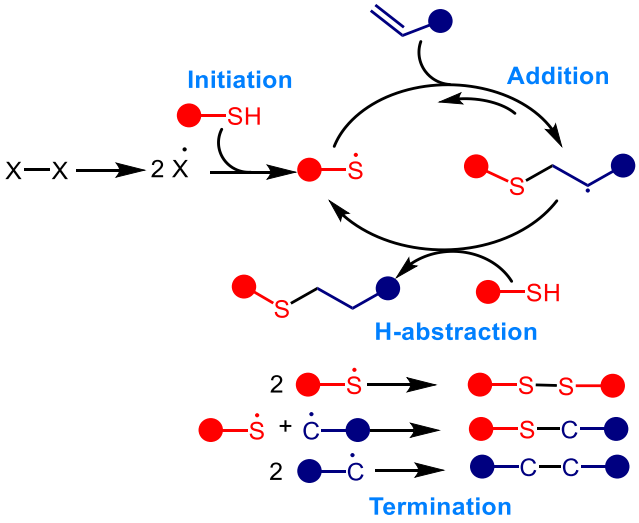

Figure I-1 Step-growth mechanism of a radical-mediated thiol–ene reaction

The kinetic of thiol-ene reaction was studied extensively by Bowman and coworkers.[36–40] They established a first-order rate kinetic model in which polymerization rate $R_p \propto [ene]^{\alpha}[RSH]^{\beta}$ the sum of the exponents being equal to 1 ($\alpha + \beta = 1$). Depending on the thiol-ene system, the two exponents α and β may be different, meaning that the overall polymerization rate depends more heavily on the concentration of one reactant over the other. The authors also insisted on addition-to-chain-transfer coefficient ratio (k_{add}/k_H) as the key factor governing the overall kinetics. The relationship between k_{add}/k_H ratio and reaction order have proved to have the following dependences:

$\frac{k_{add}}{k_H} = \frac{[RC^{\bullet}]}{[RS^{\bullet}]}$	$>> 1 \Rightarrow rate \propto = [RSH]^1$
	$\approx 1 \Rightarrow rate \propto = [ene]^{0.5}[RSH]^{0.5}$
	$<< 1 \Rightarrow rate \propto = [ene]^1$

When the chain transfer reaction is the rate-limiting step ($k_{add} >> k_H$), the overall rate depends only on the concentration of thiol. This is the typical case of allyl ethers, with the consequence that increasing the concentration of the ene does not change the reaction rate. In the case where there is no rate-limiting step ($k_{add} \approx k_H$), the overall rate is half-order with respect to thiol and ene concentrations. This often happens with norbornene-thiol or vinyl-thiol systems. The last case is where $k_{add} << k_H$, in order words, the propagation step is rate-determining, and the rate becomes first order with respect to the ene concentration. One can observe this behavior in the case of vinylsilazane-thiol systems.

1.3.1.1 Influence of thiol structure

Thiol functional groups are able to couple with almost any type of non-sterically hindered ene functional groups. Nevertheless, their relative reactivity can vary greatly depending on the substituent and steric hindrance. The most popular types of primary thiols are thiolacetates, thiolpropionates, *n*-alkyl thiols, and aromatic thiols, as shown in **Figure I-2**. Compared to other thiols in the list, *n*-alkyl thiols are the least reactive because the hydrogen atom is less easily abstracted than the other ones.[13,15,32,41,42] Thiolpropionate esters react at an increased rate compared to thiol acetates presumably because of the formation of a six-membered internal hydrogen-bonded complex between S-H with the carbonyl ester, making the S-H bond cleavage more favourable.[43,44] However, in a photochemically initiated thiol-ene reaction, there is generally no significant differences of polymerization rate among thiol acetates and propionates.[45] Recent studies have also addressed the influence of substituted-thiol on the reactivity.[46–48] Basically, the polymerization rate is found to decrease when the steric hindrance of the thiols increases. For the thiol-ene systems where the chain transfer is rate-limiting, the influence of substituted-thiol is more pronounced.

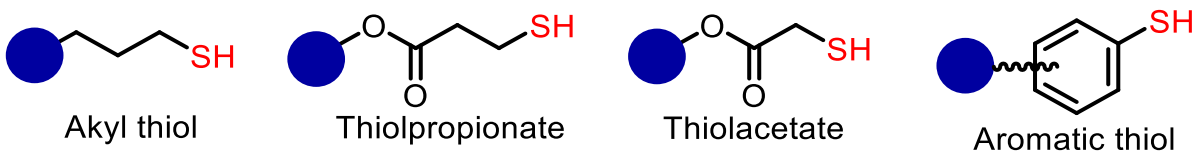

Figure I-2 Chemical structure of some common thiol functional group.

1.3.1.2 Influence of ene structure

There is a broader range of chemical structure for ene monomers, and some of the typical ene functional groups are shown in **Figure I-3**. In general, electron-rich enes are more reactive toward thiyl radicals which are intrinsically electrophilic. According to Morgan and Hoyle et al., the order of reactivity of ene toward thiol follows the trend: norbornene > vinyl ether > propenyl > alkene ≈ vinyl ester > N-vinyl amides > allyl ether ≈ allyl triazine > allyl isocyanurate > acrylate > unsaturated ester > N-substituted maleimide > acrylonitrile > methacrylate > styrene >conjugated dienes.[32,43,4950] Note that the reactivity of norbornene is exceptionally high due to a ring-strain effect. Recently, the influence of ene structure on the kinetic of radical mediated thiol-ene reaction has also been studied computationally by Northrop and Coffey.[50] The study showed good agreement with experimental results, which may serve as a basis for more accurate prediction of the reactivity of new thiol-ene systems.

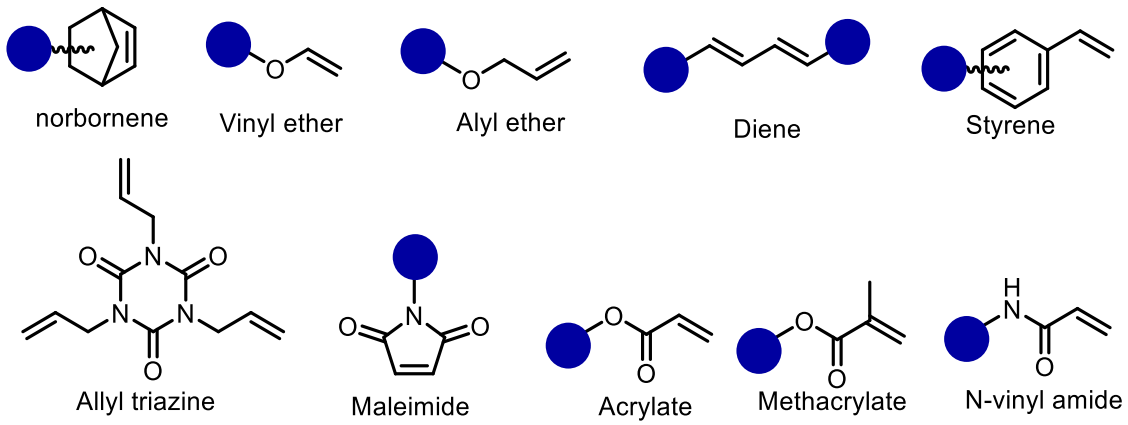

Figure I-3 Chemical structure of some common ene functional groups

1.4 Advantages compared to a conventional chain polymerization

Thiol-ene step growth polymerization has some advantages over conventional chain growth polymerization because of its distinct polymer growth mechanism (**Figure I-4**). In step polymerization, the molecular weight grows more slowly at the beginning and increases abruptly at the end of the reaction, and the monomers are consumed in the early phase of the reaction. In contrast, in chain growth polymerization, the high molecular weight polymers form early in the reaction, albeit at low conversion, leading to volumetric shrinkage of the material and ultimately significant shrinkage stress.[51] In addition, the classical free-radical

chain growth polymerizations are strongly inhibited by molecular oxygen at ambient temperature, requiring mitigation solutions such as the inclusion of physical or inert barriers or a high initiator concentration.[1,52] Overcoming these two main limitations are the main advantages of thiol-ene step growth polymerizations compared to radical chain types.[53] In addition, functionalization of the end chains is another feature of thiol-ene step growth polymerization by working under non-stoichiometric ratio of thiol and ene groups. For a synthesis performed in dispersed media, this opens the way to highly functional particles. Using such approach, biologically active ligands such as polypeptides or sugars can be covalently attached to the surface of the particles by photomodification.[18,54,55]

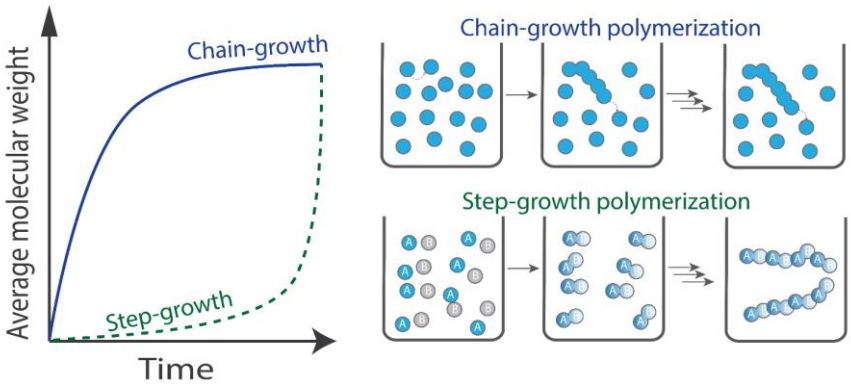

Figure I-4 Comparisons of chain-growth and step-growth reaction mechanisms

1.5 Challenges

1.5.1 Shelf-life stability of thiol-ene monomer

The shelf-life instability of thiol-ene mixture due to spontaneous polymerization is one of the main obstacles to the successful and widespread use of thiol-ene polymerization. The mechanism accounting for self-initiated polymerization has been elusive and the mitigation solution proposed by several groups[56–58] have efficacies dependent on the thiol-ene mixture chosen and the experimental conditions. The main solution to extent the shelf-life of thiol-ene mixtures involves the usage of radical stabilizers (inhibitors) including hydroquinone radical-scavengers derivatives or aluminum salts. Consequently, the type of radical inhibitor and its concentration need to be tailored according to the system used. Recently, Chen et al. suggested that secondary thiols in combination with enes have better thermal storage stability than primary thiols.[48,59] Some commercially available secondary thiols have been

reported, such as 1,4-butanediol-bis(3-mercaptobutyrate), pentaerythritol tetrakis(3-mercaptobutylate), tris(3-mercaptobutyloxyethyl) isocyanurate (see **Figure I-5**). Recently, the effect of thiol substitution on polymerization kinetics and mechanical behavior was investigated by Bowman et al.[46,60] Most stability studies were conducted under bulk conditions. It was found that the spontaneous polymerization rate can be affected by the presence of polar solvents such as water and the emulsification stage.[18,19] Therefore, this problem limits the performance of thiol-ene polymerization in dispersed media. Understanding and controlling thiol stability is necessary for further development of a photopolymerization reaction in dispersed systems. This topic is discussed in detail in Chapter II.

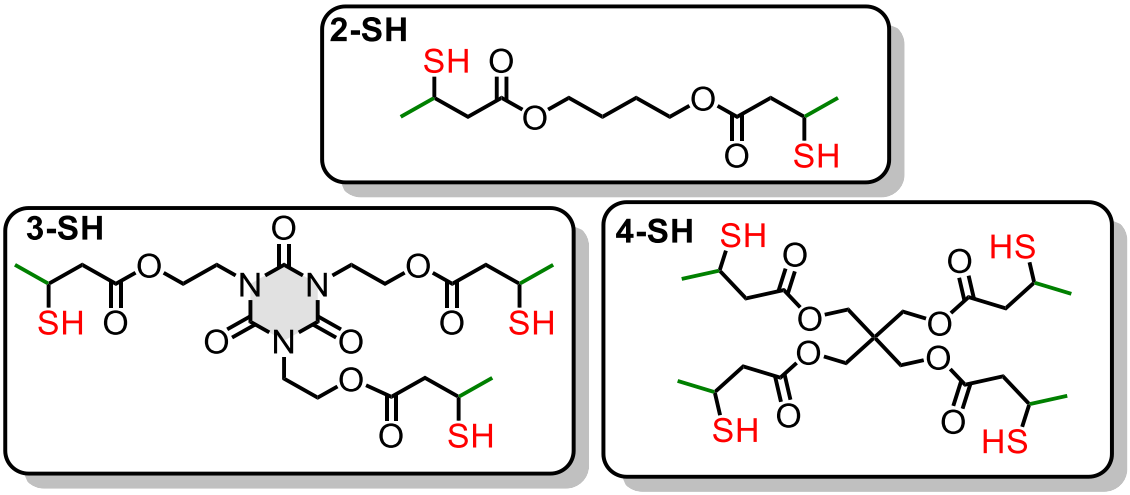

Figure I-5 Some commercial secondary thiols

1.5.2 Thiol odor

Shelf-life problems can be temporarily overcome by adjusting the concentration of radical inhibitors or using secondary thiols, as mentioned above, but thiol odor is difficult to reduce or eliminate. Selecting thiol monomers with higher molecular weights might be a good way to avoid this drawback. Miyata and co-workers have patented a series of high molecular weight thiols to avoid odor, although this strategy practically reduces their reactivity.[61] Following this approach, one could also form oligomers via a pre-polymerization step that eliminates the residual monomer and thus the unpleasant odor.[62]

2 EMULSION AND MINIEMULSION PHOTOPOLYMERIZATION

2.1 Introduction

Polymerizations in dispersed media, a large class of polymerization processes that includes emulsion and suspension polymerizations, account for approximately one fifth of the total polymer production worldwide.[4] Other processes including miniemulsion, microemulsion, dispersion, and precipitation polymerizations have less industrial importance but are well established in the academic literature. Regardless of the process, the main polymerization mechanism is based on radical chain polymerization. The typical product is a dispersion of polymer particles with diameters ranging from 10 nm (microemulsion) up to 1 mm (suspension). Among the diverse processes, emulsion polymerization has become one of most widely used for the production of polymer dispersions, with a typical particle size of 50 – 200 nm. They are often referred to as polymer colloids, synthetic latexes or emulsion polymers. Their application can be found in a wide variety of products such as rubbers, paints, coatings, adhesives, inks, and even in drug delivery systems and columns for chromatographic separations. The major reasons for this significant extent of industrial applications are due to several distinct advantages. First, water is typically used as the continuous phase, thereby reducing volatile organic compounds (or VOCs) and thus making the process more environmentally friendly. Second, heat transfer and viscosity problems in a water-based system are much less significant than in solvent-based or bulk polymerization. Third, emulsion polymerization process offers a way to prepare high molecular weight polymers at high throughput rates. UV-visible photopolymerization has emerged as one of the promising methods to upgrade the conventionally thermal/redox initiated polymerization. Finally, miniemulsion polymerization can be used to produce high volume fractions and solids contents (> 50 wt%) of polymer latexes because the scattering coefficient is lower compared to macroemulsions.

Through recent developments of energy-efficient light-emitting-diodes (LEDs), the availability of new photoinitiator systems, and reactor design, the hybrid technology named photopolymerization in (mini)emulsion has been demonstrated to be highly feasible and more eco-efficient. In the second part of this bibliographical chapter, we will review previous works on emulsion and miniemulsion photopolymerization processes.

2.2 Emulsion (photo)polymerization

In the mid-1930s, emulsion polymerization was among the first polymerization processes developed at industrial scale for the production of synthetic latexes. Nowadays, millions of tons of emulsion polymers are produced annually for various industrial products such as paints, adhesives, paper coating, etc. Furthermore, this process has also been extensively explored in many academic areas for development of novel polymer materials.[63,64] For instance, preparation of block copolymers using controlled radical polymerization in emulsion for new particle morphologies and applications.[7]

2.2.1 Preparation of emulsion

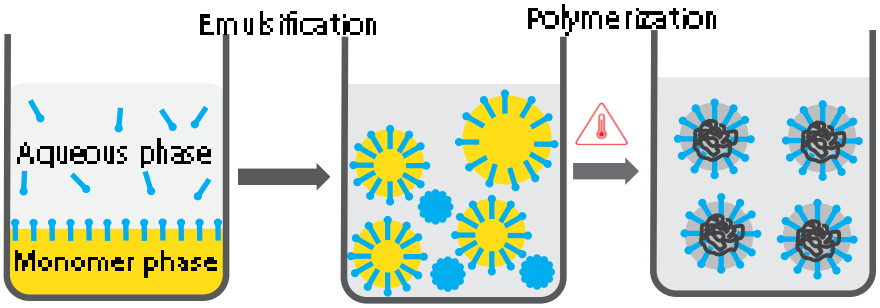

Figure I-6 General scheme of emulsion polymerization

Figure I-6 shows a general scheme of a thermal-initiated emulsion polymerization. It begins with a monomer emulsion (a class of dispersed system comprising two immiscible liquids) composed of an oil-soluble monomer and water. The main ingredients for preparation of emulsion include water, monomer, surfactant, initiator, and sometimes a buffer and/or chain transfer agents.[5,64]

- **Water** is generally the main component and acts as continuous phase which helps to maintain low viscosity and provides a good heat transfer. In addition, it is also the medium in which the monomer molecules transfer from droplets to polymer particles.

- **Monomer** should not be completely miscible nor insoluble with water. The most common monomers are styrene, butadiene, vinyl acetate, acrylates and methacrylates, acrylic acid, and vinyl chloride.

- **Surfactant** (also known as emulsifier) stabilizes the monomer droplet. It also self-assembles into micelles “solubilizing” a fraction of monomer (when it is used above its critical

micellar concentration also referred to as CMC) that may serve as the loci for nucleation of particles. Finally, it stabilizes the newly formed latex particles as well as the growing particles during polymerization. There are three types of surfactant used in emulsion polymerization: anionic, cationic, and non-ionic. Anionic surfactants are the most commonly employed.

- **Radical thermal initiator** is usually water-soluble. The most widely used are potassium, sodium and ammonium persulfates. In the cases where the polymerization needs to be carried out at low temperatures, a two-component redox system can be used, for example *tert*-butyl hydroperoxide and sodium metabisulfite. There are also other methods to generate radicals such as photochemical initiators. This component is normally introduced just after emulsification step or during the course of polymerization.

Preparation of monomer emulsion is the first step in emulsion polymerization which plays a critical role in controlling the properties of final latex products. It is usually carried out in stirred-tank reactors by mechanical agitation. The starting emulsion is not thermodynamically stable, and the polymerization is generally initiated just after this stage. The reactor is heated up and an aqueous shot of thermal initiator is added to start the polymerization.

During an *ab initio* emulsion polymerization of sparsely water-soluble monomers such as styrene, i.e. without the initial presence of any preformed latex (seed), three distinct intervals can be observed: (I) particle nucleation, (II) particle growth, and (III) further polymerization after the monomer droplets have disappeared.[65] These three intervals are depicted in **Figure I-7**.

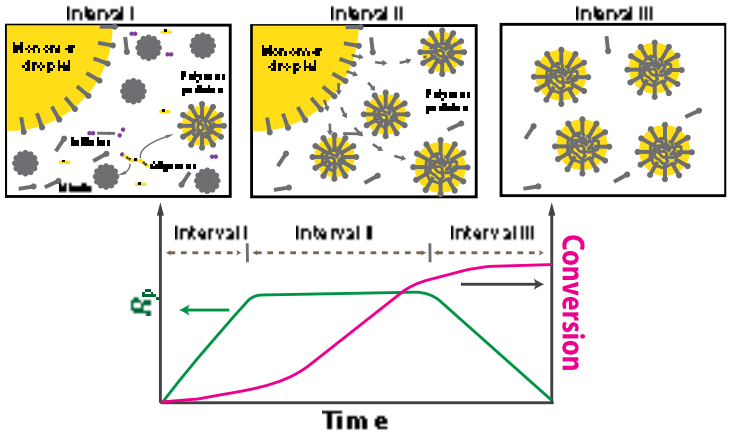

Figure I-7 Schematic illustrations of emulsion polymerization based on Harkins theory.

In interval I (Nucleation), the decomposition of thermal initiator in aqueous phase forms primary radicals initiating the polymerization. Subsequently, these radicals react with a small amount of monomer soluble in aqueous phase and generate oligoradicals. The fate of these growing radicals in interval I can be twice. Several nucleation mechanisms have been proposed including micellar, homogeneous and coagulative, and droplet nucleation, which will be discussed in the following sections. During the interval I, the number of particles increase gradually and reach constant when the nucleation is ceased. In this stage, monomer is consumed typically in the range of 0-10%. In interval II, no new particle is formed, and the particle is growing via monomer diffusion through continuous phase. Monomer conversion is stopped at about 40% at the end of this interval. Interval III which occurs typically above 40% of monomer conversion is marked by the absence of monomer droplet. Gradual depletion of monomer inside polymer particles causes the rate of polymerization to decrease progressively until the end of reaction.

2.2.2 Particle formation

The mechanism of particle formation in emulsion chain-growth polymerization is complex and has been the subject of many investigations since the late 1950s, but essentially for a chain-growth polymerization mechanism. Reviewed by many authors, this subject is briefly presented in the following section.[6,64,66–68]

2.2.2.1 Micellar nucleation

If a surfactant is used at above CMC, micelles are present. Under these conditions, micelles are small, swollen with monomers, and much more numerous than the monomer droplets. Their diameters are about 10 nm, and their number density is on the order of 10^{17}-10^{18} L^{-1}.[6,64] They can capture radicals formed in aqueous phase and become one of the reaction loci and nucleation site. This *micellar nucleation* mechanism was originally proposed by Harkins in 1947. Briefly, the oligoradicals formed by adding a few units of monomer in aqueous phase become hydrophobic enough to be captured by micelles. Such mechanism is thought to be predominant in emulsion polymerization system of relatively hydrophobic monomers including styrene, butyl acrylate or 2-ethylhexyl acrylate when [surfactant] > CMC. Consistent with this belief, an increase of the number of micelles generally results in a proportional increase in the number of particles.

Following the qualitative picture of Harkins, Smith and Ewart applied a quantitative treatment of the mechanism in 1948.[69] They derived the famous relation for the number of polymer particles N_p depending on surfactant [S] and initiator concentration [I] : $\boldsymbol{N_p \propto [S]^{0.6} \times [I]^{0.4}}$. This relation is rarely in agreement with experimental results. It is valid only for some hydrophobic monomers in a limited range of conditions and cannot be used as an evidence for a predominant micellar nucleation mechanism.

2.2.2.2 Homogeneous nucleation

If there is no added surfactant, or if the emulsion polymerization is performed below CMC, the particles form preferentially in the aqueous upon precipitation of oligoradicals. The primary particles are stabilized by (ionic) fragments originating from the initiator decomposition and/or adsorbed surfactant molecules. The particle formation in such case is known as *homogeneous nucleation* (Priest, 1952; Fitch and Tsai, 1971).[70,71] This mechanism is believed to prevail or to be significant in a system including water-soluble monomers such as methyl acrylate, vinyl acetate, etc. In this case, the oligoradicals form and grow in aqueous phase until reaching its critical chain length leading to precipitation. Polymerization may continue in these nascent-nuclei to form new particles by swelling monomer or capturing another oligoradicals. Later on, Gilbert and co-workers proposed that the precursor particles may agglomerate significantly due to their poor colloidal stability to form new particle via a coagulation process. This new mechanism, named *homogeneous-coagulative nucleation*, is known as an extension of the homogeneous nucleation.[68,72]

2.2.2.3 Monomer droplet nucleation

This mechanism often occurs in miniemulsion polymerization but is highly unlikely in conventional emulsion polymerization.[65] The reason is that the monomer droplets are in micrometer size range and their surface areas are significantly lower than that of micelles and polymer particles, leading to inefficient capture of radicals produced in the aqueous phase to form new particles. This does not mean that none of the monomer droplets are nucleated, however, in some processes some “large “particles might be observed.[73] A sketch in **Figure I-8** summarizes the three possible modes of particle nucleation in emulsion polymerization.

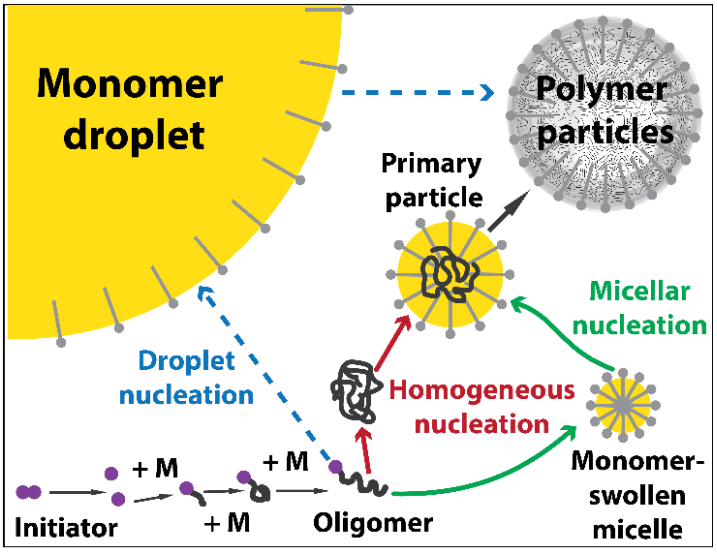

Figure I-8 Particle formation in emulsion polymerization. Monomer molecules in aqueous phase are denoted by M.

2.2.3 Emulsion photopolymerization

The emulsion photopolymerization has been developed for about four decades and it continues to grow at a sustained pace, but only in the academic literature.[11,74,75] To date, the number of studies remains limited as shown in detail by a review and a book chapter published in 2018.[4,76] This section does not intend to be exhaustive and a summary, but instead, to highlight some state-of-the-art and the most comprehensive studies in the subject. The studies published before 2018 were summarized in **Table I-1**, only the articles of the last 3 years were commented in detail (appear in red in **Table I-1**) Over the last years, the main objective has been to increase the irradiated reactor volume fraction. The issue of emulsion polymerization is that initiation occurs in the presence of micrometric and strongly light-scattered monomer droplets. This feature often impedes the progress in emulsion photopolymerization. In order to improve light penetration in emulsion, and thus increasing initiation efficiency, a general strategy has been to use visible-light instead of UV radiation.

To initiate emulsion polymerization, the Cunningham group utilized in 2018 a water-soluble organotellurium chain transfer agent which can undergo photocleavage upon an irradiation of a white LED lamp.[77] The emulsion photopolymerization was demonstrated to have controlled/living characteristics and was recently applied to prepare CO_2-switchable polymer particles via using CO_2-switchable organotellurium water-soluble agent.[78] In another

type of controlled/living radical polymerization, Wang and coworkers implemented a photo-induced atom transfer radical polymerization (photo-ATRP) of (meth)acrylates monomers in emulsion.[79] The catalyst system was based on the interaction between $CuBr_2$/Tris(2-pyridylmethyl)amine complex and SDS as surfactant, which efficiently controlled ATRP polymerization of *n*-butyl methacrylate and *n*-butyl methacrylate under violet LED (λ_{max} = 394 nm, 2.6 mW cm^{-2}). The method offers many key advantages, such as low catalyst loading, facile preparation of block copolymers in an open-to-air system using glucose oxidase.

Table I-1 Summary of main studies describing emulsion photopolymerization reported.

Monomer	Surfactant	(Photo)initiator	Lamp [irradiation time]	Particle diameter (nm)	Ref.
Styrene or MMA/AA	SDS	AIBN, 1,3-Diphenylacetone Di-tert-butyl ketone Dihydroxyacetone	450 W, medium-pressure Hg-arc, 313 nm (K_2CrO_4)	-	11,80–82
Vinyl acetate	APOENPES, POENPE	Potassium persulfate	500 W, high-pressure Hg-arc [< 180 min]	-	83,84
MMA	DTBA/SDS	-	125 W, medium-pressure Hg-arc [24 h]	-	85
MMA	Surfiniferter (4-thiobenzoyl sulfanylmethylsodium benzoate)		125 W, medium-pressure Hg-arc [24 h]	300-400	86
Styrene	SDS	Irgacure 2959 2,2-Dimethoxy-2-phenylacetophenone	375 W, high-pressure Hg-arc, 365 nm [150 min]	24-139	87
MMA	CTAB	$FeCl_3$	1000 W, high-pressure Hg-arc, 20 mW cm^{-2} [10 min]	20-90	88
Styrene	Surfactant-free	Sodium salt of bis(mesitoyl)phosphinic acid	60 LEDs per meter, LED 465 nm	80-400	89
Styrene/MMA	SDS	Benzoin	125 W, medium-pressure Hg-arc [180 min]	100-700	90
Styrene/n-isopropyl acrylamide		2-[p-(2-hydroxy-2-methylpropiophenone)]-ethylene glycol methacrylate	150 W, doped medium-pressure Hg-arc [60 min]	260	91
Styrene	SDS	Irgacure 819/BAG	2 fluorescent tubes (white light), 2 × 18 W, 0.5 mW cm^{-2} [< 300 h]	100 0.1-10 µm (coagulum)	92
Styrene/Butyl methacrylate (BuMA)/MMA	SDS	Irgacure 819 /acetic acid-modified BAPO	450 W, medium-pressure Hg-arc, [36.5 to 146 s]	50	93
MMA	Brij98/SDS/ CTAB	Organotellurium, CTA/4,4'-azobis(4-cyanovaleric acid)	6 W, LED Visible range, 50% Filter [Up to 9 h]	45-350	77

Monomer	Surfactant	(Photo)initiator	Lamp [irradiation time]	Particle diameter (nm)	Ref.
Styrene	SDS	Acridine orange (dye) /Disulfide (oxidant)/ NHC borane	Visible LED strip, no details concerning irradiance [6 – 10 h]	60-330	94
MMA/tBuMA	Brij 98	N-(3-(dimethylamino)propyl)-2-methyl-2-(methyltellanyl)propenamide	6 W, white light emitting diode (LED) [100 min at 65°C	112	78
MMA/EMA/LMA/BA/BuMA	SDS	poly(ethylene oxide) 2-bromophenylacetate PEO_{2K}-BPA/$CuBr_2$/TPMA/NaBr /TEA	UV lamp (λ_{max} = 365 nm, 4.9 mW cm^{-2}, MelodySusie®) Violet LEDs (λ_{max} = 394 nm, 2.6 mW cm^{-2})	22-117	79
Styrene/BMA/MA	-	g-CN (CM, CMD, PhCMp, vTA-CMp and $CMSO_3$)	50 W LED daylight sources (20 cm apart from each other) [overnight]	160-500	95
MMA	SDS	Acridine orange (dye) /Disulfide (oxidant)/ NHC borane	Visible LED strip, no details concerning irradiance [6 – 10 h]	71-154	96

Recently, graphite carbon nitride (g-CN) was used as a visible-light photoinitiator and Pickering stabilizer for emulsion photopolymerization of styrene and two methacrylate monomers, as shown in **Figure I-9**.[95] g-CN has a suitable band gap as a photocatalyst that can generate electrons and holes under light excitation. The author showed that the radical polymerization process was largely initiated by holes, i.e., the radicals formed by the oxidation of oxygen and water to form initiating radicals (i.e., $OH^{\cdot}$, $O_2^{-\cdot}$ and $HO_2^{-\cdot}$). By replacing g-CN into a more specialized material with unique photoluminescent properties (quantum dots PhCMp: derived from a phenyl group modified cyanuric acid/melamine complex), photoluminescent latex particles were produced for potential application in biomedicine and bioimaging.

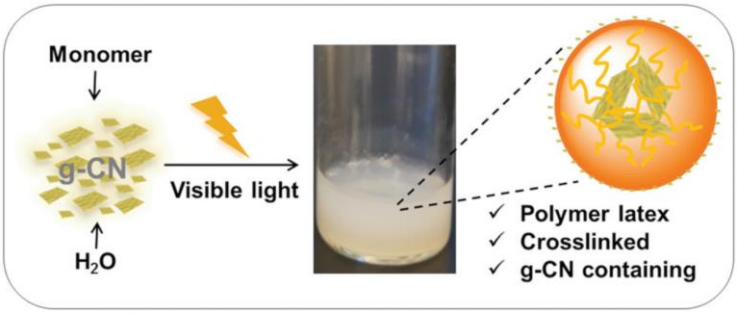

Figure I-9 The process of emulsion photopolymerization initiated and stabilized by g-CN, reproduced after publication.[95]

In 2018, Lacôte and collaborators developed a new three-component visible-light photoinitiator system for the emulsion polymerization of styrene. The system contains acridine orange (AO), water-soluble diphenyl disulfide, 2,4-dimethyl-1,2,4-triazol-3-ylideneborane (N-heterocyclic carbene borane **1**). Under blue light irradiation, the photoreduction of the disulfide 2 by AO leads to the formation of thiyl radicals (**3•**). Subsequently, this thiyl radical (**3•**) abstracts a hydrogen atom from NHC-borane 1, to afford an initiating NHC-boryl radical (**1•**), as shown in **Figure I-10**.[94] Recently, the extension of this process to methacrylate monomers was demonstrated by the same group.[96] Interestingly, thiyl radicals (**3•**) alone were also efficient in initiating the emulsion polymerization of MMA with a solids content up to 40%, while much lower rates and final monomer conversions were observed with styrene. Such discrepancy may be due to the higher propagation constant of MMA and its greater solubility in water. The new, simplified visible-light initiation system allowed access to a wide range of poly(meth)acrylate latexes.

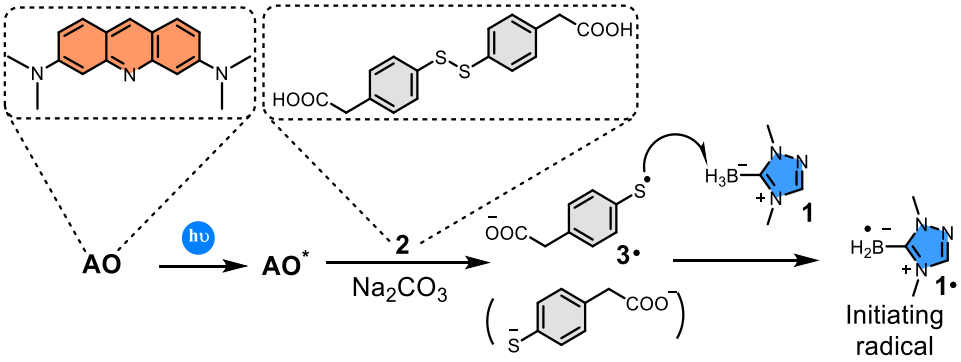

Figure I-10 Formation of boron-centered initiating radicals in water by irradiation with visible-light, inspired after publication.[96]

2.3 Miniemulsion (photo)polymerization

Miniemulsion polymerization can be considered as a variant process of emulsion polymerization, in which droplet nucleation is favored by a significant reduction in monomer droplet size. When the monomer droplets of an emulsion are reduced to the 50-500 nm range, a fraction can act as “nanoreactor” of polymerization. Miniemulsion polymerization was first studied by Ugelstad and coworkers in early in 1970-1980s in development of an industrial polyvinylchloride process.[7,64]

2.3.1 Formulations

Miniemulsion is an oil-in-water dispersion with droplet size in the range of 50-500 nm and stability from hours to months. its size and stability are in between macroemulsion and microemulsion, as illustrated in **Figure I-11**. The typical formulation of a monomeric miniemulsion is similar to that of a macroemulsion. It contains water, surfactant, initiator, and monomer. The only difference is the presence of a hydrophobic agent (costabilizer) in the organic phase to limit (and delay) droplet the destabilization of the droplets by diffusion of the monomer from smaller to larger droplets (Oswald ripening). The costabilizer, typically hexadecane or cetyl alcohol, must have a low or a moderate molar mass and low water-solubility.[97,98]

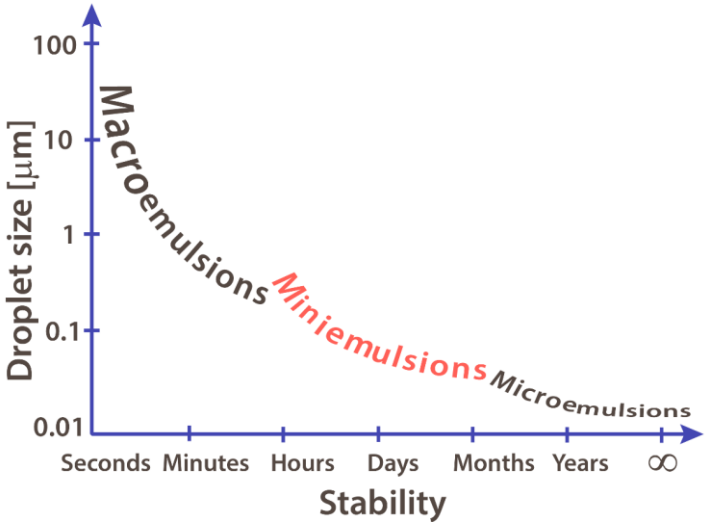

Figure I-11 Relative stability as a function of droplet size for the three classes of emulsions (reproduced form Emulsion polymerization and Emulsion Polymers).[64]

2.3.2 Preparation of monomer miniemulsion

Monomer miniemulsions are normally formed by a high energy homogenization procedure in which droplets of a coarse emulsion are broken down into smaller ones by using high-energy emulsification devices such as an ultrasonication probe or a high-pressure homogenizer. However, such high energy requirement impedes the large-scale implementation of miniemulsion polymerization. Therefore, many efforts have been devoted to developing low-energy alternatives such as emulsion inversion point (EIP)[99], phase inversion temperature (PIT)[100] and membrane emulsification method.[101,102] Concerning its

stability, miniemulsions are thermodynamically unstable, but kinetically metastable. In other words, miniemulsion are not indefinitely stable, but are stable as long enough (over hours to months) for the polymerization to be carried out.

2.3.3 Particle formation

2.3.3.1 Droplet nucleation

Droplet nucleation is desired in a miniemulsion polymerization. At the end of emulsification process, monomer droplets of relatively small size (50 – 500 nm) are formed. In an ideal "one-to-one" copy process (which is not often the case), one droplet should be converted into one particle. Therefore, there is no monomer transport through the aqueous phase and no contribution from homogeneous nucleation. It is worth noting that the concentration of free surfactant in the aqueous phase is generally lower than its CMC to prevent the occurrence of micellar nucleation. Provided that all secondary nucleation mechanisms are halted, particle number can be controlled by the initial number of monomer droplets. Practically, efficient droplet nucleation is achieved only for monomers with limited water-solubility, such as styrene, butyl methacrylates and acrylate.[103,104] This unique mechanism makes miniemulsion polymerization a powerful method to encapsulate water-insoluble materials into latexes particles,[105–107] to create hybrid particles,[108,109] nanocomposites,[110] nanocapsule,[111,112] and to conduct controlled/living radical polymerization.[102,113,114]

2.3.4 Miniemulsion photopolymerization

The nanometer size of monomer miniemulsion, typically in the range of 50-500 nm, makes them advantageous for a photoinitiated polymerization because they have a lower light-scattering coefficient compared to macroemulsions. The first miniemulsion photopolymerization was reported by Liu and co-workers in 2007.[115] A miniemulsion of methyl methacrylate was prepared using ionic surfactant (SDS) and cetyl alcohol as costabilizer. Photopolymerization was carried out at ambient temperature under UV-light (maximum at 365 nm) using Irgacure 184 (1-Hydroxy cyclohexyl phenyl ketone) as radical photoinitiator, resulting in a stable latex without coagulation. By adding a catalyst (4-hydroxy-2,2,6,6- tetramethyl-piperidinyloxy or HTEMPO), the authors found that the controlled/living photopolymerization in miniemulsion was achieved. Over the past fifteen years, a great deal

of effort has been made by many groups to advance miniemulsion photopolymerization. Of particular interest has been the use of visible-light (blue and green LED) as an effective initiation source.[113,116] Their works were discussed in detail in previous review by Chemtob et. al, and will not be repeated in this chapter.[4] The main works released before 2018 were summarized in **Table I-2**. Only the studies published over the last three years will be discussed thoroughly (in red in **Table I-2**). It is worth noting that among the 24 studies dealing with miniemulsion photopolymerizations, only two focuses on thiol-ene step growth polymerization. Studies on miniemulsion photopolymerization released over the last 5 years are commented in detail in the next section.

Table I-2 Main studies describing miniemulsion photopolymerization from 2007-2021 (Last studies are highlighted in red).

Monomer	Surfactant (costabilizer)	Photoinitiator	Lamp [irradiation time]	Particle diameter (nm)	Ref.
MMA	SDS (cetyl alcohol)	Irgacure 184	UV 365 nm, 3.5 mW cm^{-2} [70 min]	70-150	[115]
Vinyl acetate	SDS	AIBN, I-PDMS-I	125 W Philips HPK, 2.5 mW cm^{-2} [16 h]	160-360	[117]
MMA	Tween 80 (Tetradecane)	Benzoyl peroxide	200 W, high-pressure Hg arc, 0.83 mW cm^{-2} [60 min]	100-200	[118]
MMA	SDS (hexadecane)	Irgacure 184	300 W, medium-pressure Hg-Xe arc, 350 nm, 1.16 mW cm^{-2}	90-126	[119]
MMA/BA/ AA	Dowfax 2A1 (hexadecane)	Irgacure 819, Darocur 1173 Irgacure 184 2,2-Dimethoxy-2-phenylacetophenone	200 W high-pressure Hg-Xe arc, 180 mW cm^{-2} [20-140 min]	50-60	[120]
MMA/BA/ AA	SDS (hexadecane)	Irgacure 819, Darocur 1173, Irgacure 184, 2,2-Dimethoxy-2-phenylacetophenone, Irgacure 2959, Irgacure 907	200 W, high-pressure Hg-Xe arc > 300 nm, 4 - 200 mW cm^{-2}	60-90	[121]
MMA/BA/ AA	SDS/ Dowfax 2A1 (hexadecane)	Irgacure 907 Self-initiation	200 W, high-pressure Hg-Xe arc > 300 nm, 4 - 200 mW cm^{-2} 150 W, medium-pressure Hg-arc [20 -140 min]	55-75	[122]
MMA/MAA /HEMA Polyurethane	SDS/ Dowfax 2A1 (Octadecyl acrylate)	Irgacure 184	20 “black light” tubes, 315 – 400 nm, 2.5-7 mW cm^{-2} [1.5 – 15 min]	150-190	[123,124]
MMA/BA/ AA	SDS (Octadecyl acrylate)	Self-initiation	200 W, high-pressure Hg-Xe arc, 633 mW cm^{-2}	40-300	[125]
Styrene/BA	Dowfax 2A1 (Octadecyl acrylate)	TPO	20 “black light” tubes, 315 – 400 nm, 2.5 – 7 mW cm^{-2} [1.5 – 15 min]	80-190	[126]

Monomer	Surfactant (costabilizer)	Photoinitiator	Lamp [irradiation time]	Particle diameter (nm)	Ref.
MMA/BA/AA	SDS (Octadecyl acrylate)	Irgacure 2959 Irgacure 819	200 W, high-pressure Hg-Xe arc > 300 nm, 965 mW cm^{-2} [1000 s]	40-300	127
MMA/BA/AA	SDS (Octadecyl acrylate)	Self-initiation	150 W, medium-pressure Hg-arc [< 6 h]	40-115	17
MMA/BA/AA	SDS (hexadecane)	Irgacure 2959	18 W, "black light" tube, 280 - 410 nm, external, 3 mW cm^{-2} [5 and 20 min]	40-100	128
MMA/MAA /HEMA Polyurethane	SDS/ Dowfax 2A1 (Octadecyl acrylate)	Darocur 1173 Irgacure 2959 TPO Irgacure 184	20 "black light" tubes, 315 – 400 nm [12 - 16 min]	150	129
Oligomeric acrylated resin	(hexadecane)	Irgacure 184/benzophenone	150 W, medium-pressure Hg arc, 35 mW cm^{-2} [60 min]	40-500	130
Dithiol-Diene	SDS (hexadecane)	Irgacure 2959	200 W, high-pressure Hg-Xe arc, > 300 nm 965 mW cm^{-2}, radiant exitance : 588 mW cm^{-2} [5 -220 min]	100-150	17,131
Styrene	Dowfax 8390 (Hexadecane)	Photo redox catalyst: fac-[Ir(ppy)3] / 3-benzylsulfanylthiocarbonylsulfanyl propionic acid	LED strip, 460 nm, 0.73 mW cm^{-2}, [120 h]	>200	113
BA/BuMA	SDS (hexadecane)	Diphenyl(2,4,6-trimethylbenzoyl)phosphine oxide (TPO)	18 W, "black light" tube, 280 - 360 nm, 2.6 mW cm^{-2}, [27 s]	120	132
BA	SDS (hexadecane)	TPO	18 W, "black light" tube, Osram, 280 - 360 nm, 2.6 mW cm^{-2}, [27 s]	120	133
Hexyl acrylate	SDS (pentadecane)	Benzoin methyl ether	8 W, 5 UV tubes, 365 nm, 2.2 – 3.7 mW cm^{-2} [0 – 30 min]	100-200	134
Styrene	Lutensol AT50 (hexadecane)	Irgacure 819	UV LED, 365 nm, 44.2 - 68 mW cm^{-2}, [10 – 60 s]	120-160	135
Oligomeric acrylated resin	(hexadecane)	Irgacure 184/benzophenone	100 W, medium-pressure Hg arc, > 340 nm, [< 250 s]	40-500	136
BuMA	SDS (hexadecane)	4-cyano-4[(dodecylsulfanylthiocarbonyl)sulfanyl pentanoic acid)] as photoiniferter	LED strip, 530 nm, 2.5 m, 14.4 W/m, 25 LEDs [20 h]	100-200	116
Norbornene	CREMOPHOR CO40, CREMOPHOR RH60, Merpol® HCS, Tween®20 or Brij®S100 (hexadecane)	$IMesH^+BPh4^-$/ITX	Lightningcure® Hamamatsu medium pressure mercury-xenon lamp, (20 mW cm^{-2} at 365 nm) [30 min]	74-147	137

Monomer	Surfactant (costabilizer)	Photoinitiator	Lamp [irradiation time]	Particle diameter (nm)	Ref.
Triethylene glycol divinyl ether	SDS/ polyvinylpyrrolidone/ Pluronic (hexadecane)	Triarylsulfonium hexafluoroantimonate salts, 50 wt% in propylene carbonate	LC8 Lightningcure, Hamamatsu, mercury lamp [5-15 min]	173-177	138
BA/BuMA	SDS (Hexadecance)	ethyl α-bromoisobutyrate /$CuBr_2$/TPMA/NaBr	UV lamp (λ_{max} = 370 nm, 5 mW cm^{-2}, MelodySusie®)	110-167	139
Norbornene	Brij®S100 (hexadecane)	$IMesH^+BPh4^-$/ITX	LED lamp novaLIGHT LED 100–365 from Peschl Ultraviolet at 365 nm 130 mW cm^{-2} [5-60 min]	95-156	140
MMA	SDS (hexadecane)	TPO	14.4 W LED strip (5050 SMD, 60 LEDs per meter, 405 nm [2-10 min]	211-909	141
HDDA	Hitenol BC-20/ Noigen RN20 DOTAP/ AUBDMAB	Irgacure 184	12 W UV lamp (UVP, Upland, USA) [2.5 h]	109-231	142
Dithiol-diene	SDS (hexadecane)	Irgacure 2959	UV 385 nm [4 h]	210-330	143

Ring-opening metathesis photopolymerization (ROMP) in miniemulsion was largely unexplored until 2018, when Pichavant et al. presented a photolatent ROMP catalyst formed in situ by the reaction between a photogenerated N-heterocyclic carbene (NHC) ligand and an inactive ruthenium procatalyst (**Figure I-12**).[137] The borate anion (Ph_4B^-) transfers an electron to the excited triplet state of ITX (^{3}ITX*) to form the radical anion $ITX^{\bullet-}$ which subsequently undergoes a hydrogen abstraction step with the azolium cation $NHCH^+$ to yield the expected free NHC ligand for the catalyst. The authors showed that the resulting NHC-ruthenium catalyst is able to initiate ROMP of norbornene in miniemulsion, leading to stable poly(norbornene) latexes with particle size in the range of 100 nm. However, the final conversion and solids content in this study were low at 55% with 20% solids content. Recently, the authors improved the operating conditions by using a ring-shaped LED photoreactor to achieve a conversion of more than 90% and latex with a solids content of 10% (**Figure I-12**).[140]

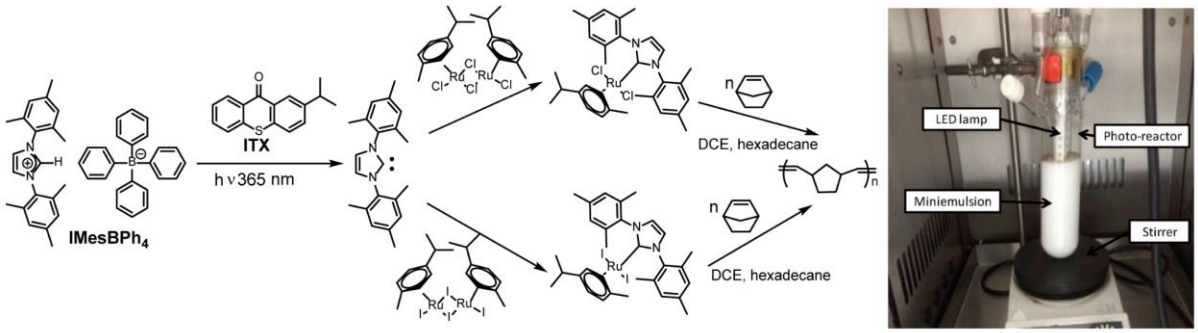

Figure I-12 The mechanism of in situ formation of ROMP-catalyst and experimental set-up using annular LED photoreactor, reproduced after publications.[137,140]

Miniemulsion polymerization is a convenient technique to prepare polymer nanocapsules.[111] Recently Artusio et al. reported a new way to produce nanocapsules by cationic UV-triggered miniemulsion polymerization (**Figure I-13**).[138] The miniemulsion photopolymerization of triethylene glycol divinyl ether was controlled at the oil/water interphase using triarylsulfonium hexafluoroantimonate salts as photoinitiator. The authors focused on formulation design with various surfactants and their concentration, as well as initiator and successfully fabricated nanocapsules with diameters of about 200 nm.

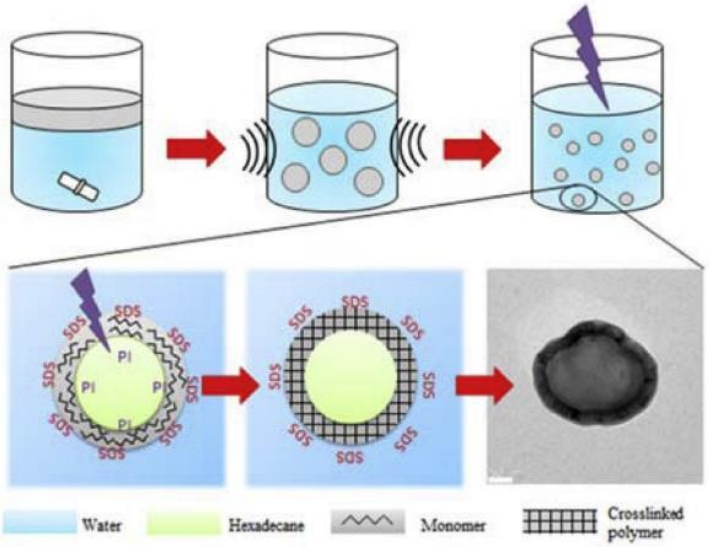

Figure I-13 Experimental scheme for the preparation of nanocapsules by of miniemulsion photopolymerization, reproduced after publication.[138]

In the field of controlled/living radical polymerization (CLRP) in miniemulsion, two reports[113,116] on photoinduced energy/electron transfer-RAFT polymerization were

summarized in **Table I-2**. The studies are characterized by two important features: the use of energy-saving LEDs that emit in the visible range (blue and green light), and a low catalyst loading (50 ppm based on the monomer) or even catalyst-free. Another photoinduced CLRP in miniemulsion was developed by Wang et al. in 2018.[139] A photo-mediated atom transfer radical polymerization (photo-ATRP) of (meth)acrylates was successfully implemented in miniemulsion media. The polymerization processes involved an ion-pair catalyst formed by the interaction of Cu/tris(2-pyridylmethyl)amine) and SDS as an anionic surfactant. The ion-pair catalyst was efficient in controlling ATRP reactions of *n*-butyl acrylate and *n*-butyl methacrylate under UV irradiation (MelodySusie® UV lamp λ_{max} = 370 nm, 5 mW cm^{-2}). Low catalyst concentration (100 ppm), high solids content of up to 50%, well-defined properties and kinetically temporal control are among the key advantages of this study. Nevertheless, the efficiency of photoinduced CLRP batch processes remained generally low (> 70% monomer conversion, associated with a long reaction time of 12 hours), which might be due to the light penetration problems of UV lamp.

Performing miniemulsion photopolymerization in a continuous flow reactor can be a good pathway to accelerate the reaction kinetic. Nauman et al. applied this approach with an additional focus on particle size control.[141] Monomer miniemulsions were prepared via membrane emulsification. Basically, the oil phase (methyl methacrylate, diphenyl(2,4,6-trimethylbenzoyl)phosphine oxide as photoinitiator, and hexadecane as costabilizer) was mixed with aqueous solution of sodium dodecyl sulfate (SDS). The mixtures were passed through membranes with different pore sizes. The resulting monomer miniemulsions with various average diameters were subsequently polymerized in a continuous tubular flow photoreactor (**Figure I-14**). The study showed that particle size can be controlled by using appropriate surfactant concentration as well as a radical scavenger (sodium nitrite) in aqueous phase. The specific role of sodium nitrite is to suppress radicals in aqueous phase generated by radical desorption of monomer droplets, thus preventing the secondary homogeneous nucleation. Although fast polymerizations (10 minutes) and particle size control were described, the emulsification process took up to 20-40 hour.[101] Future developments should aim at a higher throughput of the emulsification process to increase the overall efficiency of the continuous miniemulsion photopolymerization process.

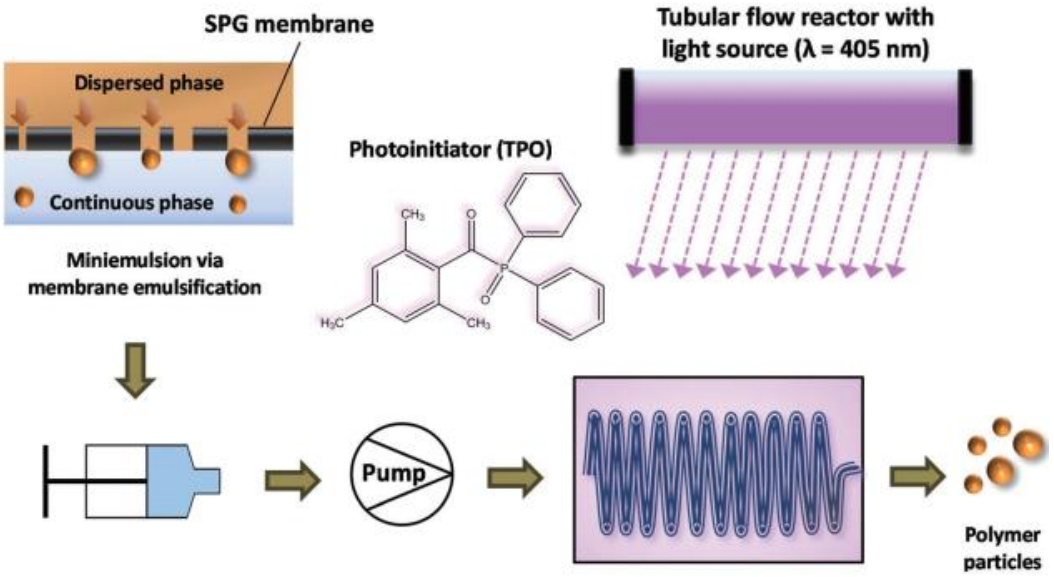

Figure I-14 Schematic illustration of membrane emulsification followed by photopolymerization in continuous flow, reproduced after publication.[141]

The latest study in this fields is the application of miniemulsion photopolymerization to prepare dipolar colloidal particles.[142] A miniemulsion of hexanediol diacrylate (HDDA) containing polarizable materials and photoinitiator was emulsified and stabilized by a non-ionic surfactant. The miniemulsion droplets were subsequently embedded in agarose gel to preserve their stability before polymerization. This strategy allows the author to prepare a ranges of dipolar particles for potential applications in colloidal liquid crystal for instance.

3 CONCLUSION

Photopolymerization in dispersed media has proven to be extremely practical due to the mild reaction conditions at room temperature and many attractive features such as spatial and temporal control. With the progress of energy-saving technology, near-UV and visible-light (LED) have been used as efficient light sources to initiate photopolymerization in emulsions or miniemulsions. Nevertheless, current studies are still strongly focused on the development of latexes based on chain growth polymerization. It is expected that the scope and applications of this process may be expanded by a step-growth polymerization such as thiol-ene polymerization in the coming years.

CHAPTER II. UNDERSTANDING THE MECHANISM OF THIOL-ENE SPONTANEOUS POLYMERIZATION

1 INTRODUCTION

The radical-initiated addition of thiols to alkenes to yield thioether products has been known for more than a century.[13,14] However, it is only since the 2000s that this reaction has been the subject of a renewed interest as part of efforts to find chemical reactions meeting the "click" chemistry criteria.[144] As small molecule reactions, thiol-ene reactions have mostly been used for anchoring a catalyst on a polymer support,[145] patterning surfaces,[146] or functionalizing biological molecules[147] (e.g., peptide[148] or carbohydrate[149]). However, the major use for thiol-ene reaction is in polymerization.[15] Generally, a thiol-ene step polymerization involves a radical photoinitiator and neat monomers with two or more SH/C=C groups per molecule in order to generate a crosslinked structure. As is often the case in photopolymerization, the applications focus on film curing used as coatings or photoresists.[21] When a solvent is present, other polymer products may be formed including hydrogels,[150] latexes,[151] and dendrimers.[152] The resulting step-growth poly(thioether)s have been proposed as an alternative to conventional chain-growth polymers (e.g., acrylic polymers) since they circumvent some limitations including oxygen inhibition, stress relaxation and heterogeneous network formation.[16] Despite these advantages and a growing number of publications, research on thiol-ene step-growth (photo)polymerization crucially never succeeded in getting established as a solid alternative to conventional chain-growth photopolymerization.

The inherent limitations of thiol-ene chemistry and poly(thioether)s have contributed to this situation. The very low odor detection level of low-molecular-weight thiols is often advanced as a disadvantage.[153] However, thiols are used today in many chemical manufacturing processes (e.g., chain-transfer agent in radical polymerization[154]) or as components of commercial products (e.g., cleaners or hair care products[155]). A second problem is the sub-ambient glass transition temperature (T_g) of poly(thioether)s leading to poor mechanical properties.[21] Significant efforts have contributed to overcome this limitation including the increase of crosslinking density,[156] the mixing with high T_g resins,[157] and the introduction of stiffer polymer backbones[158] or crystalline domains.[17] A last significant and unresolved problem of thiol-ene systems is spontaneous polymerization.[22] Lack of chemical stability has been reported in the literature for a broad range of thiol-ene monomers, generally in the absence of solvents, at ambient temperature and under conditions avoiding the formation of radicals.[23–25] Premature polymerization prevents storage and shipment of

thiol-ene formulations, or at best, reduce shelf life.[26] Additionally, the lack of photolatent systems adds complexity and cost to the polymerization process. The inability to precisely control the onset of polymerization (temporal control) also precludes modern photopolymerization technologies like photolithography or 3D printing.[159]

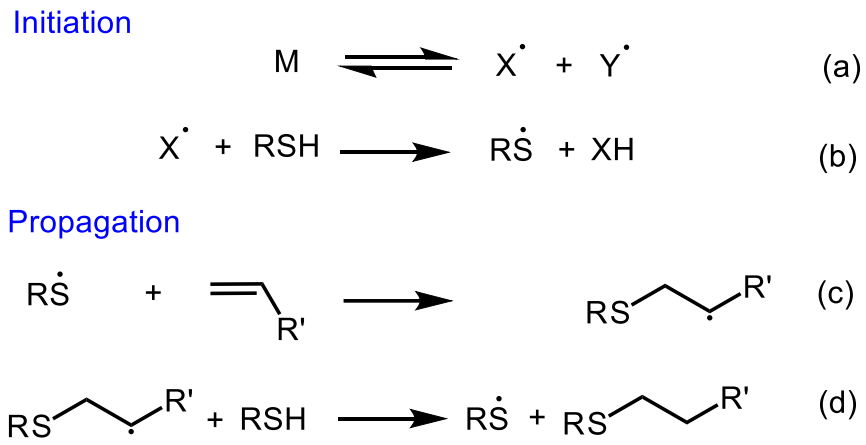

Scheme II-1 Radical chain reaction scheme of a self-initiated thiol-ene polymerization. M can be an alkene or a thiol. Termination reactions are not detailed but include a number of recombination's of carbo-centered and thiyl radicals.

The mechanism of spontaneous thiol-ene polymerization is not well established.[56,160] It is considered to involve a self-initiated polymerization process since the thermal homolysis of impurities present in the monomers (e.g., peroxides or hydroperoxides) is assumed to be negligible.[161] Other monomers susceptible to self-initiated polymerization are reported in the literature, including styrene,[162] methyl methacrylate[163] and some donor/acceptor monomer pairs.[164] Unlike thiol-ene systems, their self-polymerization proceeds at very slow rates at ambient temperature and can be effectively stopped with inhibitors. The difference between thiol-ene monomers and other self-initiating monomers can be understood by considering the self-initiated thiol-ene polymerization as a conventional *radical chain reaction* consisting of the usual initiation, propagation, and termination reactions (**Scheme II-1**). The initiation involves the thermal generation of primary radicals ($X^{\bullet}$ and $Y^{\bullet}$) from the monomer itself (**Scheme II-1**, (a), self-initiation step). The mechanism of this reaction for thiol-ene monomers is unclear although several hypotheses (discussed in the next section) were put forward. In most self-initiated polymerizations, this first step is a chemical equilibrium strongly displaced backward, that is, strongly favorable to reactant (monomer), therefore the formation of $X^{\bullet}$ is slow and very limited. Thiols can rapidly transfer a hydrogen atom to most types of radicals.[144]

Therefore, the second part of the initiation involves the reaction of X• to a thiol molecule (RSH) to produce the chain-initiating radical RS• (**Scheme II-1**, (b), self-initiation step). Propagation consists of a group of two reaction steps: *addition* and *H-abstraction*. The initiating radical RS• can add to the C=C bond to form a carbon-centered radical via a reversible process (**Scheme II-1**, (c), propagation step). This latter subsequently abstracts a hydrogen atom from another thiol molecule to yield the desired thioether product and a new thiyl radical needed to begin a new cycle (**Scheme II-1**, (d), propagation step). The propagation cycle is repeated a number of times and allows the growth of polymer chains. Compared to other monomers, the self-initiated polymerization of some thiol-ene systems is more difficult to control because of two characteristics. Firstly, the probability of self-initiation at ambient temperature may be assumed to be higher due to a lower activation energy. Secondly, the two propagation steps (c) and (d) of a thiol-ene polymerization may be very fast, even at ambient temperature, due to high addition and H-abstraction rate constants, k_{add} and k_H, respectively. Thus, polymerization can start even when the concentration of initiating radicals is low. As predicted by Le Chatelier's principle, the consumption of initiating radicals drives forward the self-initiation equilibrium (**Scheme II-1**, (a)) leading to an enhancement of the phenomenon. The efficiency of radical inhibitors in producing stable thiol-ene mixtures is generally limited because the rapid propagation steps compete with the inhibition reaction.[23,56,160,165]

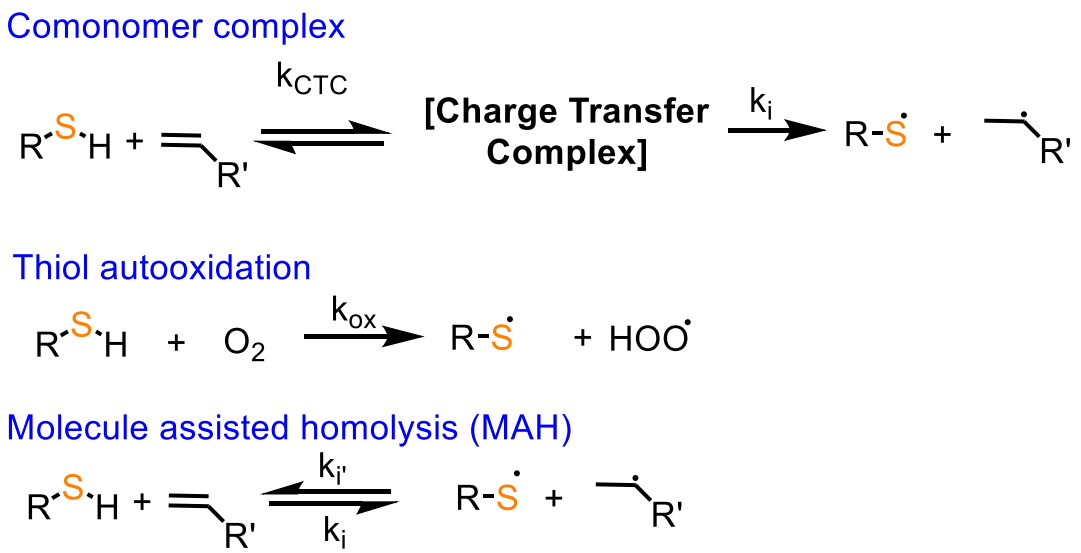

Scheme II-2 Putative mechanisms of the self-initiation of a thermal thiol-ene polymerization.

Three main mechanisms of self-initiated thiol-ene polymerization have been suggested in the literature (**Scheme II-2**). The first mechanism involves the participation of a *comonomer complex*. For example, Klemm et al. provided spectroscopic evidence (UV-vis, NMR) that supports the formation of a ground-state charge-transfer complex between a thiol and an alkene.[166,167] This latter is postulated to undergo a redox reaction yielding primary radicals. A second mechanistic hypothesis suggests that thiyl radicals are produced by oxidation of thiols by molecular oxygen (air).[168] The reaction of thiols and thiyl radicals with molecular oxygen has been the subject of intensive investigations[169] since the pioneering work of Kharasch on thiol−olefin cooxidation (TOCO) process. A third mechanism would imply the molecule-assisted homolysis (MAH) where the homolytic cleavage of the S-H bond could be assisted by hydrogen transfer to alkene to form a C-H bond.[170] A large body of evidences points out that styrene self-initiated polymerization proceeds by MAH between a Diels-Alder dimer and a monomer molecule.[171] Currently, there is no consensus as to the correct (or at least dominant) mechanism because there is a lack of experimental data. Understanding spontaneous initiation of radical chain reactions is generally challenging because it is based on slow and equilibrium reactions, but the elucidation of a dominant self-initiation mechanism would be a major contribution to the development of the thiol-ene polymerization field. By this way, more efficient mitigation strategies could be found to prevent premature polymerization. The present research aims to elucidate the main mechanism(s) of self-initiation of thiol-ene monomers, and to determine the factors that underlie the reactivity of a self-initiated thiol-ene polymerization, in particular as regards to experimental conditions (solvent, atmosphere) and the structure of ene and thiol compounds.

To address these questions, diallyl adipate (**DAA**), diallyl phthalate (**DAP**), di(ethylene glycol) divinyl ether (**DVE**) are used as model alkenes (**Figure II-1**). The advantage of allyl esters and vinyl ethers is their inability to homopolymerize or to react by thiol-Michael reaction (nucleophilic addition of thiolate to alkene) due to their electron-donating substituents. Thus, the radical-mediated thiol-ene polymerization is considered to be the predominant process in the presence of thiols. The reactivity of these 3 dienes with a series of 5 dithiols (acetate **1**, propionate **2**, tri(ethylene glycol) **3**, alkylsulfide **4**, hexane **5**, **Figure II-1**) was investigated under conditions avoiding the intentional formation of radicals. To provide insight into the underlying factors that govern the self-initiation mechanism of neat thiol-ene monomers,

three areas are studied thoroughly: *self-initiated polymerization kinetics* in bulk and in solution, *thiol solvation*, and *identification of initiating radicals*.

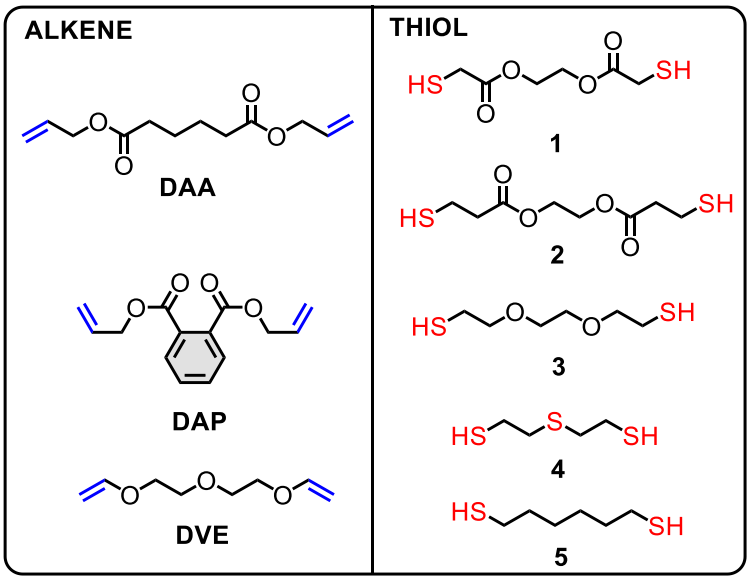

Figure II-1 Chemical structures of bifunctional thiols and alkenes

2 EXPERIMENTAL SECTION

2.1 Materials

Diallyl phthalate (**DAP**, TCI, 99%), diallyl adipate (**DAA**, TCI, 99.8 %), di(ethylene glycol) divinyl ether (**DVE**, BASF), ethylene glycol bismercaptoacetate (**1**, TCI, 97.5%), ethylene glycol bis(3-mercaptopropionate) (**2**, TCI, 98.1%), 2,2-(ethylenedioxy)diethanedithiol (**3**, TCI, 99.6%), 2,2'-thioldiethanethiol (**4**, Bruno Bock, 98.7%), 1,6-hexanedithiol (**5**, TCI, 99.1%) were used as received without further purification to be as near of real conditions of use (with some exceptions noted in the text). Diphenyl(2,4,6-trimethylbenzoyl)phosphine oxide (**TPO**, TCI, > 98%) and 2-isopropylthioxanthone (**ITX**, Aldrich, analytical standard) were used as photoinitiators and photosensitizer, respectively. N-*tert*-butyl-α-phenylnitrone (**PBN**, TCI > 98%) was used as spin trapping agent. Dibutyl disulfide (TCI, > 98.5%), cumyl hydroperoxide (TCI, 80.5%), copper (II) sulfate pentahydrate (Carl Roth, >99%) were used as impurities. All solvents were used with analytical grade without further purification.

2.2 Methods

2.2.1 Self-initiated thiol-ene bulk polymerization - Monitoring of the reaction kinetics by Fourier Transform - Near IR spectroscopy (FT-NIR).

For experiments in the presence of air, stoichiometric amounts of dithiol and diene monomers were mixed in a 1 mL centrifuge tube and 0.25 mL of this mixture were immediately transferred to a 2-mm thick quartz cuvette (internal volume: 700 µL, width: 10 mm). The cuvette without stopper was placed vertically into the closed chamber of a Bruker FTIR (IFS66/s) spectrometer. The FTIR spectra were recorded at room temperature and regular intervals during a total period of 14 h. For experiments in the presence of inert atmosphere, thiol and ene monomers were degassed separately by three successive freeze-thaw cycles and stored under nitrogen. Mixing of the two monomers and transferring the mixture to a 2-mm thick quartz cuvette closed by a rubber-cap were also carried out under nitrogen. The chemical stability of the thiol-ene mixtures was studied in the NIR region of 4000-6500 cm^{-1} with a DTGS detector. Each of the IR spectra obtained from the spectrometer is an average of ten scans, each with a resolution of 4 cm^{-1}. Spectra were taken at intervals varying between 0.5 and 10 min depending on the system reactivity. The second overtone stretch of the CH of the alkene group at 6130 cm^{-1} was used to calculate the conversion (**Figure-S II-1A**). Calibration and method validation were carried out by ^{1}H NMR (**Figure-S II-1B**). It is useful to note that the kinetic profiles were not significantly changed when the cuvette was exposed to daylight light (**Figure-S II-1C**). Additionally, premature polymerization was slowed down but not prevented when thiols were purified by passing through an aluminium oxide column (**Figure-S II-1D**). This control experiment adds support to a purely thermal self-initiated polymerization which is sensitive to the presence of small concentrations of impurities (see section 3.1.2 for details).

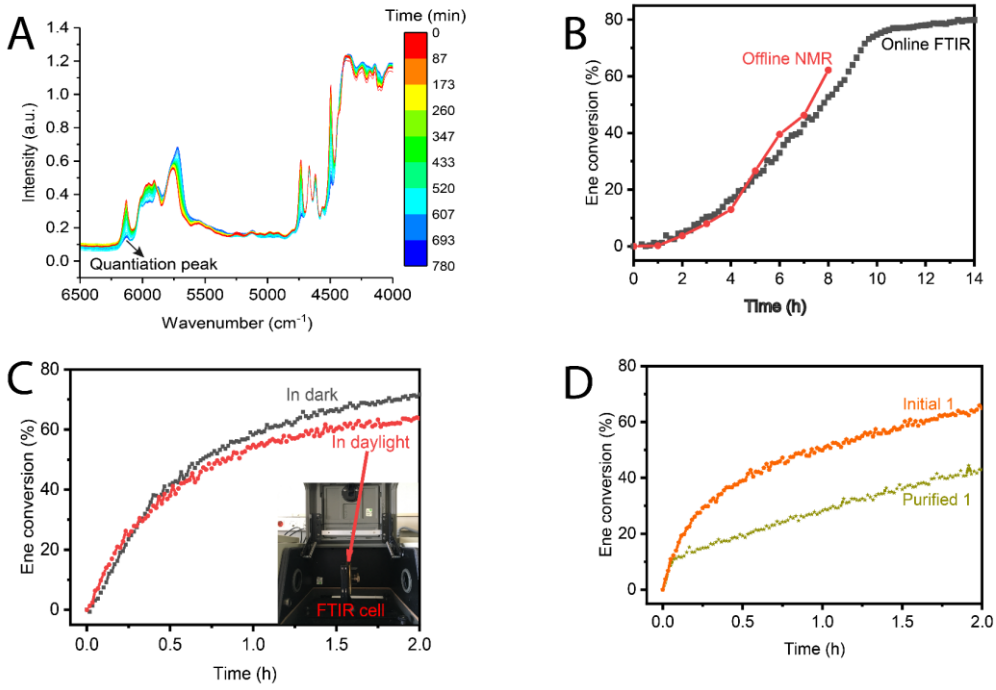

Figure-S II-1 (**A**) FTIR spectra of **DAP-3** mixture showing the evolution of the peak at 6130 cm^{-1}, (**B**)Comparison between ene conversion determined by offline ^{1}H NMR (dots) and online FT-NIR (squares), (**C**) dependence of ene conversion on storage time for stoichiometric polymerization of bulk **DAA-1** performed under air, (**D**) dependence of ene conversion versus time on the thiol stoichiometric polymerization of DAA-1. Dithiol 1 was purified after passing through an aluminum oxide column (activated, neutral, Brockmann I, 150 mesh, Sigma Aldrich Product number 199974). Briefly, 5 g of dithiol 1 was passed through a short column (12 mm ID) packed with 5 g of aluminum oxide.

2.2.2 Photoinitiated thiol-ene bulk polymerization - Monitoring of the reaction kinetics by real-time FT-IR spectroscopy.

Stoichiometric amounts of dithiol and diene monomers were mixed in a 5 mL amber vial containing 1 mol% of TPO photoinitiator with respect to the monomers. The thiol-ene mixture was sandwiched between two KBr crystals using a 100 µm Teflon O-ring spacer. The resulting unit was then compressed in a Presslok demountable cell holder and inserted inside the horizontal sample chamber of an iS50 spectrometer (Thermo Fisher Scientific). Irradiation by a 385 ± 5 nm LED lamp (LC-L1V3, Hamamatsu, 22.2 mW cm^{-2}) was led into the spectrometer chamber by means of a flexible light guide. The light guide was positioned at a distance of 5 cm from the KBr crystals to ensure complete radiation exposure of

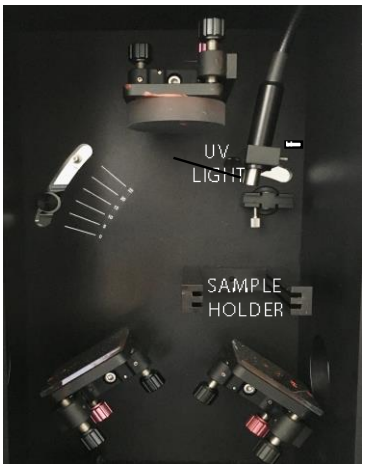

Figure-S II-2 Experimental set-up for real-time FTIR monitoring of photopolymerization

the sample. The light guide was also tilted at an angle of 5° so that it did not block the path of the IR beam (**Figure-S II-2**). The FTIR spectra were acquired in transmission mode using a MCT detector. The spectra were recorded during 120 s in the 2000-7000 cm^{-1} range, with a spectral resolution of 8 cm^{-1} and an interval of 0.14 s. The ene conversion was calculated from the C-H stretch of allylic double bond at 3100 cm^{-1}.

Thiol-ene polymerization rate. The general thiol-ene polymerization rate expression is given below (see Cramer et al. Macromolecules 2003, 36, 7964-7969 for more details)[37]

$$R_p = \sqrt{\frac{R_i}{2k_t}} \times \frac{1}{\sqrt{\frac{1}{(k_{add}[C=C])^2} + \frac{1}{(k_H[SH])^2} + \frac{1}{(k_{add}k_H[C=C][SH])}}}$$

R_i: initiation rate

k_t: rate constant for termination

k_H: rate constant for H-abstraction of thiols by carbon-centered radicals

$k_{\{add\}}$: rate constant for addition of thiyl radicals onto alkene

In the case of allyl esters presented in the study, the addition rate constant is much greater than the H-abstraction rate constants ($k_{\{add\}} >> k_H$). For this particular case, the polymerization expression given below simplifies in a way that R_p becomes first order, and dependent only on thiol concentration (H-abstraction is the rate- limiting step).

$$R_p = \sqrt{\frac{R_i}{2k_t}} \times k_H[SH]$$

2.2.3 Thiol solvation by ^{1}H NMR spectroscopy.

A $CDCl_3$ solution of thiol **1** at a concentration of 63 mM was placed into a 5-mm o.d. NMR tube. The tube was fitted with a rubber septum and 5 µL of tetramethylsilane were injected. NMR spectra were recorded by means of a Varian 300 spectrometer (300 MHz). A known volume of the solvent (or alkene) of interest was added to the NMR tubes to obtain a 24 molar excess relative to the thiol and the spectrum was recorded after injection. The chemical shifts were measured relative to the signal of tetramethylsilane. Delta chemical shift value was calculated as followed: $\Delta Hz = (\delta_{SH---solvent} - \delta_{SH}) \times 300$.

2.2.4 Electron paramagnetic resonance (EPR).

A *tert*-butylbenzene solution of 100 mM thiol **1** and 30 mM PBN was placed into a 6-mm o.d. EPR tube. If the thiyl radical (**1•)** presents in the thiol **1**, the following PBN-radical adduct (**Figure-S II-3**) is expected to be give raise a resonance signal.

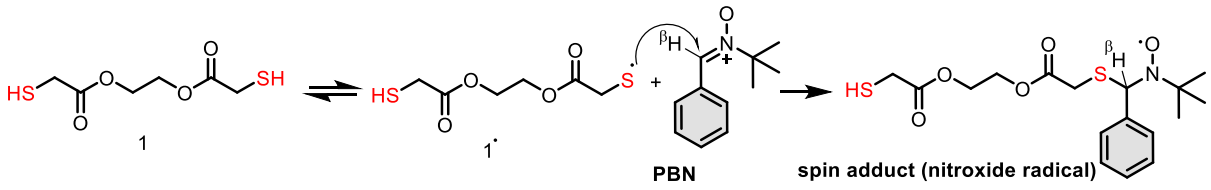

Figure-S II-3 PBN react with thiyl radical 1• to form nitroxide radical

The tube was fitted with a rubber septum, and the EPR spectrum was recorded by means of a Bruker EMX-plus EPR spectrometer. The EPR spectrum was recorded after 15 scans (modulation amplitude: 1G, receiver gain: 1.10^5, power: 6.325 mW, time constant: 20.48 ms) and simulated using WINSIM software. The simulation gives the hyperfine splitting constants for the PBN spin adducts (nitrogen and β-hydrogen a_N = 14.10 ± 0.1 G , and a_H = 2.57 ± 0.1 G, respectively)

For control experiments, ITX (10 mM) was added to the thiol-PBN solution and the EPR tube was irradiated in a circular photochemical reactor equipped with 25 LEDs (385 nm, 2.7 mW cm^{-2}) for 5 min. Thiyl radical formed via photochemical sensitization was trapped by PBN (**Figure-S II-4**) .The hyperfine splitting constants a_N, and a_H found in this experiment were used as reference values to confirm the thiyl radical.

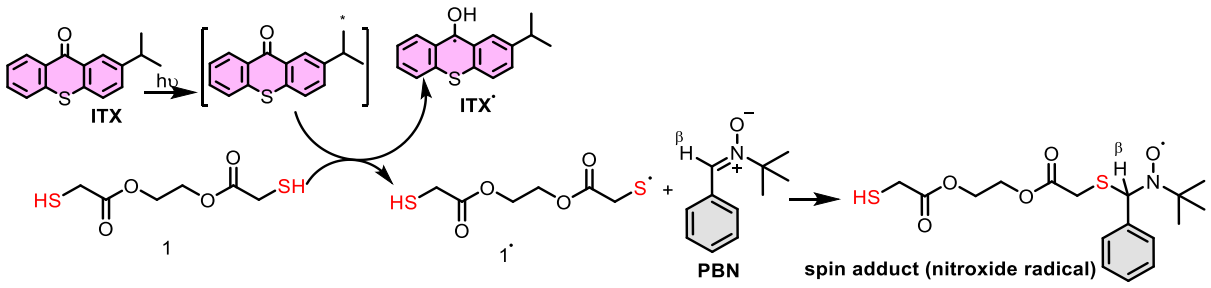

Figure-S II-4 Thiyl radical 1• is formed via photochemical sensitization using ITX and subsequently trapped by PBN.

In experiments involving the addition of solvent (or alkene), the solutions were placed in a 1-mm o.d. capillary tube before measurement.

3 RESULTS AND DISCUSSION

3.1 Self-initiated polymerization kinetics

3.1.1 Bulk polymerization

Preliminary experiments show that spontaneous thiol-ene polymerization rates can vary significantly with the solvent used, the reaction vessel or the number of samples taken for analysis. To avoid repeatability problems and obtain reproducible kinetic data, the polymerization was thus carried out with neat reactants (without solvent and initiator). Its progress was also monitored online by FT-NIR without periodic sample removal for analysis. [174] Bulk polymerization involving stoichiometric amounts of thiol and ene functional groups was performed at ambient temperature in a closed 2-mm thick spectroscopic cuvette placed in the dark chamber of a spectrometer.

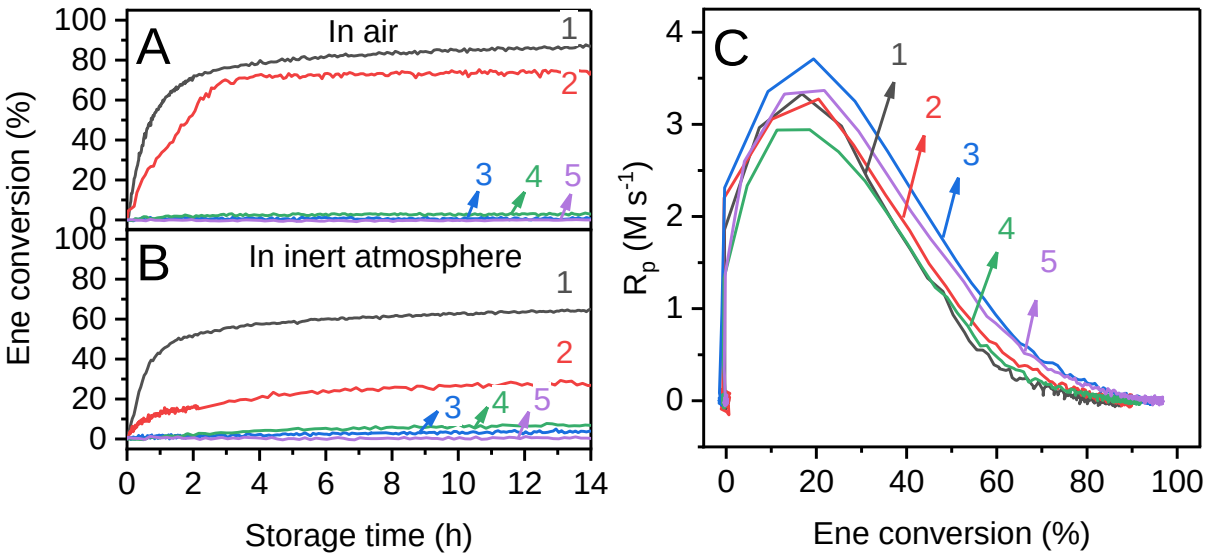

Figure II-2 Dependence of storage time on monomer (alkene) conversion for stoichiometric polymerization of bulk DAA-thiol (**1**, **2**, **3**, **4** and **5**) mixtures performed either in the presence of air (**A**) or under inert atmosphere (**B**). Polymerization was carried out at ambient temperature in the dark and under nonradical-inducing conditions. The disappearance of the second overtone stretch of the CH of the alkene group at 6130 cm^{-1} allows to evaluate ene conversion as a function of storage time. Photopolymerization rate versus ene conversion plot for a photoinitiated polymerization involving the same thiol-ene mixtures is shown in **C** (irradiance = 22.2 mW cm^{-2}, [TPO] = 1 mol%).

Figure II-2 displays plots of **DAA** conversion as function of time (up to 14 h) in presence of 5 different thiols (**1**-**5**) in the presence of air (**A**) or in inert atmosphere (**B**). In the presence of air, only **DAA-1** and **DAA-2** monomer mixtures readily undergo a premature

polymerization. However, the polymerization rates are significantly lower under inert atmosphere. This behavior indicates that one of the self-initiation mechanisms may be oxygen-assisted or/and moisture-assisted (propagation reactions are insensitive to oxygen and water).[52] The other thiols stand in marked contrast, since their polymerizations proceed at very slow rates (**3**, **4**) or does not take place (**5**) both in the presence of air and under nitrogen. It seems therefore that the reactivity of thiols depends on the inductive characteristics of their substituent since thiols bearing an ester substituent (**1**, **2**) having a marked electron-withdrawing character readily undergo a self-initiated polymerization with **DAA**. However, it remains to differentiate the respective contributions of self-initiation and propagation on the overall polymerization rate. As shown by modelling and experimental kinetic measurements,[37,50] the rate-limiting step for the thiol-ene polymerization involving allyl esters like **DAA** is H-abstraction ($k_{add}/k_H >> 1$). Under these conditions, the polymerization rate (R_p) expression simplifies as detailed in section 2.2.2. R_p depends on thiol concentration and a combination of rate and rate constants: R_I (self-initiation rate), k_t (rate constant for termination) and k_H (rate constant for H-abstraction).

$$R_p = \sqrt{\frac{R_i}{2k_t}} k_H [Dithiol]$$

One may reasonably assume that k_t and thiol concentration are in the same order of magnitude for the various **DAA**-thiol systems. Hence, k_H and R_i seem to be the most important factors in determining the value of R_p. To compare the value of k_H between the different thiols, the same series of **DAA**-dithiol mixtures is subjected to a photoinitiated polymerization using diphenyl 2,4,6 trimethyl-benzoyl phosphine oxide (TPO) as radical photoinitiator. Under these conditions, a reasonable assumption is to consider R_i constant irrespective of the monomer. **Figure II-2C** shows the plots of photopolymerization rate *versus* ene conversion for the five **DAA**-thiol systems in presence of TPO. There is little or no difference in reactivity, suggesting that k_H is of the same order of magnitude irrespective of the thiol involved. This result is consistent with literature data that the rate of H transfer depends mainly on the stability of the carbon-centered radical intermediate (unchanged in the series),[36] and to a lesser extent on thiol substituent.[172] Consequently, $\mathrm{R_p} \propto \sqrt{\mathrm{R_i}}$ in the different self-initiated **DAA**-thiol systems and the faster self-initiated polymerization rates observed for **DAA**-**1** and **DAA**-**2** (**Figure II-2A and 2B**) may be reasonably ascribed to a greater self-initiation rate.

To know whether these results obtained with **DAA** can be generalized, the same self-initiated bulk polymerization was carried out with **DAP** and **DVE** (**Figure II-1**) using the same set of thiols (**1**-**5**) as co-monomer. A number of interesting observations can be made from **Figure II-3** showing the initial polymerization rates (R_p^0) (**A**) and ene conversions after 14 h (**B**) in the presence of air and under nitrogen. The order of reactivity for the series of thiols (**1** > **2** > **3**-**4**-**5**) remains essentially the same irrespective of the alkene used. This confirms that the inductive characteristics of the thiol substituent have a significant effect on the initiation rate, and therefore, on the self-initiated polymerization rate. For a given alkene, the highest polymerization rates and conversions are achieved again with thiols **1** and **2** having an electron-withdrawing ester carbonyl substituent. For a given thiol, the reactivity is enhanced when vinyl ethers (**DVE**) are involved compared to allyl esters (**DAA**, **DAP**). A possible explanation may imply increase propagation rates due to the higher electron density of the C=C bonds of **DVE**. The polymerization rate is also slower with **DAP** compared to **DAA,** presumably because of steric effects decreasing propagation rates. However, these two explanations do not consider the possible effect of alkene structure on self-initiation rate. Finally, the case of **DAP** is particularly interesting because, unlike **DAA** and **DVE**, the polymerization is completely halted in an inert atmosphere irrespective of the thiol used. The addition of water does not change the kinetic profile , indicating that molecular oxygen plays a larger role than atmospheric moisture in the self-initiation mechanism.

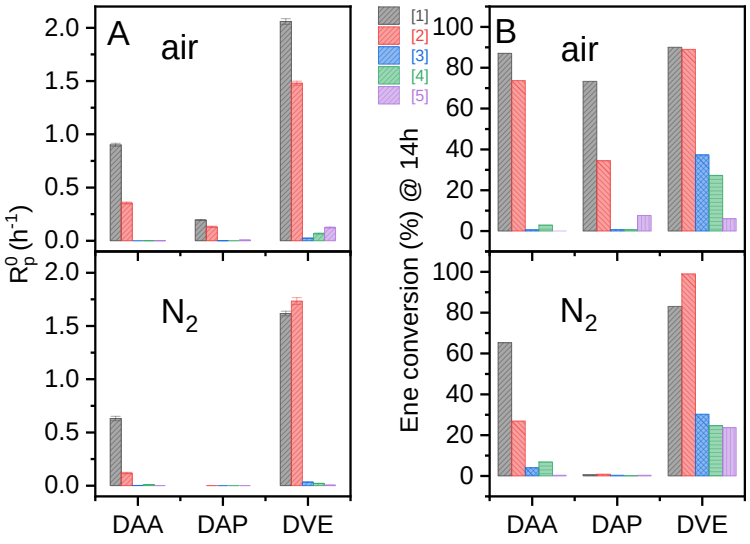

Figure II-3 . Initial polymerization rates (R_p^0) (**A**) and ene conversion after 14 h (**B**) in the presence of air and under nitrogen for **DAA**, **DAP** and **DVE.**

3.1.2 Effect of impurities

DAA-1 (1:1 equiv) is used as a model thiol-ene couple to gain insight into the effect of impurities on the course of a self-initiated bulk polymerization. **Table II-1** compares the relative initial polymerization rates in presence of four likely contaminants of thiol monomers: water, disulfide (dibutyl disulfide), hydroperoxide (cumyl hydroperoxide) and copper(II) salt ($CuSO_4$). Thiols may absorb small amounts of water and oxygen on contact with atmospheric air. Disulfide is the product of oxidative coupling of thiols and (hydro)peroxide is a common impurity resulting from air oxidation (autooxidation). Metal traces contamination may result from contact with metallic surfaces, which can catalyze the auto-oxidation of thiol to thiyl radicals. It is shown that, only Cu^{2+} and water accelerate the self-initiated polymerization relative to the reaction with neat monomers. Thus, only a minor part of the initiation is assumed to occur by homolysis of disulfide or hydroperoxide. Acceleration of reactivity observed in presence of copper ions suggests that one of the self-initiation reactions may be catalyzed by a transition metal compound. Similarly, the increased polymerization rates in presence of water demonstrate that specific solvation and polarization effects may be important in thiol-ene self-initiation mechanism. However, the effect of water is not systematic as previously mentioned since the polymerization rates of DAP-thiol systems are much less sensitive to water.

Table II-1 Dependence of self-initiated polymerization rate of **DAA-1** ([DAA] = [1] = 5.19 M) on impurities (relative to polymerization rate of a system without solvent).

Run	Concentration of impurity (M)	Relative R_p / Bulk (h^{-1})
Bulk DAA:1 (Reference)	-	1 ± 0.2
+ Water	0.52	5.5 ± 0.2
+ Dibutyl disulfide	0.05	0.8 ± 0.2
+ Cumyl hydroperoxide	0.10	1.1 ± 0.2
+ Cu^{2+}	1.56×10^{-5}	6.8 ± 0.2

3.1.3 Solution polymerization

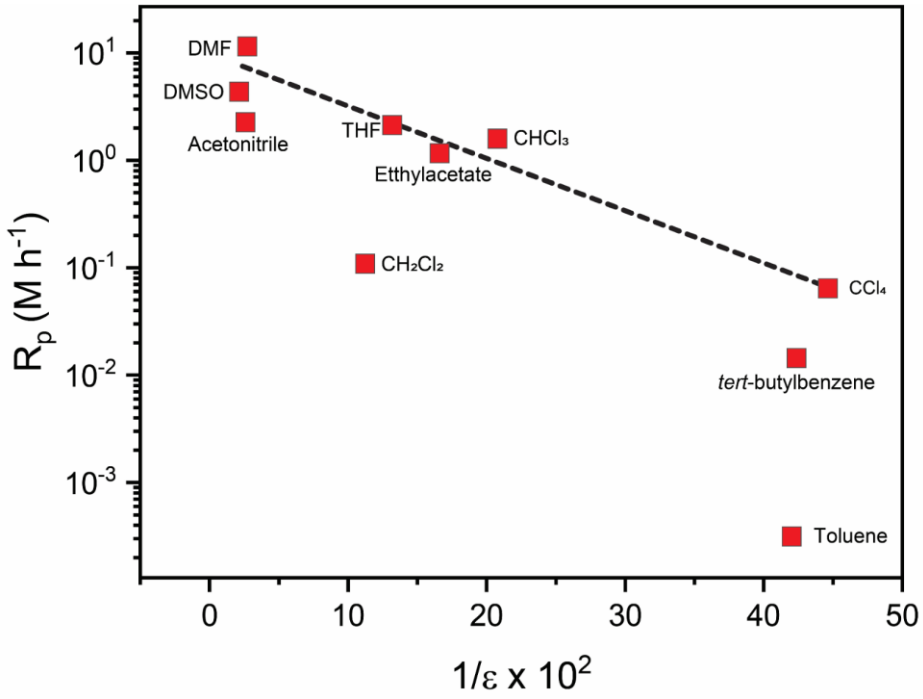

Figure II-4 Relationship between the polymerization rate of **DAA:1** in various solvents and the reciprocal dielectric constant of the solvent at ambient temperature. The polymerizations involve a mixture **DAA**:**1**:solvent = 1:1:2 equiv.

DAA-**1** was then used as model thiol-ene couple to determine the importance of solvent effects on self-initiated polymerization rates. Using a solution of **DAA**:**1** in different solvents (2 equiv), **Figure II-4** shows the polymerization rates as a function of the inverse of the solvent dielectric constants (ε). There is a general trend toward an increase of the overall reaction rate with increasing solvent polarity. The order of reactivity is DMF > DMSO >acetonitrile > THF > $CHCl_3$ > ethyl acetate > CH_2Cl_2 > CCl_4 > *tert*-butylbenzene > toluene. The few exceptions to this generalization (below the straight line) involve CH_2Cl_2 and the aromatic solvents (toluene, *tert*-butylbenzene). The polymerization rate is increased by about 2 orders of magnitude when polymerization is carried out in DMF (ε = 36.71) compared to CCl_4 (ε = 2.24). In *tert*-butylbenzene (ε = 2.36) and toluene (ε = 2.38), the polymerization can be even suppressed.

Even if the nature of the solvent can affect the rate of polymerization by changing the propagation rate constant, it is generally not as strong as observed in our investigation. An additional bias can be attributed to the dependence of polymerization rates on the solubility of molecular oxygen that varies with the solvents mentioned and used. However, this

argument can be minimized by the fact that the solvent accounts for less than 40% of total volume in most experiments. In addition, oxygen solubility is lowest in the solvents (DMF or DMSO) where the reactivity is the highest. Therefore, it seems more reasonable to assume a much larger effect of solvent polarity on the self-initiation reaction rate than oxygen solubility. More polar solvents could drive the self-initiation equilibrium toward the production of more radical species X$^{\bullet}$, and therefore RS$^{\bullet}$ (**Scheme II-1**, (a) and (b)), resulting in faster polymerization rates. This points out the importance of solute-solvent interactions. The solvation of thiol by solvents and alkene molecules is discussed further in section II.

3.2 Thiol solvation

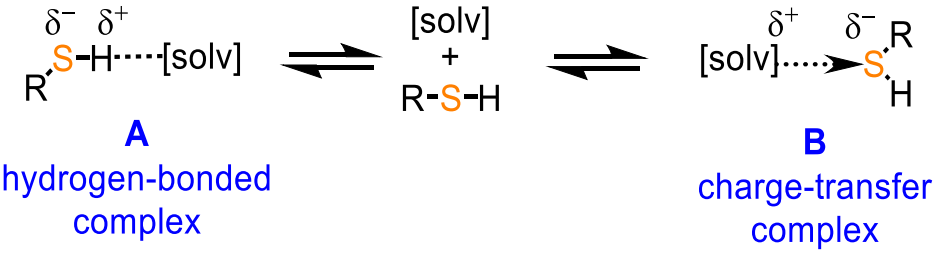

Scheme II-3 Equilibrium occurs between "free" and associated thiol and solvent molecules. Two preferential association modes involving thiols are expected to form, a hydrogen-bonded complex (**A**, left) and a charge-transfer complex (**B**, right).

Thiols can be involved in two major types of intermolecular interactions (**Scheme II-3**).[173] First, weak H bonds can form between thiols (proton donor) and polar solvents (proton acceptor): RSH•••solv (**Scheme II-3**, **A**). Second, the site of high electron density of a polar solvent (e.g., free electron pairs) can interact with the sulfur atom of the thiol (electron acceptor) resulting in a charge-transfer complex: solv→S(H)R (**Scheme II-3**, **B**). It is expected that the equilibrium between free and associated thiol and solvent (olefin) molecules may affect the self-initiation rate on the basis of the experimentally observed effect of the solvent on polymerization kinetics.

3.2.1 Thiol-solvent interactions

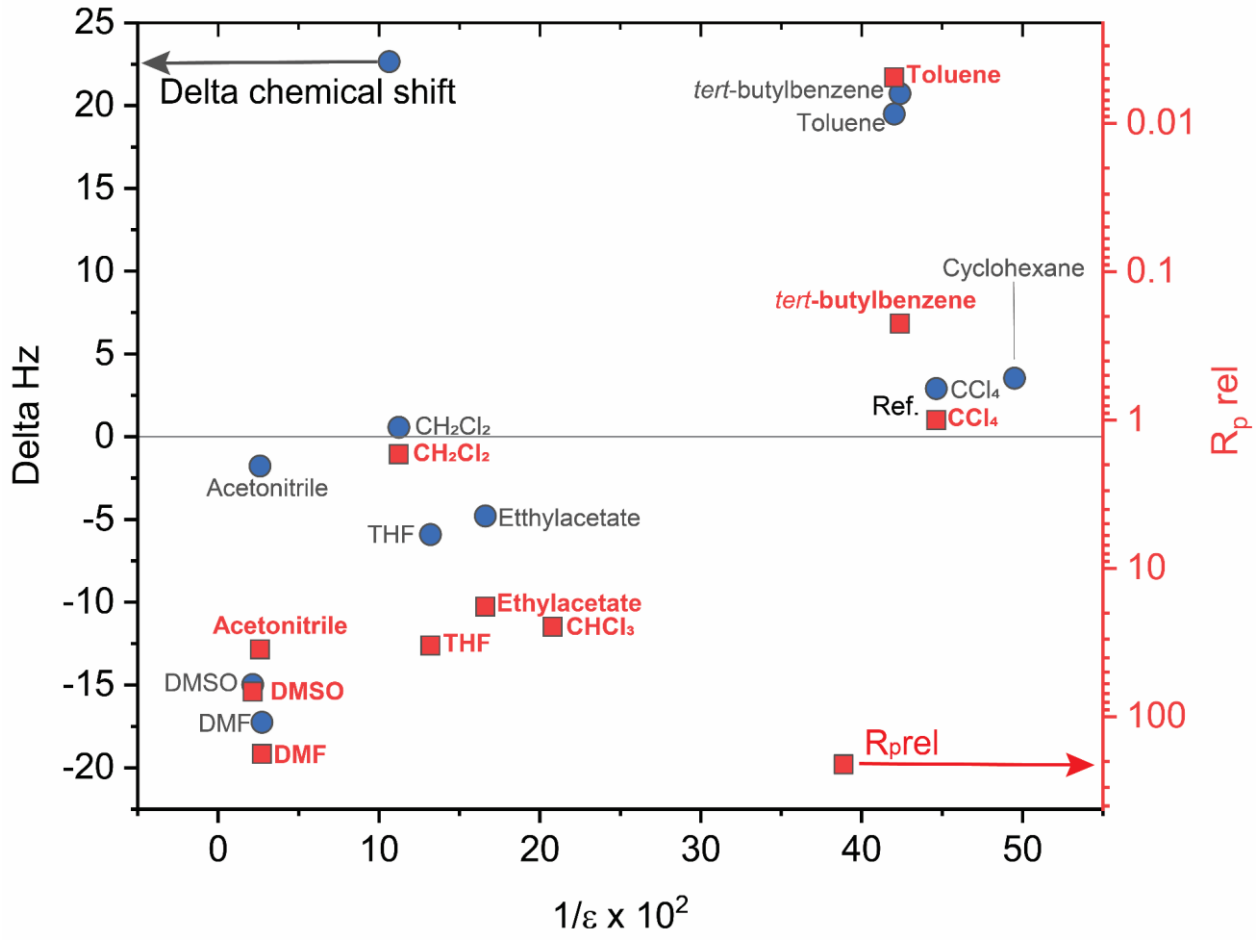

Figure II-5 Change in the chemical shift (circle) of the SH group of thiol acetate **1** in a variety of solvents of different dielectric constant (ε) (**1**:solvent = 1:24). The ^{1}H NMR experiments were carried out in $CDCl_3$ in which specific solute-solvent interactions are considered to be minimal. In $CDCl_3$, the sulfhydryl proton appears as a triplet peak at 2.03 ppm. Solvent effect on the relative polymerization rate (R_p) of **DAA:1** in the same series of solvents (square) taking as reference CCl_4. Polymerizations involve a mixture **DAA**:**1**:solvent = 1:1:2 equiv.

^{1}H NMR is the most direct method to study the nature of thiol solvation in presence of a variety of solvents.[174] **Figure II-5** displays the change of chemical shift (ΔHz) of the sulfhydryl proton (SH) for thiol acetate **1** in $CDCl_3$ after adding an excess of solvent (24 equiv). The chemical shifts are plotted against the inverse of the dielectric constant (1/ε) to elucidate the effect of solvent polarity. As reported in the literature, a downfield shift (negative ΔHz) indicates that H-bonding becomes the dominant mode of interactions, while an upfield shift (positive ΔHz) evidences a major contribution from charge-transfer interactions (**Figure II-6**).[174] For polar solvents of high dielectric constants (DMF, DMSO), the pronounced downfield chemical shift indicates strong H-bonding. With poorly polar solvents (THF, ethyl

acetate), the downfield chemical shift is more limited reflecting weaker thiol-solvent interactions. For inert solvents (cyclohexane or CCl_4) and also CH_2Cl_2, the chemical shift is hardly affected. Thus, the magnitude of the chemical shift varies significantly depending on the solvent polarity and the strength of the hydrogen-bonded complex (solvation). **Figure II-5** reproduces on the same plot the kinetic data of solution polymerization (**Figure II-4**) to show the relationship between the change of ΔHz and R_p of **DAA**:**1** induced by the presence of various solvents. With the group of non-aromatic solvents, the correlation of chemical shift (ΔHz) with $1/\varepsilon$ is analogous to the correlation with R_p. Reactivity is increased in presence of highly hydrogen bonding solvents. The second group of aromatic solvents (*tert*-butylbenzene, toluene) is an exception to the previously observed trend since a marked upfield chemical shift is observed in this case. It is likely that the predominant solvation proceeds by charge-transfer complex between the thiol and the aromatic π system of the solvent. Despite absolute values of ΔHz comparable to those of highly polar solvents, the polymerization in presence of aromatic solvents shows negligible reactivity.

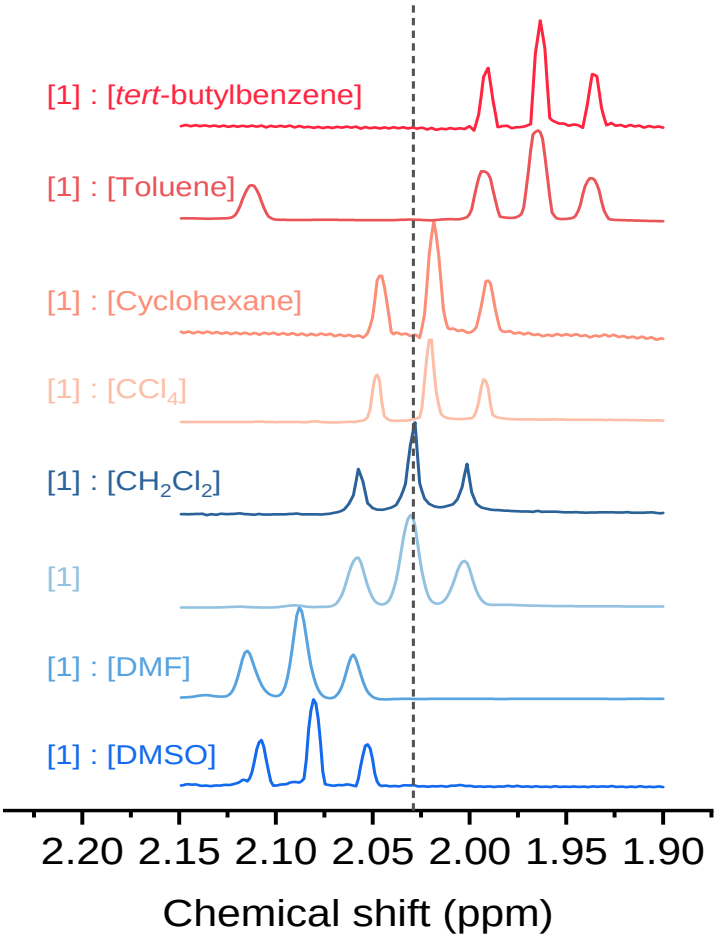

Figure II-6 The chemical shift of the sulfhydryl proton in thiol **1** in $CDCl_3$ was observed after adding an excess of solvent (24 equiv). A downfield shift (DMF, DMSO) corresponds to a negative chemical shift ΔHz, while a upfield shift (CCl_4, toluene, tert-butylbenzene) corresponds to a positive chemical shift ΔHz.

3.2.2 Thiol-alkene interactions

The ^{1}H NMR spectra of the thiols **1**-**5** were also examined in the presence of an excess of alkene (**DAP**, **DAA** or **DVE**) under the same conditions as chosen for the solvents (ene:thiol molar ratio = 24). As can be seen in **Figure II-7**, a downfield shift of SH protons is mostly encountered for **DAA** and **DVE** while an upfield shift is generally found with the aromatic derivative **DAP**. Thus, the general behavior of thiol-alkene solvation is qualitatively analogous to that of thiol-solvent systems with a distinct behavior depending on the presence of an aromatic group. With the non-aromatic alkenes (**DAA**, **DVE**), H-bonding is the major mode of interactions with thiols, presumably through the electron-rich C=C bond behaving as H acceptor. In this case, one would expect to find a more pronounced downfield chemical shift when the thiol is more acid, that is, when the S-H bond is polarized by electron withdrawing

groups. In support of this assumption, the order of downfield deviation of **1**, **2** and **3** in presence of **DAA** or **DVE** is consistent with the order of acidity **1** > **2** > **3**, and points to stronger H-bonded complexes. However, the trend is not universal and can be circumvented by alterations, in particular for thiols **4** and **5**. Deviations from this order indicate in this case specific interactions. The benzenoid alkene (**DAP**) behaves similarly to the aromatic solvents with the predominance of donor-acceptor complex interactions. With poorly polarized thiols **4** and **5** for example, the marked upfield deviation reflects the predominance of electron-donor complex as expected. But the change of chemical shift is close to zero or even slightly negative with more polarized thiols (**1**-**3**), suggesting that the effect of charge-transfer complexation on ΔHz is compensated by H-bonded complexation having an opposite effect on the chemical shift. This trend can be rationalized in terms of equilibrium between two types of complexes (**Scheme II-3**).[175]

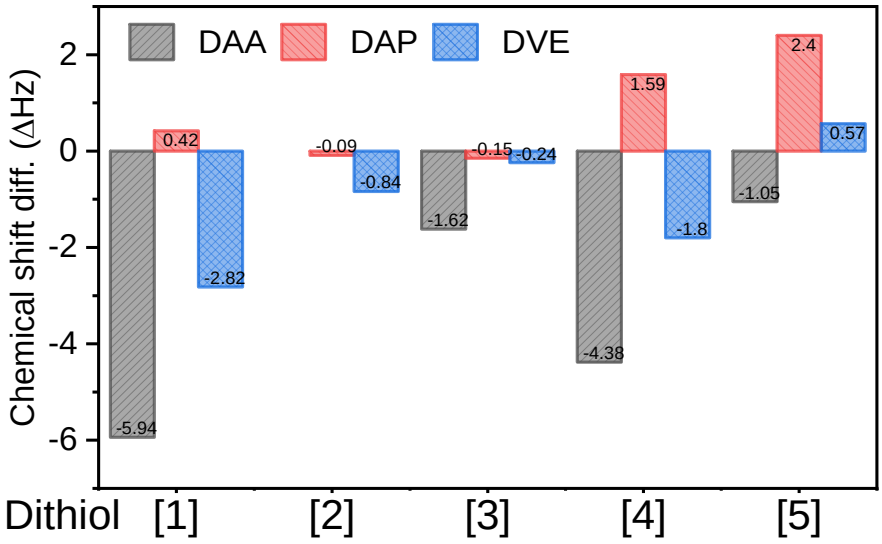

Figure II-7 Change in the chemical shift of the SH group of thiols **1**-**5** after addition of an excess of alkene **DAA**, **DAP** or **DVE** (thiol:alkene = 1:24). The ^{1}H NMR experiments were carried out in $CDCl_3$ with a thiol concentration of 0.06 M. For **DAA**:**2** pair, the chemical shift was not accessible because of overlapping signals.

The relationship between bulk self-initiated polymerization rate (R_p) and thiol-alkene solvation (ΔHz) is shown in **Figure II-8** for two representative cases, **DVE** (**A**) and **DAP** (**B**), depending on whether the alkene is aromatic or not. With the exception of thiol **4**, there is a trend toward a higher reactivity of thiol-**DVE** bulk systems when the thiol favors strong H-bonding (negative ΔHz). Therefore, **DVE** behaves in a manner generally similar to non-aromatic solvents. On the other hand, **DAP** stands in marked contrast with the other alkenes.

The charge-transfer complex observed in this case is globally detrimental to the reactivity. With poorly polarized thiols (**4**, **5**), this latter charge-transfer complexation is the dominant interaction, and the polymerization is strongly inhibited. With polarized thiols (**1**, **2**), the polymerization is only slowed down presumably because of an equilibrium with the H-bonded complex. Similar conclusions about the solvation of thiol can be obtained by FTIR spectroscopy by the examination of the effects of increasing amount of solvent (or alkene) on its FTIR spectrum.

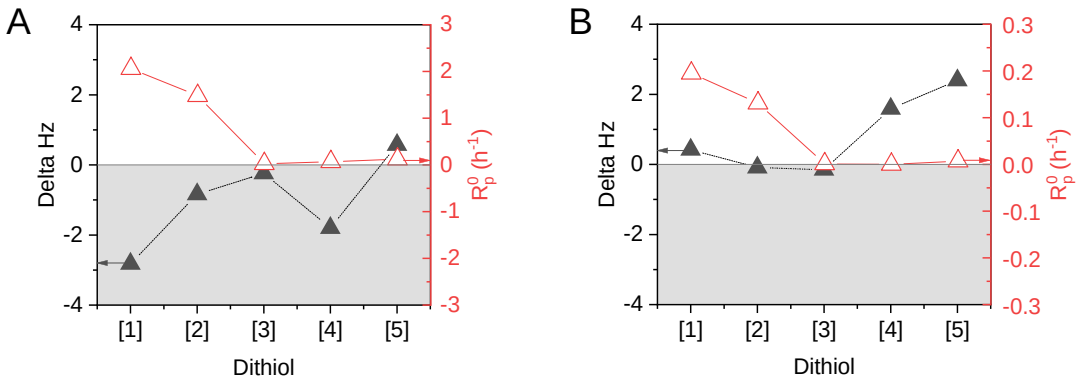

Figure II-8 Self-initiated polymerization rate (R_p^0, open triangle) of stoichiometric bulk mixtures of **DVE**-thiol (**A**) and **DAP**-thiol (**B**) depending on the thiol used (**1**-**5**). Change in the chemical shift (ΔHz, solid triangle) of the SH group in $CDCl_3$ in the thiol-ene mixture ([thiol] = 63 mM).

3.3 Nature of the initiating radicals

Most of the evidence to support and elucidate the self-initiation mechanism in thiol-ene polymerization has been so far indirect, consisting of kinetic and spectroscopic data. The major problem in ascertaining whether self-initiation occurs is to identify the primary or/and initiating radicals (**Scheme II-1**, (a) and (b)). Radical-trapping using *N-tert*-butyl-α-phenylnitrone (PBN) is especially useful for this purpose since it allows the detection by EPR of various short-lived radicals as their nitroxyl radical adducts.[144,176] To study the type and concentration of primary/initiating radicals, a mixture of thiol and PBN acting as radical scavenger was prepared, and the EPR spectra of the possible radical adducts were then analyzed.

3.3.1 Effect of thiol substituent

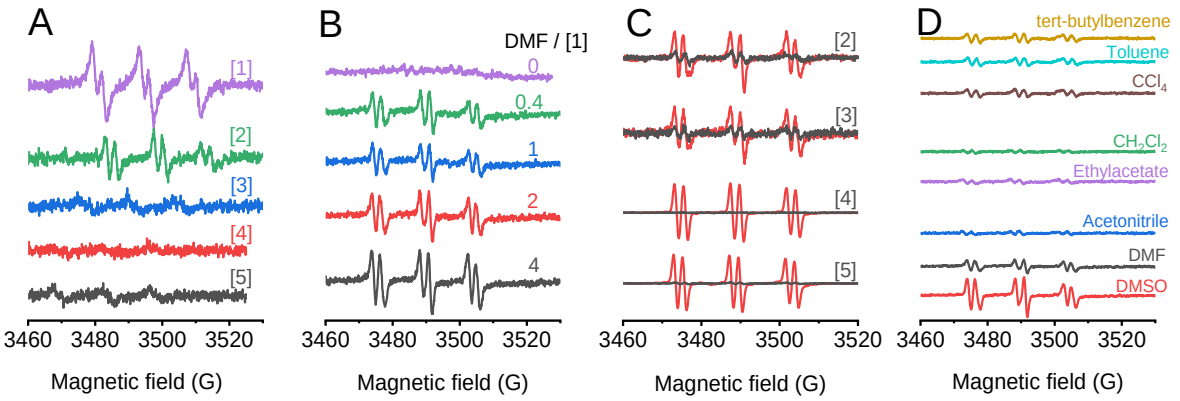

Figure II-9 . EPR spectra of thiols 1-5 in tert-butylbenzene. B. EPR spectra of thiol 1 with increasing amounts of DMF (0.4 – 4 equiv). C. EPR spectra of thiols 2-5 before and after addition of DMF (2 equiv). D. Effect of solvents on the EPR spectrum of 1 (solvent : thiol = 2:1 equiv).

The EPR spectra of mixtures of 30 mM PBN, 100 mM thiol (**1**-**5**) in *tert*-butylbenzene under air are displayed in **Figure II-9A**. After 15 scans, only thiols **1** and **2** bearing an ester substituent show an intense six-line spectrum with a well resolved hyperfine structure indicative of a single type of radical that we assume to be a thiyl radical. However, to support our assignment there are no adequate literature data of PBN/RS$^{\bullet}$ spin adducts[177,178] (except for the glutathiyl radical[179]). To ascertain the presence of RS$^{\bullet}$ for thiols **1, 2** and **3**, the expected thiyl radicals can be generated photochemically upon irradiating (385 nm) the same thiol/PBN mixture in the presence of isopropyl thioxanthone (ITX, 10 mM). Upon electronic excitation, ITX is known to induce an intermolecular abstraction of a hydrogen atom from RSH. For thiols **1**-**3**, we find that the EPR spectra of the irradiated samples are analogous to those of neat thiols. Therefore, the control experiments validate PBN as a spin-trapping probe and support the chemical nature of the trapped radicals (**Figure II-10**). The most probable mechanism is that self-initiation occurs in a single step (without intermediate primary radicals) and involves the formation of thiyl radicals from the thiol, then capable of initiating a thiol-ene polymerization. Contrary to thiols **1** and **2** with an ester substituent, the thiyl radical concentration is very small for **3**, and below the limits of detection for **4**, **5**. Clearly, the yield of thiyl radicals is dependent on the electronegativity of the thiol substituents. This trend is also in line with the thiol-ene polymerization rates increasing in the order **1** > **2** > **3**-**4**-**5** (**Figure II-3**).

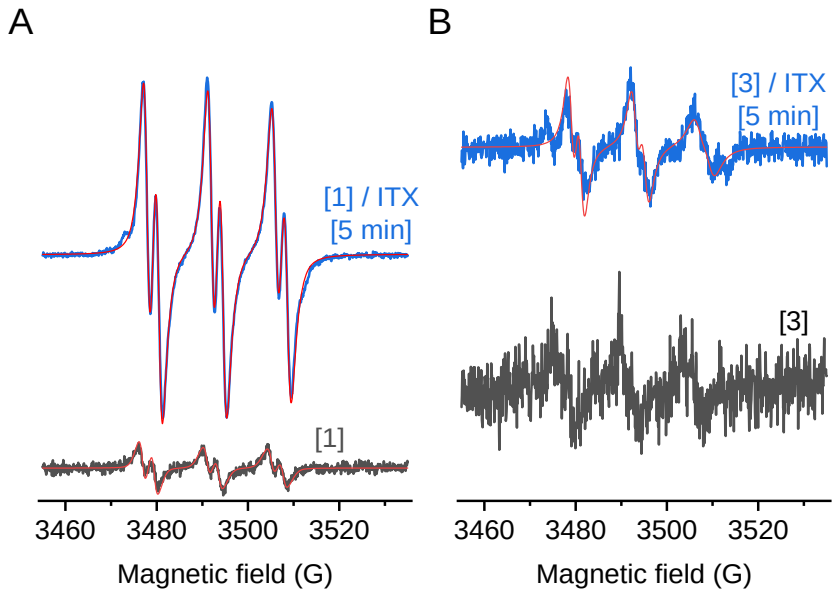

Figure II-10 The EPR spectra of the mixture 30 mM PBN, 100 mM thiol (**1** or **3**) in tert-butylbenzene with or without ITX (10 mM). The samples containing ITX were irradiated at 385 nm (2.7 mW cm^{-2}) for 5 min to generate the thiyl radical via H-abstraction. The experiment involving ITX shows a similar, but increased EPR signal compared to the system without sensitizer (ITX).

3.3.2 Effect of solvent

Figure II-9B shows the effect applied by DMF, a strong hydrogen-bonding solvent, on the EPR spectrum of neat **1**. An increasing DMF/thiol ratio (from 0.4 to 4) causes a significant increase of the EPR spectrum intensity indicating the production of more thiyl radicals. As shown in **Figure II-9C**, a similar effect of DMF (2 equiv) has been observed for thiol **2**, but also for the less polarized thiols **3**-**5**. DMF is expected to give rise to hydrogen bonding interactions with thiols even in the absence of strong electron-withdrawing substituent. Additional support for the role of thiol-solvent hydrogen bonded complex in the formation of thiyl radicals comes from the effect of solvent polarity on the concentration of thiyl radicals. **Figure II-9D** shows the EPR spectra of a system consisting of a mixture of thiol **1** (1 equiv) and various solvents (2 equiv). As expected, the abstraction of the sulfhydryl hydrogen is favored in highly polar solvents (DMF, DMSO) in which thiol-solvent H-bonded complex are present. In contrast, weakly polar (ethyl acetate, CH_2Cl_2) or apolar (aromatic) solvents (CCl_4, toluene, *tert*-butylbenzene) limit significantly or suppress the production of thiyl radicals. Clearly, there is a relationship between the formation of H-bonded complex, a higher yield of thiyl radicals, and greater polymerization rates in solution (**Figure II-4**).

3.4 Discussion

3.4.1 Role of thiol air oxidation in the self-initiation of thiol-ene polymerization

In our search for a consistent mechanism accounting for the self-initiation of thiol-ene polymerization, we have highlighted that atmospheric oxygen, thiol substituent and solvation have a significant effect on the rates of self-initiation and polymerization. These coherent and convergent elements provide a basis for stating that (initiating) thiyl radicals may be formed by air oxidation of thiols through dissolved molecular oxygen in the thiol-ene mixture.

$$RSH + O_2 \rightarrow RS^{\bullet} + HOO^{\bullet}$$

The reaction may involve a proton-coupled electron transfer from thiol to molecular oxygen (**Scheme II-4**), probably occurring inside the solvent cage. The process is initiated by an electron transfer from the thiol to molecular oxygen (O_2) yielding superoxide anion ($O_2^{\bullet -}$) and the thiyl radical cation ($RSH^{\bullet +}$). The latter species efficiently deprotonates to the corresponding thiyl radical ($RS^{\bullet}$) capable to initiate a polymerization. Hence, the self-initiation mechanism could proceed without prior formation of thiolate or the need for a metal catalyst. In this respect, it bears resemblance to the initiation of a thiol-olefin cooxidation (TOCO) reaction,[175] thiol oxidation into disulfides[173] or thiol-disulfide exchange.[180] Recently, this mechanism was also postulated to explain the atmospheric oxygen-promoted addition of thiol to alkene.[181] In agreement with our study, H-bonding influenced the extent and efficiency of coupling. More generally, our data support that the driving force for thiol oxidation is the polarization of the S-H bond. A polarized S-H bond causes the activation energy of oxidation to decrease, thereby making the transfer of electron to an oxygen molecule more facile. As depicted in **Scheme II-4**, an electron-withdrawing substituent (**i**) and hydrogen-bonded complexes (**ii**) seem to function in a similar way, activating the thiol by means of its polarization.

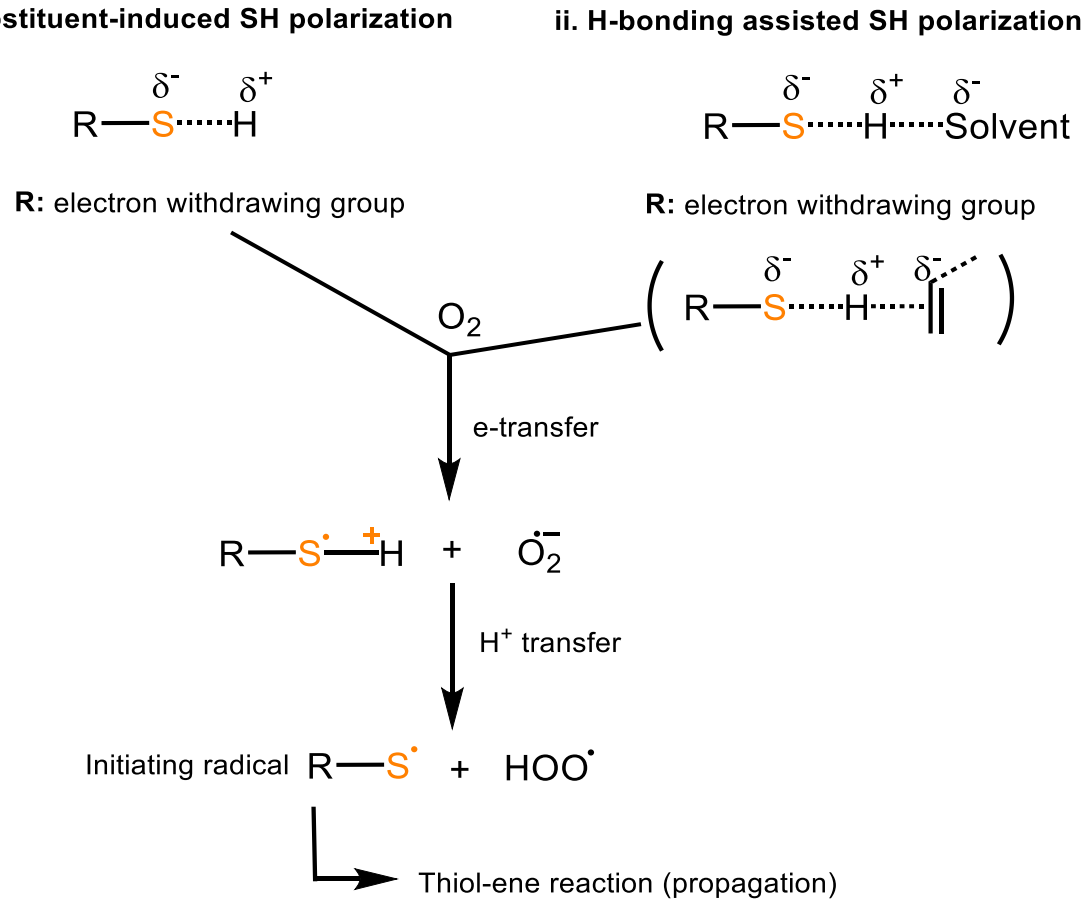

Scheme II-4 Polarization of S-H bond induced by thiol substituent or H-bonding with solvent or alkene.

i. *A thiol substituent* effect on the self-initiation rates is evident when the thiol-ene polymerization is carried out in bulk media. Irrespective of the alkene used, the self-initiated polymerization proceeds systematically at an accelerated rate when the thiol bears an electron withdrawing substituent (**1**, **2**). In the case of allyl esters, the difference of polymerization rates is attributed to a more efficient initiation step promoted by thiol polarization and, to a much lesser extent, to higher propagation rates. The self-initiation rate seems to be a function of the relative substituent-induced polarization of thiol, i.e., the relative acidity of the thiol. Spin-trapping experiments further support this rationale. Thiyl radicals are readily formed provided that the thiol substituents have sufficient electron-withdrawing character (**1** or **2**). The influence of H-bonding on S-H polarization is minimized in this case by the use of low concentration of thiols (0.1 M) and an apolar solvent (*tert*-butylbenzene).

ii. Solvent-thiol and alkene-thiol H-bonded complexes have been evidenced by ^{1}H NMR. The formation of solvent-thiol H-bonded complex is generally favored by the electron-donating property of the solvent and an electron withdrawing character of the thiol substituent, although deviations from this behavior are found under certain conditions, in particular with aromatic solvents as discussed in the next section. As demonstrated for the **DAA**:**1** pair, adding a H-bonding solvent (water, DMF, DMSO, etc.) or increasing its amount results in a higher concentration of thiyl radicals and faster self-initiated polymerizations. Alkenes behave somewhat similarly to the solvents, although relatively little data are available because of the limited number of alkenes tested. With allyl esters (**DAA**, **DAP**), the polymerization rate is not negligible when acid thiols (**1** or **2**) promote H-bonding. When the electron-withdrawing ability of the thiol substituent is insufficient, only weak dispersion forces or dipole-dipole forces arise. S-H polarization is not strong enough in this case to drive the self-initiation towards the production of thiyl radicals, explaining the much lower reactivity observed with thiols **3**-**5**. The situation is very different for vinyl ether (**DVE**) since the higher electron-donating character of the olefin drives both high initiation and propagation rates, allowing self-initiated polymerization to proceed even when the thiol has a poor acidity.

In summary, estimating the extent of thiol polarization is a reasonable approach to evaluate the effect of monomers' structure or solvent on the rate of self-initiation. It may be used to give a general idea of the behavior to be expected from a thiol-ene monomer pair that has not been studied from the point of view of its storage stability. In spite of this success, there are two deficiencies of the S-H polarization scheme that need clarifications: the effects of aromatic solvents (alkenes) and of an inert atmosphere on the self-initiated polymerization rate.

3.4.2 Effect of aromatic compounds

In the presence of polar solvents and alkenes, thiol solvation is generally dominated by H-bonded complexes. An exception to this behavior is found with aromatic solvents (alkenes). In this case, electron acceptor-donor interactions also arise, and two types of complexes may competitively form with consequences on reactivity. Two different situations are encountered depending on the position of the equilibrium. In the first case, there is a dominant contribution of the charge-transfer complex which is reflected by a strong upfield

deviation of the S-H protons in ^{1}H NMR. A prime example is the self-initiated polymerization of **DAA**-**1** in presence of *tert*-butylbenzene or toluene. In this case, the polymerization is strongly inhibited. Consistent with these results, Szmant and coworkers found a decreased rate of oxidation of various thiols into disulfide when an aromatic solvent is added.[173] In bulk conditions, the charge-transfer interactions are prominent for **DAP** with thiols **4** and **5**, and the polymerization rates are similarly negligible. In the second case, the charge-transfer complex is in equilibrium with the H-bonded complex. The mix of contributions is not easily determined experimentally, but the opposite effects of the two complexes on the chemical shift result in values close to zero. This special situation is encountered when **DAP** is polymerized with thiols **1**-**2**. The electron withdrawing character of the substituents of the two thiols drives the equilibrium toward more H-bonded complexes allowing thiol oxidation to proceed, and as a consequence, self-initiated polymerization takes place.

3.4.3 Effect of inert atmosphere

Only the polymerization of **DAP**-thiols is halted in nitrogen atmosphere. In contrast, **DAA** and **DVE** can undergo self-initiated polymerization with most thiols in inert atmosphere, but the polymerization rates are appreciably slower than the corresponding polymerizations under air. The finding that atmospheric oxygen is not necessarily required for the self-initiated polymerization to proceed is not without ambiguity about the role of thiol oxidation by air as sole mechanism responsible for self-initiation. Firstly, our experimental data can be reconciled with the thiol oxidation mechanism by considering the difficulty to remove completely atmospheric oxygen. In addition, thiyl radicals may already be present in the neat thiol before mixing with the alkene. EPR spectra of thiols supports the presence of thiyl radicals in thiols **1**-**3** without the assistance of H-bonding solvents and even when the samples are prepared under nitrogen. Their presence may be ascribed to thiol oxidation promoted by the substituent-induced polarization of the S-H bond as discussed above. This assumption is backed by the observation that polymerization rates are enhanced with the aging of the thiol (**Figure II-11**). This result can be explained with a slow oxidation of thiols by air during storage increasing the concentration of thiyl radicals.

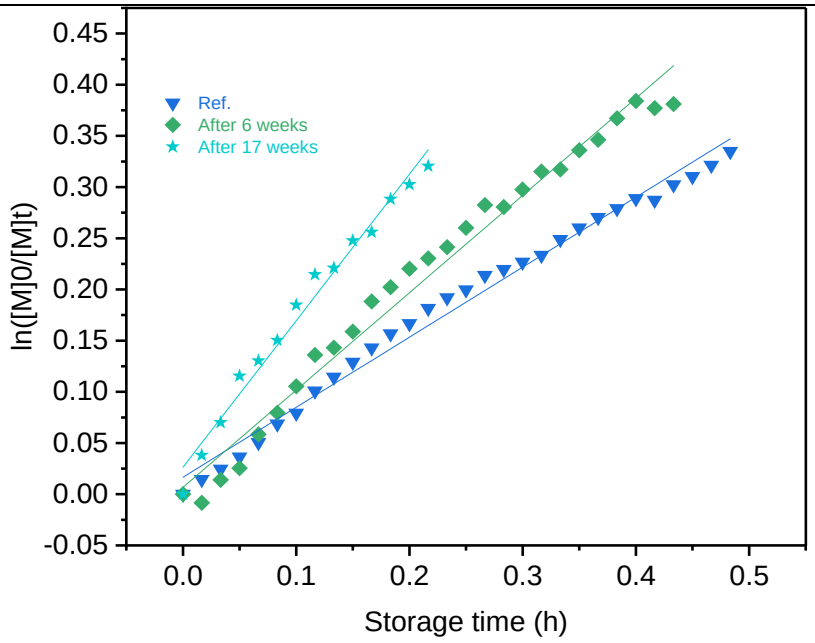

Figure II-11 Effect of thiol aging time on monomer (alkene) conversion for stoichiometric polymerization of bulk **DAA**-**1**. The experiment was performed under air and at ambient temperature **DAA** with dithiol **1**. Ref. corresponds to a freshly opened thiol bottle.

However, the most plausible explanation would be to consider a contribution of a second concurrent self-initiation reaction proceeding without the assistance of molecular oxygen. *Hydrogen atom abstraction from the thiol* (homolysis) is another route yielding thiyl radicals. In presence of alkene, the homolysis of S-H σ-bond is coupled to the addition of the resulting H$^{\bullet}$ to the π-bond of the alkene (**Scheme II-5**).[24] The driving force is thus the formation of C-H bond at the olefin that reduces the endothermicity of S-H homolysis.[182] For this reason, it is referred to as "alkene-assisted homolysis",[183,184] or in a more general way as a MAH. The occurrence of a MAH of S-H as initiation mechanism was originally reported by the groups of Pryor[170,171,185] and Nuyken,[25,186] then more recently by Metzger et al.[184,187]

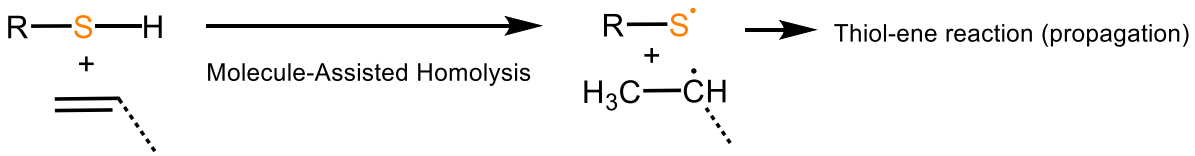

Scheme II-5 General mechanism of MAH of thiol by alkene

This bimolecular reaction has no transition state (kinetic barrier) because the combination of two radicals proceeds without energy of activation. Therefore, the activation

energy equals the reaction enthalpy $\Delta_r H$ estimated by DFT calculations. It is found that the reaction enthalpy of a H transfer from thiol **1** to **DAA** amounts to $\Delta_r H_{298} \approx 160$ kJ/mol and does not vary significantly with the nature of the alkene. This value is significantly higher than found in many MAH reactions.[182] In comparison, the activation energy for thermal initiator decomposition is in the range 120–150 kJ/mol.[161] The high endothermicity of MAH thiol hemolysis predicts that polymerization proceeds only at very low rates at ambient temperature which may appear at first glance in contradiction with the experimental results. Elucidation of that point would require a complete kinetic study, but there are arguments in favor of the MAH mechanism. The rate of producing primary radicals (R_i) by MAH is certainly very weak. However, equation 1 describes that for the representative case of allyl ester-thiol, the polymerization rate depends only on the square root of the initiator concentration. In contrast, R_p shows a first-order dependence on [Thiol] and k_H, showing their higher importance in a chain radical process. In our case, bulk conditions ([thiol] = 5.2 M) and the use of the most reactive alkenes[188] (allyl esters display the highest k_H: $10^6 – 10^7$ M^{-1} s^{-1}) may increase R_p to a level allowing the polymerization to proceed. In addition, the formation of olefin-thiol complex that is reminiscent of the MAH may modify the activation energy for initiation. Further work is required to substantiate the role of MAH in the thiol-ene self-initiated polymerization.

4 CONCLUSION

A number of thiol-ene monomer pairs have been shown to undergo self-initiated polymerization under air or nitrogen atmosphere. The self-initiated thiol-ene polymerization is a complex reaction system that may consist of competitive parallel reactions. This study focuses on the role of one-electron transfer reactions from thiol to molecular oxygen in the self-initiation process. There is some evidence that thiol oxidation by air plays a major role in the self-initiation of a spontaneous thiol-ene polymerization, in particular when the reaction is carried out under air. The self-initiated thiol-ene polymerization is depicted as a radical chain reaction involving the initial formation of thiyl radicals by the reaction of atmospheric oxygen with preferentially polarized thiols. H-bonding with electron-donating alkenes or solvents molecules (proton acceptor) or/and electron-withdrawing substituents of the thiol activates the S-H bond, making thiol oxidation easier, and polymerization faster due to a higher production of thiyl radicals. Additional support for an increased formation of thiyl

radicals originates from radical-trapping experiments. In reaction systems under exclusion of molecular oxygen, only a minor part of the initiation may occur by this oxidation manifold. It is likely that an additional contribution from molecule-assisted homolysis (MAH) of thiols occurs. Despite these new results, some mechanistic aspects of thiol-ene self-initiated polymerization require further investigation, in particular the contribution of MAH relative to thiol oxidation by air.

Nevertheless, our findings give useful practical information for preventing (or at least limiting) self-initiated thermal thiol-ene polymerization. For this purpose, three levers affecting the rate of thiol oxidation by air are available: S-H bond polarization, reaction atmosphere and thiol purity.

i. Any factor contributing to decrease thiol polarization may reduce self-initiation rate. Thiols substituents with electron-donating ability or negligible inductive properties are most appropriate. Alkenes or solvents (if the system is in solution) with less electron donating ability can also reduce the extent of hydrogen bonding-induced polarization. Interestingly, aromatic monomers or solvents seems to decrease the intrinsic polarity of the thiols due to charge-transfer interactions.

ii. The self-initiation rates are generally slower when the thiol-ene mixture is stored under a nitrogen atmosphere. However, except for a few cases (including the aromatic alkene DAP), the absence of air does not ensure a complete latency.

iii. The use of sufficiently pure reactants, in particular thiols, is apparently an important feature. The presence of disulfides and adventitious peroxides may not be as much of a problem. Self-initiation more likely involves catalytic metal traces, or water as hydrogen-bonding solvent, but not systematically.

CHAPTER III. THIOL-ENE MINIEMULSION PHOTOPOLYMERIZATION

Parts of this chapter were published in the article Le, C. M. Q.; Vidal, L.; Schmutz, M.; Chemtob, A. Droplet nucleation in miniemulsion thiol–ene step photopolymerization Polym. Chem., **2021**,*12*, 2084-2094 https://doi.org/10.1039/D1PY00139F

1 INTRODUCTION

Radical-mediated thiol–ene chemistry refers to the addition of thiyl radicals to C=C double bonds.[144] Thiol–ene reactions are most commonly photoinitiated, and generally employed for the synthesis of cross-linked poly(thioether) materials via photopolymerization.[153] The acrylic family of polymers is presently the overwhelming choice in the field of industrial photopolymerization.[12,189] But, thiol-ene systems have gained acceptance in overcoming the problems associated with monomer toxicity or volume shrinkage.[51] The result has been the development of niche products,[35] including for example, non-cytotoxic hydrogels[190] or low shrinkage dental materials.[191]

Acrylate and methacrylate monomers are also key players in emulsion polymerization, another industrially useful polymerization process.[67] The resulting acrylic waterborne polymer dispersions are formed by a radical chain polymerization.[192] The distinguishing characteristic of a thiol-ene polymerization is that polymer chains grow through a stepwise reaction between ene and thiol functional groups of reactants.[193] Also, by using a stoichiometric amount of bifunctional ene and thiol reactants, there is evidence that poly(thioether) latexes of practical utility can be formed, i.e. with a molecular weight of about one to several tens of thousands g mol^{-1}.[151] However, unlike thiol-ene photopolymers, the share hold by thiol-ene latexes has remained limited, and no commercial product has emerged yet.[4,28] The main examples result from a miniemulsion photopolymerization,[17,131,194–201] and to a less extent, dispersion[202,203] and emulsion[151,204] (photo)polymerizations. Suspension photopolymerization has been also described,[205,206,54,207,208] but this process does not result in polymer colloids (average particle diameter < 1 µm), but in micrometer solid beads (0.1 - 10 mm). Although copolymers of acrylic and methacrylic acids and esters account for a major fraction of all industrial latexes, they have significant drawbacks. Among them are the inhibition of the polymerization by oxygen and the chain transfer reactions to polymer that hinders the control of chain structure.[209] Thiol-ene polymerization exhibits numerous characteristics that can address these drawbacks, some directly related to its distinct step polymerization mechanism. For example, the thiol-ene polymerization is relatively insensitive to oxygen. Further, branching and cross-linking can be accurately tuned by varying the monomer functionality since there is virtually no chain transfer to polymer.[210] Some authors have already taken advantage of some

opportunities,[211] but further research efforts are required to tap the full potential of thiol-ene step photopolymerization in dispersed media.

The most used process in this field is miniemulsion thiol-ene polymerization.[17,131,194–201] Involving smaller and therefore less scattering monomer droplets (50 -500 nm) than an emulsion polymerization, it has the added advantage of imparting greater radiation penetration within the reactor. In addition, the desired particle nucleation mode occurs via radical capture into the monomer droplets, subsequently converted into polymer particles.[212] Consequently, when a step polymerization is confined to droplets containing a stoichiometric amount of ene and thiol functional groups, the equilibrium can be driven toward high molecular weights.[131] However, six years after the first example of thiol-ene miniemulsion photopolymerization,[17] the question of droplet nucleation efficiency is still largely unanswered. In contrast, there are extensive studies regarding chain radical polymerization in miniemulsion.[213–215] Regardless of the type of polymerization, the goal of a miniemulsion polymerization is to nucleate most of the initial monomer droplets and minimize homogeneous nucleation*;* i.e. the fact that oligomeric radicals instead of entering into the droplets can precipitate in the aqueous phase to form particles.[209] The relative extents of droplet and homogeneous nucleation are expected to vary in a thiol-ene step polymerization compared to a conventional radical chain polymerization due to distinct relationships between molecular weight and the percent conversion of monomer.[216] For fundamental and practical reasons, it is therefore of interest to discuss the set of reaction conditions for the robust droplet nucleation of thiol-ene monomer miniemulsions.

This chapter begins with the preparation and the batch photopolymerization of an aqueous model miniemulsion based on diallyl phthalate (**DAP**) and 2,2-(ethylenedioxy)diethanedithiol (**3**) (see chemicals structures in **Figure III-1**) with sodium dodecyl sulfate (SDS) as the surfactant and hexadecane (HD) as the costabilizer. The weight fraction of monomers was kept constant at 20 wt%, and a water-soluble radical photoinitiator (TPO-Li) of the monoacylphosphine oxide family was chosen. Using an appropriate concentration of radical scavenger (quinone), it was possible to achieve a chemically stable **DAP-3** miniemulsion. Under these conditions, droplet stability, polymerization kinetics, molecular weight progress and particle size distribution could be determined. However, it was difficult to adequately discuss the mechanism of particle nucleation with this system because

of the limited droplet stability. Upon decreasing the weight fraction of monomer to 1 wt%, monomer droplets possessing photolatency, size monodispersity and stability were eventually obtained. Emphasis was placed on understanding the reaction parameters which are important in favoring droplet nucleation, i.e., *droplet size*, *initiator solubility* and *monomer solubility*.[209] Initiators and thiol-ene monomers of different chemical structures have been used for this purpose (see **Figure III-1** for details). Comparison of particle size (number) and droplet size (number) was exploited to evaluate qualitatively the extent of droplet and homogeneous nucleation.[101] However, a major problem is generally the lack of precision and accuracy in the determination of droplet and particle size distribution, possibly leading to erroneous conclusions about the nucleation mode.[98] To minimize interpretations errors, the size distribution determined by dynamic light scattering (DLS) was compared with the one given by transmission electron microscopy (TEM).

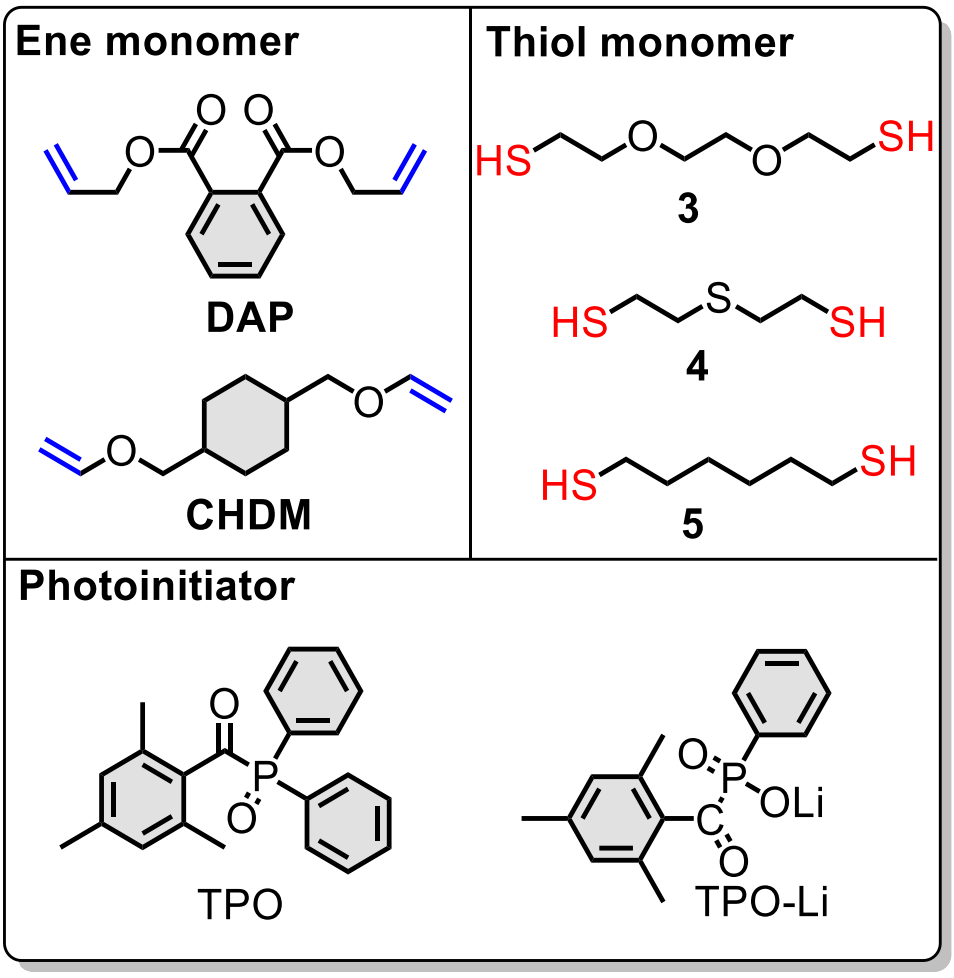

Figure III-1. Chemical structure of radical photoinitiators, dithiol and diene monomers.

2 EXPERIMENTAL SECTION

2.1 Materials

Diallyl phthalate (**DAP**, 99%, water solubility: 0.15 mg/mL), 2,2-(ethylenedioxy)diethanedithiol (**3**, 99.6%, water solubility: 11.4 mg/mL), 1,6-hexanedithiol (**5**, > 99.1%, water solubility: 0.15-0.27 mg/mL), 2,5-di-tert-butylhydroquinone (**DBHQ**, > 98%), pyrogallol (**PY**, 99%), sodium dodecyl sulfate (**SDS**, 98%), hexadecane (**HD**, > 98%) lithium phenyl(2,4,6-trimethylbenzoyl)phosphinate (**TPO-Li**, > 99%) and diphenyl(2,4,6-trimethylbenzoyl)phosphine oxide (**TPO**, > 98%) were purchased from TCI Chemicals. 2,2'-thiodiethanethiol (**4**, 98.7%, water solubility: 0.62 mg/mL) is a gift from Bruno Bock. 1,4-bis[(vinyloxy)methyl]cyclohexane (**CHDM**, > 98%, water solubility 0.025 mg/mL) is a gift from BASF. Dimethyl sulfoxide-d^6 (DMSO-d^6, 99.5% D) was bought from Eurisotop. All chemicals were used without further purification.

2.2 Synthesis

Miniemulsion thiol-ene photopolymerization was prepared as follow. A monomer phase containing **3** (1.70 g, 9.2 mmol), DAP (2.3 g, 9.2 mmol), DBHQ (40.5 mg, 50 mM with respect to monomer), and HD (0.16 g) was mixed in a 25 mL vial. The organic phase was then mixed with 16 mL of an aqueous phase containing SDS (0.14 g, 3.5 wt%/monomer, 30 mM in water). A macroemulsion was formed by high-speed mixing with Ultra-Turrax equipped with 8 mm dispersing tool, setting at 20 000 rpm for 5 min. The resulting macroemulsion was further emulsified by using a Branson sonifier SFX250 for 5 min at 90% amplitude and pulse mode 5 s ON / 1 s OFF cycles. A portion of 10 g of miniemulsion was mixed with 2 mL of a TPO-Li solution (20 mg/mL, 2 % w/w respect to monomer) in a 20 mL cylinder vial. The sample was placed at the center of a circular photoreactor fabricated by wrapping a 3 meter of UV-LED strip (SMD3528 type, 60 LEDs/m, 385-390 nm) onto inner-wall of a quartz cylinder (ID 80mm × H 100 mm) (**Figure**

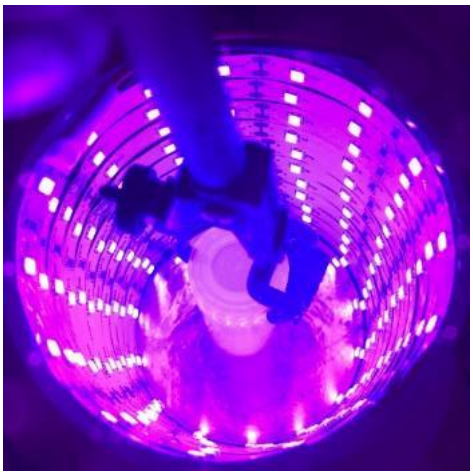

Figure III-2 Photochemical set-up for UV-initiated miniemulsion photopolymerization

III-2). The sample was irradiated for 20 min at room temperature while maintain stirring at 1100 rpm (irradiance = 3.7 mW cm^{-2}).

2.3 Characterization

2.3.1 Nuclear magnetic resonance (NMR)

The chemical stability of monomeric miniemulsion after sonication was monitored by ^{1}H-NMR spectroscopy. At a determined time, a 30 µL aliquot was diluted in 570 µL DMSO-d^{6} for measurement of ene conversion. Integral areas for the methylene protons at 4.7 ppm and 4.25 ppm, corresponding to the proton in monomer and polymer product, were used to evaluate ene-conversion.

2.3.2 Size exclusion chromatography (SEC)

Molecular weight and its polydispersity were measured by SEC (Agilent 1260 Infinity) using THF as an eluent. The solvent was pumped through a set of columns (Polymer Laboratories ResiPore, nominal particle size: 3 µm; porosity: 2 µm) composed of a guard column (50 × 7.5 mm) and two columns (300 × 7.5 mm). The flowrate was set at 1 mL/min and the column temperature was controlled at 35°C. The system was then calibrated using universal calibration standards (EasiVial polystyrene standards from Agilent). The dried latexes were dissolved in THF to give a final concentration of 5 mg/mL and filtered through a 0.2 µm PTFE membrane before injection. The Agilent GPC/SEC software and multi-detector were used to determine the molecular weight data.

2.3.3 Dynamic light scattering (DLS)

Droplet and particle sizes were determined by DLS (VASCO particle size analyzer-Cordouan technologies) with a 658 nm laser source and a detector set to a scattering angle of 135°. The latexes were diluted in deionized water to reach 0.1 % solid before measurement. The diluted sample was transferred to DLS cell, and the Dual Thickness Controller (DTC) was set as DOWN. Each sample was acquired 10 times by statistical mode with the signal to noise limit 1 %. The z-average diameter D_z(DLS) and polydispersity index PdI^{DLS} were computed by NanoQ software version 2.6 using cumulant data analysis mode. Using the particles refractive index, the inverted Mie algorithm was applied to determine a number-average diameter D_n

and a weight-average diameter D_w. The goal was to put DLS-based and TEM-based measurements on a common basis to make a comparison possible.[217]

For size distribution measurements of monomer miniemulsions (monomer weight fraction: 1 and 20 wt%), 20 µL samples were placed on the measurement cell and the Dual Thickness Controller (DTC) was set as DOWN mode, resulting in a thin film of miniemulsion of approximate 100 µm thickness (factory setting).

2.3.4 Transmission electron microscopy (TEM)

In cryo-TEM analysis, a drop of 5 µL sample (0.1 – 1 wt%) was deposited on copper grid covered with carbon film which was rendered hydrophilic using an ELMO glow discharge unit (Cordouan Technologies, France). The grid was placed in a home-made freezing chamber maintained at 22°C and a relative humidity at 80% before plunging into liquid ethane held at −190 °C by liquid nitrogen. The grid was mounted onto a cryo holder (Gatan 626, Pleasanton, CA, USA) and observed under low dose conditions in a Tecnai G2 microscope (FEI, Eindhoven, Netherland) at 200 kV. Images were acquired using an Eagle slow scan CCD camera (FEI). In negative stain TEM analysis (NS-TEM), a drop of 5 µL ethanol was applied onto copper grid covered with a plain carbon film for 1 min. The excess solvent was drained by touching the grid to the edge of a filter paper. Then a drop of 5 µL latex sample (0.1 wt%) was applied. After 1 min of interaction, the excess was removed, and the residue was immediately stained by 5 µL staining solution (2 wt% sodium phosphotungstate in water) for 1 min. The grid was fully dried by filter paper. The NS-TEM images were obtained by a JEOL ARM-200F (JEOL, Tokyo, Japan) instrument working at 200 kV. The images were recorded with a Gatan camera (Orius 1000 model). Regardless of the technique, the number of particles were counted by using ImageJ software. The number-average diameters ($D_n = \sum n_i D_i / \sum n_i$, where n_i is the number of particles of diameter D_i) and volume-average diameters ($D_w = \sum n_i D_i^4 / \sum n_i D_i^3$) were calculated. Polydispersity index $PdI^{TEM} = (\sigma / D_n)^2$ is defined as the squared ratio of the standard deviation (σ) of the particle diameter distribution divided by the number-average diameter. PdI^{TEM} was used to estimate the width of size distribution.

2.3.5 Turbiscan

The droplet stability of the **DAP-3** miniemulsions was measured at 30 °C in a Turbiscan LAbexpert (Formulaction). The thiol-ene miniemulsion was transferred to a customized glass

vial designed for Turbiscan analyzer and loaded into the instrument. A near-infrared light source (880 nm) was sent to a sample and the backscattered signal (BS) (45° from the incident radiation) was recorded as a function of position (from top to bottom of the vial), enabling the detection of the migration phenomena. Then BS signal was collected as a function of storage time. The measured BS signal subtracted with the first measurement (time zero) yielded ΔBS (%). All BS signals were calibrated with Teflon standards. The backscattered light, which depends on the droplet mean diameter and on the monomer weight fraction, provides a useful measurement of the droplet stability.[218]

3 RESULTS AND DISCUSSION

3.1 Miniemulsion step photopolymerization of DAP-3

3.1.1 Chemical stability of monomer miniemulsion

Miniemulsions containing a weight fraction of 20 wt% in DAP (diene) and **3** (dithiol) monomers have been obtained in three stages: firstly, the preparation of an organic monomer phase including HD as a costabilizer (against Ostwald ripening), secondly, its coarse dispersion in an aqueous phase surfactant continuous phase, and thirdly, its emulsification using ultrasonication to form fine droplets typically in the 50- 500 nm size range. There are many reports in the literature about the limited shelf-life stability of thiol-ene systems, generally in bulk without the use of solvent.[23,169,219,220] The reasons are their very rapid polymerization rates and sensitivity to the presence of small concentrations of impurities and other adventitious radicals. The situation is even more complex for a thiol-ene miniemulsion because it involves a multicomponent system and several preparation steps. In spite of these problems, a chemical stability is desired for the polymerization to be temporarily controlled. In addition, a premature reaction may affect droplet break-up and droplet size distribution by changing the composition and viscosity of the dispersed phase.[221]

Figure III-3A shows the temporal evolution of ene conversion (see representative ^{1}H NMR data in **Figure III-3B**) in the dark of a **DAP-3** miniemulsion, taking the end of ultrasonication as the initial time of measurements. Using an initiator-free system, the functional group consumption stands at 84% just after sonication with a standard deviation of 15% (the experiment was replicated 3 times). It is extremely difficult to obtain reproducible kinetic data because polymerization proceeds at very rapid rates. Control measurements of

monomer conversion after each preparation stage shows that the main source of premature reaction is the last step of ultrasonication. In the first steps, **DAP-3** mixture in bulk or dispersed in water can be also subjected to spontaneous reaction, but at much lower conversion rates than the sonicated samples. The ability of ultrasonication to cause radical polymerizations has been reported in the literature.[222] Ultrasonic cavitation generates very high local temperatures and pressures, resulting in bond breakage and the formation of radicals, such as hydroxyl radicals (OH•) when it proceeds in water.[223] Although difficult to solve, the problem of spontaneous thiol-ene reaction may be circumvented by the addition of phenolic radical inhibitors added to the organic phase.

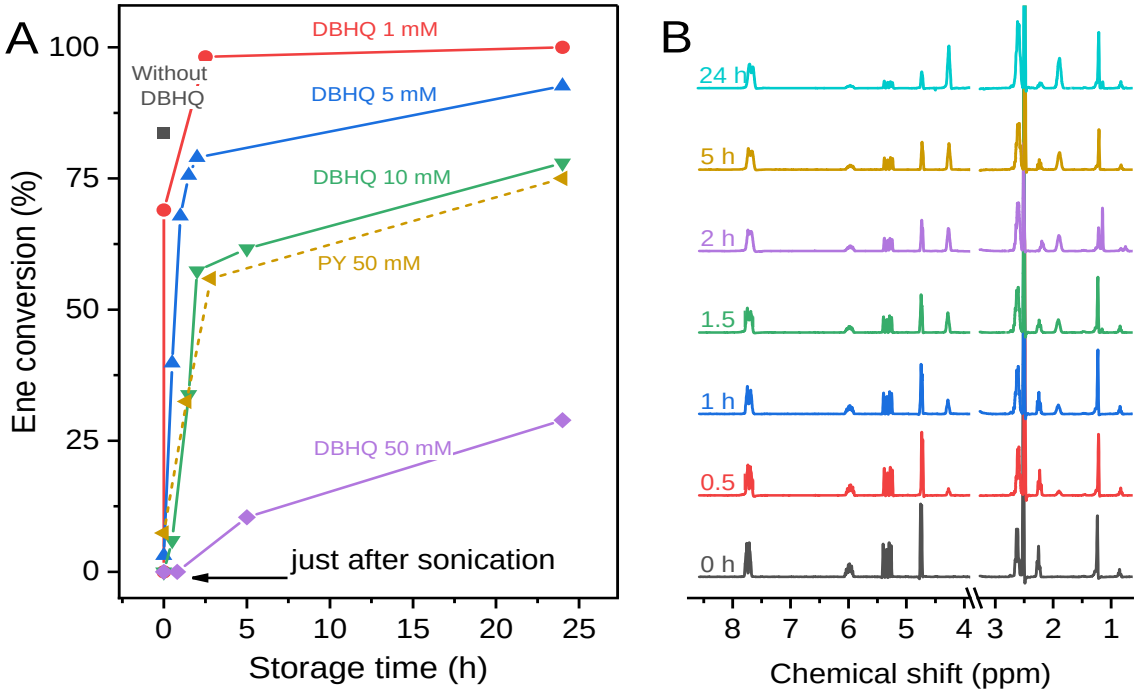

Figure III-3 (A) Ene conversion as a function of storage time of **DAP-3** aqueous miniemulsion (20 w% monomer phase content, [SDS] = 3.5 w%/monomer). (B) ^{1}H NMR spectra in DMSO-d^{6} of a **DAP-3** miniemulsion (20 w% monomer phase content) containing 10 mM of DBHQ (radical inhibitor) as a function of storage time (in the dark and at ambient temperature). t = 0 is the first measurement just after ultrasonication.

Two types of radical stabilizers of different solubility in aqueous and organic phase – pyrogallol (PY) and 2,5-di-tert-butylhydroquinone (DBHQ) – were evaluated by comparing their ability to prevent miniemulsion polymerization.[56] PY and DBHQ have partition coefficients (*log P*) of 0.79 and 2.44 respectively, suggesting different locations. While DBHQ is mostly encapsulated in monomer droplets, PY is distributed between the two phases. As shown in **Figure III-3A**, when used at similar concentration (50 mM with respect to monomer),

the PY-stabilized miniemulsion exhibits a conversion of 30% after 1 h storage time while DBHQ-stabilized analogue is almost unconverted. Note that 4-hydroxyphenol is another effective radical stabilizer for thiol-ene miniemulsion employed by Patton et al.[17] Consequently, DBHQ was used as radical inhibitor in the rest of the study. The other challenge is to use it at minimal concentration to limit detrimental effects on the final values of monomer conversion and molecular weight. **Figure III-3A** depicts the ene conversion as a function of storage time for a range of DBHQ concentrations (1 - 50 mM). There is a trend indicating a better shelf-stability upon increasing the inhibitor content. At 50 mM of DBHQ, monomer conversion remains at 0% just after sonication, and is less than 10% within the next five hours. For a monomer miniemulsion, preserving the chemical stability in the order of several minutes to several hours is generally sufficient to give time for the operator to conduct polymerization and to obtain reproducible results.

3.1.2 Monomer droplet stability

Stability of a miniemulsion droplet is achieved provided that the destabilization rate by coalescence and Ostwald ripening are sufficiently low.[212] Kinetically stable monomer droplets (i.e., having both colloidal and diffusional stability) can be obtained by appropriate choice/concentration of surfactant and costabilizer. Few detailed stability studies of thiol-ene monomer miniemulsions have been reported in the literature.[131] A stability study based on Turbiscan data measuring backscattered light over storage time is presented in **Figure III-4A** for a **DAP-3** miniemulsion with or without radical inhibitor. In the DBHQ-based monomeric miniemulsion, a change in backscattered signal (ΔBS) occurred in the matter of minutes, indicating a poor stability. The constantly fluctuating backscattering signal arises because the limited chemical stability may interact in a complex manner with droplet stability. This system is, therefore, not a true miniemulsion in the sense that it is not stable over a period of weeks or months. However, the destabilization is slow and moderate (without apparent phase separation), which implies that a photopolymerization remains possible if it is performed just after sonication. Conversely, the stability of the miniemulsion was strongly improved in the absence of radical inhibitor, and this latter was stable for at least 5 h. This miniemulsion contains a significant fraction of polymer because of the self-initiated polymerization induced by sonication discussed previously. It is known that the inclusion of a water-insoluble monomer-soluble polymer can significantly reduce diffusional degradation,[224] and therefore,

explains that a kinetically stable miniemulsion could be produced in this case. The fact that the droplet stability depends on the *in situ* formed polymeric costabilizer points out that Ostwald ripening is the predominant destabilization process in the first unreacted miniemulsion.

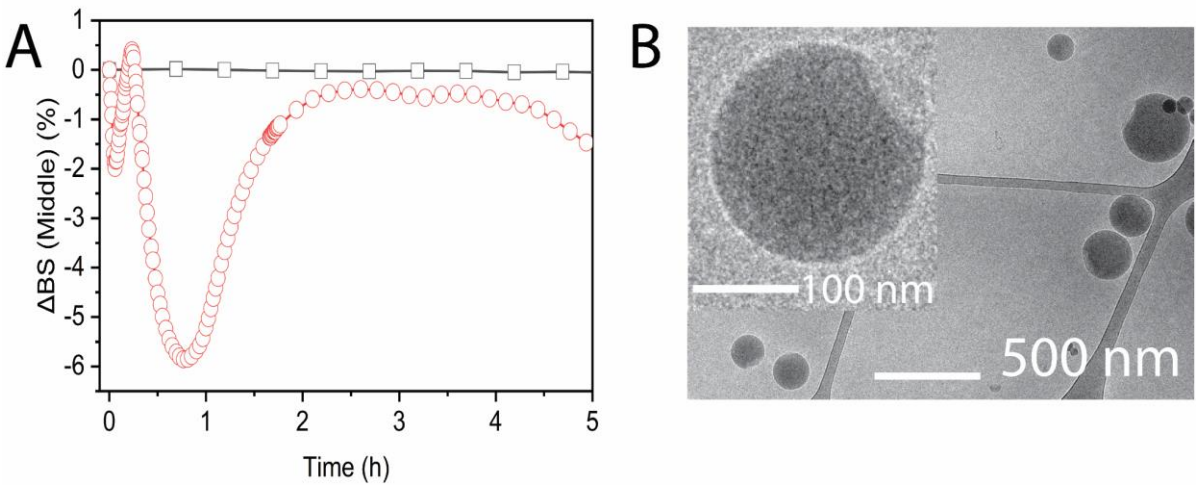

Figure III-4 (A) Variation of backscattered signal (ΔBS) in the middle of the measuring vial as a function of storage time for a **DAP-3** miniemulsion prepared without DBHQ (square) and with 50 mM DBHQ as radical stabilizer (circle). (B) cryo-TEM image of a **DAP-3** miniemulsion containing DBHQ, implying that the observed monomer droplets do not contain polymer. SDS was used at 3.5 w%/monomer.

The limited solubility of HD in **DAP-3** monomer mixture may account for the poor costabilizing properties. Not easily evidenced at the macroscopic level, the insolubility could be revealed through a cryo-TEM image of the monomer droplets. **Figure III-4B** shows a typical image of a **DAP-3** miniemulsion. The droplets have a broad size distribution (60 – 350 nm) and a number-average diameter of approximately 152 nm. At higher magnification, one can observe in most droplets the existence of a separate and brighter HD phase. Similar phase segregation into a Janus structure has been observed previously in immiscible polymer blends and microspheres.[225] In comparison to a core-shell architecture, an anisotropic biphasic morphology is more thermodynamically favorable due to minimization of interfacial surface area.[226] In addition to HD phase separation, the water-solubility of **3** (15 mg/mL at 25°C) is thought to be another contributing factor to the Ostwald ripening.

3.1.3 Polymerization kinetics and molecular weight progress

A photopolymerization was performed with a 50 mM DBHQ-stabilized **DAP-3** miniemulsion (just after ultrasonication) containing the water-soluble photoinitiator TPO-Li.

The conversion-time curve obtained by a series of ^{1}H-NMR measurement at different irradiation times is shown in **Figure III-5A, B**. Despite high scattering of miniemulsion droplets and low irradiance of LED light (3.7 mW cm^{-2}), a full conversion was achieved in less than 5 min. Note that the reaction was extended to 20 min, however, to favor the formation of high-molecular-weight polymer that in step-growth polymerization is only significant at the last percentage of reaction conversion. Despite the high concentration of radical inhibitor, the polymerization kinetic remains fast without any apparent induction period. The reasons lie on the initiation efficiency and the high addition (k_{add}) and hydrogen transfer (k_H) rate constants governing the thiol-ene polymerization of DAP and **3** monomers. The values of k_{add} and k_H are in the range of 10^4-10^6 L mol^{-1} s^{-1} at ambient temperature, typically in the same range as the propagation rate constants of conventional acrylates.[36]

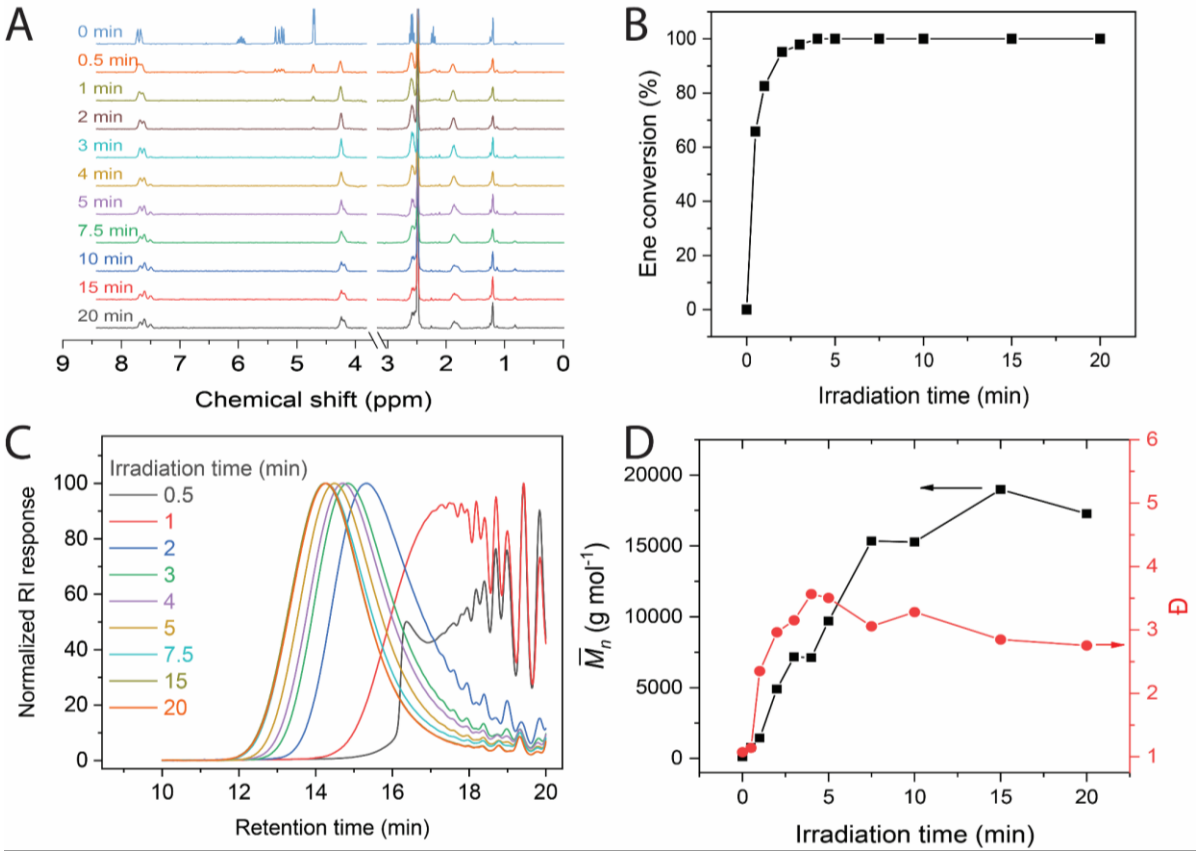

Figure III-5 (A) ^{1}H NMR spectra in DMSO-d^6 during a **DAP-3 (with 50 mM DBHQ)** miniemulsion photopolymerization for different irradiation times. Monochromatic irradiation at 385 nm, I = 3.7 mW cm^{-2}. (B) Conversion-time curve for a **DAP-3** miniemulsion photopolymerization using the water-soluble photoinitiator TPO-Li. (C) Series of SEC traces during a **DAP-3** miniemulsion photopolymerization. (D) Dependence of number-average molecular weight ($\bar{M}_n$) and dispersity ($Đ$) on irradiation time. SDS was used at 3.5 w%/monomer.

To investigate the evolution of molecular weight during photopolymerization, aliquots of the reaction medium were withdrawn at defined intervals between 30 s and 20 min, quenched with DBHQ before SEC analysis. **Figure III-5C,D** shows a series of SEC traces and the growth of number-average molecular weight ($\bar{M}_n$) of poly(thioether) samples as well as molecular weight dispersity (*Đ*) as a function of irradiation time. The polymerization reaction has a typical kinetic profile of a conventional step-growth polymerization, in which high molecular weight is only obtained at very high conversion. At the end of the reaction, a polymer with $\bar{M}_n$ = 17,000 g mol^{-1} and *Đ* = 2.8 was achieved, which are reasonable values for a step-reaction polymerization.

3.1.4 Colloidal properties of polymer particles

Due to their sub-ambient glass transition temperature, poly(thioether) particles are not adapted to analysis by conventional TEM. This technique involves the drying of the latex, with possible alterations of particle shape and size.[227] By contrast, negative staining (NS) and cryo-TEM have been found to be more appropriate than conventional TEM for the observation of soft particles.[228] As shown in the cryo-TEM pictures of **Figure III-6A**, the particles derived for **DAP-3** polymerization were homogeneous with a spherical shape. A significant number of particles (> 700) were counted for estimating a number-weighted mean diameter ($D_n^{\mathrm{cryo-TEM}}$). As shown in the size distribution plot, $D_n^{\mathrm{cryo-TEM}}$ was evaluated at 63 nm with a relatively broad size distribution ($PDI^{cryo-TEM}$= 0.14). **Figure III-6B** is an image of the same latex sample, but negatively stained with phosphotungstic acid. As indication of successful negative staining, the particles appear as low contrast objects with a darker halo surrounding them.[229] Consistently, a negative stain does not penetrate the object, but coats the surface, obscuring the object itself and all internal structural details, and resulting in such characteristic footprint like aspect. As can be seen in **Figure III-6B**, the number-weighted mean diameter $D_n^{\mathrm{NS-TEM}}$ (73 nm) calculated from more than 150 particles is relatively consistent with those given by cryo-TEM. The slight deviation has been ascribed to the presence of few larger particles (> 150 nm) resulting in a broader size distribution (PDI^{NS-TEM} = 0.25). Their absence in the cryo-TEM picture means that the negative stained object may suffer locally from a dehydration followed by coalescence.

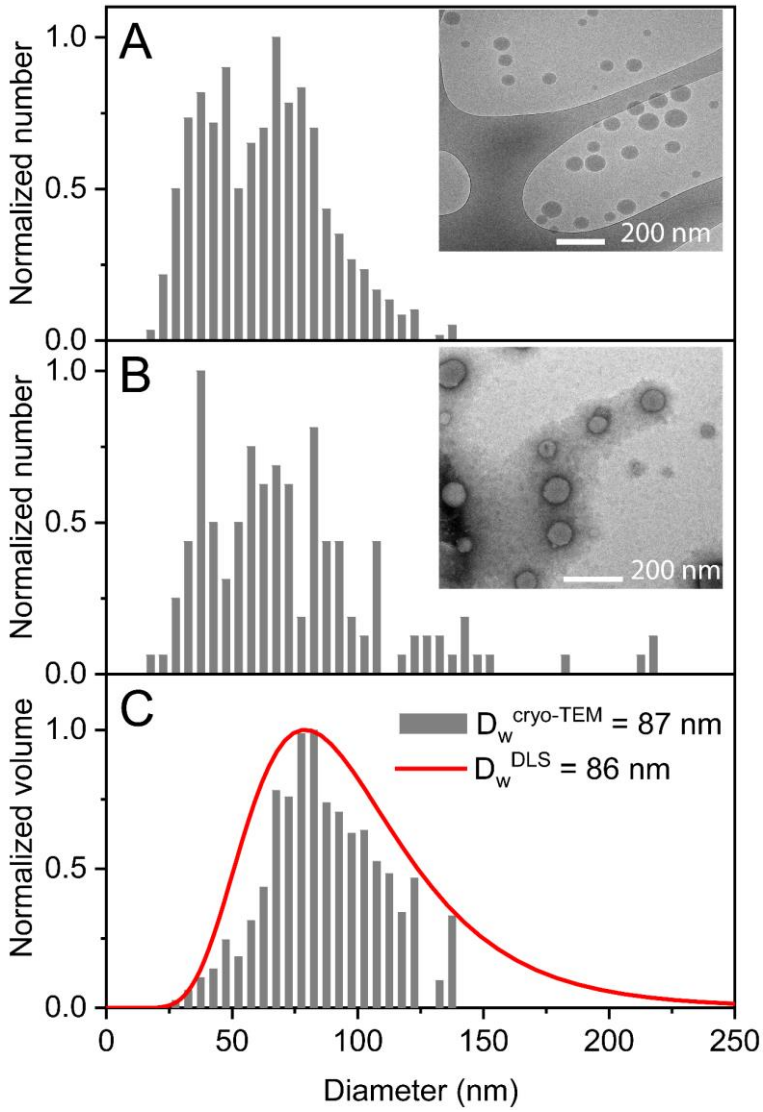

Figure III-6 (A) Cryo-TEM image of a latex obtained via **DAP-3 (with 50 mM DBHQ)** miniemulsion photopolymerization and the corresponding number-weighted size distribution. (B) NS-TEM image of the same latex and the derived particle number size distribution. (C) Comparison of volume-weighted size distributions derived from DLS and cryo-TEM for a latex based on **DAP-3**. The standard deviations for the volume-weighted diameters are 2.0 nm ($D_w^{cryo\text{-}TEM}$) and 2.6 nm (D_w^{DLS}). SDS was used at 3.5 w%/monomer.

An intensity-weighted mean diameter, also referred to as z-average diameter, was typically obtained by DLS (using the conventional cumulant method). Using the same poly(thioether) sample, **Figure III-6C** shows an intensity-weighted mean diameter (D_i^{DLS}) of 93 nm and a broad size distribution (PDI^{DLS} = 0.18). We should note that this diameter cannot be compared directly with a number-weighted mean diameter derived from electron microscopy measurements (although they are both hydrodynamic diameters). This difference and the broad size distribution of the sample can explain the larger particle size found in DLS compared to TEM. To make a comparison possible between the two methods, the DLS

intensity-weighted diameters and the TEM number-weighted diameters were both converted to volume-weighted mean diameters (D_w), the former using the Mie theory, and the latter by calculation (see experimental section for details). As shown in **Figure III-6C**, a good agreement was found between the two volume-average size distributions given by cryo-TEM and DLS analysis.

3.1.5 Approaching particle nucleation mode

Investigating droplet nucleation requires the availability of reliable droplet and particle size data.[209] In the case of **DAP-3** system, the latter can be obtained but not the former because of the limited colloidal stability of the monomeric miniemulsion discussed previously. Under these conditions, the reader is cautioned that the droplet size data are not reliable enough. Misinterpretation of DLS size data due to poor monomer miniemulsion stability can have a significant impact on the conclusions that are reached with regard to the nucleation mode. Nevertheless, a first reasonable approach for investigating particle formation mechanism involves comparing only the DLS size distributions of polymer particles and monomer droplets. As depicted in **Figure III-7A**, the two plots show Gaussian distributions appreciably shifted, with limited overlap. This suggests that the general trend is a predominant homogeneous nucleation over droplet nucleation.

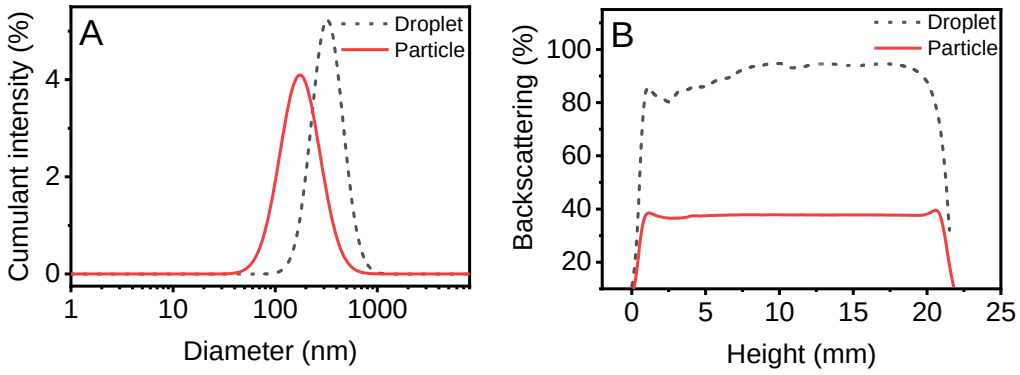

Figure III-7 (A) DLS size distributions in the **DAP-3 (with 50 mM DBHQ)** miniemulsion photopolymerization. Dotted line: monomer (before irradiation); solid lines: particles (after polymerization, 20 min at ambient temperature). (B) Evolution of backscattering signal as measured by Turbiscan. SDS was used at 3.5 w%/monomer.

In addition, the reaction was accompanied by a sharp drop of the backscattered signal ΔBS as can be seen in **Figure III-7B**. Such evolution of optical properties can be reconciled with the course of a polymerization where homogeneous nucleation plays a major role. In such

case, the nucleated particles have a limited concentration in monomer, and their growth proceeds by mass transfer from the non-nucleated droplets acting as reservoir like in the same manner as for emulsion polymerization. Light scattering intensity drops as a result of the disappearance of monomer droplets, which are significantly larger than the particles. In the case of a predominant droplet nucleation, the expected similarity between droplet and particle size distributions would imply rather that the scattering properties are essentially unchanged.

3.2 Investigation of droplet nucleation

3.2.1 Methodology

To study accurately how the particles are formed, it is necessary to start the miniemulsion polymerization with photolatent, stable and monomodal thiol-ene monomer droplets. In our case, a decrease of the monomer weight fraction was the only way of meeting these three requirements. Stable **DAP-3** droplets could be generated by means of a monomer weight fraction of 1 wt%. Similarly, the miniemulsion was emulsified using SDS, costabilized by HD, and made chemically inert by DBHQ. It is useful to mention that SDS concentration was kept at 6.0 mM, below CMC, so that the contribution of micellar nucleation is neglected. Evidence for the formation of a kinetically stable monomeric miniemulsion is based on DLS and Turbiscan data provided in **Figure III-8**. In these conditions of droplet stability, one can safely examine the effect of three experimental parameters known to have a significant impact on droplet nucleation: *initiator solubility*, *initial droplet size* and *monomer solubility*. By comparing droplets and particles with regard to their size distribution and number (the concentration of polymer particles in units of number of particles per liter) in each case, it is possible to ascertain whether droplet nucleation occurs, and, if it does, its extent relative to homogeneous nucleation.

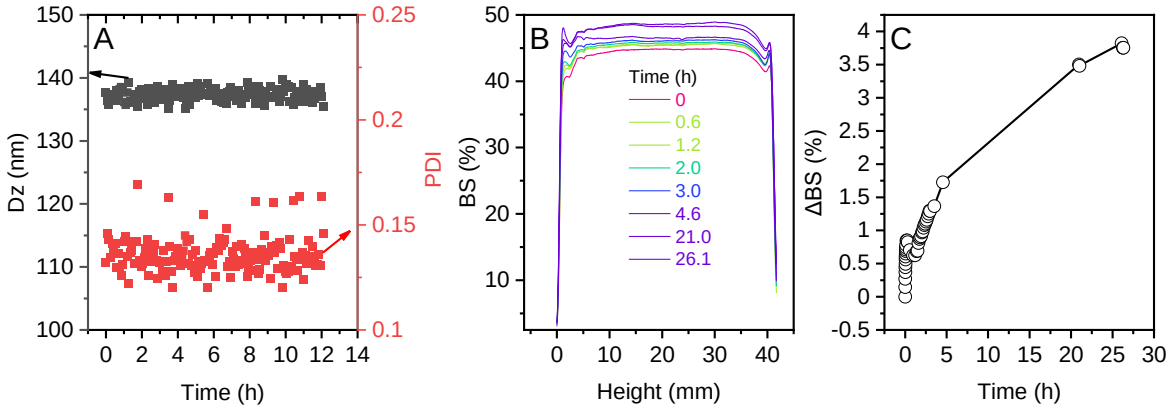

Figure III-8 Droplet stability of a **DAP-3 (with 50 mM DBHQ)** miniemulsion having a monomer weight fraction of 1 wt%. (A) Temporal evolution of z-average diameter (D_z analysis with time interval of 5 min for 12 h). The result shows that the droplet size is unchanged over a period of 12h; (B) Backscattering signal (BS) as a function of sample height for different storage times (Turbiscan analysis at ambient temperature); (C) Variation of BS as a function of storage time, t = 0 is the time just after ultrasonication. SDS was used at 35 w%/monomer, equal to 12 mM based on water.

3.2.2 Effect of initiator solubility

Two radical photoinitiators from the same monoacylphosphine oxide family were employed: TPO as oil-soluble photoinitiator and the water-soluble salt analogue TPO-Li used previously (see chemical structures in **Figure III-1**). **Figure III-9A,B** compares the size distributions of droplets and particles in each case and using two independent methods: DLS (top) and TEM (middle). An advantage of using miniemulsions with low monomer concentration in DLS is the absence of the need for dilution, thus limiting the risk of monomer dissolution and droplet size variation. Regarding TEM, particle size data were collected from NS-TEM images (**Figure III-9C**), while droplet size data were obtained by cryo-TEM analysis. Regardless of the initiator solubility, the starting miniemulsion is monomodal and has an intensity-average diameter of about 175 ± 11 nm. The nucleation is completely different whether the initiator is water-soluble or not. When using TPO-Li (**A** for DLS data and **B** for TEM data), the size distribution of the droplets significantly deviates from that of the particles irrespective of the method used. The ratio of number of particles over number of droplets (N_p/N_d) was estimated at 8.2 (DLS data). Homogeneous nucleation appears therefore to be the predominant particle nucleation process, but droplet nucleation may be very slightly present. The good agreement of DLS (**A**) and TEM (**B**) data supports the validity of this conclusion. This is also consistent with the previous observation at a higher monomer weight fraction (see section CHAPTER III.3.1.5). The situation is much different for the miniemulsion containing TPO in the droplet core. In this case, droplets and particles exhibit similar size

distributions whether determined by DLS (**A'**) or TEM (**B'**), and N_p/N_d was estimated at 0.9 (DLS data). The fact that the number of particles derives directly from the number of droplets indicates a predominant droplet nucleation. The explanation for this effect is that water-insoluble initiator reduces the probability of forming oligoradicals in water, and therefore, the extent of homogeneous nucleation. The situation is quite different with TPO-Li, the water-soluble radicals are unlikely to be captured by the existing droplets/particles, leading to a predominant homogeneous nucleation.

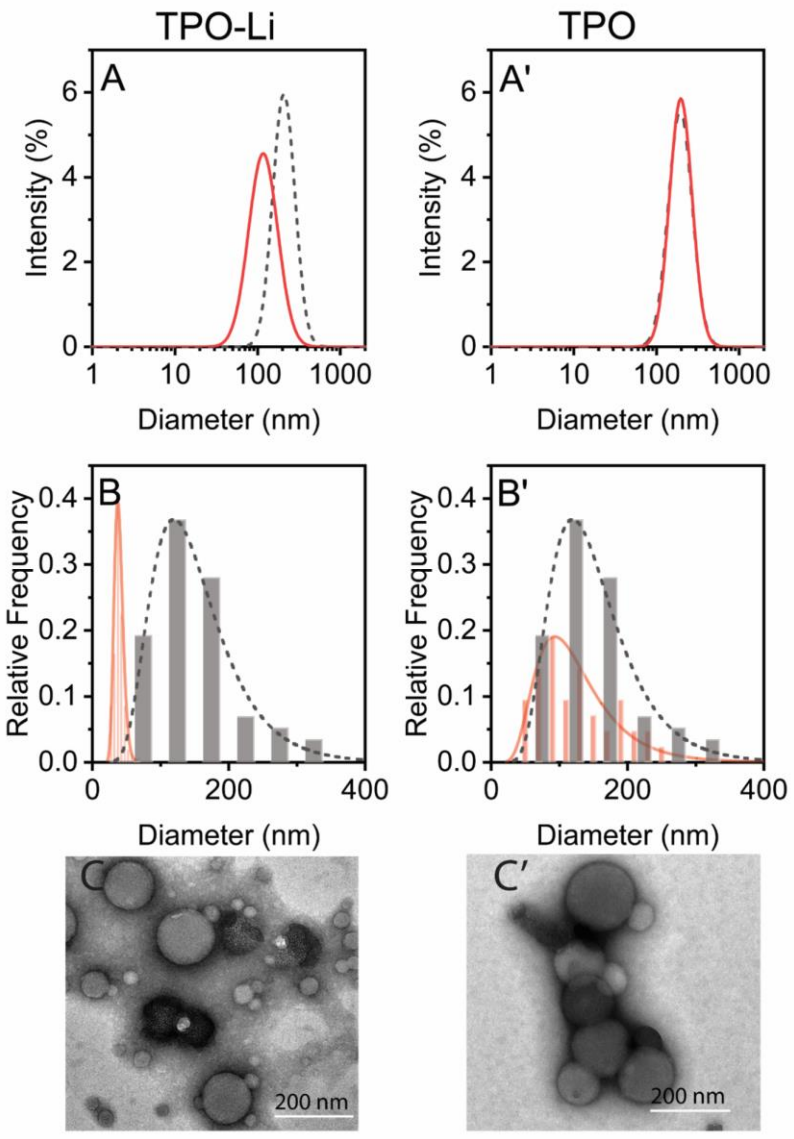

Figure III-9 DLS (top) and TEM (bottom) size distributions in a **DAP-3 (with 50 mM DBHQ)** miniemulsion photopolymerization with a weight fraction in monomer of 1 wt% using TPO-Li (A, B) or TPO (A', B') as initiator. Dotted line: monomer droplets; solid line: polymer particles. In TEM data (B and B'), the droplet size distributions were determined using cryo-TEM while particle size distribution derived from NS-TEM. NS-TEM pictures of **DAP-3** latexes obtained by miniemulsion photopolymerization using TPO-Li (**C**) and TPO (**C'**). SDS was used at 35 w%/monomer, equal to 12 mM based on water.

3.2.3 Effect of SDS concentration

In this second series of experiments, the SDS concentration was varied (3, 6, 12 and 24 mM) as a means of obtaining a set of 4 types of stable droplets of different sizes. This has implied that in certain cases the surfactant concentration exceeds CMC ([SDS] ≥ 12 mM), therefore, micelles are present and micellar nucleation may occur. The resulting droplets have an intensity-average diameter (D_d) of 104-210 nm. Based on DLS data, a systematic comparison of droplet and particle size distributions is presented in **Table III-1** and **Figure III-10**. In the presence of the water-insoluble initiator TPO (**A'**, **B'**, **C'** and **D'**), a robust droplet nucleation operates regardless of the droplet size. With the water-soluble initiator TPO-Li (**A**, **B**, **C** and **D**), the extent of droplet nucleation increases appreciably as droplet size decreases. For the lowest droplet size (D_d = 104 nm), a good correspondence between particle and droplet size distribution and a N_p/N_d ratio very close to 1 were found. It is likely that radical capture in particles can be enhanced by reducing the initial droplet size, improving droplet nucleation efficiency.

Table III-1 Influence of water-solubility of photoinitiators on nucleation mechanism. Monomer content was kept at 1 %wt/aqueous phase, and PI content 2 %wt/monomer.

Initiator	[SDS] (mM)	D_d (nm)	D_p (nm)	N_p/N_d
TPO-Li	24	104 ± 2	102 ± 2	1.1
	12	133 ± 5	103 ± 5	2.1
	6	183 ± 6	91 ± 2	8.2
	3	210 ± 5	154 ± 5	3.8
TPO	24	124 ± 3	127 ± 2	0.9
	12	138 ± 1	136 ± 3	1.0
	6	166 ± 5	173 ± 5	0.9
	3	221 ± 5	221 ± 7	1.0

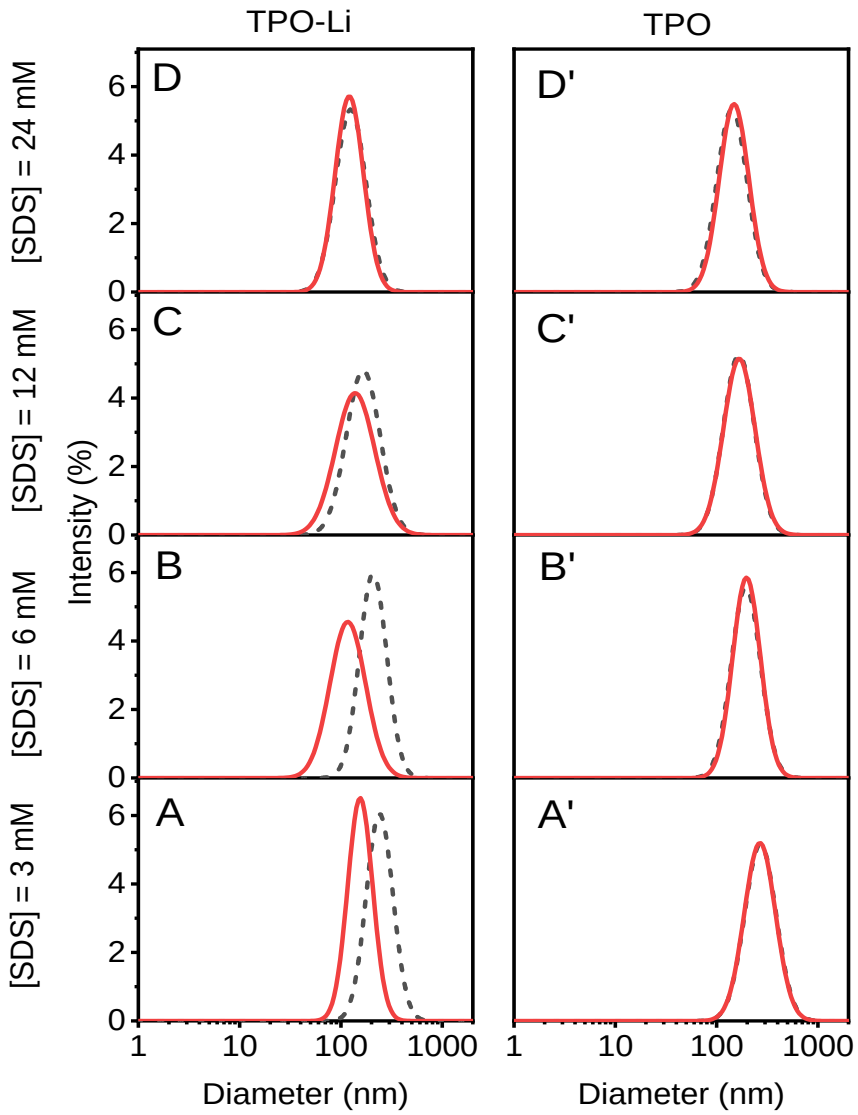

Figure III-10 Droplet size distribution (dotted line) and particle size distribution (solid line) in **DAP-3 (with 50 mM DBHQ)** miniemulsion photopolymerization (monomer content: 1 wt%) using TPO-Li (left column), and TPO (right column); at [SDS]= 3 mM (A, A'), 6 mM (B, B'), 12 mM (C, C'), and 24 mM (D,D').

To evaluate the validity of this interpretation, particle size distributions were also evaluated from negative stained TEM images of the 8 latexes (**Figure III-11**), four containing TPO and four other containing TPO-Li. A reasonable assumption based on the previous experimental results is to consider that the TPO-initiated systems undergo a prominent droplet nucleation, irrespective of surfactant concentration. Under these conditions, the particle size distribution should be the replica or the "one to one" copy" of the initial droplet size distribution. Based on this assumption, one can distinguish two behaviors for the TPO-Li-initiated systems in agreement with the DLS results. At low SDS concentration (**A**: 3 mM and **B**: 6 mM), a population of particle smaller than the starting droplet population (TPO-derived

latex) suggests a substantial droplet nucleation. At high SDS concentration (**C**: 12 mM and **D**: 24 mM), the particle size distribution is somewhat similar to that of the droplets, suggesting a dominant droplet nucleation. The driving force is the increase probability of radical capture by monomer droplets when their diameter is reduced to about 100 nm. Thus, when droplet size is small enough, the size distribution of particles is not dependent on whether the initiator is soluble in water.

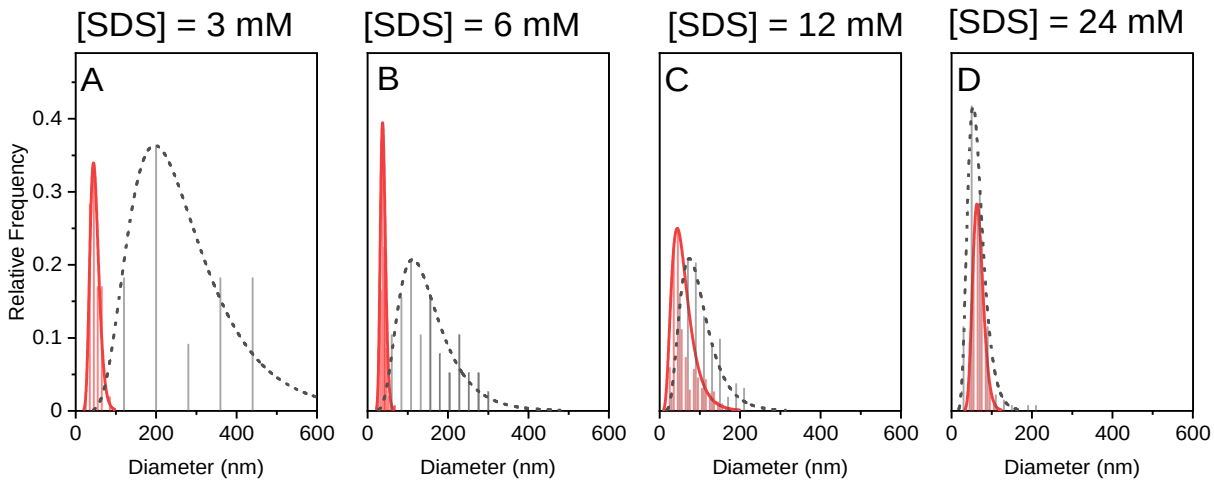

Figure III-11 Effect of initiator solubility on particle size distribution (derived from NS-TEM imaging) of a latex derived from a **DAP-3 (with 50 mM DBHQ)** miniemulsion (monomer content: 1 wt%) prepared at different surfactant concentrations: Dotted line : TPO as an initiator ; solid line : TPO-Li as an initiator.

3.3 Effect of monomer solubility

In miniemulsion radical chain polymerization, it is well established that the use of more water-soluble monomers can increase the occurrence of homogeneous nucleation by reducing radical desorption rate and nucleation duration. Thus, it is important to determine in what extent a similar dependency exists for miniemulsion thiol-ene polymerization. For this purpose, a range of thiol and ene monomers of different water solubility compared to the reference monomers **3** and DAP have been employed (see chemical structures in **Figure III-1**). For thiol monomers, the water insolubility decreases in the order: 3 < 4 < 5. For the ene monomer, the order is following DAP < cyclohexyl divinylether (CHDM). The water-solubility values are given in the experimental section. By combining these monomers, four thiol-ene miniemulsions composed of a monomer phase of decreased water-insolubility have been prepared: **DAP-3** (ref.) < **DAP-4** < **DAP-5** < **CHDM-5**. The existence of stable and photolatent droplets was firstly ascertained. As shown in **Figure III-12**, all TPO-initiated polymerizations

show similar profiles of droplet and size distributions, suggesting that the droplet nucleation is not affected by the change of monomer water-solubility. More surprising is that homogeneous nucleation is operative in all systems initiated by TPO-Li, even when the most water-insoluble thiol-ene couple **CHDM-5** is employed. A word of caution regarding this comparison is that the droplet size differs depending on the monomer composition, so direct comparison is not possible.

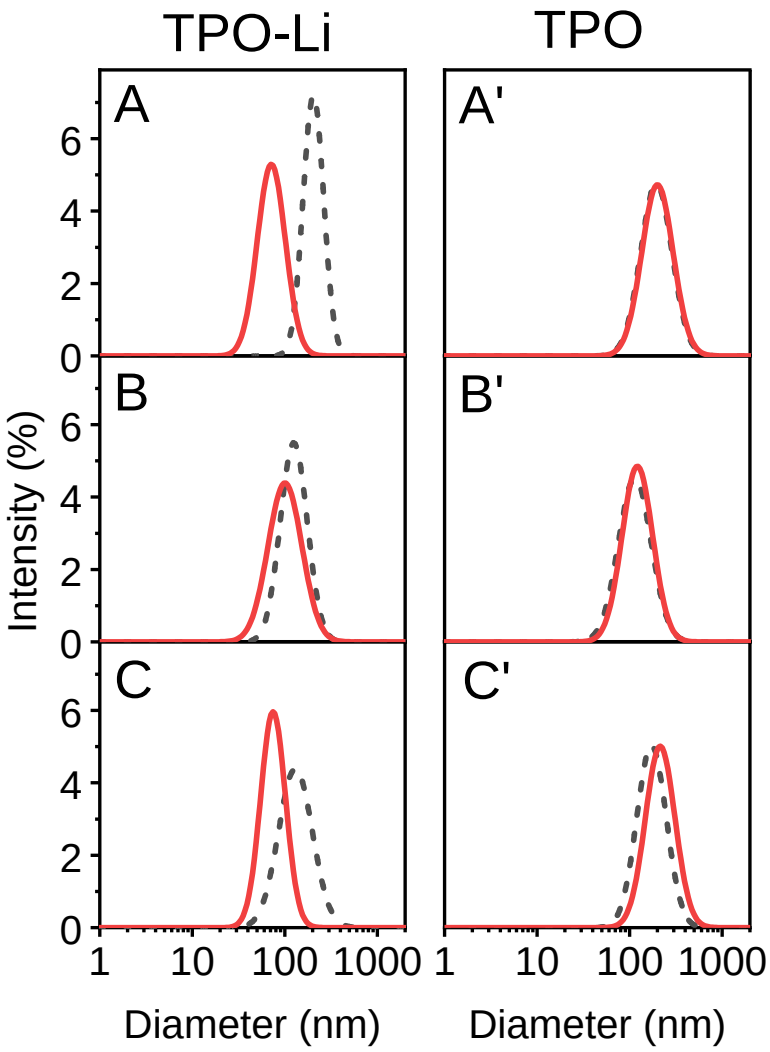

Figure III-12 DLS size distribution of latex and droplets derived from **DAP-4** (A), **DAP-5** (B), and **CHDM-5** (C) using TPO-Li as the water-soluble initiator and SDS as the surfactant ([SDS]= 6 mM), monomer mixtures were stabilized with **50 mM DBHQ**. A', B' and C' are analogous distributions when the water-insoluble initiator TPO was used.

4 CONCLUSION

A wide variety of thiol-ene monomers have been successfully polymerized by miniemulsion thiol-ene step photopolymerization in the literature, but the question of particle nucleation mechanism has remained elusive. This study lays the foundation for

favoring droplet nucleation, which is the preferred nucleation mode in a miniemulsion polymerization. It has been postulated that the specific stepwise mechanism of a thiol-ene reaction could reduce the extent of droplet nucleation and increase the probability of forming polymer particles by homogeneous nucleation. These assumptions are justified on the basis that in a step polymerization the size of the polymer chains increases at a relatively slower pace compared to an analogous chain polymerization, resulting in extended stay of oligomeric radicals in the aqueous phase and higher radical desorption rate.

Involving a model **DAP-3** diallyl ester-dithiol miniemulsion, the first part describes the great difficulty of obtaining a chemically stable miniemulsion. Thiol-ene monomer miniemulsions are highly susceptible to thermal self-initiated polymerization in the dark because of facile production of adventitious radicals during sonication. The use of radical inhibitor at relatively high concentration (DBHQ at 50 mM in monomer) was found to be a practical solution for the **DAP-3** system. However, a persistent problem is that concentration and type of radical inhibitor must be adjusted to each thiol-ene miniemulsion to impart long-term chemical stability. Efforts to overcome this problem will require a better understanding of the self-initiation mechanism to allow the prediction of thiol-ene monomer spontaneous reactivity. Another difficulty arises because of the poor monomer droplets stability. This was assigned to Ostwald ripening and to the limited solubility of HD (costabilizer) in the monomer mixture. The reader is also cautioned that a high thiol-ene droplet stability can be mistakenly achieved by the slow increase in molecular weight due to sonication-induced polymerization. In our case, the limited droplet stability of the **DAP-3** miniemulsion did not prevent a subsequent polymerization. Reproducible kinetic data were achieved when the miniemulsion was photopolymerized in batch just after ultrasonication. Using a 20 mL sample with a 20 wt% monomer phase, high-molecular-weight products were obtained by employing a water-soluble initiator (TPO-Li) at 385 nm. Despite broad droplet size distribution, large droplet size (170 nm) and moderate irradiance (3.7 mW cm^{-2}), the reaction times were reasonable (20 min).

For an accurate determination of particle nucleation mode, thiol-ene droplets with a low monomer weight fraction (1 wt%) were prepared. Under these conditions, they possess chemical stability, droplet stability and monomodal droplet size distribution. Several reaction parameters must be controlled for droplet particle nucleation to proceed successfully. Using

a water-soluble initiator, droplet nucleation generally coexists with homogeneous nucleation (mixed nucleation mode) except when the droplet size was reduced to 100 nm. Conversely, a water-insoluble initiator results in a predominant droplet nucleation irrespective of droplet size and monomer water-solubility. Presumably, the driving forces of this robust droplet nucleation are the water-insolubility of the radicals (favoring a reaction confined to the droplets) and the high reaction rates (minimizing the mass transfer of monomer from droplets to particles). This suggests that using a water-insoluble initiator is the best way to promote a high droplet nucleation efficiency in miniemulsion thiol-ene photopolymerization. However, our approach is not without limitations. Firstly, the low used solids content can disfavor radical capture by droplets, and secondly, no quantitative analysis is proposed when a mixed nucleation mode is operative.

CHAPTER IV. THIOL-ENE EMULSION PHOTOPOLYMERIZATION

Parts of this chapter were published in the following two articles:

1. Le, C. M. Q.; Schmutz, M.; Chemtob, A. Ab Initio Batch Emulsion Thiol–Ene Photopolymerization. Macromolecules **2020**, *53*, 2369-2379 DOI: 10.1021/acs.macromol.0c00265.
2. Le, C. M. Q.; Schrodj, G.; Ndao, I.; Bessif, B.; Heck, B.; Pfohl, T.; Reiter, G.; Elgoyhen, J.; Tomovska, R.; Chemtob, A. Semi-Crystalline Poly(thioether) Prepared by Visible-Light-Induced Organocatalyzed Thiol-ene Polymerization in Emulsion. Macromol. Rapid Commun. 2021, e2100740 DOI: 10.1002/marc.202100740.

1 INTRODUCTION

Polymerization in dispersed systems is one of the most used techniques for the production of polymers.[230] A significant example is *emulsion polymerization*, a widely used process industrially that results in polymer dispersions with a typical average diameter in the 50 – 200 nm range.[66,231,232] Compared to solution polymerization, emulsion polymerization involves much more mechanistic events that govern the rate of formation and growth of polymer particles.[233,234] Over the last 70 years, understanding and predicting these events has been a major challenge for the academic community, with the goal of controlling the multiple characteristics of dispersed polymers: particle size and molecular weight distribution, polymer composition and architecture, etc.[65,69] The complex nature of emulsion polymerization has not hindered the large scale use of "emulsion polymers" in many different industrial fields including coatings, adhesives, inks and non-woven textiles.[63] Today, emulsion polymerization is still at the forefront in the field of eco-efficient production of polymers. Its sustained development is ensured by new environmental regulations and some key technical advantages of latex products including low viscosity, high molecular weights, heat removal capacity and water as possible continuous phase, etc.[235] However, all current commercial emulsion polymers (styrene-butadiene, acrylic, vinyl acetate…) are exclusively prepared by chain radical polymerization carried out in tank reactors using thermal or redox radical initiator.[209] Although further progress should be made in the future, all advances will necessarily be limited by the boundaries imposed by the mechanism of chain radical polymerization.

Very few step polymers – mostly polyesters – could be prepared by aqueous emulsion polymerization,[236–240] and never with a clear picture of the operating mechanism. To achieve high-molecular-weight products by step polymerization, a number of experimental criteria must be fulfilled that are difficult to reconcile with an emulsion polymerization in water: very high monomer conversions (> 98%), the absence of side reactions (to avoid stoichiometric imbalance of functional groups), and an efficient removal of the by-products (to shift the equilibrium in the direction of the polymer).[216,241] In this context, miniemulsion polymerization has proven to be better suited than emulsion polymerization for the synthesis of step polymers in water because mass transfer of monomer through aqueous phase is avoided, thus decreasing the risk of side reactions.[212] Using this technique, step

polymerization in miniemulsion gave rise to a number of latexes based on epoxy,[242] polyurethane,[243] polyester,[244] poly(dimethylsiloxane),[245] poly(thioether)[17,131] and a broad range of waterborne "step polymer-acrylics" hybrids.[246] However, by comparison with a (macro)emulsion, the preparation of a monomer miniemulsion adds complexity and cost in the form higher energy consumption and equipment investment.[98] This explains why this technique has not yet undergone a large-scale industrial implementation.[247] Currently, the preferred method towards waterborne step polymer dispersions still involves a solution polymerization in non-aqueous media, followed by redispersion in water through ionic groups attached to the polymer backbone or external surfactants.[248]

Emulsion polymerization being the workhorse process for the production of dispersed polymers, further research is therefore required to overcome the technical challenges of emulsion step polymerization.[249] In a seminal work, Shipp et al.[204] reported in 2017 a promising example of radical-mediated thiol-ene step polymerization in emulsion. Starting from polyfunctional thiol and alkene monomer emulsions, submicron-sized poly(thioether) particles with linear or cross-linked structure were achieved using a thermal radical initiator. Compared to other step polymerizations, thiol-ene polyaddition features indeed several characteristics able to push up molecular weights such as high conversions, absence of by-product and no side-reaction with water.[15,41] Although a significant amount of experimental data was reported in this aforementioned study, issues related to polymerization kinetics, particle size distribution and molecular weight progress are still poorly understood, particularly with regard to differences with the well-studied chain radical polymerization in emulsion. Additionally, the fundamental mechanisms that dictate particle formation in a step radical polymerization in emulsion need to be further clarified. Two important aspects are the effects of monomer polarity on particle size and the dependencies of surfactant concentration on the final number of particles. Investigation of these issues will help control the properties of the final latex.

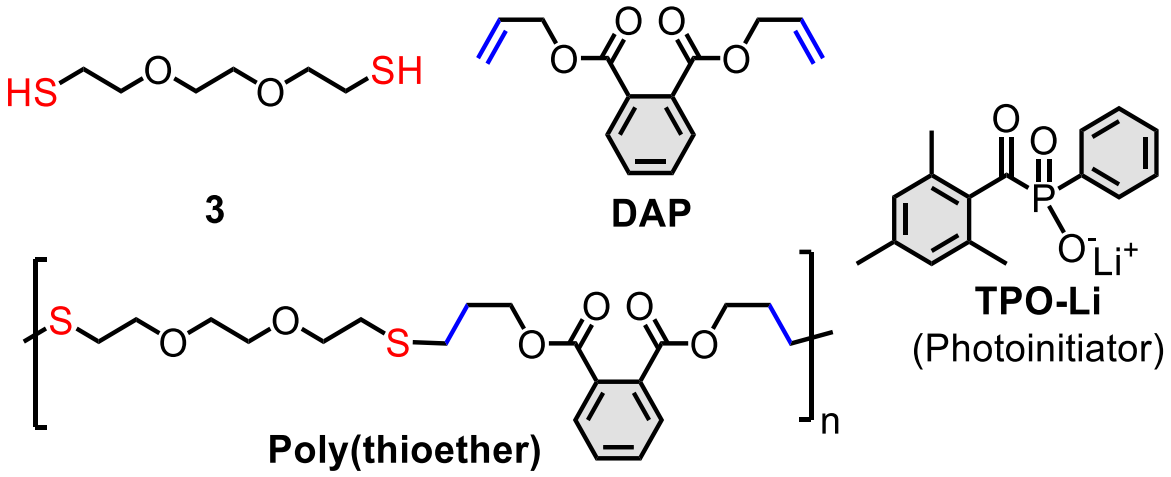

Scheme IV-1. Chemical structure of diene and dithiol monomers DAP and **3** respectively, water-soluble radical photoinitiator (TPO-Li), and poly(thioether) derived from **DAP-3** thiol-ene polyaddition.

To address these questions, we have studied the batch photoinduced thiol-ene polyaddition of an aqueous surfactant-stabilized emulsion prepared with the bifunctional monomers diallyl phthalate (DAP) and 2,2-(ethylenedioxy)diethanedithiol (**3**) (1:1 equiv.) at 25°C (**Scheme IV-1**). To be very close to the operational conditions of a conventional emulsion polymerization, we have used sodium dodecyl sulfate (SDS) as the surfactant and a water-soluble photoinitiator lithium phenyl(2,4,6-trimethylbenzoyl)phosphinate (TPO-Li). Photopolymerization (λ_{max} = 385 nm, 3.7 mW cm^{-2}) has resulted after 20 min in a conversion of monomers higher than 99 %, a coagulum-free poly(thioether) latex with a solids content of 10 wt%, and stable particles having an average diameter of 60 nm. Despite significant radiation attenuation due to the multiple scattering of micron-sized monomer droplets, faster polymerization rates and higher molecular weights were achieved compared to a control experiment involving a water-soluble redox initiator. The fact that our emulsion step polymerization is photochemically initiated opens up new possibilities for improving temporal control of reaction and tuning molecular weight tunable through irradiance. To prove the versatility of our process, the effect of latex solids content (5 – 40 wt%) and non-stoichiometric thiol-ene ratio have been also studied. Finally, to clarify the nucleation mechanism, we have determined the number of particles per unit volume of water (N_p) as function of surfactant concentration.

2 EXPERIMENTAL SECTION

2.1 Materials

All monomers were used as received including diallyl phthalate (**DAP**, TCI 99 %), diallyl terephthalate (**DATP**, TCI, 99.4 %), diallyl isophthalate (**DAIP**, TCI 99.7 %), diallyl adipate (**DAA**, TCI 99.8 %), di(ethylene glycol) divinyl ether (**DVE**, BASF), 1,4-bis[(vinyloxy)methyl]cyclohexane (**CHDM**, BASF > 98%), 2,2-(ethylenedioxy)diethanedithiol (**3**, TCI 99.6 %), DL-dithiothreitol (**6**, TCI > 98 %), ethylene glycol bismercaptoacetate (**1**, TCI, 97.5%), ethylene glycol bis(3-mercaptopropionate) (**2**, TCI 98.1%), 2,2'-thioldiethanethiol (**4**, Bruno Bock 98.7%), 1,6-hexanedithiol (**5**, TCI 99.1%). 2,5-di-tert-butylhydroquinone (**DBHQ**, TCI 99.3 %) was used a radical stabilizer for monomer mixture. Aqueous phase is comprised of sodium dodecyl sulfate (**SDS**, TCI 98 %), lithium phenyl(2,4,6-trimethylbenzoyl)phosphinate (**TPO-Li**, TCI 99.3 %) and double distilled water. Other chemicals include L-ascorbic acid (Sigma Aldrich, 99%), hydrogen peroxide (Carlo Erba, 30%) and iron (II) sulfate heptahydrate (Merck, > 80%). Dimethyl sulfoxide-d^6 (DMSO-d^6, 99.5% D) was purchased from Eurisotop and other solvents were used with analytical grade without further purification.

2.2 Synthesis

2.2.1 Photoinitiated thiol-ene emulsion polymerization

A photolatent organic phase consisting of a 1:1 stoichiometric mixture of thiol and ene functional groups was prepared by adding **dithiol 3** (1.70 g, 9.2 mmol, 1 equiv.), **DAP** (2.30 g, 9.2 mmol, 1 equiv.) and DBHQ (40.5 mg, 0.178 mmol, 0.02 equiv.) to a 10 mL vial. 1 g of the resulting organic solution was then transferred to a 20 mL soda-lime glass vial (outer diameter: 25 mm, height: 70 mm). To this latter was added an aqueous phase consisting of TPO-Li (20 mg, 0.067 mmol, 0.03 equiv.), SDS (35 mg, 3.5 wt% with respect to monomers, 13.5 mM in water) and 9 mL of deionized water. A coarse emulsion with an organic phase content of 10 wt% was prepared using Ultra-Turrax® T25 homogenizer (IKA-Werke equipped with 8 mm dispersing tool) at 20 000 rpm for 5 min. Alternatively, a magnetic stirrer (RCT-basic from IKA-Werke) can be used to form the monomer emulsion upon operating at 1100 rpm for 20 min. In both cases, the monomer droplets were relatively unstable and coalesced if agitation was stopped, causing a phase separation. Thus, photopolymerization was performed

immediately after emulsion preparation at room temperature inside a LED circular photochemical reactor.

The photoreactor was constructed by winding a 385 nm LED strip (SMD3528, 60 LED/Meter, LightingWill, length: 1000 mm) around a quartz cylinder (internal diameter: 80 mm, length: 100 mm). Irradiation was maintained for 20 min, while the vial was kept under continuous magnetic stirring (1100 rpm). The vial was placed centrally in the photoreactor where it received at its surface an irradiance (*I*) of 3.7 mW cm^{-2}. *I* value was measured by a calibrated silicon photodiode radiometer (S120VC, Thorlabs) (see experimental setup at **Figure III-2**). At given irradiation times, 50 µL aliquots were withdrawn of the vial for analysis of monomer conversion, particle size and molecular weight.

2.2.2 Redox initiated thiol-ene emulsion polymerization of DAP-3

A similar **DAP-3** monomer emulsion was produced upon replacing the water-soluble photoinitiator in the aqueous continuous phase by a mixture of ascorbic acid (16.5 mg, 0.094 mmol, 0.04 equiv.) and $FeSO_4$ (0.49 mg, 0.003 mmol, 0.0014 equiv.) acting as reductant and catalyst respectively.[250] The polymerization was initiated by introducing 9.7 µL of a 30% wt H_2O_2 solution (0.094 mmol, 0.04 equiv.) into the 20-mL vial containing the coarse emulsion. The reaction was stirred by magnetic stirring at 1100 rpm for 20 min.

2.3 Characterization

2.3.1 Nuclear magnetic resonance (NMR)

Evolution of ene and thiol conversions during the reaction was monitored by ^{1}H-NMR and ^{13}C-NMR spectroscopy. All NMR spectra were recorded in DMSO-d^6 on a Varian 300 – MR. All chemical shifts were reported in parts per million (ppm) relative to the residual DMSO-d^6 (δ 2.50 ppm). At least 64 scans were recorded for each spectrum. Typically, a 30 µL aliquot was charged into an NMR tube containing 570 µL of DMSO-d^6 and the spectrum recorded. For each trial, ene conversion was determined upon comparing the integration area of resonances of methylene protons attached to a vinyl group (−CH=CH_2) in DAP at 4.75 ppm and that of the same methylene protons in the polymer at 4.25 ppm. Thiol conversion was calculated based on the change in the integral value for the sulfhydryl proton at 1.58 ppm at the beginning and after a selected time (**Figure V-1**). For the analysis of the poly(thioether),

water was evaporated from the latex, and the solid was then purified with methanol and dried under vacuum.

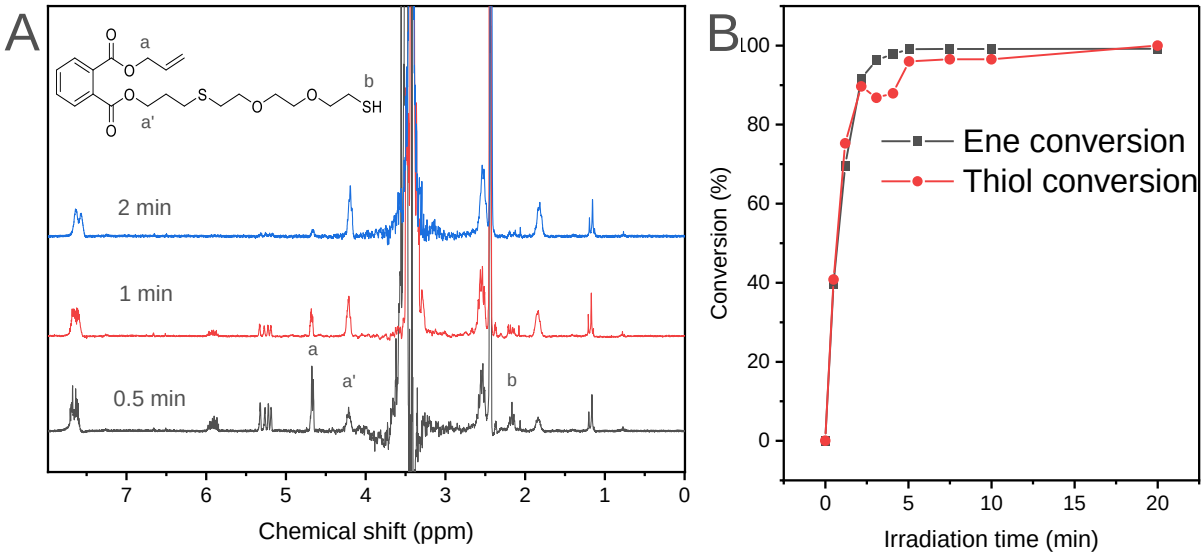

Figure IV-1 (**A**) ^{1}H-NMR in DMSO-d^{6} taken at different times during emulsion photopolymerization of **DAP-3**. For the determination of thiol and ene conversion by mean of ^{1}H-NMR, the equations used are Conv.(ene) = $A_{a'}/(A_a+A_{a'})$ and Conv.(SH) = 1-$[(A_b)_t/(A_b)_{t0}]$. (**B**) Typical thiol and ene conversion-time curves with conversion values obtained from ^{1}H NMR data (Irradiation at 385 nm, I = 3.7 mW cm^{-2}, 20 min). Thiol and ene conversion can be determined with a good level of precision, but only until a maximum value of 90% conversion for thiol. Below this threshold value, a nice synchronicity between thiol and ene conversions is observed. But above this value, a high signal-to-noise ratio is found for the resonance of the sulfhydryl protons, which affects the precision of SH conversion.

2.3.2 Size exclusion chromatography (SEC)

Number–average molecular weights $\bar{M}_n$ and weight-average molecular weights $\bar{M}_w$ were measured by SEC (Agilent 1260 Infinity) containing a G1314B variable wavelength detector operating at 254 nm, a G7800A multidetector suite consist of a refractive index detector and a viscosimeter detector and using THF as eluent. The solvent was pumped through a set of columns (Polymer Laboratories ResiPore, nominal particle size: 3 µm; porosity: 2 µm) composed of a guard column (50 × 7.5 mm) and two columns (300 × 7.5 mm). The flowrate was set at 1 mL min^{-1} and the column temperature was controlled at 35 °C. The system was then calibrated using calibration standards (EasiVial polystyrene standards from Agilent). A portion of 50 µL latex sample was placed into a vial and water was removed by a nitrogen flow. The residue was rinsed with 0.5 mL of methanol and subsequently with 0.5 mL of water. The purified latex was dried under vacuum at room temperature for 2 hours. The mass of polymer in vial was recorded before dissolution in THF. The volume of THF was

adjusted to give a final concentration 5 mg mL^{-1} and the polymer solution in THF was filtered through a 0.2 µm PTFE membrane before injection. Agilent GPC/SEC software and multi-detector were used to obtain the molecular weight data.

2.3.3 Dynamic light scattering (DLS)

Particle size and its distribution were determined by DLS (VASCO particle size analyzer-Cordouan technologies). Details are described in Chapter III 2.3.3

The number-particle size distributions were exported to a worksheet to calculate the volume-average particle diameter: $D_v = \sqrt[3]{\frac{\sum(n_i \times D_i^3)}{n_i}}$ where n_i is the number fraction of particles of diameter D_i. The number of particle per L water of the latex (N_p) is then derived from D_{avg} as follow: $N_p = \frac{6 \times m_{mon} \times x}{\pi \times D_{avg}^3 \times \rho_{pol} \times V_{aq}}$ where m_{mon} is the monomer mass, x is the monomer conversion, V_{aq} is the aqueous phase volume in L, and ρ_{mon} is the density of polymer.[251] The average of N_p and it standard deviation (SD) for each sample is reported as $\overline{N_p} \pm SD$.

2.3.4 Transmission electron microscopy (TEM)

Particle analysis by cryo-TEM is described in detail in Chapter III 2.3.4.

2.3.5 Turbiscan

Backscattering value was determined by using multiple light scattering (Turbiscan LAB, Formulaction). Given the instability of the macroemulsion, the as-prepared **DAP-3** emulsion was immediately transferred to 20 mL testing tube and placed in the measurement chamber. Technical details are described in Chapter III, 2.3.5

3 RESULTS AND DISCUSSION

3.1 Reaction kinetics, particle size and molecular weight progress

The thiol-ene photopolymerization of a conventional oil-in-water emulsion requires specific conditions of implementation: bicomponent and micro-sized **DAP-3** monomer droplets (1:1 equiv.), a water-soluble photoinitiator (TPO-Li), and an aqueous continuous phase containing a surfactant (SDS) at a concentration above the CMC. For ensuring effective temporal control, the starting emulsion must also be chemically stable before exposure to

irradiation, which is generally a challenge with thiol-ene formulations.[56,58,160] Di(tert-butyl)-1,4-hydroquinone (DBHQ), a typical radical inhibitor, was thus added to the **DAP-3** organic phase (0.02 equiv.). This was found to be an efficient means to prevent premature thiol-ene emulsion polymerization and maintain a minimum chemical stability of 2 h. Without stabilizer, ene conversion was nearly 60 % after emulsification, whether the initiator was present or not. This result lends confidence that for this thiol-ene couple, the instability is mainly assigned to a radical mediated thiol-ene reaction. The precise mechanism accounting for the spontaneous generation of radicals in this complex biphasic system is discussed in **Chapter II**. To compensate for the inhibitor presence, an appropriate excess of photoinitiator (0.03 equiv.) was used.

Starting with a DBHQ-stabilized **DAP-3** emulsion, the ene conversion-time curves in **Figure IV-2** support the photolatency of monomer droplets not exposed to UV radiation (plot **a**) and the role of light (385 nm, monochromatic LED) as the main trigger of polymerization (plot **b**). Even at low irradiance (3.7 mW cm^{-2}), a conversion of approximate 99% was achieved in less than 5 min. However, continuous irradiation was maintained for 20 min because it is known that step polymerization shows the presence of high-molecular-weight polymers only near the very end of the reaction. Despite of the inhibitor, no induction period was visible because its duration may be too short to be detected by an offline technique such as ^{1}H NMR spectroscopy (used here to monitor the concentration of monomer in the reaction vessel).

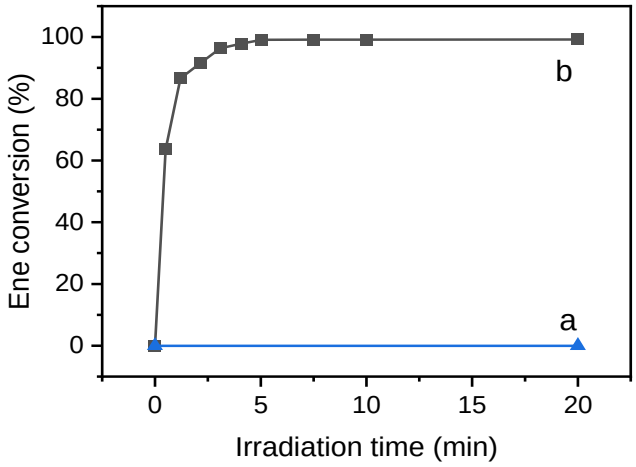

Figure IV-2. Conversion-time curves for **DAP-3** emulsion photopolymerization. Plot **a**: without irradiation; plot **b**: monochromatic irradiation at 385 nm, I = 3.7 mW cm^{-2}. Irradiation was performed in a LED circular photochemical reactor (see experimental section for details). DAP-3 was stabilized with 50 mM DBHQ.

Remarkably, the very high backscattering signal caused by the emulsified micron-sized droplets of monomer did not prevent high polymerization rates (Backscattering values before and after irradiation are shown in **Figure IV-3**). In addition, precise measurement of reflectance revealed a significant decrease after polymerization. The fact the reaction medium becomes less scattering is consistent with the disappearance of large monomer droplets by diffusion through the aqueous phase into much smaller polymer particles of lower scattering efficiency.[218]

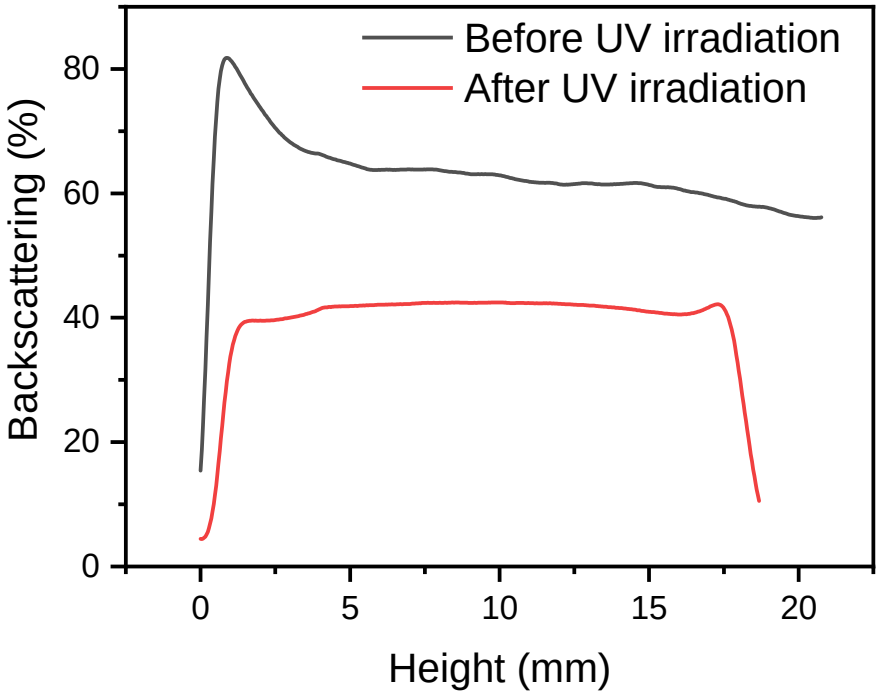

Figure IV-3 Backscattering percentage measured for a **DAP-3** macroemulsion measured over the sample height (0 – 20 mm) before irradiation (grey solid line) and after photopolymerization (red solid line) (see detailed at section 2.3.5). DAP-3 was stabilized with 50 mM DBHQ.

The thiol conversion-time curve was difficult to obtain because the sulfhydryl protons of **3** could not be quantified without ambiguity by ^{1}H NMR when conversions become large. However, a mass polymerization involving only the thiol-ene reactants, clearly established the synchronicity of thiol and ene functional groups' conversion (**Figure IV-4**). The similarity of thiol and ene kinetic data support that allyl ester cannot undergo homopolymerization, and that the predominant reaction is thiol-ene radical addition. In agreement with this, ^{1}H and ^{13}C NMR analysis of the polymer latex confirmed that the polymer backbone exhibits a high density of thioether units (**Figure IV-5**).

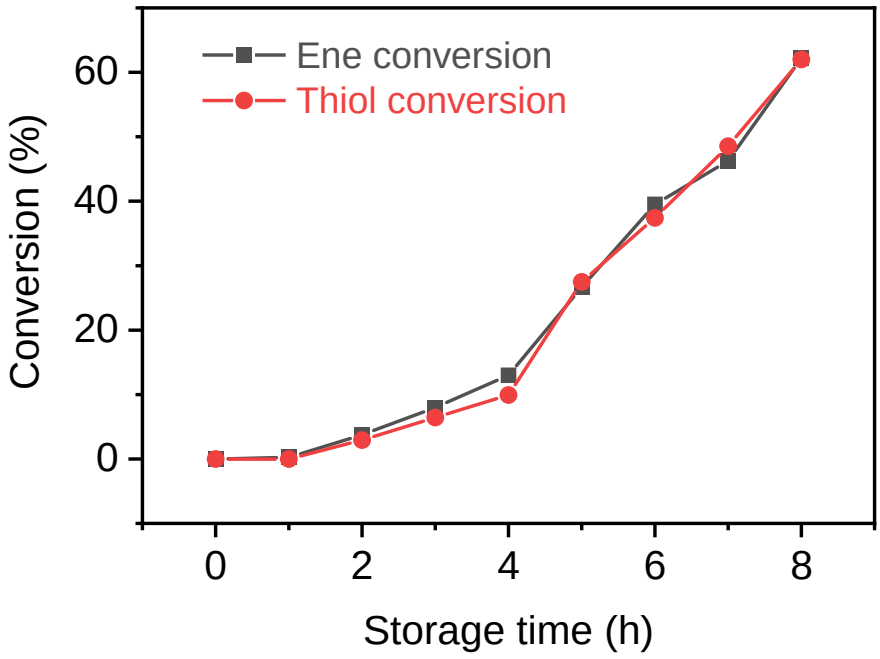

Figure IV-4 Thiol and ene conversion-time curves for the bulk polymerization carried out without initiator.

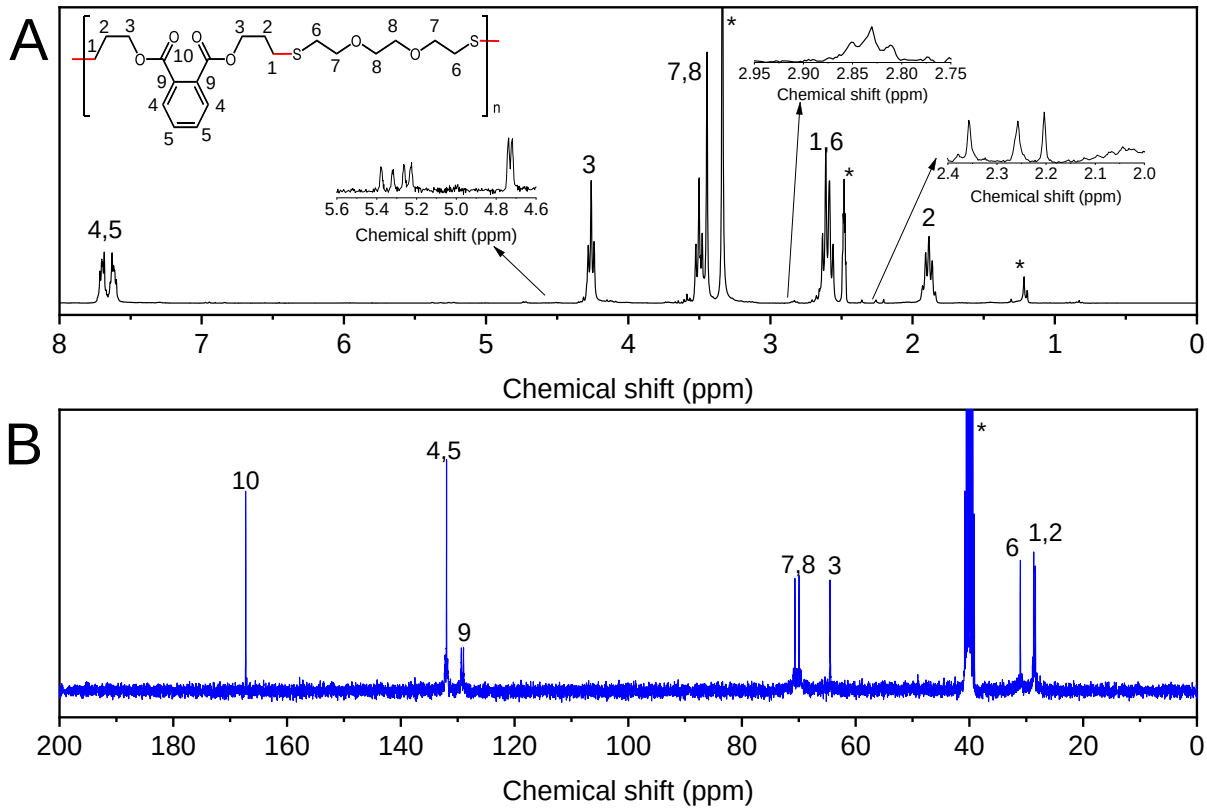

Figure IV-5 (A) ^{1}H-NMR spectrum and (B) ^{13}C-NMR spectrum in DMSO-d^{6} of the latex derived from **DAP-3** emulsion photopolymerization. Irradiation at 385 nm, I = 3.7 mW cm^{-2}, 20 min.

Direct imaging of the polymer particles using microscopy required the use of cryo-TEM. A first attempt with conventional TEM showed that the soft poly(thioether) particles had coalesced upon drying due to their sub-ambient glass transition temperature.[252] As shown in **Figure IV-6A**, the latex is almost monomodal and near-spherical in shape. The particles display a number-average diameter of 62 nm, that is customary in emulsion polymerization, and a relatively broad size distribution (PdI^{TEM} = 0.14). The intensity-average diameter (z-average) obtained from DLS analysis was significantly higher (98 nm), while the size dispersity remained in the same order of magnitude (PdI^{DLS} = 0.15). DLS measures typically show larger sizes than found in microscopic studies.[253] The fact that the sample is not monodisperse accounts for this discrepancy. With a size range spanning 25 – 125 nm, the largest particles have a scattering cross-section 4 orders of magnitude greater than the smallest ones. Therefore, intensity-average value is further weighted towards the minor population of larger particles due to their higher scattering efficiency. Using Mie theory (see experimental section for details), it was possible to calculate number-average and volume-average distributions, making possible the comparison between DLS- and TEM-based data. **Figure IV-6B** shows on the same plot the excellent agreement between the two methods as regards with volume and number distribution analysis. Process replicability was also verified as shown by a standard deviation for intensity-average diameters lower than 5 nm (**Table IV-1**). The process is also robust since the water-soluble photoinitiator can be added either before or after the preparation of the monomer emulsion with no impact on reaction rates and particle size.

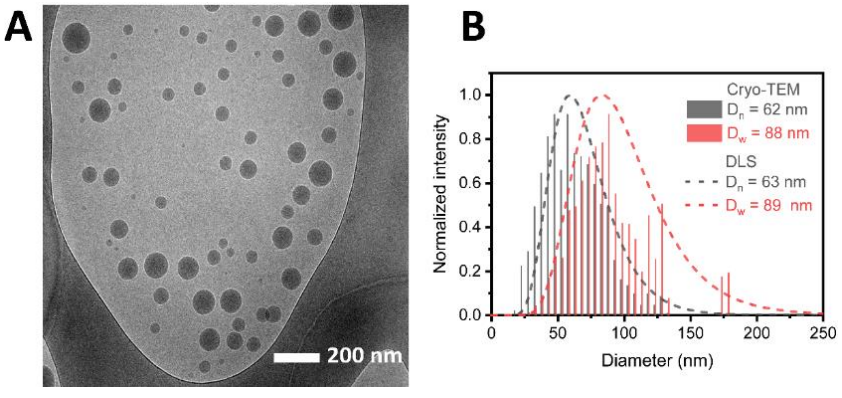

Figure IV-6. A: Cryo-TEM image of a latex obtained by **DAP-3** emulsion photopolymerization. **B**: Volume-average and number-average distributions obtained from cryo-TEM-based measures (bars) and determined from DLS data (dashed line) after conversion of intensity distribution through Mie theory. D_n and D_w are respectively number-average and volume-average diameters. DAP-3 was stabilized with 50 mM DBHQ.

Table IV-1 Reproducibility experiments for the emulsion photopolymerization of **DAP-3**.

Run	z-average diameter nm	PDI^{DLS}	$\bar{M}_n$ kg mol^{-1}	$\bar{M}_w$ kg mol^{-1}	Đ
1	94.4	0.15	12.6	36	2.8
2	93.4	0.19	-	-	-
3	100.0	0.17	-	-	-
4	104.0	0.17	13.8	43.8	3.2
5	104.0	0.14	15.7	45.8	2.9
6	91.6	0.18	-	-	-
7	102.0	0.17	13	34.3	2.6
8	93.9	0.18	16.6	54.9	3.3
9	99.3	0.18	12.2	29.8	2.4
Average	98.0	0.17	13.5	37.9	2.8
Standard dev.	4.8	0.01	1.36	6.7	0.3

Figure IV-7A shows the evolution of number-average molecular weight ($\bar{M}_n$) and molecular weight dispersity ($Đ = \bar{M}_w/\bar{M}_n$) as function of ene-conversion. At the end of irradiation (20 min), the molecular-weight distribution was relatively broad (Đ = 2.8), and a maximum ($\bar{M}_n$) value of 14,000 g mol^{-1} was achieved. This latter value is reasonable from the practical viewpoint and given the difficulty of obtaining high-molecular-weight polymers in a step polymerization. Significant increase in molecular weights was reported near the very end of the reaction (> 97% conversion), consistently with a step polymerization. However, the polymerization slightly departs from the normal step pathway as revealed a comparison with Carothers equation ($DP_n = \frac{1}{1-conv}$) (**Figure IV-7B**). In our case, a higher number-average degree of polymerization was obtained at moderate percent of conversion (60 – 95%). The underlying reason is unclear at this time although such evolution was observed in certain step polymerizations, which involves fast reactions rates and separation of monomers in two phases.[254,255] Under these conditions, monomers can react preferentially at the interface with the growing polymer chain ends instead of creating new chains, thus driving higher molecular weights. It is hypothesized that such interfacial polymerization may occur in our system, primarily dictated by the high-rate constants of thiol-ene reaction and distinct partitioning of **3** and DAP in aqueous phase and polymer particles based on their different solubility in water (**3** has a water solubility about 80 times higher than DAP). The fact that almost complete

conversion was achieved with a 1:1 stoichiometric ratio suggests that partitioning effects are not overly significant. However, further study is necessary to understand these results.

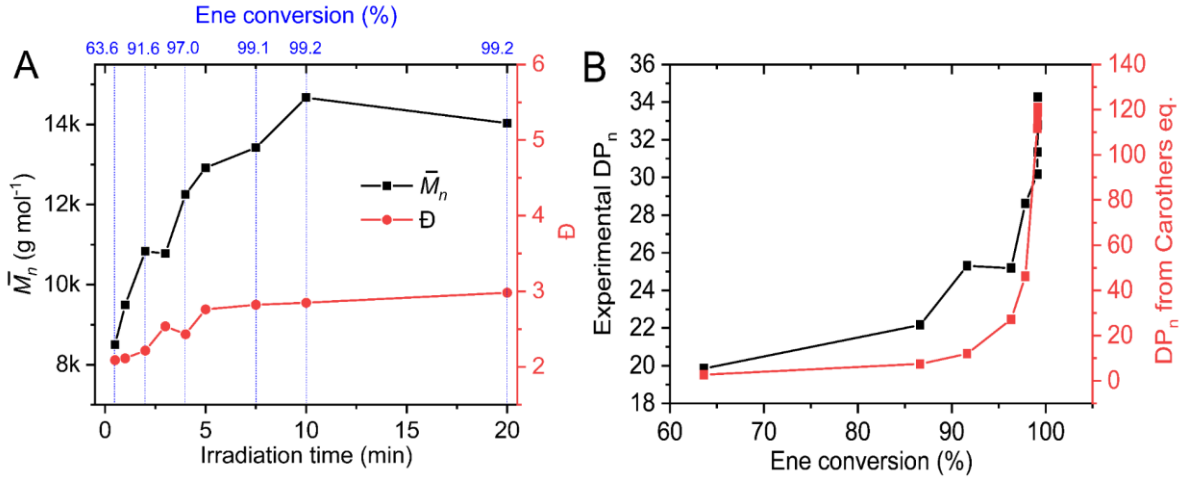

Figure IV-7. A: Dependence of number-average molecular weight ($\bar{M}_n$) and dispersity (Đ) on monomer conversion and irradiation time for emulsion photopolymerization of **DAP-3** at 25°C. The vertical blue lines show the corresponding ene conversion at a specific irradiation time. B: Comparison between experimental number-average degree of polymerization (DP_n) and theoretical values derived from Carothers equation (DP_n=1/(1-Conv.) for two monomers in equimolar quantities) as a function of ene conversion.

A salient feature of thiol-ene polymerization compared to chain-growth polymerization is its insensitivity to oxygen inhibition.[256] This was firstly confirmed by unchanged polymerization kinetics and particle size when purging the reactor with nitrogen to flush out oxygen (**Table IV-2**). On the other hand, lower $\bar{M}_n$ values levelling off at approx. 10 300 g mol^{-1} were systematically obtained in photopolymerization under nitrogen atmosphere. We postulated that atmospheric oxygen might cause a loss of thiol groups by thiol air oxidation. Although the net result of a stoichiometric imbalance between the functional groups is normally a decrease the degree of polymerization, the opposite trend was found in our case. This is probably due to the formation of thiyl radical-terminated chain ends by air oxidation and their subsequent bimolecular coupling reaction to yield disulfide bonds.

Table IV-2 Influence of different parameters on emulsion photopolymerization of **DAP-3** thiol-ene couple. **EP1** (reference sample): solids content 10 wt%, [DBHQ] = 50 mM (based on monomer vol.), photoinitiator (TPO-Li) 2 wt% with respect to monomer weight added before emulsification, [SDS] = 13.5 mM (based on water vol.), LED Irradiation at 385 nm, I = 3.7 mW cm^{-2}, 20 min; **EP2:** TPO-Li was added after emulsification; **EP3**: the macroemulsion was purged with nitrogen for 20 min before photopolymerization.

Sample name	z-average diameter nm	PDI^{DLS}	$\bar{M}_n$ kg mol^{-1}	$\bar{M}_w$ kg mol^{-1}	Đ
EP1 (ref.)	97.8 ± 5.1	0.17 ± 0.01	13.5	37.9	2.8
EP2	101.5 ± 3.1	0.15 ± 0.07	-	-	-
EP3	98.9 ± 2.2	0.17 ± 0.07	10.3	24.3	2.3

The validity of this assumption was assessed by exposing the two latexes produced under air and nitrogen to a reducing solution containing DL-dithiothreitol. As shown in

Figure IV-8A, only the latex produced under air showed a reduction of molecular weight from 13,500 to 9,300 g mol^{-1} and a narrowed molecular weight distribution (Đ = 2.2). Moreover, a close inspection of the ^{1}H-NMR spectra in DMSO-d^6 (

Figure IV-8B) revealed that only this latex displayed disulfide-adjacent methylene protons (-S-S-C*H*$_2$-CH_2) appearing as a distinctive triplet at 2.83 ppm. After treatment with DL-dithiothreitol, this resonance almost vanished, thereby providing evidence of S-S bonds in the original polymer backbone. Conversely, the resonance assigned to monosulfide-adjacent methylene protons (-S-C*H*$_2$-CH_2) – resulting from thiol-ene addition and arising at 2.68 ppm – was not affected by DL-dithiothreitol in both cases. In all polymers, the triplet peak from the terminal thiol protons (1.58 ppm) was also not detected, consistently with the high ene conversion (> 99%) determined by NMR. Consequently, it is not possible to assume for a reaction performed in ambient conditions that the initial thiol-allyl stoichiometric ratio is the effective stoichiometric ratio throughout the polymerization from start to finish. However, a quantitative analysis of the polymer ^{1}H and ^{13}C NMR spectra reveals that an average polymer chain contains 99% thioether monomer and only 1% of disulfide linkages. Except for the occasional presence of S-S bonds, thiol-ene polymerization with no possibility of chain transfer yields only linear poly(thioether) chains without branching. Therefore, the final polymer composition and structure are well-defined because only dictated by the alternating sequence of DAP-3 units.

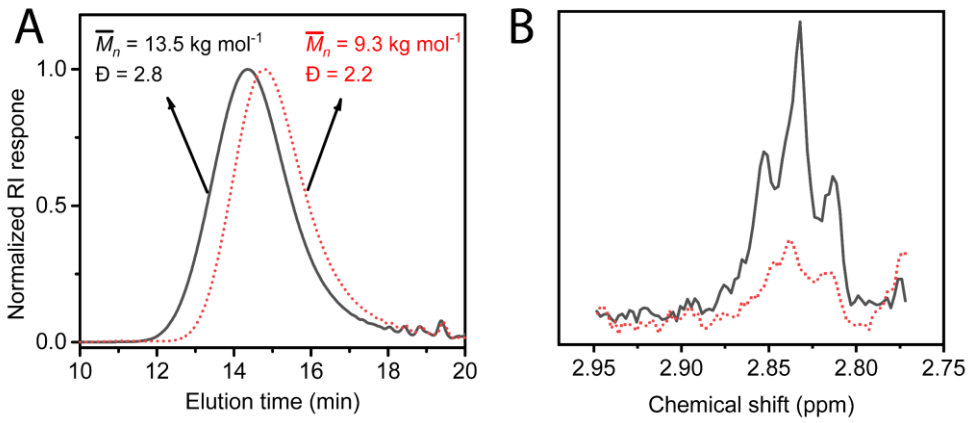

Figure IV-8. Effect of reducing agent (DL-dithiothreitol) on the SEC profile (A) and ^{1}H NMR spectrum in $CDCl_3$ (B) of a poly(thioether) latex produced under air by **DAP-3** emulsion photopolymerization. Solid line: as-synthesized latex. Dotted line: the same latex after treatment with DL-dithiothreitol (excess amount in DMSO-d^6, 12 h at room temperature). The NMR spectrum shows the 2.75 – 2.95 ppm region with the triplet resonance of the disulfide-adjacent methylene protons (-S-S-CH_2-CH_2) centered at 2.83 ppm. DAP-3 was stabilized with 50 mM DBHQ.

3.2 Key features of emulsion thiol-ene photopolymerization

Photochemically initiated thiol-ene emulsion polymerization has several advantageous features, that are successively highlighted in the following section: (**i**) temporal control of reaction, (**ii**) molecular weight tunable by irradiance, (**iii**) latex functionalization, (**iv**) high solids content latex, and (**v**) lower particle size and higher molecular weights compared with conventional redox initiators.

(i) Temporal control of **DAP-3** emulsion polymerization was investigated by switching on/off the irradiation source at different times over the course of the reaction. The instant on/off capacity of LED is indeed a distinctive advantage compared to conventional UV arc radiation sources. As can be seen in **Figure IV-9**, monomer conversion occurred only when the reactor was placed under UV exposure, while an almost complete and instantaneous interruption was observed when the irradiation was stopped. This result can be understood on the basis of faster termination rate constants (k_t = 2 x 10^8 L mol^{-1} s^{-1}compared to rate constants controlling propagation (k_{add} = 2 × 10^6 L mol^{-1} s^{-1} and k_H = 2 × 10^5 L mol^{-1} s^{-1}).[51] This distinctive feature is of interest to limit the risk of runaway reaction whereas the continuous generation of radicals cannot be stopped in a thermal polymerization due to thermal inertia. Keeping the same light dose as for continuous irradiation, similar monomer conversion (> 99%) and intensity-average diameter (95 nm) were achieved.

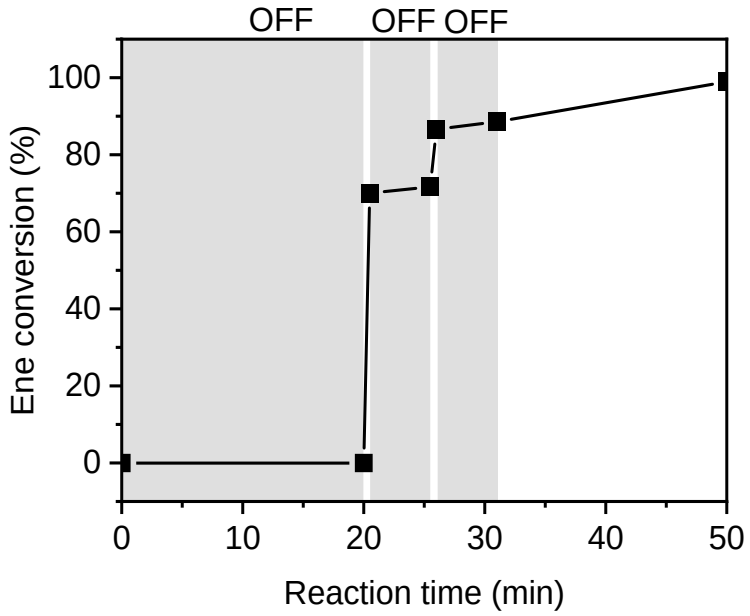

Figure IV-9. Effect of discontinuous irradiation on ene conversion-time for **DAP-3** emulsion photopolymerization. Grey areas correspond to periods of non-UV exposure while the white areas the system was exposed to radiation for 30 s. Irradiation was performed in a LED circular photochemical reactor: λ_{max} = 385 nm, I = 3.7 mW·cm^{-2}. DAP-3 was stabilized with 50 mM DBHQ.

(ii) **Figure IV-10A** is the evolution of molecular weight as a function of irradiance. At very low irradiance (0.4 mW cm^{-2}), only moderate molecular weights were found (3,800 g mol^{-1}). The main reason is probably that irradiation time of 20 min is not sufficient, leading to low monomer conversion (34%) and large particle sizes (> 600 nm). In the 0.9-3.7 mW cm^{-2} irradiance range, an almost full conversion (> 99%) could be reached after 20 min. While particle sizes were slightly changed (90 – 120 nm), number-average molecular weights progressively increased from 7,000 to 13,000 g mol^{-1}. This trend illustrates the dependence of molecular weight on the concentration of initiating radicals and demonstrates the ability to control the molecular weight by tuning irradiance. It is possible that slightly greater conversions achieved at higher irradiance (not easily detectable by ^{1}H NMR) account for the higher $\overline{M}_n$ values found experimentally.

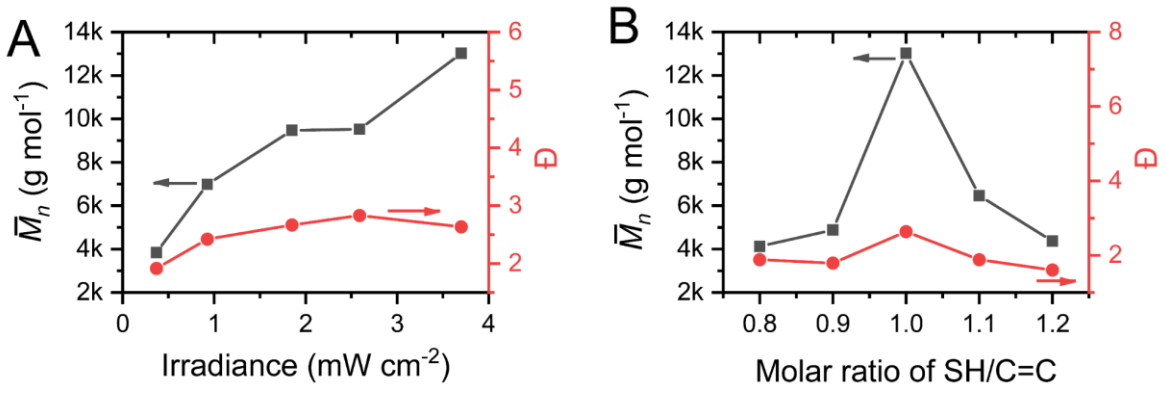

Figure IV-10. In A, a 1:1 thiol-ene ratio was used; in B, an irradiance of 3.7 mW·cm^{-2} was chosen, in both cases the irradiation time at 385 nm was 20 min. DAP-3 was stabilized with 50 mM DBHQ.

(iii) Another critical feature of thiol-ene step growth polymerization is its potential to control functional groups on the surface of the particles by using off-stoichiometric monomer feed ratios. **Figure IV-10B** shows the variation of molecular weight depending on thiol:ene stoichiometric ratio. As expected, a stoichiometric imbalance in ene or thiol caused a drastic decrease of $\bar{M}_n$ from 13,500 to 6,400 g mol^{-1} with a narrowing of dispersity from 2.6 to 1.9. Functionalization is therefore coupled to molecular weight, which is less desirable than if functionalization could be achieved independently. Nevertheless, polymers could be formed despite a significant difference in stoichiometry of functional groups. This result provides further support for an interfacial polymerization mechanism that is much less dependent on stoichiometry than a solution or mass polymerization.

(iv) All previous photopolymerizations targeted latexes with a solids content of 10 wt% (weight of solid material/weight of latex). However, much higher solids contents are generally desired for latex based on chain polymerization to maximize the reactor production and minimize transport costs.[257] To evaluate the flexibility of our process, the organic phase content was varied from 5 to 40 wt% while keeping surfactant concentration at 3.5 wt% (with respect to monomers) and the irradiation conditions unchanged. The effect on particle size and molecular weights are shown in **Figure IV-11**. Particle diameter gradually increased from 80 to 160 nm at higher solids content, but without noticeable variation in particle size distribution (PdI^{DLS} = 0.18) and conversion (> 98-99%). Conversely, molecular weight was lowered to 8,500 g mol^{-1}. It is likely that at higher solids content, slightly lower conversions were obtained, thus requiring probably more irradiation time to achieve higher molecular weights. However, one must emphasize the possibility to produce a latex with a high solids

content (40 wt%), reasonable molecular weights, without residual monomer (intrinsic property of a step polymerization) and no coagulum.

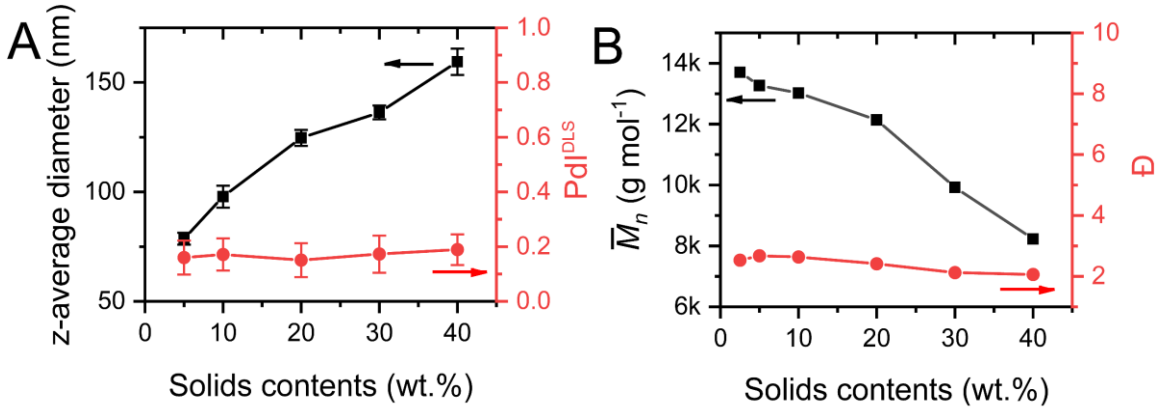

Figure IV-11. **A**: Effect of solids content on particle average diameter (z-average values) and size distribution (PdI^{DLS}) (A); **B**: Effect of solids content on molecular weight ($\bar{M}_n$) and polydispersity (Đ). DAP-3 was stabilized with 50 mM DBHQ and SDS amount was kept at 3.5 w%/monomer.

(v) Conventional emulsion polymerization generally relies on thermal initiators operating at a minimum temperature of 75 °C for their decomposition. Conversely, water-soluble redox initiators can be exploited at room temperature, and make possible a comparison with our photoinitiated system since the polymerization can be carried out at 25°C in both cases. We used a tricomponent system based on hydrogen peroxide (oxidant) together with ascorbic acid (reductant) and ferrous ion (catalyst), that is a common water-soluble redox initiator.[250] As can be seen in **Table IV-3**, redox initiation yielded broader particle size distribution (PdI^{DLS} = 0.22), much larger average-diameter (422 nm) and was marked by a 2-fold decrease in molecular weight (6,800 g mol^{-1}) compared to TPO-Li photoinitiator. The difference of results can be interpreted on the basis of distinct rates of radical generation. Despite non-homogeneous and limited radiation distribution, it is expected that a photochemical initiation produces a higher rate of initiation, thus increasing the number of polymer particles formed. We should note that high particles numbers are associated with small particle size. Higher polymerizations rates can be driven by a higher number of particles in a photochemically induced polymerization. Conversely, radical generation by redox initiator may be less efficient at 25°C, leading to smaller number of particles, and lower molecular weights.

Table IV-3. Effect of initiator on latex properties derived from **DAP-3** (thiol:ene = 1:1 equiv.) emulsion photopolymerization performed at 25°C.

Initiator	D_z nm	PdI^{DLS}	ene Conv. %	$\bar{M}_n$ kg mol^{-1}	Đ
TPO-Li[a]	97.8 ± 5.1	0.17	> 99	13.5	2.8
Ascorbic acid/H_2O_2/Fe^{2+} [b]	422 ± 30	0.22	> 99	6.8	2.6

Irradiation at 385 nm, I = 3.7 mW cm^{-2}, 20 min. [a] 0.03 equiv. of the water-soluble radical photoinitiator TPO-Li was used, [TPO-Li] = 7 mM. [b] The mixture of ascorbic acid/H_2O_2/Fe^{2+} (0.04:0.04:0.001 equiv.) acts as a redox initiator.

3.3 Fundamentals of particle formation

A detailed understanding of the mechanisms that govern particle formation is essential in emulsion polymerization because they dictate the final particle size (D_n) and number (N_p) (in a batch polymerization), which are fundamental properties of a latex. Particle formation mechanisms are complex, and the insight given by mechanistic approaches (radical entry and exit, aqueous events) and experimental methods have been instrumental to understand the formation mechanism in an emulsion polymerization proceeding by a radical chain polymerization. There are three main mechanisms of particle formation, namely, micellar, homogeneous, and droplet nucleation, as discussed in **CHAPTER I.2.2.2**. However, their relative contribution can vary significantly depending on surfactant concentration, monomer's water-solubility, and size of monomer droplet.[6] Under conventional emulsion polymerization conditions, where the monomer droplet formed in the micrometer range size, particle formation by droplet nucleation can be considered as insignificant. Attention is therefore focused on the other two mechanisms, which control particle number of the latex. It is well-accepted that homogeneous nucleation is the active mechanism at surfactant concentrations below its critical micelle concentration (CMC). At above CMC, both micellar and homogeneous nucleation operate simultaneously but with different extents. There is a general consensus that micellar nucleation may be the predominant mechanism of particle formation for monomer having water solubility less than 15 mM. On the other hand, there is the broad opinion that the higher the water-solubility of the monomer, the higher is the likelihood of homogeneous nucleation, even in the presence of micelles. The higher there is the equilibrium monomer concentration in the aqueous phase, the higher is the probability that a monomer initiation and propagations take place in water.[64] However, it is generally very difficult to prove unambiguously which of the two nucleation mechanisms is

predominant despite the very high number of publications on this subject. Whichever particle formation mechanism is dominant, an important consideration for the latex preparation is to be able to predict and explain the dependence of N_p on the surfactant concentration [S], initiator concentration [I], temperature and the monomer used. There is an extensive literature on this subject for chain growth emulsion polymerization. Since the pioneering work of Smith and Ewart. This alter suggested that above the CMC for a dominant micellar nucleation, the final particle number should be proportional to $[I]^{0.4}[S]^{0.6}$. Subsequent work demonstrated the same exponents can be predicted from a homogeneous nucleation model and cannot be used as a proof to support a micellar nucleation mechanism. Fitch, Gardon, Sutterlin, El-Aasser, demonstrated a wide range of exponents, but many studies reported a sigmoidal curve of log N_p vs log [S] with a dependence of $x = 0.6$ for reasonable water-insoluble monomers, above CMC and up to a limiting [S].

With the advent of step polymerization in emulsion such as emulsion thiol-ene polymerization, it is important to know whether changes in the particle formation mechanism and the dependence of N_p occur. In order to gain a clearer picture about particle formation in a thiol-ene step-growth emulsion polymerization, we studied firstly the influence of monomer polarity on particle size using a range of thiols (**1**-**6**) and ene (**DVE**, **DAP**, **DAA**, **CHDM**) having different water solubility (**Scheme IV-2**). To move forward, the effects of thiol/ene monomer polarity and the plot N_p =f([S]) was then investigated thoroughly. The region above the CMC was under scrutiny to assess the dependence of N_p on [S].

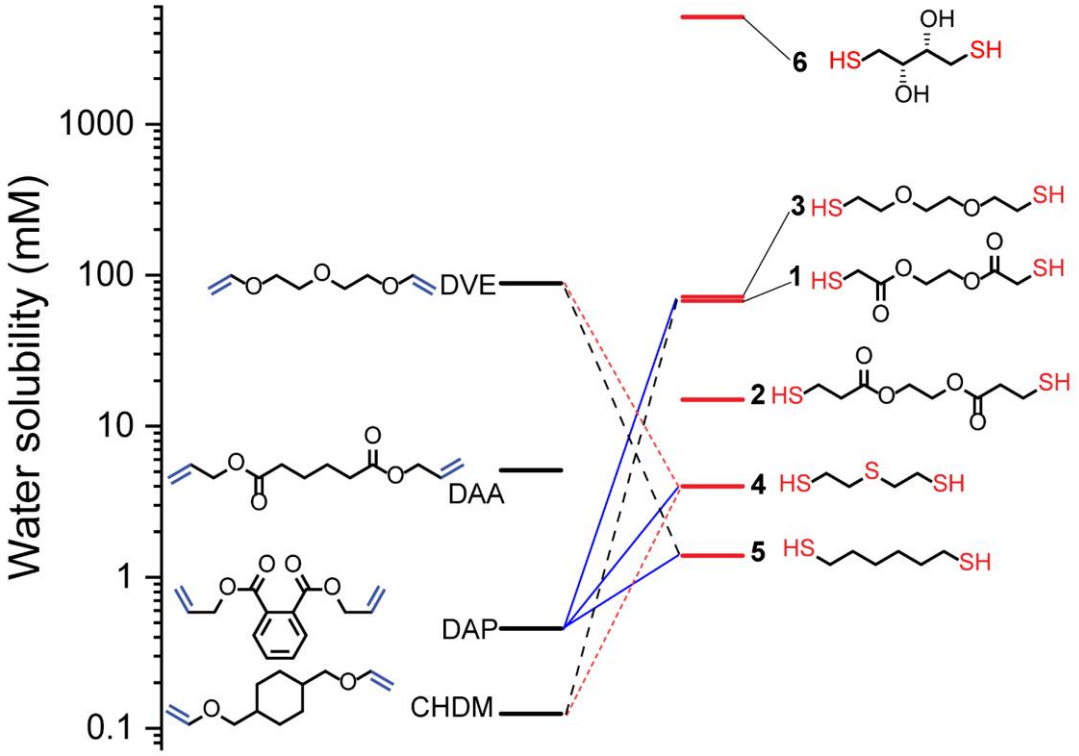

Scheme IV-2 Experimental plan for investigating the influence of [SDS] on N_p.

3.3.1 Influence of monomer polarity on particle size

Two sets of polymerization were conducted: **DAP** with a series of thiols (**1**-**6**), and thiol **3** with a series of enes (**DVE**, **DAP**, **DAA**, **CHDM**). At the end of each reaction, conversion in ene functional group, molecular weight, and particle size were determined (**Table IV-4**). In all cases, quantitative conversions were achieved, $\bar{M}_n$ ranged from 4.5 to 13.5 kg mol^{-1} and $Đ$ spanned from 2 to 4. Considering particle size, the general trend is that smaller particle sizes are obtained upon decreasing thiol or ene monomer's polarity. For example, using **DAP** as ene, particle size went from 187 nm (D_z) for the most water-soluble dithiol (**6**) to below 100 nm for some dithiols of very limited water-solubility (**4** and **5**). A similar behavior is observed when polymerizing thiol **3** with various enes. The z-average diameter is inversely dependent on the ene monomer solubility: 185 nm for **DVE**, the most water-soluble ene *versus* 64 nm for **CHDM** showing the lowest solubility in water. The density of surfactant molecules adsorbed at the particle surface controls particle size, and is strongly dependent on the polymer (monomer) polarity. An increased polymer's (monomer 's) hydrophilicity leads to a higher probability of particle coagulation and greater particle sizes, in line with the trend observed experimentally. To gain deeper insight into the way the particles are formed, we

have examined the evolution of the number of particles per liter of latex (N_p, L^{-1}) as a function of surfactant concentration.

Table IV-4 Influence of monomer polarity on final particle size and distribution. All of the formulations were prepared at [SDS] = 13.2 mM and [TPO-Li] = 7.5 mM. Emulsion photopolymerizations were conducted at 25°C, irradiation time 20 min, UV-LED 385 nm, 3.7 mW cm^{-2}. Monomers were stabilized with 50 mM DBHQ/monomer volume and conversion in all cases > 90%

Diene	Water solubility (mM)	Dithiol	Water solubility (mM)	$\bar{M}_n$ (kg mol-1)	Đ	D_z (DLS) (nm)
DAP	0.46 ± 0.27	6	5.1 x 10^3	5.5	2.6	187
		3	72 ± 10	13.5	2.8	98
		1	67 ± 28	6.7	2.3	69
		2	15 ± 0.8	4.5	2.0	118
		4	4 ± 0.1	9.3	2.4	77
		5	1.39 ± 0.39	7.6	2.9	53
DVE	86.6 ± 0.6	3	72 ± 10	9.1	1.8	185
DAA	5.1			5.4	2.1	111
DAIP	0.2			10.9	4.0	103
DATP	0.17			10.4	2.3	67
CHDM	0.13			6.2	1.9	64

3.3.2 Influence of monomer polarity on particle size (number)

3.3.2.1 Analysis of particle size

To calculate N_p (L^{-1}), we employed volume –average diameters (D_v) determined by DLS and cryo-TEM was used subsequently to verify the validity of our approach. To this purpose, three latexes samples **DAP-3**, **DAP-4** and **DAP-5** were prepared using a constant SDS concentration (20 mM) and subsequently analyzed by cryo-TEM. The results are provided in **Table IV-5** and **Figure IV-12**. There is a good agreement between the number-average particle diameters (D_n) and volume-average particle diameters (D_v) found with the two techniques. This lends confidence to the values of N_p determined from $D_v(DLS)$. The intensity-weighted average particle size ($D_z(DLS)$) exhibits a discrepancy for the latex derived from **DAP-5** due to a presence of a small fraction of large particles. For the sake of comparison, it is therefore preferable of not using D_z values for calculation of N_p. With the exception of **DAP-3**, the PdI^{TEM}

values of **DAP-4** and **DAP-5** latexes are significantly smaller than PdI^{DLS} since electron microscopy can overcome the strong dependence of detector-response with respect to the large particles. Because PdI^{TEM} provides a better representation of particle size distribution, it is then used for comparison. As can be seen in **Figure IV-12**, **DAP-3** presents a much broader particle size distribution compared to **DAP-4** and **DAP-5**. This could result from a mixed mode of homogeneous nucleation (secondary nucleation) and micellar nucleation due to the high-water solubility of dithiol **3**.

Table IV-5 Particle size characterization for latexes prepared with **DAP** and thiols (**3**-**5**) at [SDS]= 20 mM.

	D_n (nm)	D_v (nm)	D_z (nm)	PdI^{DLS}	D_n (nm)	D_v (nm)	PdI^{TEM}
DAP-3	59	68	99	0.15	61	69	0.15
DAP-4	35	39	57	0.19	37	40	0.09
DAP-5	17	21	38	0.22	18	20	0.10

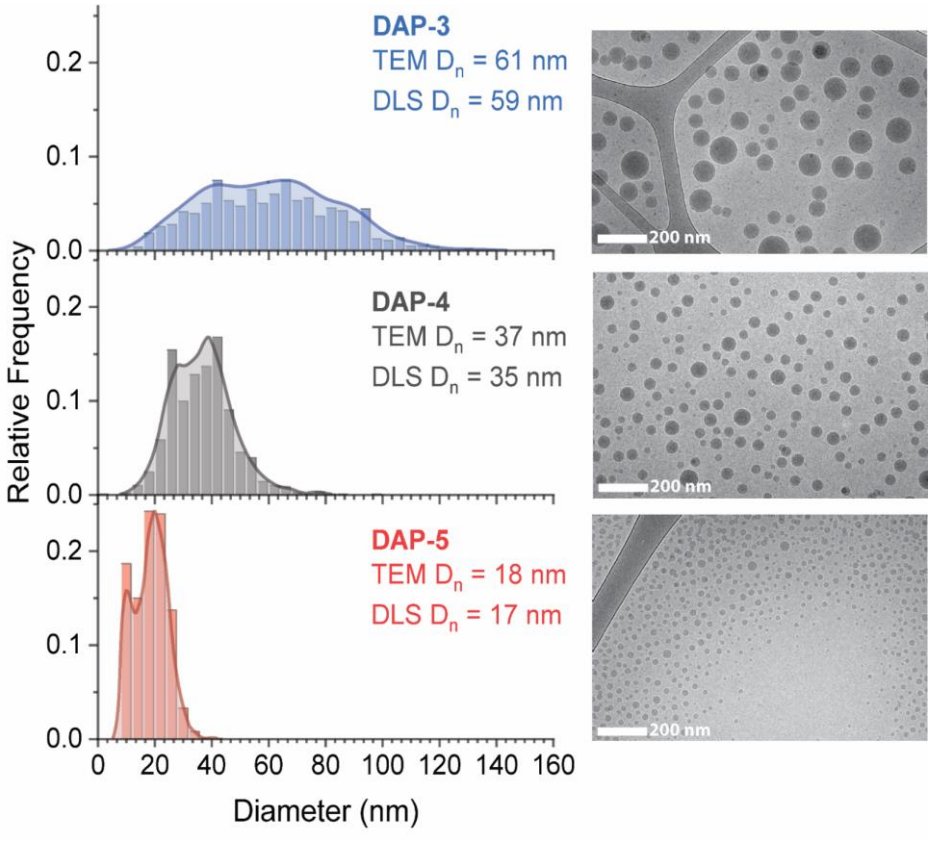

Figure IV-12 Particle size distributions of three latexes, prepared at [SDS]= 20 mM. Data were fitted with kernel density estimation functions. In all cases the bin size is 4 nm, and Scott's rule was used to determine the bandwidth. Histograms are based on analysis of 1089 particles(**DAP**-**3**), 1192 particles (**DAP**-**4**) and 2845 particles (**DAP**-**5**). Monomers were stabilized with 50 mM DBHQ/monomer volume.

3.3.2.2 Number of polymer particles and effect of surfactant concentration

Case of DAP. Three separate sets of experiments were conducted using **DAP** in conjunction with three dithiols of different water-solubilities: **3** (high), **4** (medium), **5** (low). [SDS] was varied from 0.1 mM to 200 mM. **Figure IV-13** is a plot of N_p as a function of [SDS] in logarithmic scale for the three latexes prepared with **DAP** and three dithiols of variable water-solubility: **3** (high), **4** (medium), **5** (low). Regardless of the thiol, it is clear that the plot $N_p \propto [SDS]^x$ cannot be fitted by a single exponent of x. A typical sigmoidal shape is visible, where four regimes depending on the surfactant concentration can be distinguished, each characterized by a different x value.

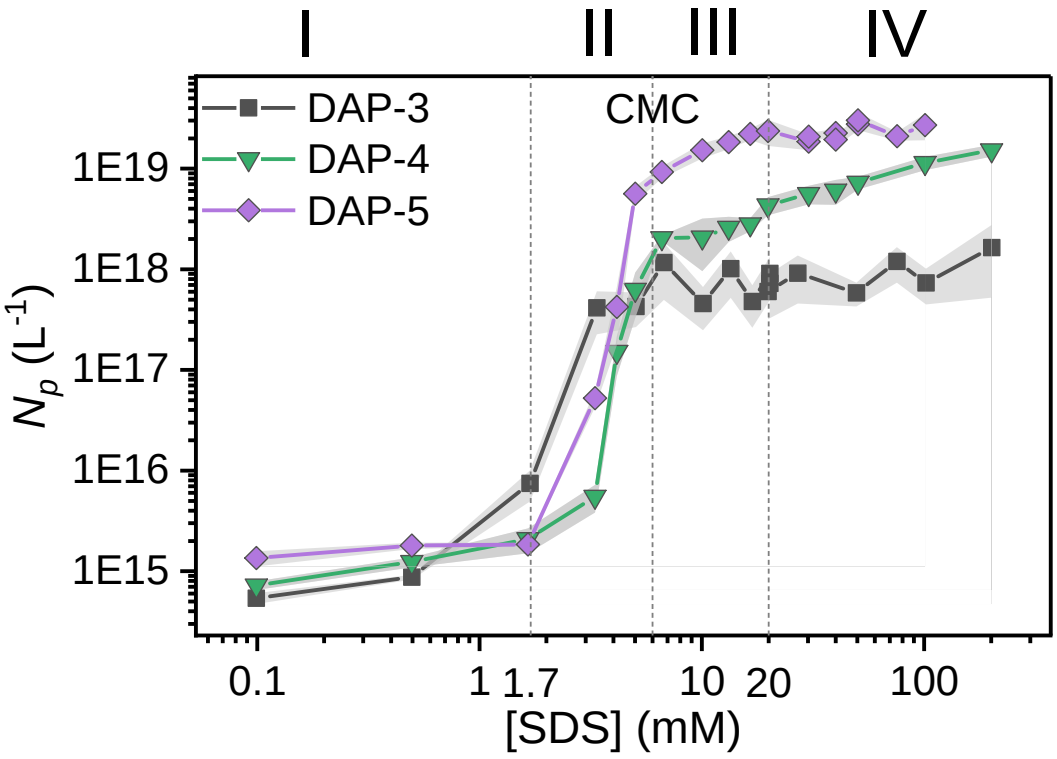

Figure IV-13 Particle number as a function of [SDS] for **DAP**-dithiol systems.

Clearly, for 0.1 mM < [SDS] < 2 mM (region I), the surfactant has negligible effect on N_p (x = 0) and homogeneous nucleation is the only active nucleation mechanism. There is a sudden change in N_p when [SDS] is closed to its CMC (region II), particularly pronounced for thiols with medium (**4**) and low water-solubility (**5**). The spike in N_p occurs at [SDS] of about 3 to 6 mM. This agrees with the CMC value of SDS reported in literature which varies in a wide

range from 1.7 to 9 mM, we adopt a CMC of SDS at 6 mM as reported by Sütterlin.[258–260] In addition, this region is also marked by a change of the latex optical properties, from turbid to translucent. The lower the water-solubility of the thiol monomer (the resulting polymer), the more steeply rises the particle number near CMC. Such steep rises in particle number near CMC might be accounted for the occurrence of a second mode of particle formation via micellar nucleation (**Figure IV-14**).

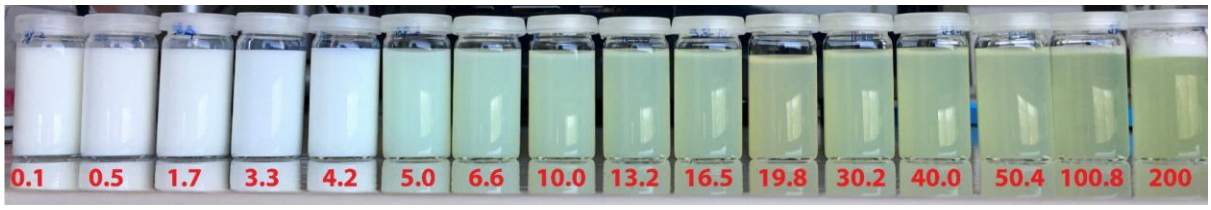

Figure IV-14 The transmission of the latex increases upon increasing SDS concentration, from left to right the concentration of SDS increase in the range of 0.1-200 mM, **DAP-5** system.

At [SDS] > CMC (region III) in **DAP-3** system, N_p is relatively independent of [SDS] over a broad range of concentrations (x = 0.17).[151] In contrast, the **DAP-4** and **DAP-5** systems exhibit a steady increase of N_p vs [SDS], with x = 0.65 and 0.77, respectively. Clearly, the exponent decreases with increasing thiol water-solubility. This reflects a growing agglomeration tendency due a reduced effectiveness of adsorption on particle surface, in other words, the surface concentration of surfactant molecule (Γ, in mol/cm^2) is likely to be smaller on a more hydrophilic polymer particle surface which disfavors the packing of surfactant necessary to obtain minimum particle size. At SDS concentration above 20 mM, a last region IV can be defined where x = 0.65 for **DAP-4** (**Figure IV-15**) and x = 0 in the case of **DAP-5**. The decline of x is not easy to understand and may be explained by a more effective SDS adsorption on the particle surface in the case of **DAP-4**.

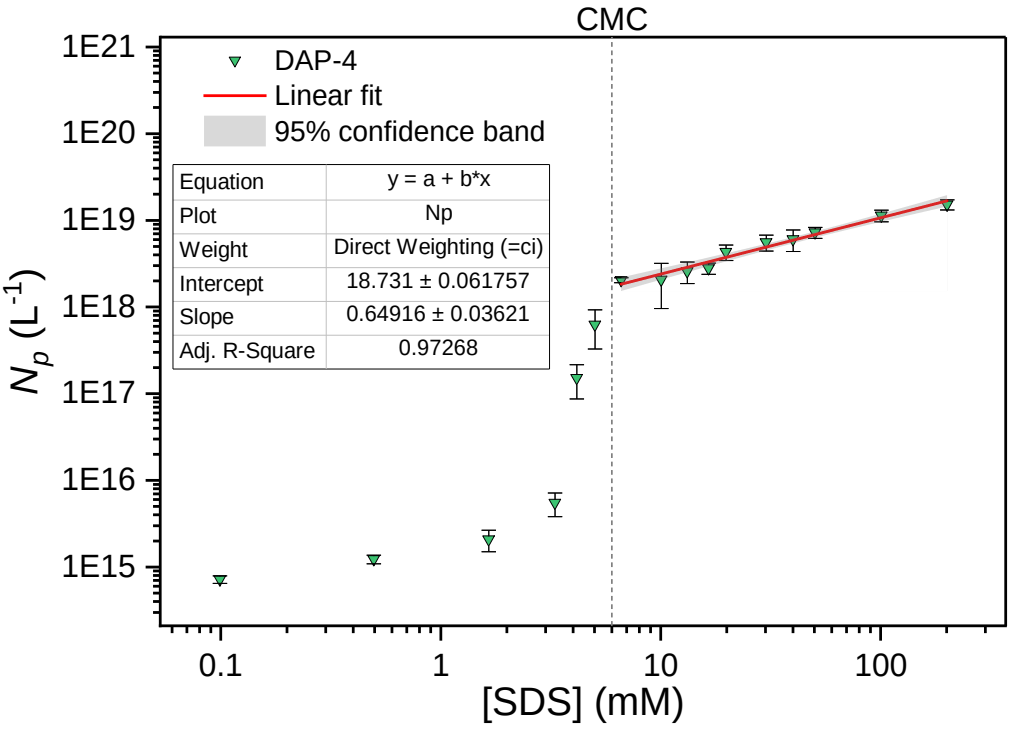

Figure IV-15 Linear-fitting is applied for **DAP-4** system

Case of CHDM and DVE. Likewise, we have investigated the dependence of *x* in the region III (20 mM > [SDS] > CMC) for poly(thioether)s prepared with two other dienes, **CHDM**, less water-soluble than **DAP**, and **DVE**, more water-soluble than **DAP** (**Scheme IV-2**) using again the same three thiols (**3**-**5**). The $N_p \propto [SDS]^x$ plots shown in **Figure IV-16** all exhibit a sigmoidal shape. Interestingly, *x* remains at a high level for the three latexes prepared with **CHDM** (plot **A**) whatever the thiol used: *x* = 0.75 (**3**), *x* = 1.05 (**4**) and *x* = 0.96 (**5**). Even with the most water-soluble thiol **3**, step polymerization with highly water-insoluble **CHDM** drives a sufficiently low polar particle surface to allow the surfactant adsorption, resulting in a high value of x. Conversely, when choosing the more water-soluble **DVE** (plot **B**), there is no clear dependence of N_p on [SDS] at above CMC for thiols **3** (*x* < 0) and **4** (x = 0.21). The reduced adsorption efficiency of SDS on the more polar surface results in a higher agglomeration tendency, and the incapacity for more surfactant molecules to adsorb onto particle surface to further reduce particle size above CMC. Only the copolymerization of **DVE** with the most water-insoluble thiol **5** enables to increases the adsorption effectiveness, resulting in a *x* value of 0.66.

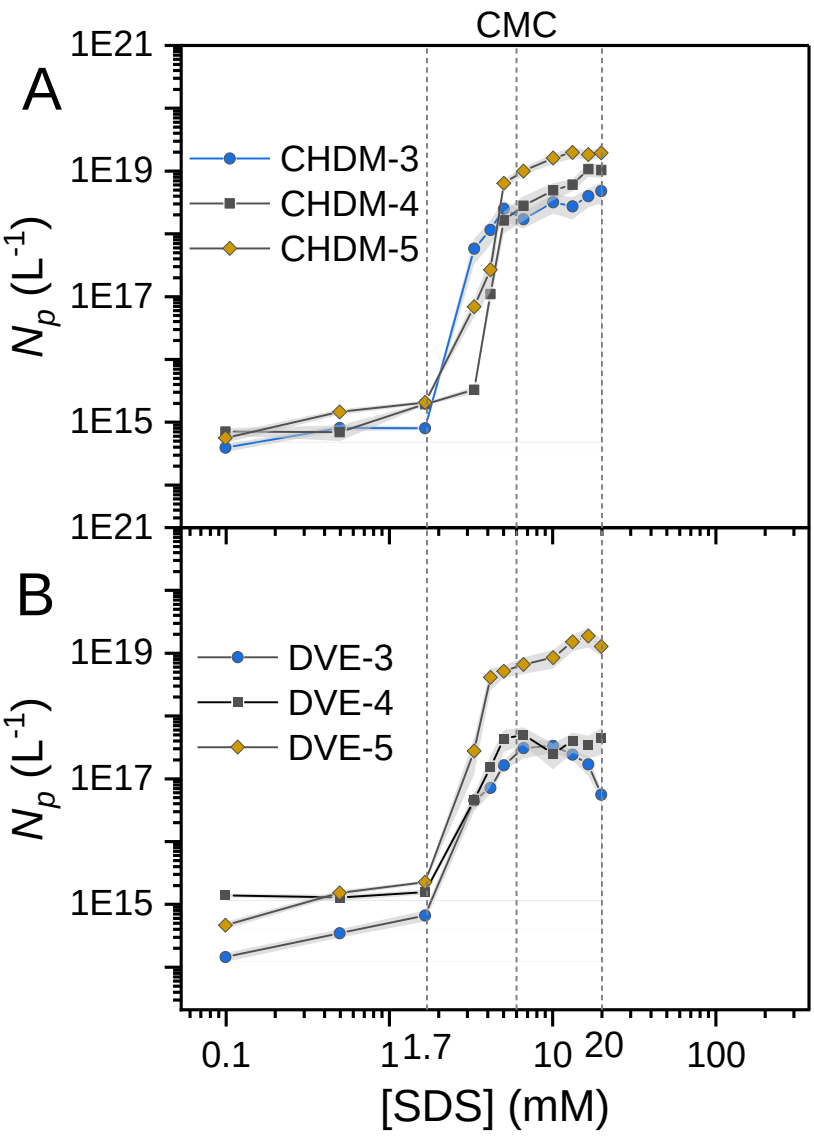

Figure IV-16 Particle number as a function of [SDS] for some diene-dithiol systems.

Finally, we tried to correlate the values of *x* with the water-solubility of both thiol and ene compounds. As shown in **Figure IV-17**, above CMC, *x* decreases with either thiol or ene polarity. One can draw a parallel with an emulsion chain-growth polymerization for which a similar tendency has been reported.[259–261] Nevertheless, due to a distinctive step mechanism, there is a complex interplay between monomer solubility and *x* in a thiol-ene emulsion polymerization. As expected, the combination of two highly water-insoluble co-monomers (e.g. **CHDM**- **5**) drives a high value of *x*, whereas the coupling of two water-soluble monomers (e.g. **DVE**-**3**) gives a value close to zero or negative. More complex and difficult to predict is the combination of two co-monomers of opposite water-solubility. Interestingly, when the monomer mixture contains at least a highly water-insoluble component (e.g. **CHDM** or thiol

5), it is experimentally found that a *x* value close to **1** can be achieved even in the presence of a highly water-soluble counter-part such as **DVE** or thiol **3**.

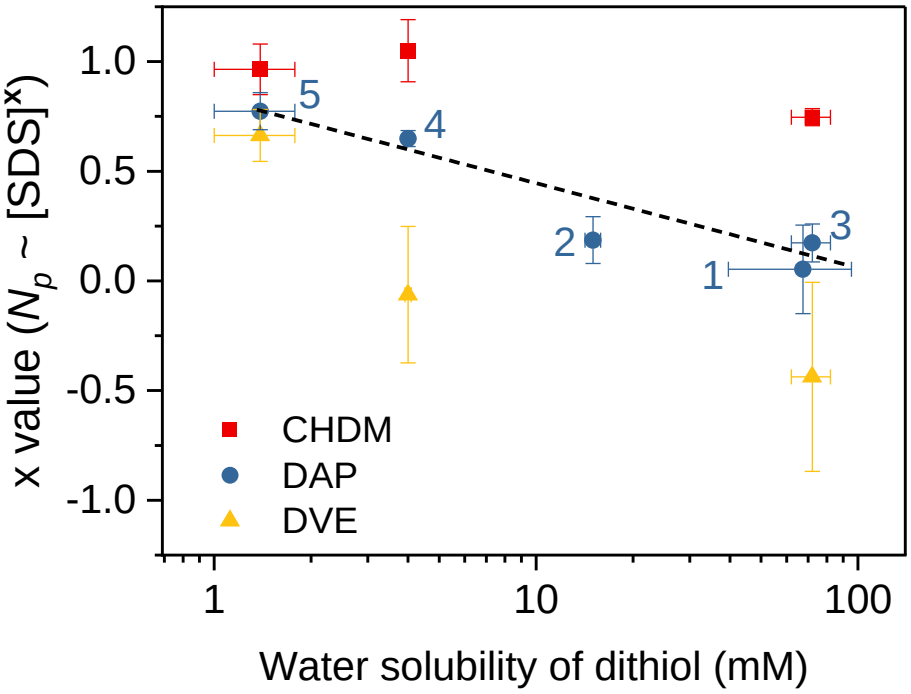

Figure IV-17 Dependence of exponents x of ($Np \propto [SDS]^x$) water solubility of monomer.

4 CONCLUSION

A systematic investigation on thiol-ene emulsion step photopolymerization in water at 385 nm was performed. Linear polymer nanoparticles with size lower than 100 nm could be synthesized from two bifunctional monomers **3** and DAP using experimental conditions very close to a conventional chain emulsion polymerization. Compared to other step polymerizations carried out in aqueous emulsion, thiol-ene polymerization has the advantage of being able to simultaneously attain both high reaction rates and reasonable molecular weights ($\bar{M}_n$ >13,000 g mol^{-1}). This new emulsion thiol-ene photopolymerization process also exhibits several advantages: stable poly(thioether) latex can be produced without high energy homogenization, at low irradiance and up to 40 wt% solids contents. The ability to harness the inherent advantages of light overheat for creating the initiating radicals has been exploited since temporal control and tuning reaction of molecular weight by irradiation intensity were demonstrated.

To gain a better understanding of particle formation during photopolymerization of thiol-ene emulsions, we systematically investigated the effect of monomer/polymer polarity

on particle size using different thiol-ene monomer mixtures. The evolution of N_p was plotted against [SDS] for different monomer systems. It was found that the sigmoidal shape of the relationship $N_p \sim [SDS]^x$ resembles that of a conventional chain-growth emulsion polymerization. Moreover, the exponent *x* above the CMC of SDS decreases with increasing polarity of the monomer, regardless of whether it is a dithiol or a diene. This study provides a practical approach to better control the particle size of the latexes by adjusting the surfactant concentration.

CHAPTER V.EXPANDING THIOL-ENE EMULSION PHOTOPOLYMERIZATION PROCESS: PHOTOCATALYSIS AND PHOTOREACTOR

1 VISIBLE-LIGHT PHOTOCATALYZED THIOL ENE EMULSION POLYMERIZATION

1.1 Motivation

The radical addition of a thiol S-H bond across an alkene is one of the archetypal "click" reactions. Its high significance in macromolecular synthesis and biochemistry mainly resides in the high efficiency of the carbon-sulfur bond-forming reaction and a broad functional group tolerance. Generally, the radical thiol-ene reaction is initiated by thermal[262] or photochemical means.[263] The decomposition of a radical (photo)initiator yields some primary radicals that abstract a hydrogen radical from thiols to form thiyl radicals. These latter species then initiate the typical thiol-ene polymerization that consists of alternating radical propagation and chain transfer reactions. Since the pioneering work of Yoon in 2013,[264] a number of redox photocatalysts are also known to mediate visible-light radical thiol-ene reactions. The main class of compounds includes transition metal complexes ($Ru(bpz)_3(PF_6)_2$,[264] $Ru\text{-}(bpy)_3Cl_2$,[265,266] $Ir(ppy)_3$[267]), metal oxide particles (TiO_2,[268] BiO_2[269]), as well as various organic photocatalysts (acridinium derivatives,[270–272] eosin–Y,[267,273–276] *N*-hydroxyphtalimide,[277] phenyl-glyoxylic acid[278]). With very few exceptions,[265,266] the mechanism is considered to involve the direct photooxidation of thiol by the electronically excited catalyst to generate a thiyl radical cation. Its subsequent deprotonation generates a thiyl radical, which is then involved in the classical thiol−ene reaction cycle as described previously. Most photocatalytic chromophores typically absorb at longer wavelengths than radical photoinitiators, and therefore are more compatible with multiple functionalized organic structures, very common in organic chemistry. Additionally, a photoredox catalysis proceeds in principle by a radical chain process mechanism involving some catalyst-regenerating turnover steps, which help minimizing the amount of catalyst used. Although many studies concluded the ease of accomplishing the thiol-ene reaction with relatively high yield (70–90%) and a minimum of side reactions, they also reported that long irradiation times (1−24 h), high catalyst loading (1-10% mol) or high irradiance were required. The studies of Yoon are an exception to this generalization.[264,265] These limitations explain that photocatalytic thiol-ene polymerization is used to much lesser extent than the corresponding small molecule reaction. From the practical viewpoint of obtaining high yields of a high-molecular-weight product, such thiol-ene step polymerizations must be run with a stoichiometric ratio of bifunctional ene and thiol monomers in a manner

allowing to obtain very high conversions (> 98-99%). The synthesis of low molecular weight telechelic poly(thioether) was described using *fac*-Ir(ppy)$_3$[279] and 4-(diphenylamino)benzaldehyde as photocatalyst.[280] Higher molecular weights and reaction rates were attained by Boyer[281] and Konkolewicz[282] through a different reaction mechanism involving an additional redox mediator, an amine or alkyl halide respectively, which circumvents the slow rate of direct photooxidation of thiol with the photocatalyst.[283]

To further expand the visible-light mediated photocatalytic thiol-ene polymerization, we describe herein an industrially relevant emulsion polymerization process to prepare linear semicrystalline poly(thioether) latexes in water, using eosin-Y disodium (EY^{2-}) as photocatalyst.[276,284] We have been successful in designing a process using low irradiance (< 5 mW cm^{-2}), applying accessible (LED) irradiation sources, using low catalyst loadings (< 0.1% mol), achieving fast reaction time scales (< 1 h), and working with a high selectivity and a wide range of monomers. All these features are in agreement with the criteria defined by Bowman for a "photoclick" reaction.[55] Additionally, the process description is accompanied by a detailed mechanistic investigation.

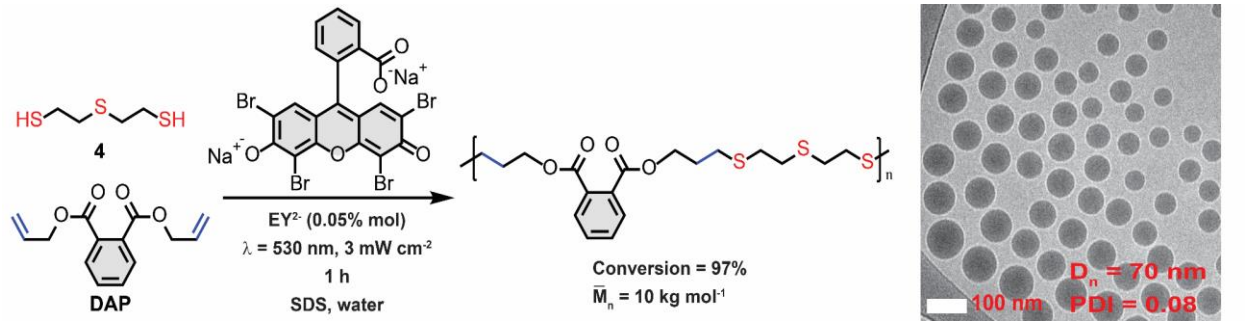

Scheme V-1. Reference thiol-ene monomer system and photocatalyst used in this study. Monomer emulsion was prepared at concentrations of SDS = 13.5 mM , EY^{2-}= 0.29 mM/water (0.05% mol / monomers) and a phosphate buffer (pH 8.0, 0.01 M) and irradiated by green LED (λ = 530 nm, I = 3 mW cm^{-2}) for one hour under magnetic stirring at 1100 rpm.

1.2 Experimental section

1.2.1 Materials

Monomers including diallyl phthalate (**DAP**, TCI, 99.0%), diallyl terephthalate (**DATP**, TCI, 99.4%), diallyl adipate (**DAA**, TCI, 99.8%), di(ethylene glycol) divinyl ether (**DVE**, BASF, > 98.0%), 1,4-bis[(vinyloxy)methyl]cyclohexane (**CHDM**, BASF, > 98.0%), 2,2'-thioldiethanethiol (**4**, Bruno Bock, 98.7 %) were used as received. Eosin disodium (**EY^{-2}**, TCI, > 95.0%), sodium

dodecyl sulfate (**SDS**, TCI, 98%) sodium phosphate monobasic and dibasic (Sigma Aldrich, >99%) and deionized water were used to prepared aqueous solutions. All solvents were used with analytical grade without further purification.

1.2.2 Synthesis

1.2.2.1 General procedure for the emulsion polymerization.

In typical reaction, monomer phase composed of a 1:1 stoichiometric mixture of thiol and ene functional groups was prepared by mixing **dithiol 4** (0.4000 g, 2.54 mmol, 1 equiv.), DAP (0.633 g, 2.54 mmol, 1 equiv.) to a 20 mL soda-lime glass vial (external diameter: 25 mm, height: 70 mm). To this latter was added an aqueous phase composed of EY^{2-} (2 mg, 0.0026 mmol, 0.02 % w/w monomer), SDS (35 mg, 3.5 % w/w with respect to monomers, 13.5 mM in water) and 9 mL of phosphate buffer 0.01 M. A coarse emulsion with an organic phase content of 10 w% was prepared using Ultra-Turrax® T25 homogenizer (IKA-Werke equipped with 8 mm dispersing tool) at 15 000 rpm for 10 min. The photopolymerization was performed immediately after emulsification at room temperature inside a LED circular photochemical reactor constructed by green LED strip (530 nm, 3 mW cm^{-2}) around a quartz cylinder (id: 80 mm, length: 100 mm). Irradiation was maintained for 60 min, while the vial was kept under continuous magnetic stirring (1100 rpm). After the reaction was completed, 50 µL aliquots were withdrawn for determination of monomer conversion (^{1}H-NMR) and particle size (cryo-TEM analysis). The remained latex was precipitated in 200 mL absolute ethanol. The polymer was collected by filtration and washed thoroughly with excess ethanol and finally dried under vacuum.

1.2.3 Characterization

1.2.3.1 Nuclear Magnetic Resonance (NMR)

The conversion in ene groups before and after irradiation was determined by ^{1}H-NMR in DMSO-d^6. A portion of 30 µL aliquot was dissolved in 570 µL DMSO-d^6. The integral of methylene protons 4.7 and 4.25 assigned respectively to proton in monomer and polymer were used for determining the conversion (see chapter IV 2.3.1) . Latexes that were insoluble in DMSO were dried after addition of radical stabilizer (pyrogallol, 1 % w) and then dissolved in $CDCl_3$ for ^{1}H-NMR measurement (Varian 300-MR)

1.2.3.2 Size exclusion chromatography (SEC)

The polymer molecular weights and their dispersity were measured by SEC (Agilent 1260 Infinity) using THF as an eluent. Detailed protocol is described in Chapter III and IV.

1.2.3.3 Dynamic Light Scattering (DLS)

Particle size and particle size distribution of the latexes were analyzed by DLS using a VASCO particle analyzer (see detailed description in characterization sections of Chapter III and IV)

1.2.3.4 Transmission Electron Microscopy (TEM)

Cryo-TEM images of the latex were acquired according to the procedure described in Chapter III.

1.2.3.5 Steady-state fluorescence quenching

The steady-state fluorescence quenching studies were carried out with a spectrofluorometer FP-8200 (Jasco Corporation, Japan) equipped with a xenon lamp. The excitation was set at 517 nm and the emission was monitored at 537 nm. The excitation and emission bandwidths (5 nm) and scan rate (1000 nm/min) were kept constant. The samples were prepared by mixing 0.1 mL EY^{-2} solution (10 µM in water) with various volumes of a **dithiol 4** solution (500 µM in water) in a set of five volumetric flasks. The flasks were completed to 10 mL mark with distilled water. These solutions were transferred to a quartz cell (4 x 1 x 1 cm) and the emission intensity of EY^{-2} were in turn collected without degassing.

1.2.3.6 UV-vis spectroscopy

UV-vis studies were conducted on a V730 UV-vis spectrometer (Jasco Corporation, Japan) operating at 1.0 nm bandwidth, scan speed 1000 nm/min. For the formation of ground state charge transfer complex study, 2 mL of EY^{-2} solution (2 µM in water) were mixed with increasing volumes of a second EY^{-2} solution containing **dithiol 4** (EY^{-2} 2 µM and **dithiol 4** 1.3 mM) in a quartz cuvette (4 × 1 × 1 cm). UV-vis spectra were recorded after each injection. For the evaluation of EY^{-2} concentration remaining after reaction, spectra of the solutions

comprising of 0.1 mL macroemulsion (before) and latex (after) in 3.9 mL DMSO were recorded.

1.2.3.7 Differential Scanning Calorimetry (DSC)

A Mettler Toledo DSC1 was used for thermal analysis. The DSC program was set from -100 to 150°C. The heating and cooling rate were 5 and 10°C/min under nitrogen atmosphere.

1.2.3.8 X-ray diffraction

X-ray diffraction (XRD) measurements were carried out in reflection mode using a D500 X-ray powder diffractometer (Siemens, Germany) with Cu-Kα radiation source (λ = 0.1542 nm) and scintillation counter. The diffractometer was equipped with a heated sample holder (Paar, Austria). The degree of crystallinity can be estimated by comparing the peak area of the amorphous polymer with that of the crystalline phase. % crystallinity = (area of crystalline peaks/total area)*100.[285]

1.2.3.9 Polarized light microscopy

The polarized light microscopy experiments were carried out with a crossed polarizers setup using a Zeiss A1 microscope equipped with a CCD camera, Axiocam ICc 1 (Zeiss, Germany). In this setup, the polarizer was placed in the light path before the sample and the analyzer, a second polarizer with a polarization direction perpendicular to the first polarizer, was positioned in the optical path behind the objective and before the CCD-camera. As plane-polarized light interacts with an anisotropic, birefringent sample, two wave components, which are polarized in perpendicular planes, are generated. Due to the different velocities of the two components by propagating through an anisotropic sample, these wave components are phase-shifted and recombine with constructive and destructive interference by passing the analyzer, which is used as a contrast for imaging anisotropic materials.

1.3 Results and discussion

1.3.1 Formulation and control experiments

We began our investigations by examining the radical thiol-ene polymerization of an emulsion based on 2,2'-thioldiethanethiol (**dithiol 4**) and diallyl phthalate (DAP) (**Scheme V-1**). A macroemulsion was prepared by mixing the mixture of thiol-ene monomers (10 %w) with an aqueous phase containing sodium dodecyl sulfate (SDS) as surfactant (13.5 mM), EY^{2-}

as photocatalyst (0.29 mM in water, 0.05% mol/monomers) and a pH = 8 phosphate buffer (0.01 M). The resulting emulsion was irradiated for one hour under green light (530 nm, I = 3 mW cm^{-2}). A stable colloidal latex suspension was obtained, displaying a high monomer conversion (> 97%), moderate molecular weights ($\overline{M_n}$ = 10 kg mol^{-1}) (**Figure V-1**) and an average diameter of 70 nm (number average diameter determined by cryo-TEM) (**Scheme V-1**). All the experimental data are summarized in **Table V-1** (entry **1**). ^{1}H NMR analysis established that linear polymer chains were formed, composed almost exclusively of thioether repeating units (CH_2-CH_2-S-). Only a small fraction of disulfide bonds was detected (2-3%). No sulfone or sulfoxide group was observed, ruling out the possibility of over-photooxidation reactions of the thioether units.[267]

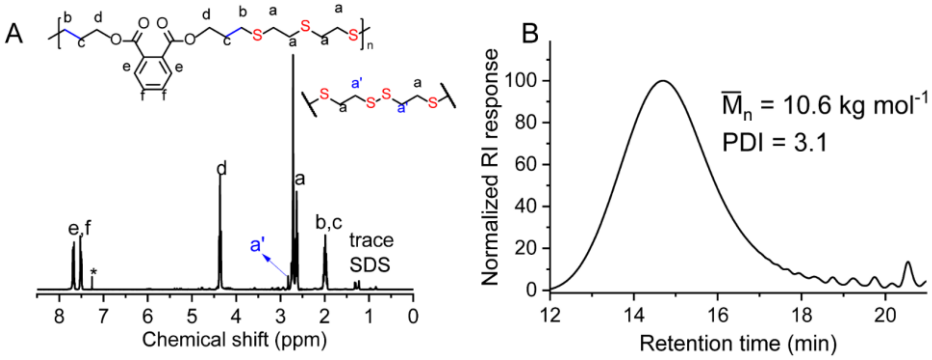

Figure V-1 ^{1}H-NMR ($CDCl_3$) spectrum (**A**) and GPC trace (**B**) of dried poly(thioether)s resulting from photocatalytic emulsion thiol-ene polymerization of **DAP-4**.

We performed two control experiments which proved that in the absence of catalyst or light no monomer conversion occurred (**Table V-1** entries **2**-**3**), supporting the photolatency of the thiol-ene monomer mixture and the initiating role played by the excited photocatalyst. Using instead of EY^{2-} other organic dyes like rose Bengal or acridine yellow (**Table V-1** entries **4**-**5**) was possible but did not provide any beneficial effect. Because it is known that photoredox systems are pH-sensitive, we also studied the effect of pH in the range 5-8. Lower and higher pH values were avoided to limit photocatalyst decomposition and undesirable thiol-Michael reactions. We observed that a pH of 8 yielded the highest conversions and molecular weights (**Table V-1** entries **6**-**8**). In the course of a more exhaustive survey of the role played by molecular oxygen ($^3O_2$), we found that the reaction can be conducted either in the presence of air, or under rigorously degassed conditions (**Table V-1** entry **9**).

Table V-1 Reference and control experiments. Yields determined by ^{1}H-NMR, molecular weights by SEC using THF as eluent.

Entry	Condition	pH	Catalyst	Ene conversion [%]	$\overline{M_n}$ [g mol^{-1}] / Đ
1	Green light	8	EY-Na_2	97	10600 / 3.1
2	Green light	8	No	0	-
3	No light	8	EY-Na_2	0	-
4	Green light	8	Rose Bengal	67 ± 14	-
5	Blue light	Not controlled	Acridine yellow	>96	7100 / 2.5
6	Green light	5.5	EY-Na_2	94	6940 / 2.3
7	Green light	7.2	EY-Na_2	>96	9910 / 2.7
8	Green light	7.4	EY-Na_2	>96	9070 / 2.8
9	Green light Under N_2	8	EY-Na_2	96	4200 / 2.0

1.3.2 Investigation reaction mechanism

In the case of eosin photosensitization, two competitive mechanisms can take place: (i) the first one involves the proton-coupled electron-transfer reaction from a thiol to generate a thiyl radical as described previously (type I mechanism); (ii) the second one is the oxidation of the thiol by singlet oxygen ($^1O_2$) (type II mechanism). This latter reactive oxygen species can result from an energy transfer from $^3EY^{2-*}$ to $^3O_2$.

(i) **Type I mechanism**:

$$^3EY^{2-*} + RSH \rightarrow RSH^{\bullet+} + EY^{\bullet 3-}$$

$$RSH^{\bullet+} \rightarrow RS^{\bullet} + H^+$$

(ii) **Type II mechanism**:

$$^3EY^{2-*} + {}^3O_2 \rightarrow EY^{2-} + {}^1O_2$$

$$^1O_2 + RSH \rightarrow RSH^{\bullet+} + O_2^{\bullet-}$$

$$2RSH^{\bullet+} + 2O_2^{\bullet-} \rightarrow H_2O_2 + RS^{\bullet} + O_2$$

To gain better insight into the primary mechanisms, we compared the polymerization kinetics of a **DAP-4** emulsion in air and under nitrogen. As shown in **Figure V-2A**, the reaction rate in the presence of air was approximate twice as fast as under nitrogen, resulting in significantly higher molecular weights (particle size and polymer structure were found to be similar). To substantiate whether singlet oxygen could interfere, the same experiment was

performed in the presence of air and sodium azide (4.3% mol) acting as singlet oxygen quencher (azide ion is a common reagent to physically quench $^1O_2$).[286] Under these conditions, no deleterious effect on monomer conversion was observed[286] (**Figure V-2B**). Our conclusion is that the type I mechanism prevails, but that molecular oxygen is likely to be involved in a reaction regenerating the photocatalyst, resulting in increased rates of the reaction due to a higher EY^{2-} concentration (*vide infra*).[287] In support of the minor role of reactive oxygen species, a fully converted latex illuminated in the presence of 0.5% mol of EY^{2-} for 14 h did not yield sulfoxide or sulfone as oxidation products (**Figure V-2C**). Finally, **Figure V-2D** shows a "light/dark" experiment in which the progress of the polymerization was examined for alternating periods of irradiation and darkness. Clearly, monomer conversion required constant irradiation and conversion ceased during the periods of darkness. As widely discussed in the literature,[288] this result does not mean that a chain radical process did not occur but rather illustrates the short life times of thiyl and carbon-centered radicals. Fast reactions and low catalyst loadings can be reconciled with a chain radical process.

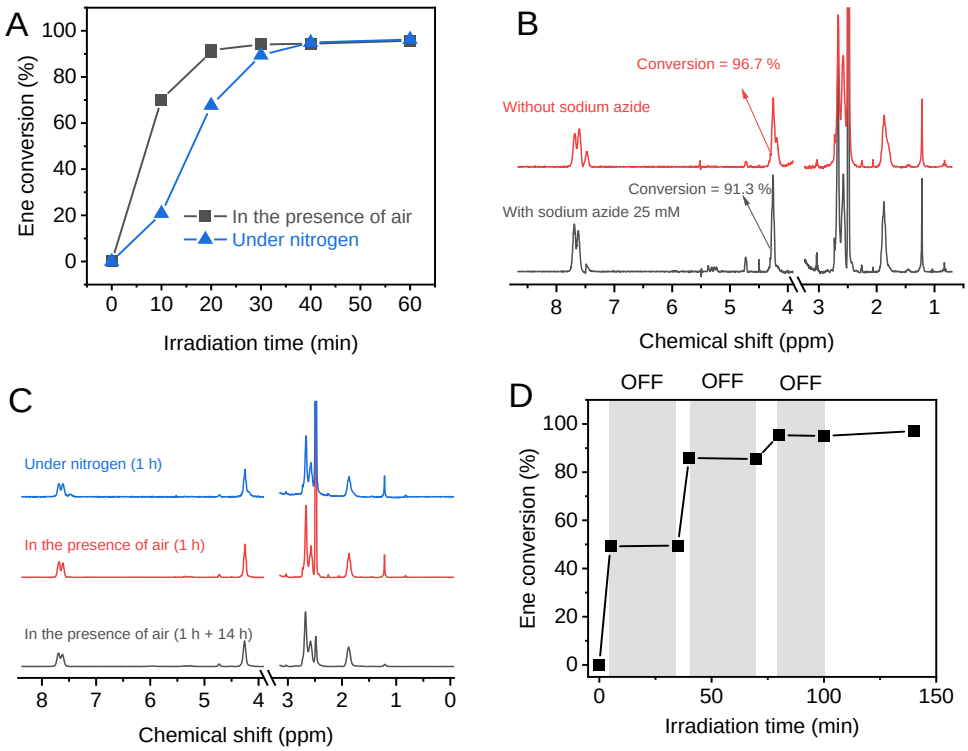

Figure V-2: Influence of atmospheric air on the reaction kinetic (**A**), temporally controlled kinetic of the reaction under air and pH 8 (**B**), ^{1}H-NMR spectra of as-prepared poly(thioether)s were recorded in DMSO-d^6 (**C**), ^{1}H-NMR spectrum of **DAP-4** latex produced by emulsion photopolymerization after 1h irradiation. After the first irradiation, 0.45% mol of EY^{-2} was added to the latex and the sample was irradiated under constant air-bubbling for 14 h (**D**)

A number of evidence supported the electron-transfer from a thiol upon electronic excitation of EY^{2-} (type-I mechanism). According to the Rehm-Weller equation, the free energy change for an electron-transfer from thiol to $^3EY^{2-*}$ is favorable (ΔG_{et} = -0.52 V *vs* SCE). Quenching of $^3EY^{2-*}$ in the presence of **dithiol 4** was also proved by fluorescence emission experiments in which increasing amounts of dithiol were added to an aqueous solution of EY^{2-} (**Figure V-3A**). An interaction rate constant was determined by measuring the rate of fluorescence decay F_0/F at 537 nm from a Stern-Volmer plots (F_0/F=1+ K_{SV}[**4**], R^2 = 0.994, and K_{SV} = 1.44 x 10^3 M). In order to gain more insight into the quenching mechanism and to investigate the possible formation of a ground-state charge transfer complex, we also analyzed the effect of thiol concentration on the UV-Vis spectra of a binary EY^{2-}/**dithiol 4** solution in water. Addition of increasing amounts of **dithiol 4** caused a slight increase of the spectrum intensity (**Figure V-3B**), which agrees with the formation of a weak eosin/**dithiol 4** complex in water. Such complex is important because it can increase the electronic density of the excited state of eosin and favors its reductive quenching by a thiol to generate the thiyl radical cation, but only upon irradiation.[289,290] Consequently, UV-vis spectroscopy demonstrates the existence of a contribution of static quenching.

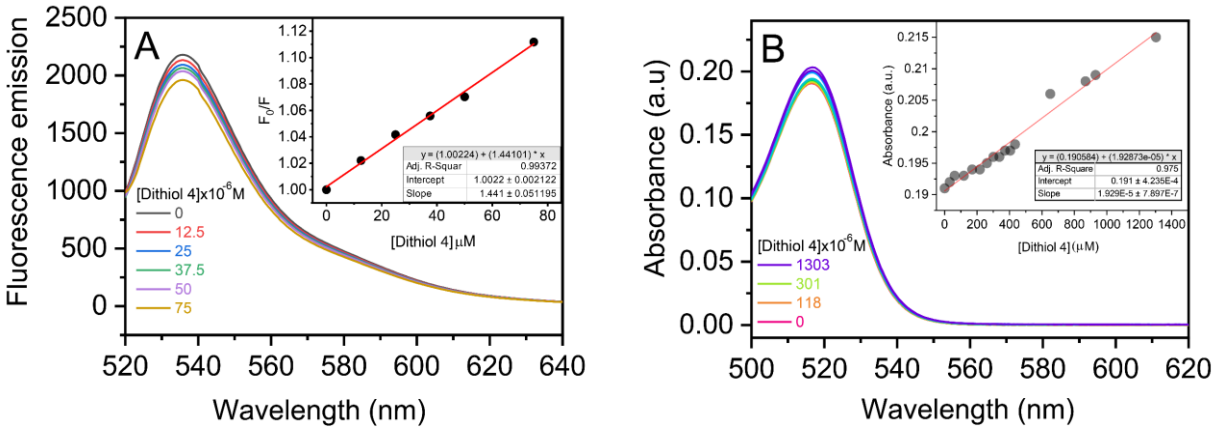

Figure V-3: Steady state fluorescence quenching of eosin (1×10^{-7} M) with **dithiol 4** in the concentration range (0-7.5×10^{-5} M) in non-degassed water (**A**) and UV-vis spectroscopy of eosin (2×10^{-6} M) with **dithiol 4** in the concentration range 0 - 1.3×10^{-3}M (**B**).

On the basis of these previous results, the following mechanism can be proposed (**Scheme V-2**). A thiyl radical cation may be generated by photooxidation of thiol with $[EY^{2-}]^*$. A subsequent proton-transfer step affords the chain-propagating thiyl radical involved in the classical radical thiol-ene chain process with ene monomer (chain propagation cycle). To close

the catalytic cycle, the photo-reduced radical trianion $EY^{\bullet 3-}$ can be oxidized to the original eosin dianion EY^{2-} by two ways: either a reaction with a carbon-centered radical to form a thioether product or a reaction with molecular oxygen to form superoxide anion ($O_2^{\bullet -}$). This latter route might explain why an acceleration of polymerization was observed when the reaction was conducted in the presence of air. The former route proceeding in the absence of molecular oxygen is consistent with the fact that high conversions can be achieved also under nitrogen.

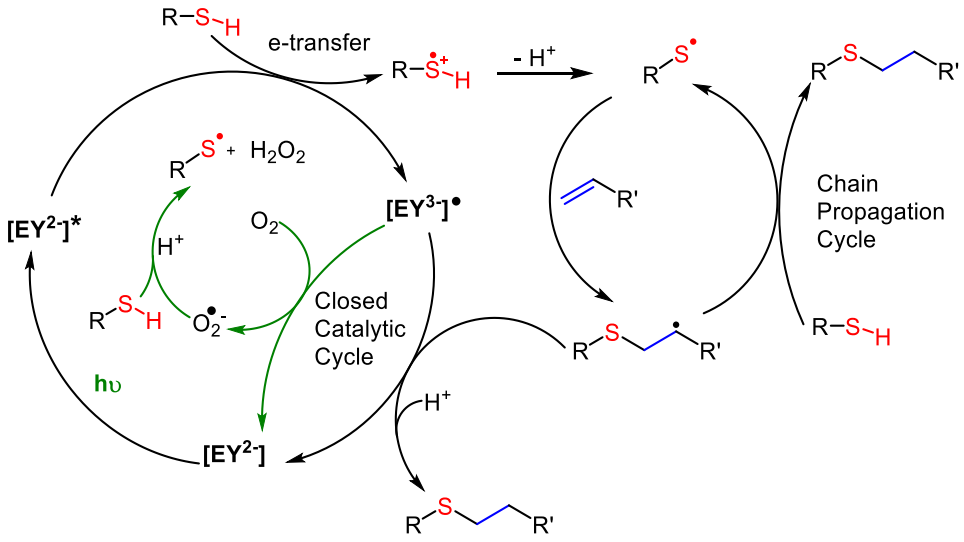

Scheme V-2. Proposed mechanism for thiol-ene polymerization under green light.

1.3.3 Preparation of semi-crystalline poly(thioether) latexes

Next, we evaluated the potential of this process for the preparation of semi-crystalline latexes. Recent studies suggested that poly(thioether) linear chains, which combine secondary attractive forces and high structural regularity, can have a high a tendency for crystallization.[291–293] To achieve better insight into the structure-property relationship, **dithiol 4** was polymerized with various diallyl esters and divinyl ethers: diallyl terephthalate (DATP), diallyl adipate (DAA), di(ethylene glycol) divinyl ether (DVE), 1,4-bis[(vinyloxy)methyl]cyclohexane (CHDM), using a similar emulsion polymerization process for all of these molecules. This approach represents a simple and versatile means of synthesizing a host of different latexes by varying the choice of the **R** and **R'** spacer groups in the dithiol (HS-**R**-SH) and the diene (H_2C=CH-**R'**-CH=CH_2). **Table V-2** provides the chemical structures of the ene monomers used (**dithiol 4** is the only dithiol used, **R** = CH_2-CH_2-S-CH_2-

CH_2) and some detailed characterization results including particle size, conversion and molecular weight. All latexes were made up of linear chains with the expected repeat units (-S-**R**-S-CH_2-CH_2-**R'**-CH_2-CH_2) (**Figure V-4**).

Table V-2. Characterization of latexes prepared by **dithiol 4** and various dienes

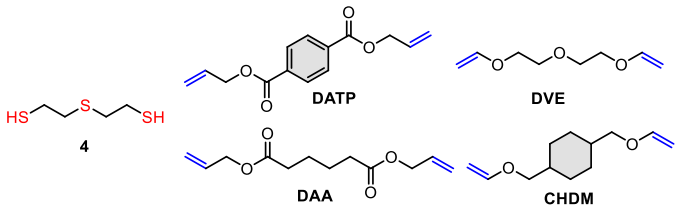

Ene	Ene conversion Conv. [%]	Z-average diameter [nm] / PDI	$\overline{M_n}$ [g mol-1] / Đ
DAP	96.7	96 ± 3 / 0.18	10600 / 3.1[c]
DATP	97.1[a]	74 ± 2 / 0.18	N/D[d]
CHDM	N/D[b]	92 ± 3 / 0.17	7800 / 2.0[e]
DAA	92.4[a]	76 ± 3 / 0.22	8500 / 2.1[e]
DVE	N/D[b]	226 ± 8 / 0.19	9800 / 2.2[e]

[a] determined by ^{1}H-NMR in $CDCl_3$, [b] no reference peak is available for calculation, [c] determined by SEC using THF eluent, [d] the polymer is neither soluble in THF nor DMF, [e] determined by SEC using DMF eluent.

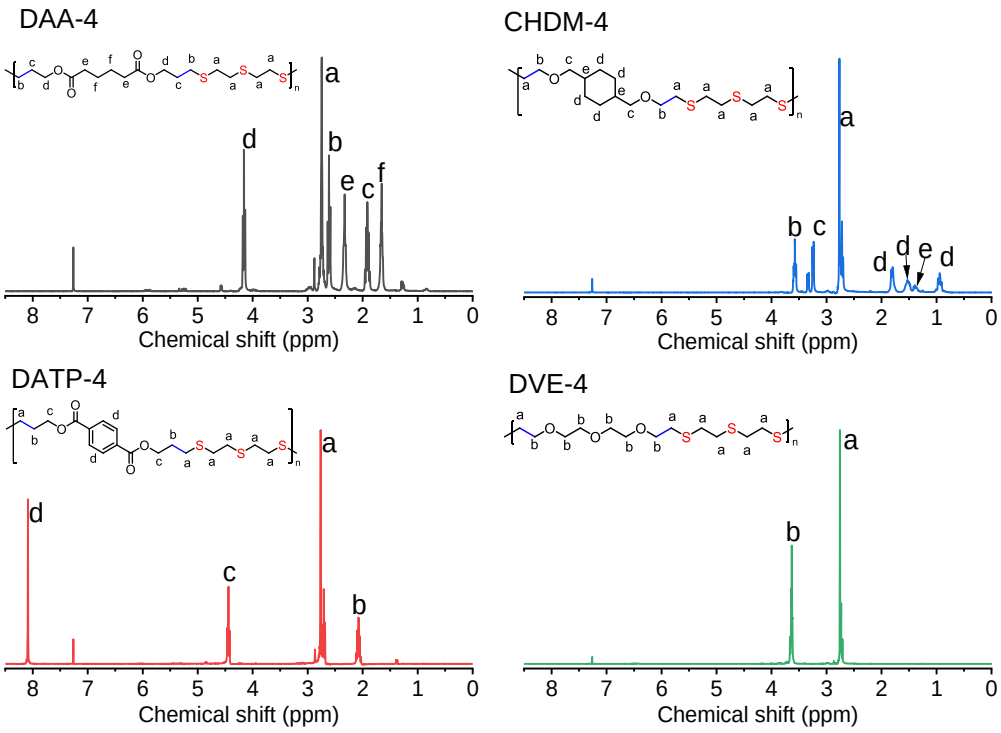

Figure V-4 ^{1}H-NMR ($CDCl_3$) spectra of dried poly(thioether)s resulting from photocatalytic emulsion thiol-ene polymerization of dithiol **4** with **DATP**, **CHDM**, **DAA** and **DVE**.

Unlike polymers derived from **CHDM** and **DAP**, the structures prepared with **DATP**, **DAA** and **DVE** were only poorly soluble at room temperature in a number of organic solvents such as acetone, ethanol, DMF, DMSO and THF, hinting indirectly at a significant fraction of less soluble crystalline domains. Crystallinity increases chemical resistance because crystalline domains can act as physical crosslinks that effectively increase secondary attractions and prevent solvation of chains. To confirm a considerable manifestation of crystalline domains in the three less soluble polymers, we performed the corresponding DSC analysis (**Figure V-5**). In addition, images obtained by polarized optical microscopy on spin-coated thin films of the polymer of **DVE-4** showed clear birefringent polygonal patterns, characteristic for coalesced crystalline spherulites (**Figure V-6A** and **B**). Interestingly, in accordance with the sequence of a first melting-, crystallization- and second melting-peak seen in the corresponding DSC heating trace (see **Figure V-5E**), two distinctly different morphologies were observed. When the sample was crystallized by quenching from the melt, which is reached at a temperature of ca. 90 °C, the films showed clear signs of Maltese cross patterns of birefringence (**Figure V-6A**), suggesting radial growth of multiple thin lamellar crystals which cannot be resolved individually by optical microscopy. However, when melting the sample of **Figure V-6A** at ca. 64 °C followed by crystallization at ca. 76 °C, a distinctly different pattern of radially arranged needle-like crystalline structures could be observed (**Figure V-6B**). From an analysis of corresponding XRD curves (**Figure V-6C**), which also indicate that two different crystalline polymorphs are responsible for the observed two melting processes, the degree of crystallinity was estimated to be in the range of 25 – 45 %. The results of XRD measurements during stepwise heating are shown in **Figure V-7**. It should be noted that crystallization of the polymer of **DVE-4** was quite fast. Depending on the thermal history and crystallization temperature, the whole sample could become crystalline within seconds to hours, as could be observed in real time by optical microscopy. Fast crystallization is also indicated by the rather narrow crystallization peaks in the DSC traces (see **Figure V-5**), suggesting that the ease of chain packing was a driving force for ordering and crystallization of these polymer chains.[294] Thus, profiting from structural regularity, compactness and some degree of flexibility, packing was facilitated in particular for poly(thioether) chains based on aliphatic dienes **DVE** (**R'** = $OCH_2CH_2OCH_2O$) and **DAA** (**R'** = $CH_2OC(O)(CH_2)_4C(O)OCH_2$).[295] Aromatic or cyclic **R'** groups present in the other dienes (**DAP** or **CHDM**) are thought to lower the tendency for crystallization by preventing close packing of polymer chains.

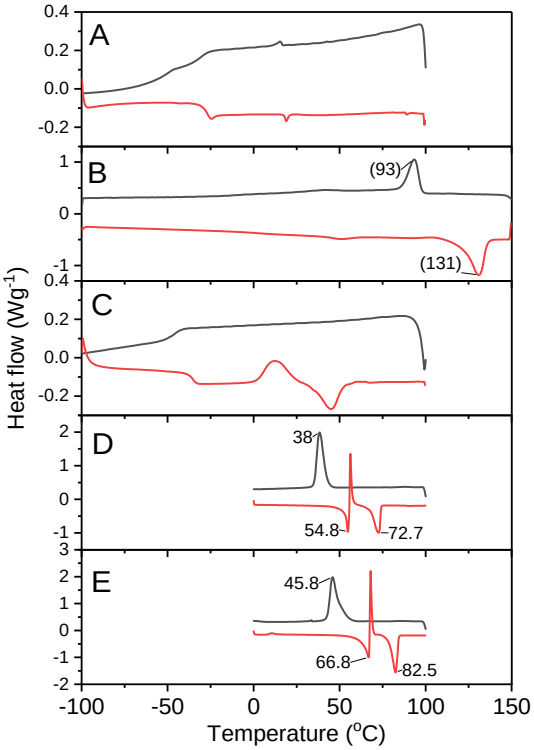

Figure V-5 DSC cooling (black) and heating (red) traces, measured at a rate of 10 K/min, for the pure polymers resulting from thiol-ene emulsion photopolymerization of **dithiol 4** with **DAP** (A), **DATP** (B), **CHDM** (C), and at a rate 5 K/min for **DAA** (D) and **DVE** (E).

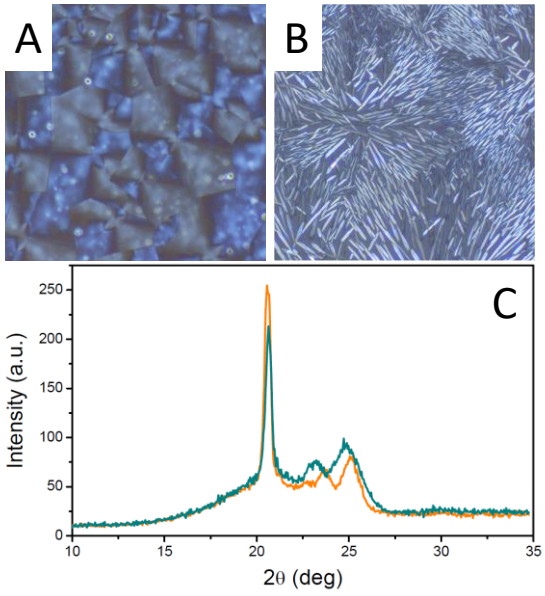

Figure V-6 Polarized optical microscopy images (size: 475×475 µm^2) of *ca.* 100 nm thick films of the polymer of **DVE-4** (**A**) Crystallized rapidly at room temperature after quenching from the molten state at 100 °C. (**B**) The sample of (**A**) was subsequently molten at *ca.* 64 °C and further heated to ca. 76°C where it crystalized in a different morphology. (**C**) Corresponding X-ray diffraction curves of analogous samples. The curves in dark cyan and orange represent the two different crystalline states at 47 °C and at 70°C, measured after 1 min and 90 min of annealing at the respective temperatures.

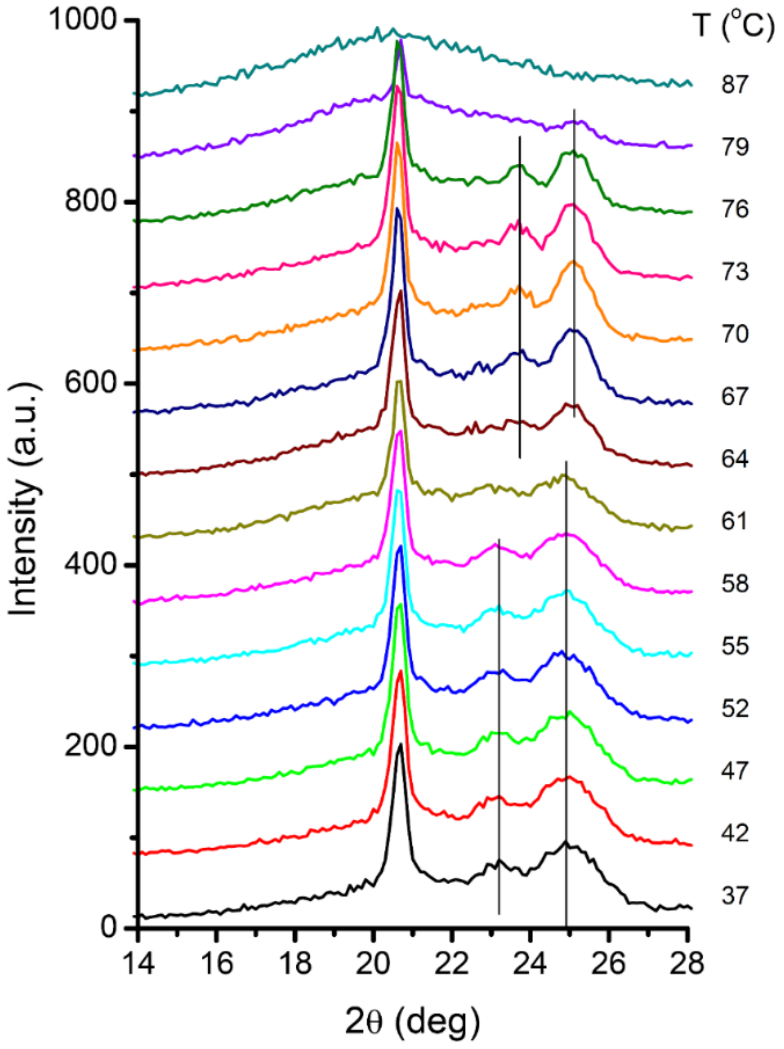

Figure V-7 XRD measurements of **DVE-4** during stepwise heating at the indicated temperatures (30 min per scan).

1.3.4 Conclusion

In conclusion, visible-light photocatalyzed thiol-ene emulsion polymerization was successfully developed using eosin disodium organic dye as photocatalyst. The process has many advantages such as low catalyst loading, absence of additive, short reaction times, low irradiance, higher reactivity under air atmosphere, and the achievement of nanolatexes of relatively high molecular weight. Using 2,2'-thioldiethanethiol as dithiol paves the way towards achieving latexes with semi-crystalline properties. Poly(thioether)s prepared with diallyl adipate or di(ethylene glycol) divinyl ether combine structural regularity, compactness and flexibility, leading to high tendency toward crystallization as proved by DSC, X-ray diffraction and polarized optical microscopy.

2 USE OF STIRRED TANK PHOTOCHEMICAL REACTOR

2.1 Motivation

The objective is to develop batch and semi-batch emulsion thiol photopolymerizations using the multipurpose photoreactor with specially designed by Peschl UV Consulting. Batch emulsion polymerization is a simple mode of operation where all ingredients (monomer, water, surfactant, initiator, etc.) are present in the reactor at the beginning of the reaction. This process is preferred in academic research but is of limited use in industry due to the difficulty of removing the heat of polymerization at high polymerization rates. In semi-batch emulsion polymerization, some of the ingredients (usually pure monomers, monomer macroemulsions, and/or initiators) are introduced into the reactor in a controlled manner at different feed rates.[6,63] This second process is more versatile than batch polymerization and is ultimately most commonly used in emulsion polymerization. Most often, a latex seed with a well-defined particle size (number of particles) is prepared and its growth is ensured by polymerizing a monomer feed or an emulsion feed with the goal of preventing the formation of new particles (secondary nucleation). In this section, we report on the feasibility of these two processes for an emulsion thiol-ene step-growth photopolymerization.

2.2 Experimental section

2.2.1 Synthesis

2.2.1.1 Batch polymerization process

A photolatent organic thiol-ene phase (40.5-40.8 g) was prepared according to **Table V-3**. An aqueous phase consisting of TPO-Li (0.400 g, 1.34 mmol, 0.0145 equiv./monomers), SDS (3.18 g, 7.8 wt.%/monomers, 30 mM in water), and 360 mL of deionized water was prepared in a 500 mL Peschl multipurpose photoreactor (**Figure V-9**). The organic phase was then added to the reactor and the resulting coarse emulsion was mixed using the Ultra-Turrax mixer equipped with 18 mm dispersing tool, set at 15000 rpm for 10 minutes. Photopolymerization was performed immediately after emulsion preparation at room temperature in the photoreactor at 385 nm (33 mW cm^{-2}). Irradiation of the reactor was carried out under magnetic stirring at 1100 rpm for 1 h. At different irradiation times, a 1 mL aliquot was taken from the top of the reactor for subsequent analysis of monomer conversion, particle size, and molecular weight.

Table V-3 Organic phase compositions used in batchwise emulsion photopolymerization.

Organic phase 1	Weight (g)	Quantity (mmol)	Organic phase 2	Weight (g)	Quantity (mmol)
DAP	24.86	99.9	DAP	23.48	94.4
4	15.62	99.9	3	17.28	94.4
DBHQ	0	0	DBHQ	0.04	0.18

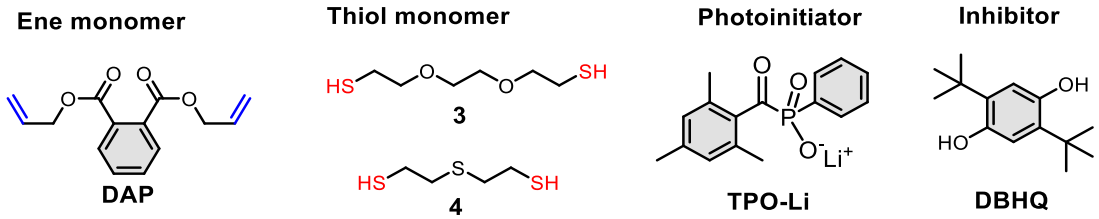

Figure V-8. Chemical structure of photoinitiator, dithiol and diene monomers.

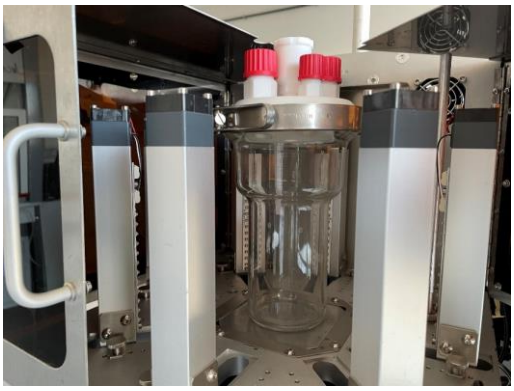

Figure V-9. Digital image of a 500 mL photoreactor.

2.2.1.2 Semi-batch polymerization process

Semi-batch emulsion polymerizations were performed using the previously synthesized seed latex based on **DAP-4** by continuously feeding a stoichiometric amount of a **DAP-4** macroemulsion or the pure monomer. The formulations are listed in **Table V-4**. The initial batch (containing the latex seed, water, TPO-Li, and SDS) was magnetically stirred at room temperature at 1100 rpm, and the LEDs were dimmed to 25% (14 mW cm^{-2}). In the case of macroemulsion feed, the pre-emulsion was prepared using the Ultra-Turrax mixer (18 mm dispersing tool) at 10 000 rpm for 10 minutes. This mixture was then fed with a syringe pump (KD scientific model KDS-100-CE) at 2 mL/min using 30 mL Omnifix latex free B.Braun syringe. The UV light was turned on when the first drop of macroemulsion was added to the reactor. For the feeding of the pure monomer, the rate was set to 35 mL/h and the same protocol was applied (see the setup in **Figure V-10**). During feeding, 1 mL of samples were removed from the reactor with a disposable syringe and transferred to vials for characterization

Table V-4 Semi-batch recipes.

	Initial charge	Macroemulsion feed	Initial charge	Neat monomer feed
Seed **DAP-4** latex	40.0 g (4.0 g of polymer)	-	40.0 g (4.0 g of polymer)	-
Water	234.0 g	90 mL	324 mL	-
SDS	0.735 g	0.35 g	1.085 g	-
TPO-Li	0.108 g	-	0.108 g	-
DAP-4 (1:1 equiv.)	-	36 g	-	36 g

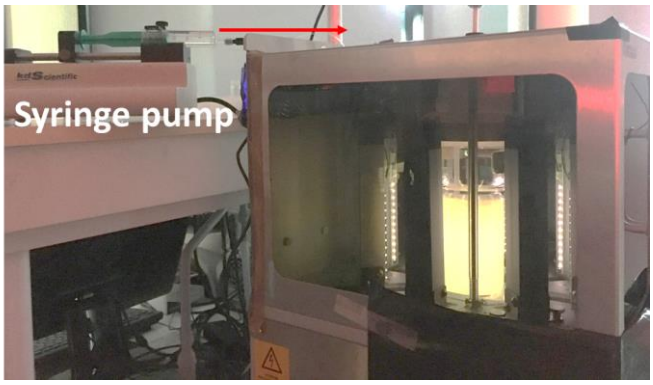

Figure V-10 Digital image of the semi-batch set-up

2.2.2 Characterizations

The determination of the ene-conversion and molecular weight of the latexes has been described in previous publication.[151] The particle size analysis by DLS are described in Chapter III. 2.3.3 and IV. 2.3.3.

2.3 Results and discussion

2.3.1 Description of the photoreactor

The first trials using Peschl multipurpose photoreactor involved thiol-ene batch emulsion photopolymerization. The photoreactor shown in **Figure V-11** is made of stainless steel with integrated IKA agitator drive on the top (or magnetic drive on the bottom). On top of the housing, we used a 500-mL stirred-tank reactor. The set-up is covered by a removable UV shield which is protected with a reed contact switch for safe operation. On top of the photoreactor platform, high powered air cooled 385 nm LED light sources are attached. The power supply and constant current drivers are integrated in the photoreactor platform. Each LED light source comes with 12 LEDs, each 2 W, so that the total LED power consumption is approx. 24 W per LED module. All LEDs can be dimmed from 10-100% (**Figure V-12**) and are equipped with a temperature sensor.

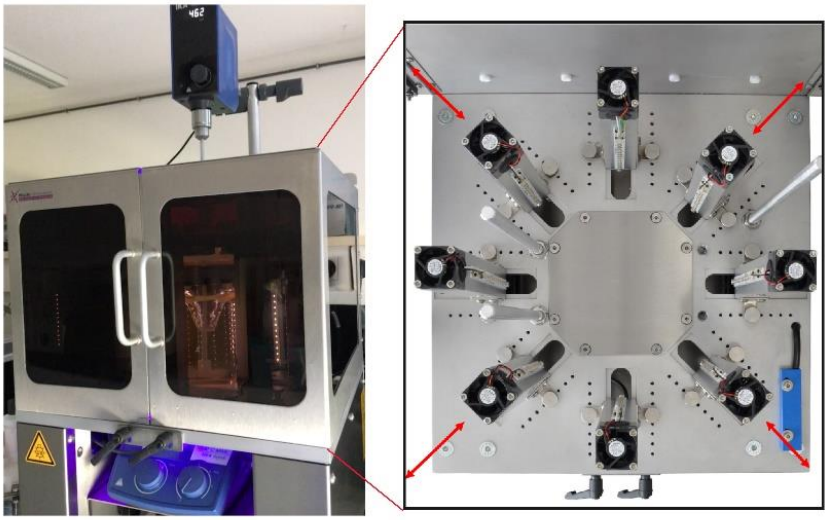

Figure V-11. Multipurpose photochemical reactor designed by Peschl UV consulting.

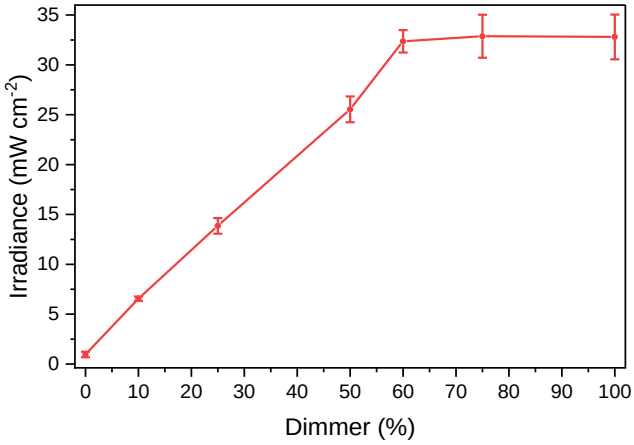

Figure V-12 Irradiance of the photoreactor measured by a calibrated silicon photodiode radiometer (S120VC, Thorlabs).

2.3.2 Batch polymerization

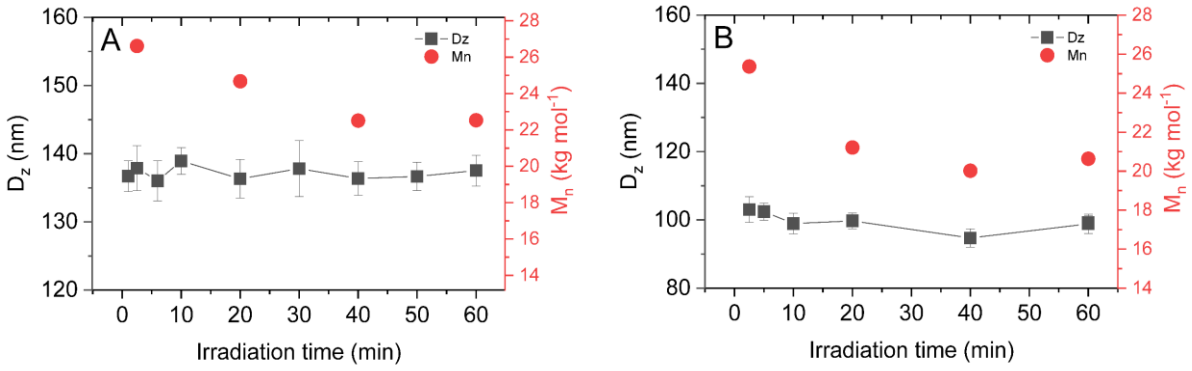

Figure V-13. Particle size and molecular weight change during **DAP-4** (**A**) and **DAP-3 (B**) batch emulsion photopolymerization in Peschl photochemical reactor. DAP-3 stabilized with 5 mM DBHQ/monomer volume and DAP-4 was used without radical inhibitor. [SDS] = 7.8 wt.%/monomers, 30 mM in water.

In the first step, the emulsion photopolymerization of **DAP-4** and **DAP-3** thiol-ene mixtures were carried out in batch at room temperature using SDS as surfactant and TPO-Li as water-soluble photoinitiator. In order to limit the reaction temperature below 35°C, the solid contents were kept at 10 wt% and the illumination time was also limited to one hour. Three parameters including monomer conversion (ene functional groups), molecular weight, and particle size were monitored during reaction at predefined time-intervals. Ene conversions determined by ^{1}H NMR spectroscopy showed a full conversion within only 2.5 min for **DAP-4** monomer system, demonstrating the possibility to obtain high molecular weight of poly(thioether) latex under this photoreactor setup. The molecular weight progress of the two monomer systems was then characterized by SEC and presented in **Figure V-13**. The two runs afforded relatively high molecular weights, above 20 kg mol^{-1}. Due to the completeness of the reactions at that time, particle size remains unchanged until the end of irradiation. This means that the particle nucleation and growth have been completed within 2.5 min. Comparing to a batch process in small scale (10 mL cylindrical vial) previously reported,[151] these results are quite promising and even better, suggesting that upscaling is feasible. Nevertheless, the fast polymerization rates underline the importance of controlling the polymerization exotherm. This can only be achieved upon adjusting irradiance, photoinitiator concentration or through the development of semi-batch operations, this latter being the second objective of this deliverable. Given that a low organic phase content (10 wt%) has been employed here, runaway may occur when implementing similar process with solids content higher than 50 wt%. Here, we used these fully characterized batchwise polymer latexes based on **DAP-4** as a well-defined seed for a subsequent seeded semi-batch emulsion polymerization.

2.3.3 Semi-batch polymerization

The main advantage of utilizing semi-batch approach is the ability to control the exothermicity of the reaction, minimize photoinitiator concentration and prevent premature thiol-ene reaction (by feeding the two monomers separately). In this process, some of the reactants (seed, photoinitiator, surfactant) are charged in the reactor at the start and the remainder is fed in a controlled way. Monomer can be added to the reactor either by neat monomer (namely monomer feed) or macroemulsion (emulsion feed). The latter approach is preferred by industry because it can achieve a better mixing. We started our scouting

experiments by this way. The macroemulsion feeding and irradiation were conducted simultaneously over a period of 1 hour. Photoinitiator concentration and irradiation were fixed to 0.3 wt%/monomer and 14 mW cm^{-2}. To avoid the formation of homogeneous nucleation which create a new population of particle, the number of seed particles (N_p) were selected at least two orders of magnitude higher than the reference value 10^{14} L^{-1}.[234] The targeted solids content was 10 wt%. N_p was measured during the reaction progress. Theoretically, N_p is expected to be constant during the course of reaction in the absence of secondary nucleation occurring in aqueous phase.[6,234,296] The variation of N_p during the feeding period is presented in **Figure V-14**. As can be seen, the emulsion feeding resulted in a decreased number of particles, indicating that particle coagulation happened (**Figure V-14A**). This can be attributed to a macroemulsion chemically instable enough and the reaction perhaps have been started in this formulation. However, a full conversion and relatively high molecular weights (10.9 kg mol^{-1}) were achieved after 1 hour of reaction, this approach requires further optimization for a better control of particle size.

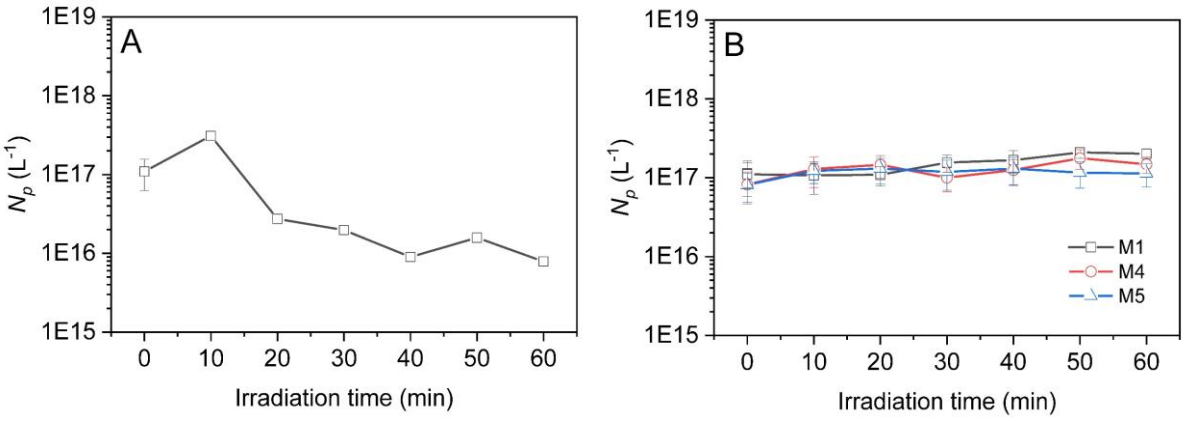

Figure V-14. The variation in N_p during the course of semi-batch emulsion polymerization of **DAP-4** using monomer emulsion feed (**A**) and neat monomer feed (**B**).

To avoid the complexity of emulsion feeding, a neat monomer mixture was fed to the reactor at different rates.[297,298]. The results are presented in **Table V-5** and **Figure V-14B.** Similar to the emulsion feeding process, we dimmed the irradiance to 25% to slowdown the photolysis rate of TPO-Li to ensure a progressive release of primary radicals. We began with a photoinitiator concentration of 0.1 wt%/monomer (run M1, **Table V-5**). Although the final conversion is low (67 %), it seems possible to prevent secondary nucleation (constant N_P throughout the polymerization is observed) (**Figure V-14B**) and without sign of coagulation.

Our efforts to increase the final conversion to reach higher molecular weights polymer by increasing photoinitiator concentration to 0.2 wt%/monomer (run M2, **Table V-5**) and 1 wt%/monomer (run M3, **Table V-5**) led to significant coagulations. There are many reasons to account for the formation of coagulum. One possibility is a polymerization in monomer droplets, which may occur when a high flux of free-radicals enter the droplets.[64] Another explanation is related to fast polymerization at high [TPO-Li] and insufficient monomer mixing. Therefore, the feeding rate of the next reaction was decreased to 35 mL/h to improve the mass transfer of the monomer (run M4, **Table V-5**). Again, the results showed that the particle number was well-controlled and no coagulation. However, the main drawback is once again a limited conversion (75%), leading eventually to low molecular weights (2300 g mol^{-1}). Concerning the effect of [SDS], it is generally recommended in a semi-batch emulsion polymerization to use a sufficient amount of surfactant to maintain colloidal stability but low enough to avoid the formation of new particles by secondary nucleation.[6,299] It is shown however that decreasing [SDS] below its critical micelle concentration (3 mM) results in significant particle coagulation (run M5, **Table V-5**). Among the five runs, M1 and M4 seem the most promising in terms of particle size control. However, the reaction conditions need to be optimized to achieve higher molecular weights.

Table V-5. Experimental conditions used for seeded semi-batch polymerization of **DAP-4**.

Run	Feeding rate of neat DAP-4 mixture (mL/h)	[SDS] mM/water	TPO-Li wt%/mon.	wt% Coagulation	Final conv. %
M1	60	13.2	0.1	0	67
M2	60	13.2	0.2	25.5	89
M3	60	13.2	1	28	91
M4	35	13.2	0.3	0	75
M5	35	3.0	0.3	7.8	86

2.3.4 Conclusion

In summary, a new photoreactor developed by PESCHL for scaling the thiol emulsion photopolymerization process was rationally implemented. It was shown that both batch and semi-batch processes are feasible. Highly efficient and fast photopolymerization and production of coagulation-free latex with high molecular weight polymer are the main

advantages of batch process. However, the solid content was intentionally limited to 10 wt% to avoid thermal runaway. Using this batch process to produce a seed latex, a more versatile semi-batch emulsion polymerization process was implemented to control the particle size and polymerization heat using the thiol-ene mixtures **DAP-4**. Nevertheless, the final conversion and molecular weight of the polymer remained limited. Future developments are underway to overcome these limitations and develop a semi-batch emulsion thiol-ene polymerization with higher solid contents.

GENERAL CONCLUSION

In this dissertation, the challenges and opportunities of thiol-ene photopolymerizations in dispersed systems were studied. The first part is devoted to a deeper understanding of the fundamental problems posed by self-initiated thiol-ene polymerization in order to facilitate reproducibility and practical implementation of photoinitiated thiol-ene polymerizations. Subsequently, two UV-driven processes of thiol-ene photopolymerization in miniemulsion and emulsion were developed where reaction kinetics, particle size, and molecular weight of polymer latexes were systematically investigated. Taking advantage of this development, the emulsion process was scaled up using a novel stirred-tank LED photoreactor. It was also adapted to low-energy visible-light sources through a photocatalyzed polymerization to prepare semi-crystalline poly(thioether) latexes. The following paragraphs summarize the main results of this work and provide some perspectives.

In **Chapter II**, the mechanisms responsible for spontaneous thiol-ene polymerization were investigated in detail in order to develop more efficient strategies to curb premature polymerization. A number of thiol-ene monomer pairs have been shown to undergo self-initiated polymerization under air or nitrogen atmosphere. This study shows that thiyl radicals formed by the oxidation of thiols by dissolved atmospheric oxygen in the thiol-ene mixture play an important role. To determine the factors underlying the reactivity, self-initiated polymerization kinetics, thiol solvation, and the nature of the initiating radicals were investigated using a variety of techniques, including real-time FTIR, ^{1}H NMR spectroscopy, and spin-trapping experiments. Our data demonstrate that the driving force for thiol air oxidation is the polarization of the S-H bond. Thiol substituents with electron-withdrawing properties and/or hydrogen-bonded thiol-solvent (or thiol-alkene) complexes promote self-initiation by increasing the polarization of the S-H bond, thereby facilitating electron transfer to molecular oxygen.

Complex and unique polymer colloids were prepared by miniemulsion photopolymerization through particle nucleation confined to monomer droplets. In **chapter III**, the reaction conditions for favoring droplet nucleation in thiol-ene step growth photopolymerization were studied using a monomer miniemulsion of diallyl phthalate and 2,2-(ethylenedioxy)diethanedithiol. Control of chemical stability is also difficult because of self-initiated polymerization caused by random radicals generated during the emulsification phase (ultrasonication). However, the addition of a suitable concentration of a radical

scavenger (quinone, e.g., DBHQ) can stop the polymerization for several hours. Under these conditions, the kinetics of batch photopolymerization, the course of molecular weight and particle size distribution were determined with reproducible results. Emphasis was placed on understanding how initiator solubility, droplet size, and monomer solubility affect droplet nucleation. To this end, reliable measurement of droplet (particle) size distribution was achieved by combining size data from dynamic light scattering and transmission electron microscopy. When a water-soluble photoinitiator is used, substantial homogeneous nucleation is observed even for highly water-insoluble monomers. Only when the droplet diameter is small enough (about 100 nm) does droplet nucleation predominate. Conversely, a water-insoluble initiator leads to robust and complete droplet nucleation regardless of the reaction conditions.

In **chapter IV**, we present for the first-time poly(thioether) latexes prepared by emulsion photopolymerization. The reaction is based on two bifunctional monomers used in the previous chapter. After 20 min of irradiation (λ_{max} = 385 nm, 3.7 mW cm^{-2}), the polymerization resulted in a conversion of over 99%, a coagulum-free poly(thioether) latex with a solids content of 10 wt%, a number average molecular weight of 14 kDa, and an average particle diameter of 60 nm. The reaction kinetics, particle size distribution and molecular weight variation were studied in detail. To clarify the factor determining particle formation, the number of particles per unit volume of water was determined as a function of surfactant concentration. It is found that the dependence of the number of particles on the SDS concentration above the CMC depends on the combined polarity (water-solubility) of the ene and thiol. The exponent x in the relationship $N_p \sim [SDS]^x$ decreases with increasing water solubility of the monomer, similarly as emulsion chain-growth polymerization. The study also shows that the solids content of the dispersion can be as high as 40%. The molecular weights remain reasonable (> 4 kDa) even when the functional groups are stoichiometrically unbalanced. In contrast to conventional thermally induced polymerization, temporal control is demonstrated by sequential "on"-"off" cycles and tuning of molecular weights is achieved by precise energetic dosing of radiation. This new step of photopolymerization in emulsion thus opens a pathway for the synthesis of linear polysulfide latex without high-energy homogenization and at low irradiance.

In the **last chapter**, we describe an extension of thiol-ene emulsion photopolymerization using a more environmentally friendly and safer visible-light. A thiol-ene emulsion photocatalytic polymerization under green light was used for the preparation of linear semi-crystalline latexes. The process involves 2,2'-thioldiethanethiol as dithiol and various dienes, low irradiance (3 mW cm^{-2}), eosin-Y-disodium as organocatalyst, low catalyst loadings (< 0.05% mol) and proceeds in fast reaction time scales (< 1 h). The resulting latexes had a molecular weight of about 10 kDa, an average diameter of 100 nm, and a linear poly(thioether) structure consisting only of thioether repeat units. A detailed mechanistic investigation reveals that an electron transfer reaction from a thiol to the excited triplet state of the photocatalyst (type I mechanism) is the most important step, while oxidation by singlet oxygen produced by energy transfer has a negligible effect (type II mechanism). Only polymers prepared with aliphatic dienes such as diallyl adipate or di(ethylene glycol) divinyl ether showed a high crystallization tendency as revealed by differential scanning calorimetry, polarized optical microscopy and X-ray diffraction. Ordering and crystallization of the poly(thioether) chains are facilitated by the ease of molecular packing due to the regular structure, compactness, and flexibility of the polymer chains. Moreover, it is possible to perform thiol-ene emulsion photopolymerization on a larger scale. A new stirred tank LED photoreactor operating at 385 nm was rationally used. It is shown that both batch and semi-batch processes are applicable. Fast photopolymerization and production of coagulation-free latex with high molecular weight polymer are the main advantages of batch process. However, the solid content was limited to 10 wt% to avoid thermal runaway. Using the latex prepared by batch process, a more versatile seeded semi-batch emulsion polymerization process was carried out. Nevertheless, final conversion and molecular weight of the polymer remain limited.

The focus of this dissertation was to answer some fundamental questions related to reaction kinetics, molecular weight evolution and particle size control, which are practically useful for further development of innovative materials and intensification of polymerization processes. There is still much room for improvement of the thiol-ene photopolymerization in dispersed systems. Among the most promising directions and important questions are.

- **To fully establish the mechanism of self-initiated thiol-ene polymerization** by understanding the contribution of MAH relative to thiol-air oxidation.

- **To mitigate the problem of self-initiated thiol-ene polymerization** by separating thiol and ene monomers. Scouting experiment has also shown that it is possible to avoid self-initiated polymerization by combining two streams of (mini-)emulsions containing separate thiol and ene monomers at the last moment before photopolymerization.
- **To synthesize new sulfur-containing latexes.** Due to the versatility of the synthesis method developed in this study, there is no limit to the number of poly(thioether) latexes that can potentially be synthesized. For example, thiol-ene emulsion photopolymerization yielded innovative poly(thioether)s with high crystallinity, especially with 2'-thiodiethanethiol (**dithiol 4**). Future development could be to investigate the relationships between polymer structure and crystallinity and their influence on the ability to form poly(thioether) films.
- **Towards visible-light.** There are still many opportunities to tap at using commercially available and affordable water-soluble dyes to perform thiol-ene polymerization in a (mini-)emulsion under visible-light irradiation.
- **Semi-batch and continuous operation modes.** Improvement of the process on an industrial scale might include further developments of semi-batch or continuous flow process to increase solids content and molecular weights.

RESUMES EN FRANÇAIS

INTRODUCTION GÉNÉRALE

Les polymères synthétiques ont pénétré presque tous les aspects de la vie humaine, des tâches quotidiennes aux techniques les plus poussées.[1,2] A ce titre, ils sont considérés comme les matériaux du vingtième siècle. La croissance des polymères synthétiques est due à leurs propriétés uniques, larges et adaptables. De nos jours, l'industrie polymère est confrontée à des défis importants tels que la limitation des ressources naturelles, les réglementations environnementales et la sensibilisation croissante des clients aux problèmes environnementaux. Dans ce contexte, des formulations sans COV, des procédés de polymérisation moins énergivores et une production minimale de déchets sont devenus des axes prioritaires de développement.[3] Aujourd'hui, deux technologies de polymérisation, la *polymérisation en milieu dispersé* et la *photopolymérisation*, sont considérées comme éco-efficientes et productrices des polymères zéro COV.[4]

- La *polymérisation en milieu dispersé*, en particulier les procédés de polymérisation en émulsion et en suspension en phase aqueuse, permet la synthèse de particules polymères de taille variable allant du nanomètre au micromètre. Elle a abouti à des applications industrielles à fort tonnage, notamment des revêtements, des textiles non tissés, des encres, ainsi que des applications de niche dans l'administration contrôlée de médicaments et les tests immunologiques.[5,6] Actuellement, la plupart des procédés de polymérisation en émulsion repose presque exclusivement sur un mécanisme de polymérisation radicalaire en chaîne utilisant des amorceurs radicalaires thermiques ou redox.[7]

- La *photopolymérisation* est un second procédé majeur de polymérisation sans COV et économe en énergie utilisé dans l'industrie. Il est bien adapté aux applications de surface et en couche mince telles que les encres, les vernis, les revêtements industriels et, plus récemment, pour la fabrication additive (stéréolithographie).[8-10] La plupart de ces applications impliquent la réticulation d'un mélange sans solvant constitué de monomères et d'oligomères réactifs. Dans ce processus, des espèces actives (principalement des radicaux) sont produites par rayonnement ultraviolet (UV) ou visible.

L'hybridation de ces deux technologies de polymérisation pourrait renforcer l'éco-efficience du procédé mais aussi de générer de nouveaux produits. Les recherches sur la *photopolymérisation en milieu dispersé* ont commencé dès les années 1980,[11] mais ce

procédé hybride n'a jamais réussi à s'imposer comme une alternative viable. Une des raisons est la pénétration limitée du rayonnement dans des systèmes dispersés diffusants. D'autres aspects entravent la progression de la *photopolymérisation en milieu dispersé*, l'absence de processus de polymérisation *ad hoc*, de photoréacteur, de lampe et de photoamorceur appropriés.[4]

Ce projet doctoral s'intéresse à la *photopolymérisation thiol-ène en milieu dispersé*. La réaction d'addition radicalaire thiol-ène est connue depuis plus d'un siècle et sa principale application est en polymérisation.[15] Généralement, une polymérisation par étapes thiol-ène implique un mélange sans solvant de monomères thiol/ène multifonctionnels et d'un amorceur radicalaire pour conduire à une structure réticulée poly(thioéther). Le mécanisme de croissance implique une série de réactions d'arrachement d'hydrogène sur le thiol et d'addition du radical thiyl ainsi formé sur l'alcène (**Scheme I-1**). Cette polymérisation radicalaire par étapes a été proposée comme alternative à la polymérisation radicalaire en chaîne conventionnelle. Cependant, elle a été rarement utilisée dans des systèmes dispersés pour produire des particules de polymère.[17-19]

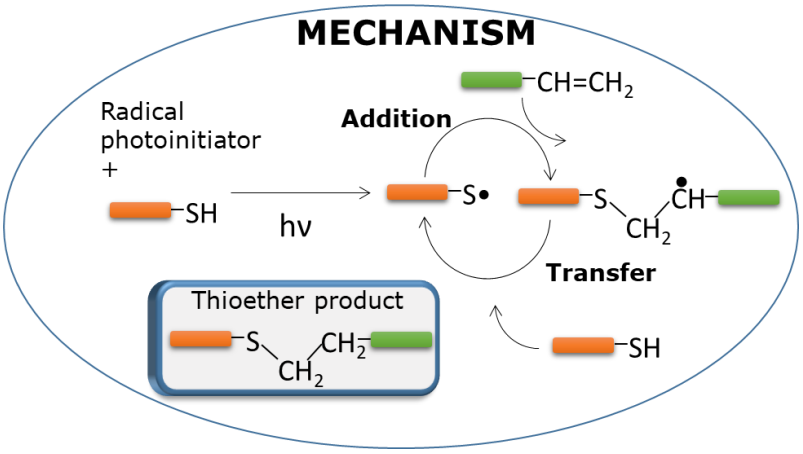

Schème I-1 Mécanisme général de la polymérisation thiol-ène

Ce projet de thèse vise à développer des procédés de *photopolymérisation par étapes thiol-ène* en milieu dispersé. L'approche principale consiste à partir d'émulsions ou de miniémulsions (nanoémulsions) de monomère dithiol-diène hautement réactives en phase aqueuse, qui sont ensuite converties en latex poly(thioéther) par une courte exposition à la lumière dans un photoréacteur. Ce procédé est pertinent en termes de contrôle de la taille

des particules, d'absence d'inhibition de l'oxygène, de sécurité grâce à sa capacité à être contrôlé dans le temps et de faible consommation d'énergie grâce à l'utilisation de photoréacteur à LED. Le mécanisme de polymérisation par étapes offre aussi des avantages: une faible teneur en monomères résiduels, une post-fonctionnalisation de la surface des particules,[18] une cristallinité des chaînes poly(thioether) ayant un impact positif sur la résistance mécanique et chimique.[20,21] Ce manuscrit se concentre sur le développement de processus de photopolymérisation par étape thiol-ène en miniémulsion et en émulsion.

Comme représenté sur le **Scheme I-2**, cette thèse est divisée en cinq chapitres, dont une section bibliographique et quatre sections de résultats expérimentaux qui abordent les principaux défis de la photopolymérisation thiol-ène en milieu dispersé :

i. Maîtriser/comprendre la *polymérisation spontanée* des mélanges de monomères thiol-ène ;

ii. Développer la *photopolymérisation thiol-ène en miniémulsion* en mettant l'accent sur le contrôle de la taille de particule ;

iii. Développer la *photopolymérisation thiol-ène en émulsion* grâce à une compréhension des mécanismes de formation des particules ;

iv. *Renforcer l'éco-efficience des procédés* grâce à l'utilisation de la photocatalyse sous lumière visible et de réacteurs photochimiques.

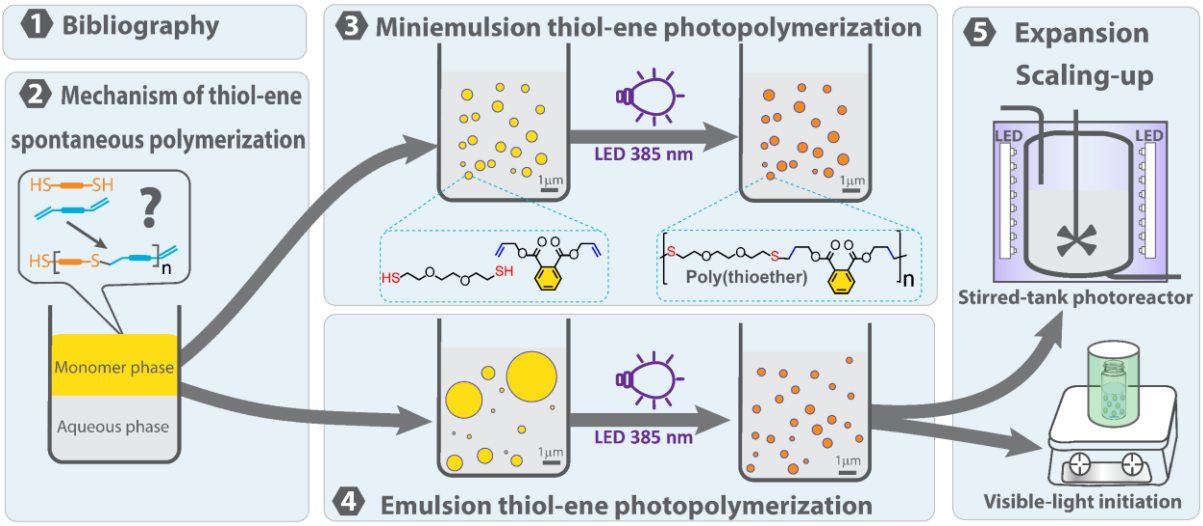

Schème I-2 Développement du procédé de photopolymérisation thiol-ène en émulsion et miniémulsion.

CHAPITRE II. COMPRENDRE LE MÉCANISME DE LA POLYMÉRISATION SPONTANÉE THIOL-ÈNE

L'addition amorcée par des radicaux des dérivés thiols sur les alcènes pour donner des produits thioéthers est connue depuis plus d'un siècle.[13,14] Cependant, ce n'est que depuis les années 2000 que cette réaction fait l'objet d'un regain d'intérêt dans le cadre de la recherche de réactions chimiques répondant aux critères de la chimie « click ».[144] Pour la réaction de petites molécules, la réaction thiol-ène oa principalement été utilisée pour ancrer un catalyseur sur un support polymère,[145] une surface,[146] ou fonctionnaliser des molécules biologiques.[147] Cependant, son utilisation principale est la polymérisation.[15] Généralement, une polymérisation par étapes de type thiol-ène implique un photoamorceur radicalaire et des monomères avec au moins deux groupes SH/C=C par molécule afin de générer une structure réticulée. Comme c'est souvent le cas en photopolymérisation, les applications se concentrent sur la réticulation sans solvant de films utilisés ensuite comme revêtements ou photoresists.[21] Lorsqu'un solvant est présent, d'autres produits polymères peuvent être formés, notamment des hydrogels,[150] des latex,[151] ou des dendrimères.[152] Les poly(thioéthers) ont été proposés comme alternatives aux polymères obtenus par polymérisation en chaîne (par exemple, les polymères acryliques) car ils contournent certaines limitations, notamment l'inhibition de l'oxygène, la relaxation des contraintes et la formation de réseaux hétérogènes.[16] Malgré ces avantages et un nombre croissant de publications, la recherche sur la (photo)polymérisation par étapes thiol-ène n'a jamais réussi à s'imposer comme une alternative solide à la photopolymérisation en chaîne.

Les limitations inhérentes à la chimie du thiol-ène et aux poly(thioéther)s ont contribué à cette situation. Les thiols sont odorants et possèdent un très faible seuil de détection pour les espèces de faible masse molaire.[153] Un deuxième problème est la température de transition vitreuse (T_g) sous-ambiante des poly(thioéther)s conduisant à de faibles propriétés mécaniques.[21] Un dernier problème important et non résolu à ce jour est la polymérisation spontanée.[22] Une instabilité chimique a été rapportée dans la littérature pour une large gamme de monomères thiol-ène, généralement en l'absence de solvants, à température ambiante et dans des conditions évitant la formation de radicaux.[23-25] La

polymérisation prématurée empêche le stockage et l'expédition des formulations thiol-ène, ou au mieux, réduit la durée de conservation.[26] De plus, l'absence de systèmes photolatents ajoute de la complexité et du coût au processus de polymérisation. L'incapacité à contrôler avec précision le début de la polymérisation (contrôle temporel) exclut également des technologies modernes de photopolymérisation comme la photolithographie ou l'impression 3D.[159]

Le mécanisme de la polymérisation spontanée thiol-ène n'est pas connu.[158 159] On considère qu'il s'agit d'un processus de polymérisation auto-amorcé puisque l'homolyse thermique des impuretés présentes dans les monomères (par exemple, les peroxydes ou les hydroperoxydes) est supposée négligeable.[161] D'autres monomères susceptibles de polymérisation auto-amorcée sont rapportés dans la littérature, notamment le styrène,[162] le méthacrylate de méthyle[163] et certaines paires de monomères donneur/accepteur.[164] Contrairement aux systèmes thiol-ène, leur auto-polymérisation se déroule à des vitesses très lentes à température ambiante et peut être efficacement arrêtée avec des inhibiteurs radicalaires. La différence entre les monomères thiol-ène et les autres monomères auto-amorcés peut être comprise en considérant la polymérisation auto-amorcée du thiol-ène comme une réaction radicalaire en chaîne classique consistant en les réactions habituelles d'initiation, de propagation et de terminaison (**Scheme II-1**). Par rapport à d'autres monomères, la polymérisation auto-amorcée de certains systèmes thiol-ène est plus difficile à contrôler en raison de deux caractéristiques. Premièrement, la probabilité d'auto-amorçage à température ambiante est plus élevée en raison d'une énergie d'activation plus faible. Deuxièmement, les deux étapes de propagation d'une polymérisation de thiol-ène peuvent être très rapides, même à température ambiante, en raison des constantes de vitesse d'addition et de d’arrachement d’H élevées. Ainsi, la polymérisation peut démarrer même lorsque la concentration en radicaux amorceurs est faible.

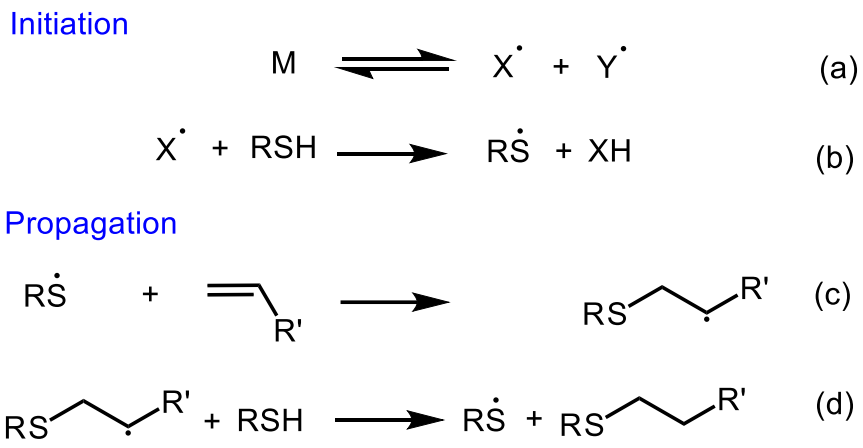

Schème V-1. Schéma de réaction en chaîne radicalaire d'une polymérisation de thiol-ène auto-amorcée.

Trois mécanismes principaux de polymérisation auto-amorcée thiol-ène ont été suggérés dans la littérature (**Scheme II-2**). Le premier mécanisme implique la participation d'un complexe de comonomères.[166] [167] Une seconde hypothèse suggère que les radicaux thiyls sont produits par oxydation des thiols par l'oxygène moléculaire (air).[168] Un troisième mécanisme impliquerait l'Homolyse Assistée par une autre Molécule (MAH) où le clivage homolytique de la liaison SH pourrait être assisté par le transfert d'hydrogène à l'alcène pour former une liaison CH.[170] Actuellement, il n'y a pas de consensus sur le mécanisme correct (ou du moins dominant) car il y a un manque de données expérimentales. Comprendre l'amorçage spontané des réactions radicalaires en chaîne est généralement difficile car il est basé sur des réactions lentes et équilibrées, mais l'élucidation d'un mécanisme d'auto-initiation dominant serait une contribution majeure au développement la polymérisation thiol-ène. De cette façon, des stratégies plus efficaces pourraient être trouvées pour empêcher une polymérisation spontanée. Ce chapitre vise à élucider le(s) mécanisme(s) principal(aux) d'auto-amorçage des monomères thiol-ènes, et à déterminer les facteurs qui sous-tendent la réactivité d'une polymérisation auto-amorcée thiol-ène, en particulier en ce qui concerne les conditions expérimentales (solvant, atmosphère) et la structure des composés ène et thiol.

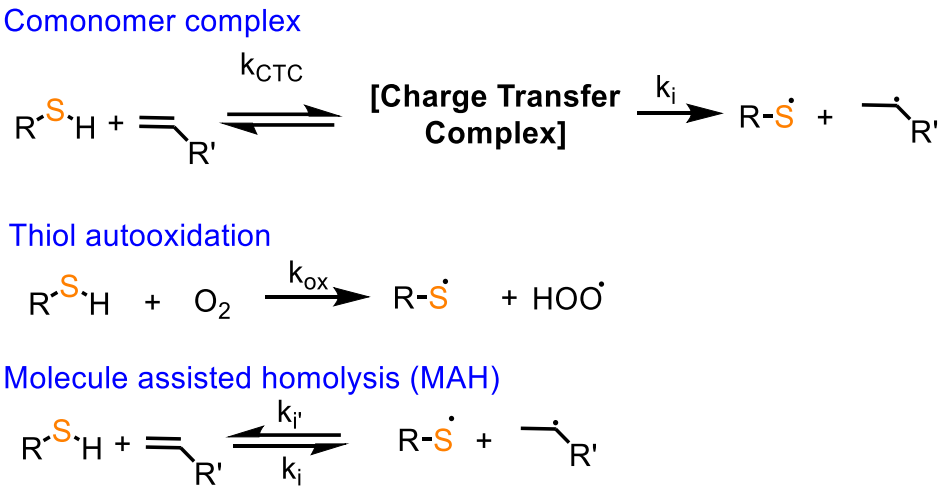

Schème V-2 Mécanismes possible de l'auto-amorçage d'une polymérisation thermique du thiol-ène.

Pour répondre à ces questions, l'adipate de diallyle (**DAA**), le phtalate de diallyle (**DAP**), le di(éthylène glycol) divinyl éther (**DVE**) sont utilisés comme alcènes modèles (**Figure II-1**). L'avantage des esters allyliques et des éthers vinyliques est leur incapacité à s'homopolymériser ou à réagir par réaction thiol-Michaël (addition nucléophile de thiolate à l'alcène) en raison de leurs substituants électro-donneurs. Ainsi, la polymérisation radicalaire du thiol-ène est considérée comme le processus prédominant en présence de thiols. La réactivité de ces 3 dienes avec une série de 5 dithiols (acétate **1**, propionate **2**, tri(éthylène glycol) **3**, sulfure d'alkyle **4**, hexane **5**, **Figure II-1**) a été étudiée dans des conditions évitant la formation intentionnelle de radicaux. Pour donner un aperçu des facteurs sous-jacents qui régissent le mécanisme d'auto-amorçage des monomères thiol-ène purs, trois domaines sont étudiés en profondeur : la cinétique de polymérisation auto-amorcée sans solvant et en solution, la solvatation du thiol et l'identification des radicaux amorceurs.

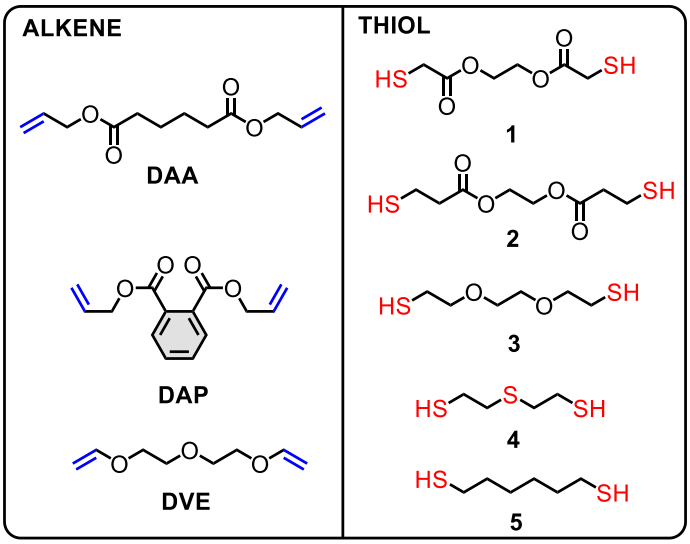

Figure V-1. Structures chimiques des thiols et alcènes bifonctionnels.

CHAPITRE III. PHOTOPOLYMERISATION THIOL-ENE EN MINIEMULSION

La famille des polymères acryliques est actuellement le choix prépondérant dans le domaine de la photopolymérisation industrielle.[12.191] Mais, les systèmes thiol-ène ont gagné en acceptation par leur aptitude à surmonter les problèmes associés à la toxicité des monomères ou au rétrécissement de volume du polymère.[51] Le résultat a été le développement de produits de niche,[35] tels que des hydrogels non cytotoxiques[190] ou des matériaux dentaires à faible retrait.[191]

Les monomères d'acrylate et de méthacrylate sont également des acteurs clés de la polymérisation en émulsion, un autre procédé de polymérisation très utile sur le plan industriel.[67] Les dispersions de polymères acryliques aqueuses résultantes sont formées par une polymérisation radicalaire en chaîne.[192] La caractéristique distinctive d'une polymérisation thiol-ène est que les chaînes polymères se forment progressivement par une réaction entre les groupes fonctionnels ène et thiol des réactifs.[193] Aussi, en utilisant une quantité stœchiométrique de monomères ène et thiol bifonctionnels, des latex de poly(thioéther) d'utilité pratique peuvent être formés, c'est-à-dire avec une masse moléculaire allant de un à plusieurs dizaines de milliers de g mol^{-1}.[151] Cependant,

contrairement aux photopolymères thiol-ène, la part détenue par les latex thiol-ène est restée limitée, et aucun produit commercial n'a encore vu le jour.[4,28] Les principaux exemples résultent d'une photopolymérisation en miniémulsion,[17,19,20,194–197,199–201] et dans une moindre mesure, la dispersion[202,203] et l'émulsion.[151,204] La photopolymérisation en suspension a également été décrite,[205,206,54,207,208] mais ce processus ne conduit pas à des colloïdes polymères (diamètre moyen des particules < 1 µm), mais à des billes solides micrométriques (0,1 - 10 mm).

Le procédé le plus utilisé dans ce domaine est donc la polymérisation en miniémulsion thiol-ène.[17,131,194–201] Impliquant des gouttelettes de monomère plus petites et donc moins diffusantes (50-500 nm) qu'une polymérisation en émulsion, elle présente l'avantage supplémentaire de permettre une plus grande pénétration du rayonnement à l'intérieur du réacteur. De plus, le mode de nucléation des particules souhaité se produit via la capture de radicaux dans les gouttelettes de monomère, ensuite converties en particules de polymère.[212] Par conséquent, lorsqu'une étape de polymérisation est confinée à des gouttelettes contenant une quantité stœchiométrique de groupes fonctionnels ène et thiol, l'équilibre peut être conduit vers des poids moléculaires élevés.[131] Cependant, six ans après le premier exemple de photopolymérisation en miniémulsion thiol-ène,[17] la question de l'efficacité de la nucléation des gouttelettes est encore largement sans réponse. En revanche, il existe des études approfondies concernant la polymérisation radicalaire en chaîne en miniémulsion.[213–215] Quel que soit le type de polymérisation, l'objectif d'une polymérisation en miniémulsion est de « nucléer » la plupart des gouttelettes de monomère initiales et de minimiser la *nucléation homogène;* c'est-à-dire le fait que des radicaux oligomères au lieu d'entrer dans les gouttelettes peuvent précipiter dans la phase aqueuse pour former des particules.[209] On s'attend à ce que la fraction de particules produites par nucléation dans des gouttelettes et par nucléation homogène varient dans une polymérisation à étapes thiol-ène par rapport à une polymérisation en chaîne en raison de relations distinctes entre la masse molaire moléculaire et le pourcentage de conversion du monomère.[216] Pour des raisons fondamentales et pratiques, il est intéressant de discuter des conditions de réaction favorisant la nucléation des gouttelettes de miniémulsion de monomère thiol-ène.

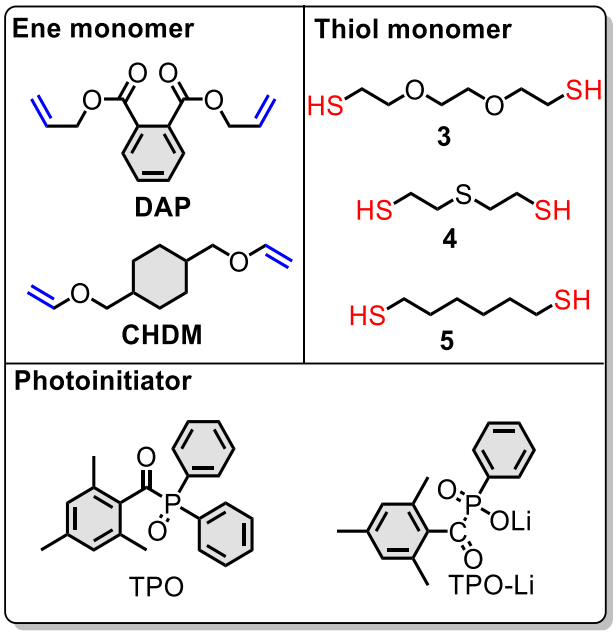

Figure III-1 Structure chimique des photoinitiateurs radicalaires, des monomères dithiol et diène.

Ce chapitre débute par la préparation et la photopolymérisation batch d'une miniémulsion modèle aqueuse à base de phtalate de diallyle (**DAP**) et de 2,2-(éthylènedioxy)diéthanedithiol (**3**) (voir les structures chimiques dans **Figure III-1**) avec du dodécyle sulfate de sodium (SDS) comme tensioactif et de l'hexadécane (HD) comme costabilisant. La fraction massique des monomères a été maintenue constante à 20 %, et un photoamorceur radicalaire hydrosoluble (TPO-Li) de la famille des oxydes de monoacylphosphine a été choisi. En utilisant une concentration appropriée de piégeur de radicaux (quinone), il a été possible d'obtenir une miniémulsion de **DAP**-**3** chimiquement stable. Dans ces conditions, la stabilité des gouttelettes, la cinétique de polymérisation, la progression de la masse molaire et la distribution de la taille des particules ont pu être déterminées. Cependant, il s'est avéré difficile de discuter du mécanisme de nucléation des particules avec ce système en raison de la stabilité limitée des gouttelettes. En diminuant la fraction massique de monomère à 1 % en poids, des gouttelettes de monomère possédant une photolatence, une monodispersité de taille et une stabilité colloïdale ont été obtenues. L'accent a été mis sur la compréhension des paramètres de réaction qui sont importants pour favoriser la nucléation des gouttelettes, c'est-à-dire la taille des gouttelettes, la solubilité de l'amorceur et la solubilité des monomères.[209] Des amorceurs et des monomères thiol-ène de différentes structures chimiques ont été utilisés dans ce but (voir **Figure III-1**). La comparaison

de la taille des particules (nombre) et de la taille des gouttelettes (nombre) a été exploitée pour évaluer qualitativement l'étendue de la nucléation homogène et dans les gouttelettes.[101]

CHAPITRE IV. PHOTOPOLYMÉRISATION THIOL-ENE EN ÉMULSION

La polymérisation en émulsion est un procédé largement utilisé dans l'industrie qui aboutit à des dispersions colloïdales de polymère avec un diamètre moyen de 50 à 200 nm.[67] [233] [234] Cependant, tous les polymères commerciaux produits par ce procédé (styrène-butadiène, acrylique, acétate de vinyle…) sont exclusivement préparés par polymérisation radicalaire en chaîne réalisée dans des réacteurs à cuve agitée.[209]

Très peu de polymères produits par polymérisation par étapes – principalement des polyesters – peuvent être préparés par polymérisation en émulsion aqueuse.[238-242] Pour obtenir des produits de haut poids moléculaire par polymérisation par étapes, il faut remplir un certain nombre de critères expérimentaux difficiles à concilier avec une polymérisation en émulsion dans l'eau : des conversions de monomères très élevées (> 98 %), l'absence de réactions secondaires (pour éviter un déséquilibre stœchiométrique des groupes fonctionnels), et une élimination efficace des sous-produits (pour déplacer l'équilibre dans le sens du polymère).[218] [243] Dans ce contexte, la polymérisation en miniémulsion s'est avérée mieux adaptée que la polymérisation en émulsion pour la synthèse de polymères par étapes dans l'eau car le transfert de masse de monomère à travers la phase aqueuse est évité, diminuant ainsi le risque de réactions secondaires.[212] Grâce à cette technique, la polymérisation par étapes en miniémulsion a donné naissance à un certain nombre de latex à base d'époxy,[242] polyuréthane,[243] polyester,[244] poly(diméthylsiloxane),[245] poly(thioéther)[17,131] et une large gamme d'hybrides "polymères-acryliques" à base d'eau.[246] Cependant, par rapport à une (macro)émulsion, la préparation d'une miniémulsion de monomères ajoute de la complexité et des coûts sous la forme d'une consommation d'énergie et d'un investissement en équipement plus élevés.[98] Ceci explique pourquoi cette technique n'a pas encore fait l'objet d'une mise en œuvre industrielle à grande échelle.[247]

La polymérisation en émulsion étant le procédé le plus courant pour la production de polymères dispersés, des recherches supplémentaires sont donc nécessaires pour surmonter les défis techniques de la polymérisation en émulsion par étapes.[249] Dans une étude fondatrice, Shipp et al.[204] ont rapporté en 2017 un exemple prometteur de polymérisation thiol-ène en émulsion. Bien qu'une quantité importante de données expérimentales ait été rapportée dans cette étude susmentionnée, les problèmes liés à la cinétique de polymérisation, à la distribution de la taille des particules et à la progression du poids moléculaire sont encore mal compris, en particulier en ce qui concerne les différences avec la polymérisation radicalaire en chaîne bien étudiée en émulsion. De plus, les mécanismes fondamentaux qui dictent la formation de particules dans une polymérisation radicalaire par étapes en émulsion doivent être clarifiés.

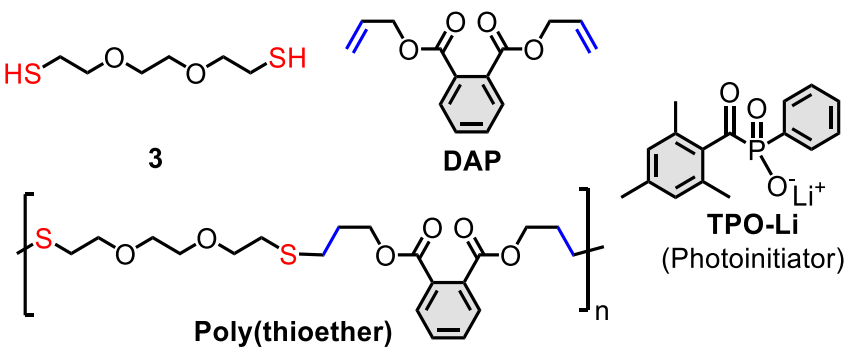

Schème IV-1 Structure chimique des monomères diène et dithiol **DAP** et **3**, photoamorceur radicalaire hydrosoluble (TPO-Li) et poly(thioéther) dérivé de la polyaddition **DAP**-**3**.

Pour répondre à ces questions, nous avons étudié la polyaddition batch photoinduite d'une émulsion aqueuse thiol-ène stabilisée par un tensioactif préparée avec les monomères bifonctionnels phtalate de diallyle (**DAP**) et 2,2-(éthylènedioxy)diéthanedithiol (**3**) (1:1 équiv.) à 25°C (**Scheme IV-1**). Pour être très proche des conditions opératoires d'une polymérisation en émulsion classique, nous avons utilisé le dodécyle sulfate de sodium (SDS) comme tensioactif et un photoamorceur hydrosoluble, le lithium phényl(2,4,6-triméthylbenzoyl)phosphinate (TPO-Li). La photopolymérisation (λ_{max} = 385 nm, 3,7 mW cm^{-2}) a entraîné après 20 min une conversion de monomères supérieure à 99 %, un latex de poly(thioéther) sans coagulum avec un contenu en solides de 10 % massique, et des particules stables ayant un diamètre moyen de 60 nm. Malgré une atténuation significative du rayonnement due à la diffusion multiple de gouttelettes de monomère, des vitesses de

polymérisation plus rapides et des poids moléculaires plus élevés ont été obtenus par rapport à une expérience témoin impliquant un initiateur redox soluble dans l'eau. Le fait que la polymérisation en émulsion soit initiée photochimiquement ouvre de nouvelles possibilités pour améliorer le contrôle temporel de la réaction et la modification de la masse molaire par l'intensité de l'irradiation. Pour prouver la polyvalence de notre procédé, l'effet de la teneur en solides du latex (5 à 40 % en poids) et le rapport thiol-ène non stœchiométrique ont également été étudiés. Enfin, pour clarifier le mécanisme de nucléation, nous avons déterminé le nombre de particules (N_p) en fonction de la concentration en tensioactif.

CHAPITRE V. PHOTOPOLYMERISATION THIOL-ENE EN ÉMULSION : PHOTOCATALYSE et PHOTOREACTEUR

Généralement, la réaction radicalaire thiol-ène est initiée par voie thermique[262] ou par des moyens photochimiques.[263] La décomposition d'un (photo)amorceur radicalaire donne des radicaux primaires qui arrache un hydrogène des thiols pour former des radicaux thiyls. Ces dernières espèces amorcent alors la réaction thiol-ène. Depuis le travail pionnier de Yoon et al. en 2013,[264] un certain nombre de photocatalyseurs redox sont également connus pour la réaction radicalaire thiol-ène sous lumière visible. La principale classe de composés comprend les complexes de métaux de transition, des particules d'oxyde métallique, ainsi que divers photocatalyseurs organiques. Le mécanisme est considéré comme impliquant la photooxydation directe du thiol par le catalyseur excité électroniquement pour générer un cation radical thiyle. Sa déprotonation ultérieure génère un radical thiyl, qui est alors impliqué dans le cycle réactionnel classique thiol-ène. La plupart des chromophores photocatalytiques absorbent généralement à des longueurs d'onde plus longues que les photoamorceurs et sont donc plus compatibles avec de structures organiques fonctionnalisées, très courantes en chimie organique. De plus, une catalyse photorédox procède en principe par un mécanisme de réaction en chaîne radicalaire impliquant certaines étapes de régénération du catalyseur, qui aident à minimiser la quantité de catalyseur utilisée. Bien que de nombreuses études aient

conclu à la facilité d'accomplir la réaction thiol-ène avec un rendement relativement élevé (70-90%) et un minimum de réactions secondaires, elles ont également signalé que de longues durées d'irradiation (1-24h), une charge élevée en catalyseur (1- 10%mol) ou une irradiance élevée étaient nécessaires.

Ces limitations expliquent que la polymérisation photocatalytique thiol-ène soit peu utilisée. Pour obtenir de rendements élevés et des polymères de fortes masses molaires élevé, de telles polymérisations par étape doivent être effectuées avec un rapport stœchiométrique de monomères bifonctionnels ène et thiol et conduire à des conversions très élevées (> 98-99%). La synthèse de poly(thioéther) téléchélique de bas poids moléculaire a été décrite en utilisant fac-Ir(ppy)$_3$[279] et 4-(diphénylamino)benzaldéhyde comme photocatalyseur.[280] Des poids moléculaires et des vitesses de réaction plus élevés ont été atteints par Boyer[281] et Konkolewicz[282] par un mécanisme de réaction différent impliquant un médiateur redox supplémentaire, une amine ou un halogénure d'alkyle respectivement, qui contourne la lenteur de la photooxydation directe du thiol avec le photocatalyseur.[283]

Pour étendre encore davantage la polymérisation photocatalytique thiol-ène sous lumière visible, nous décrivons ici un procédé de polymérisation en émulsion pour préparer des latex de poly(thioéther) semi-cristallins linéaires dans l'eau, en utilisant l'éosine-Y disodique (EY^{2-})comme photocatalyseur (**Schéma V-3**).[276,284] Nous avons réussi à concevoir un procédé utilisant une faible irradiance (< 5 mW cm^{-2}), des sources d'irradiation accessibles (LED), de faibles concentration de catalyseur (< 0,1% mol), rapide (< 1 h), sélectif et adaptable à une large gamme de monomères. Toutes ces caractéristiques sont en accord avec les critères définis par Bowman pour une réaction « photoclick ».[55]

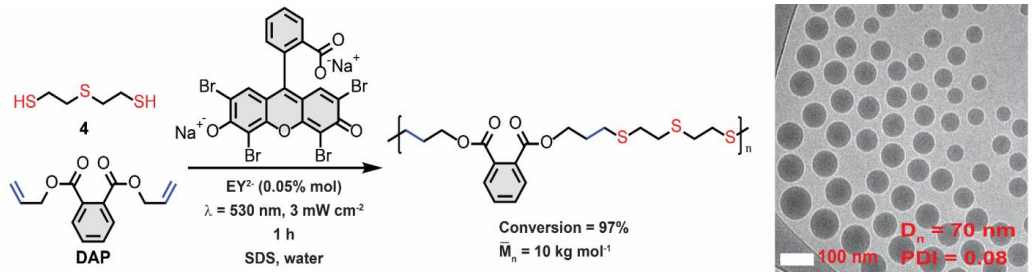

Schéma V-1. Monomères thiol-ène et photocatalyseur utilisés dans cette étude. L'émulsion de monomère a été préparée à des concentrations de SDS = 13,5 mM, EY^{2-}= 0,29 mM/eau (0,05 % mol/monomères) et un tampon phosphate (pH 8,0 ; 0,01 M) et irradiée par une LED verte (λ = 530 nm, I = 3 mW cm^{-2}) pendant une heure sous agitation magnétique à 1100 rpm.

REFERENCES

(1) Moad, G.; Solomon, D. H. T*he chemistry of radical polymerization*; Elsevier, 2006.

(2) Young, R. J.; Lovell, P. A. *Introduction to Polymers*; CRC press, 2011.

(3) Dubé, M. A.; Gabriel, V. A.; Pakdel, A. S.; Zhang, Y. Sustainable polymer reaction engineering: are we there yet? *Can. J. Chem. Eng.* **2020**. https://doi.org/10.1002/cjce.23865.

(4) Jasinski, F.; Zetterlund, P. B.; Braun, A. M.; Chemtob, A. Photopolymerization in dispersed systems. *Prog. Polym. Sci.* **2018**, *84*, 47–88. https://doi.org/10.1016/j.progpolymsci.2018.06.006.

(5) Anderson, C. D.; Daniels, E. S. Emulsion polymerisation and latex applications, Vol. 14, 2003. *Rapra Technol.*

(6) Lovell, P. A.; Schork, F. J. Fundamentals of emulsion polymerization. *Biomacromolecules* **2020**, *21* (11), 4396–4441. https://doi.org/10.1021/acs.biomac.0c00769.

(7) A. M. van Herk. *Chemistry and technology of emulsion polymerisation*; John Wiley & Sons, 2013.

(8) Dietliker, K.; Braig, A.; Ricci, A. Industrial applications of photochemistry: automotive coatings and beyond. in *photochemistry*; photochemistry; 2010; pp 344–368.

(9) *Handbook of industrial inkjet printing (A Full System Approach)*; Werner, Z., Ed.; Wiley-VCH Verlag, 2017.

(10) Wang, X.; Schmidt, F.; Hanaor, D.; Kamm, P. H.; Li, S.; Gurlo, A. Additive manufacturing of ceramics from preceramic polymers: a versatile stereolithographic approach assisted by thiol-ene click chemistry. *Addit. Manuf.* **2019**, *27*, 80–90. https://doi.org/10.1016/j.addma.2019.02.012.

(11) Turro, N. J.; Chow, M.-F.; Chung, C.-J.; Tung, C.-H. An efficient, high conversion photoinduced emulsion polymerization. magnetic field effects on polymerization efficiency and polymer molecular weight. *J. Am. Chem. Soc.* **1980**, *102* (24), 7391–7393. https://doi.org/10.1021/ja00544a053.

(12) *Photopolymerisation initiating systems:*; Lalevée, J., Fouassier, J.-P., Eds.; Polymer Chemistry Series; Royal Society of Chemistry: Cambridge, 2018. https://doi.org/10.1039/9781788013307.

(13) Hoyle, C. E.; Lee, T. Y.; Roper, T. Thiol–enes: chemistry of the past with promise for the future. *J. Polym. Sci. Part Polym. Chem.* **2004**, *42* (21), 5301–5338. https://doi.org/10.1002/pola.20366.

(14) Jacobine, A. F. Thiol-ene polymerization. in *Radiation curing in polymer science and technology*; Elsevier: London (UK), 1993.

(15) Hoyle, C. E.; Bowman, C. N. Thiol-ene click chemistry. *Angew. Chem.-Int. Ed.* **2010**, *49* (9), 1540–1573. https://doi.org/10.1002/anie.200903924.

(16) Konuray, O.; Fernández-Francos, X.; De la Flor, S.; Ramis, X.; Serra, À. The use of click-type reactions in the preparation of thermosets. *Polymers* **2020**, *12* (5), 1084. https://doi.org/10.3390/polym12051084.

(17) Jasinski, F.; Lobry, E.; Tarablsi, B.; Chemtob, A.; Croutxe-Barghorn, C.; Le Nouen, D.; Criqui, A. Light-mediated thiol-ene polymerization in miniemulsion: a fast route to semicrystalline polysulfide nanoparticles. *ACS Macro Lett.* **2014**, *3* (9), 958–962. https://doi.org/10.1021/mz500458s.

(18) Amato, D. V.; Amato, D. N.; Flynt, A. S.; Patton, D. L. Functional, sub-100 nm polymer nanoparticles via thiol–ene miniemulsion photopolymerization. *Polym. Chem.* **2015**, *6* (31), 5625–5632. https://doi.org/10.1039/c4py01449a.

(19) Jasinski, F.; Rannée, A.; Schweitzer, J.; Fischer, D.; Lobry, E.; Croutxé-Barghorn, C.; Schmutz, M.; Le Nouen, D.; Criqui, A.; Chemtob, A. Thiol–ene linear step-growth photopolymerization in miniemulsion: fast rates, redox-responsive particles, and semicrystalline films. *Macromolecules* **2016**, *49* (4), 1143–1153. https://doi.org/10.1021/acs.macromol.5b02512.

(20) Machado, T. O.; Cardoso, P. B.; Feuser, P. E.; Sayer, C.; Araujo, P. H. H. Thiol-ene miniemulsion polymerization of a biobased monomer for biomedical applications. *Colloids Surf B Biointerfaces* **2017**, *159*, 509–517. https://doi.org/10.1016/j.colsurfb.2017.07.043.

(21) Resetco, C.; Hendriks, B.; Badi, N.; Prez, F. D. Thiol–ene chemistry for polymer coatings and surface modification – building in sustainability and performance. *Mater. Horiz.* **2017**, *4* (6), 1041–1053. https://doi.org/10.1039/C7MH00488E.

(22) Kuhne, G.; Diesen, J. S.; Klemm, E. New results of the self-initiation mechanism of sh/en addition polymerization. *Angew. Makromol. Chem.* **1996**, *242*, 139–145. https://doi.org/10.1002/apmc.1996.052420109.

(23) Klemm, E.; Sensfuß, S.; Holfter, U.; Flammersheim, H. J. Free-radical stabilizers for the thiol/ene-systems. *Angew. Makromol. Chem.* **1993**, *212* (1), 121–127. https://doi.org/10.1002/apmc.1993.052120111.

(24) Hiatt, R. R.; Bartlett, P. D. The thermal reaction of styrene with ethyl thioglycolate; evidence for the termolecular thermal initiation of styrene polymerization. *J Am Chem Soc* **1959**, *81*, 1149–1154.

(25) Nuyken, O.; Reuschel, G.; Siebzehnrübl, F. Novel sulfur containing polymers. *Makromol. Chem. Macromol. Symp.* **1989**, *26* (1), 313–331. https://doi.org/10.1002/masy.19890260129.

(26) Naumann, S.; Buchmeiser, M. R. Latent and delayed action polymerization systems. *Macromol Rapid Commun* **2014**, *35* (7), 682–701. https://doi.org/10.1002/marc.201300898.

(27) Lowe, C.; Bowman, C. *Thiol-x chemistries in polymer and materials science*; Lowe, C., Ed.; Series, R. P. C., Bowman, C., Series Eds.; RSC Polymer Chemistry Series n°6; Royal Society of Chemistry, 2013.

(28) Durham, O. Z.; Shipp, D. A. Polymer colloids from step-growth thiol-x polymerizations. *Polym Rev* **2020**, *0* (0), 1–26. https://doi.org/10.1080/15583724.2020.1743307.

(29) Posner, T. Beiträge Zur Kenntniss Der Ungesättigten Verbindungen. II. Ueber Die addition von mercaptanen an ungesättigte kohlenwasserstoffe. *Berichte Dtsch. Chem. Ges.* **1905**, *38* (1), 646–657. https://doi.org/10.1002/cber.190503801106.

(30) Kharasch, M. S.; Read, A. T.; Mayo, F. R. The peroxide effect in the addition of reagents to unsaturated compounds. xvi. the addition of thioglycolic acid to styrene and isobutylene. *Chem Ind* **1938**, *57*, 752.

(31) Drake, C. D. Preparation of polymeric sulphides. US2347182A, April 25, 1944.

(32) Hoyle, C. E.; Lowe, A. B.; Bowman, C. N. Thiol-click chemistry: a multifaceted toolbox for small molecule and polymer synthesis. *Chem. Soc. Rev.* **2010**, *39* (4), 1355–1387. https://doi.org/10.1039/b901979k.

(33) Hoyle, C. E.; Lee, T. Y.; Roper, T. Thiol-enes: chemistry of the past with promise for the future. *J. Polym. Sci. Part Polym. Chem.* **2004**, *42* (21), 5301–5338. https://doi.org/10.1002/pola.20366.

(34) Killops, K. L.; Campos, L. M.; Hawker, C. J. Robust, Efficient, and orthogonal synthesis of dendrimers via thiol-ene "click" chemistry. *J. Am. Chem. Soc.* **2008**, *130* (15), 5062–5064. https://doi.org/10.1021/ja8006325.

(35) Machado, T. O.; Sayer, C.; Araujo, P. H. H. Thiol-Ene Polymerisation: A promising technique to obtain novel biomaterials. *Eur. Polym. J.* **2017**, *86*, 200–215. https://doi.org/10.1016/j.eurpolymj.2016.02.025.

(36) Cramer, N. B.; Reddy, S. K.; O'Brien, A. K.; Bowman, C. N. Thiol−ene photopolymerization mechanism and rate limiting step changes for various vinyl functional group chemistries. *Macromolecules* **2003**, *36* (21), 7964–7969. https://doi.org/10.1021/ma034667s.

(37) Cramer, N. B.; Davies, T.; O'Brien, A. K.; Bowman, C. N. Mechanism and modeling of a thiol−ene photopolymerization. *Macromolecules* **2003**, *36* (12), 4631–4636. https://doi.org/10.1021/ma034072x.

(38) Lee, T. Y.; Smith, Z.; Reddy, S. K.; Cramer, N. B.; Bowman, C. N. Thiol−allyl ether−methacrylate ternary systems. polymerization mechanism. *Macromolecules* **2007**, *40* (5), 1466–1472. https://doi.org/10.1021/ma062494b.

(39) Reddy, S. K.; Cramer, N. B.; Bowman, C. N. Thiol−vinyl mechanisms. 1. termination and propagation kinetics in thiol−ene photopolymerizations. *Macromolecules* **2006**, *39* (10), 3673–3680. https://doi.org/10.1021/ma060008e.

(40) Reddy, S. K.; Cramer, N. B.; Bowman, C. N. Thiol−vinyl mechanisms. 2. kinetic modeling of ternary thiol−vinyl photopolymerizations. *Macromolecules* **2006**, *39* (10), 3681–3687. https://doi.org/10.1021/ma0600097.

(41) Griesbaum, K. Problems and possibilities of the free-radical addition of thiols to unsaturated compounds. *Angew. Chem. Int. Ed. Engl.* **1970**, *9* (4), 273–287. https://doi.org/10.1002/anie.197002731.

(42) Hong, M.; Liu, S.-R.; Li, B.-X.; Li, Y.-S. Application of thiol-ene click chemistry to preparation of functional polyethylene with high molecular weight and high polar group content: influence of thiol structure and vinyl type on reactivity. *J. Polym. Sci. Part Polym. Chem.* **2012**, *50* (12), 2499–2506. https://doi.org/10.1002/pola.26026.

(43) Morgan, C. R.; Magnotta, F.; Ketley, A. D. Thiol/ene photocurable polymers. *J. Polym. Sci. Polym. Chem. Ed.* **1977**, *15* (3), 627–645.

(44) Kühne, G.; Diesen, J. S.; Klemm, E. New results of the self-initiation mechanism of sh/en addition polymerization. *Angew. Makromol. Chem.* **1996**, *242* (1), 139–145. https://doi.org/10.1002/apmc.1996.052420109.

(45) Türünç, O.; Meier, M. A. R. The thiol-ene (click) reaction for the synthesis of plant oil derived polymers. *Eur. J. Lipid Sci. Technol.* **2013**, *115* (1), 41–54. https://doi.org/10.1002/ejlt.201200148.

(46) Long, K. F.; Bongiardina, N. J.; Mayordomo, P.; Olin, M. J.; Ortega, A. D.; Bowman, C. N. Effects of 1°, 2°, and 3° thiols on thiol–ene reactions: polymerization kinetics and mechanical behavior. *Macromolecules* **2020**, *53* (14), 5805–5815. https://doi.org/10.1021/acs.macromol.0c00369.

(47) Wutticharoenwong, K.; Soucek, M. D. Influence of the thiol structure on the kinetics of thiol-ene photopolymerization with time-resolved infrared spectroscopy. *Macromol. Mater. Eng.* **2008**, *293* (1), 45–56. https://doi.org/10.1002/mame.200700175.

(48) Li, Q.; Zhou, H.; Hoyle, C. E. The effect of thiol and ene structures on thiol–ene networks: photopolymerization, physical, mechanical and optical properties. *Polymer* **2009**, *50* (10), 2237–2245. https://doi.org/10.1016/j.polymer.2009.03.026.

(49) Roper, T. M.; Guymon, C. A.; Jönsson, E. S.; Hoyle, C. E. Influence of the alkene structure on the mechanism and kinetics of thiol–alkene photopolymerizations with real-time infrared spectroscopy. *J. Polym. Sci. Part Polym. Chem.* **2004**, *42* (24), 6283–6298. https://doi.org/10.1002/pola.20452.

(50) Northrop, B. H.; Coffey, R. N. Thiol-ene click chemistry: computational and kinetic analysis of the influence of alkene functionality. *J. Am. Chem. Soc.* **2012**, *134* (33), 13804–13817. https://doi.org/10.1021/ja305441d.

(51) Cramer, N. B.; Bowman, C. N. Chapter 1. Thiol-ene and thiol-yne chemistry in ideal network synthesis. In *Polymer Chemistry Series*; Lowe, A., Bowman, C., Eds.; Royal Society of Chemistry: Cambridge, 2013; pp 1–27. https://doi.org/10.1039/9781849736961-00001.

(52) Ligon, S. C.; Husar, B.; Wutzel, H.; Holman, R.; Liska, R. Strategies to reduce oxygen inhibition in photoinduced polymerization. *Chem. Rev.* **2014**, *114* (1), 557–589. https://doi.org/10.1021/cr3005197.

(53) O'Brien, A. K.; Cramer, N. B.; Bowman, C. N. Oxygen inhibition in thiol–acrylate photopolymerizations. *J. Polym. Sci. Part Polym. Chem.* **2006**, *44* (6), 2007–2014. https://doi.org/10.1002/pola.21304.

(54) Durham, O. Z.; Norton, H. R.; Shipp, D. A. Functional polymer particles via thiol–ene and thiol–yne suspension "click" polymerization. *RSC Adv.* **2015**, *5* (82), 66757–66766. https://doi.org/10.1039/C5RA12553G.

(55) Fairbanks, B. D.; Macdougall, L. J.; Mavila, S.; Sinha, J.; Kirkpatrick, B. E.; Anseth, K. S.; Bowman, C. N. Photoclick chemistry: a bright idea. *Chem. Rev.* **2021**, *121* (12), 6915–6990. https://doi.org/10.1021/acs.chemrev.0c01212.

(56) Esfandiari, P.; Ligon, S. C.; Lagref, J. J.; Frantz, R.; Cherkaoui, Z.; Liska, R. Efficient stabilization of thiol-ene formulations in radical photopolymerization. *J. Polym. Sci. Part Polym. Chem.* **2013**, *51* (20), 4261–4266. https://doi.org/10.1002/pola.26848.

(57) Belon, C.; Allonas, X.; Croutxe-Barghorn, C.; Lalevee, J. Overcoming the oxygen inhibitionin the photopolymerization of acrylates: a study of the beneficial effect of triphenylphosphine. *J Polym Sci Part Polym Chem* **2010**, *48*, 2462–2469.

(58) Edler, M.; Mostegel, F. H.; Roth, M.; Oesterreicher, A.; Kappaun, S.; Griesser, T. Enhancing the stability of uv-curable thiol/vinyl carbonate resins. *J. Appl. Polym. Sci.* **2017**, *134* (24).

(59) Chen, L.; Wu, Q.; Wei, G.; Liu, R.; Li, Z. Highly Stable Thiol–Ene Systems: From their structure–property relationship to dlp 3d printing. *J. Mater. Chem. C* **2018**, *6* (43), 11561–11568. https://doi.org/10.1039/c8tc03389g.

(60) Long, K. F.; Wang, H.; Dimos, T. T.; Bowman, C. N. Effects of thiol substitution on the kinetics and efficiency of thiol-michael reactions and polymerizations. *Macromolecules* **2021**, *54* (7), 3093–3100. https://doi.org/10.1021/acs.macromol.0c02677.

(61) Miyata, H.; Ikeda, H.; Murofushi, K.; Hattori, Y.; Urakawa, K. Polymerization accelerator, curable composition, cured product, and process for producing thiol compound. US20100029876A1, February 4, 2010.

(62) Childress, K. K.; Alim, M. D.; Mavila, S.; Martinez, V.; Ding, Y.; Bowman, C. N.; Stansbury, J. W. Systematic modulation and structure–property relationships in photopolymerizable thermoplastics. *ACS Appl. Polym. Mater.* **2021**, *3* (2), 1171–1181.

(63) Chern, C.-S. *Principles and applications of emulsion polymerization*; John Wiley & Sons, 2008.

(64) Lovell, P. A.; El-Aasser, M. S. *Emulsion polymerization and emulsion polymers*; Wiley, 1997.

(65) Harkins, W. D. A General theory of the mechanism of emulsion polymerization1. *J. Am. Chem. Soc.* **1947**, *69* (6), 1428–1444.

(66) Chern, C. S. Emulsion polymerization mechanisms and kinetics. *Prog. Polym. Sci.* **2006**, *31* (5), 443–486. https://doi.org/10.1016/j.progpolymsci.2006.02.001.

(67) van Herk, A. M.; Gilbert, R. G. Emulsion polymerisation. in *chemistry and technology of emulsion polymerisation*; van Herk, A. M., Ed.; John Wiley & Sons Ltd: Oxford, UK, 2013; pp 43–73. https://doi.org/10.1002/9781118638521.ch3.

(68) Thickett, S. C.; Gilbert, R. G. Emulsion polymerization: state of the art in kinetics and mechanisms. *Polymer* **2007**, *48* (24), 6965–6991. https://doi.org/10.1016/j.polymer.2007.09.031.

(69) Smith, W. V.; Ewart, R. H. Kinetics of emulsion polymerization. *J. Chem. Phys.* **1948**, *16* (6), 592–599.

(70) Priest, W. J. Particle growth in the aqueous polymerization of vinyl acetate. *J. Phys. Chem.* **1952**, *56* (9), 1077–1082. https://doi.org/10.1021/j150501a010.

(71) Fitch, R. M.; Tsai, C. H. Particle formation in polymer colloids, iii: prediction of the number of particles by a homogeneous nucleation theory; Fitch, R. M., Series Ed.; Polymer Colloids; Springer US, 1971; pp 73–102.

(72) Coen, E. M.; Peach, S.; Morrison, B. R.; Gilbert, R. G. First-principles calculation of particle formation in emulsion polymerization: pseudo-bulk systems. *Polymer* **2004**, *45* (11), 3595–3608. https://doi.org/10.1016/j.polymer.2004.03.084.

(73) Hansen, F. K.; Ugelstad, J. Particle nucleation in emulsion polymerization. iv. nucleation in monomer droplets. *J. Polym. Sci. Polym. Chem. Ed.* **1979**, *17* (10), 3069–3082. https://doi.org/10.1002/pol.1979.170171003.

(74) Takeishi, M.; Yoshida, H.; Niino, S.; Hayama, S. Photopolymerization of styrene in water in the presence of N-Laurylpyridinium azide. *Makromol. Chem.* **1978**, *179* (5), 1387–1391. https://doi.org/10.1002/macp.1978.021790531.

(75) Lougnot, D. J.; Merlin, A.; Jacques, P.; Fouassier, J. P. Behaviour of the excited states of the initiator in a photoinduced emulsion polymerization. *Makromol. Chem. Rapid Commun.* **1980**, *1* (11), 687–691. https://doi.org/10.1002/marc.1980.030011106.

(76) Piogé, S.; Nicol, E. Chapter 18. emulsion photopolymerization. in *photopolymerisation initiating systems*; Polymer Chemistry Series; The Royal Society of Chemistry, 2018; pp 552–572.

(77) Fan, W.; Tosaka, M.; Yamago, S.; Cunningham, M. F. Living ab initio emulsion polymerization of methyl methacrylate in water using a water-soluble organotellurium chain transfer agent under thermal and photochemical conditions. *Angew. Chem. Int. Ed. Engl.* **2018**, *57* (4), 962–966. https://doi.org/10.1002/anie.201710754.

(78) Su, X.; Jiang, Y.; Jessop, P. G.; Cunningham, M. F.; Feng, Y. Photoinitiated TERP emulsion polymerization: a new member of the large family of preparation approaches for CO_2-switchable latexes. *Macromolecules* **2020**, *53* (14), 6018–6023. https://doi.org/10.1021/acs.macromol.0c00616.

(79) Wang, Y.; Dadashi-Silab, S.; Lorandi, F.; Matyjaszewski, K. Photoinduced atom transfer radical polymerization in ab initio emulsion. *Polymer* **2019**, *165*, 163–167. https://doi.org/10.1016/j.polymer.2019.01.034.

(80) Turro, N. J.; Chow, M. F.; Chung, C. J.; Tung, C. H. Magnetic field and magnetic isotope effects on photoinduced emulsion polymerization. *J. Am. Chem. Soc.* **1983**, *105* (6), 1572–1577. https://doi.org/10.1021/ja00344a025.

(81) Turro, N. J.; Arora, K. S. Magnetic effects on photoinduced emulsion polymerization. effects of lanthanide ion addition. *Macromolecules* **1986**, *19* (1), 42–46. https://doi.org/10.1021/ma00155a008.

(82) Turro, N. J.; Pierola, I. F.; Chung, C.-J. Stereochemistry of photoinitiated emulsion polymerization. *J. Polym. Sci. Polym. Chem. Ed.* **1983**, *21* (4), 1085–1096. https://doi.org/10.1002/pol.1983.170210416.

(83) Mah, S.; Lee, D.; Koo, D.; Kwon, S. Photo-induced emulsion polymerization of vinyl acetate in the presence of poly(oxyethylene) nonyl phenyl ether, a nonionic emulsifier (II). *J. Appl. Polym. Sci.* **2002**, *86* (9), 2153–2158. https://doi.org/10.1002/app.11049.

(84) Mah, S.; Koo, D.; Jeon, H.; Kwon, S. Photo-induced emulsion polymerization of vinyl acetate in the presence of poly(oxyethylene)10 nonyl phenyl ether ammonium sulfate, an anionic emulsifier (I). *J. Appl. Polym. Sci.* **2002**, *84* (13), 2425–2431. https://doi.org/10.1002/app.10531.

(85) Kwak, J.; Lacroix-Desmazes, P.; Robin, J. J.; Boutevin, B.; Torres, N. Synthesis of mono functional carboxylic acid poly(methyl methacrylate) in aqueous medium using sur-iniferter. application to the synthesis of graft copolymers polyethylene-g-poly(methyl methacrylate) and the compatibilization of LDPE/PVDF blends. *Polymer* **2003**, *44* (18), 5119–5130. https://doi.org/10.1016/S0032-3861(03)00525-1.

(86) Shim, S. E.; Shin, Y.; Jun, J. W.; Lee, K.; Jung, H.; Choe, S. Living-free-radical emulsion photopolymerization of methyl methacrylate by a surface active iniferter (suriniferter). *Macromolecules* **2003**, *36* (21), 7994–8000. https://doi.org/10.1021/ma034331i.

(87) Hu, X.; Zhang, J.; Yang, W. Preparation of transparent polystyrene nano-latexes by an uv-induced routine emulsion polymerization. *Polymer* **2009**, *50* (1), 141–147. https://doi.org/10.1016/j.polymer.2008.10.058.

(88) Zhang, H.; Zang, L.; Luo, J.; Guo, J. Preparation of poly(methyl methacrylate) nano-latexes via uv irradiation in the presence of iron aqueous solution. *E-Polym.* **2012**, *12* (1), 1–10. https://doi.org/10.1515/epoly.2012.12.1.376.

(89) Muller, G.; Zalibera, M.; Gescheidt, G.; Rosenthal, A.; Santiso-Quinones, G.; Dietliker, K.; Grutzmacher, H. Simple One-pot syntheses of water-soluble bis(acyl)phosphane oxide photoinitiators and their application in surfactant-free emulsion polymerization. *Macromol. Rapid Commun.* **2015**, *36* (6), 553–557. https://doi.org/10.1002/marc.201400743.

(90) Chicoma, D. L.; Carranza, V.; Giudici, R. Synthesis of core-shell particles of polystyrene and poly(methyl methacrylate) using emulsion photopolymerization. *Macromol. Symp.* **2013**, *324* (1), 124–133. https://doi.org/10.1002/masy.201200076.

(91) Lu, Y.; Wittemann, A.; Ballauff, M.; Drechsler, M. Preparation of polystyrene-poly(n-isopropylacrylamide) (ps-pnipa) core-shell particles by photoemulsion polymerization. *Macromol. Rapid Commun.* **2006**, *27* (14), 1137–1141. https://doi.org/10.1002/marc.200600190.

(92) Krüger, K.; Tauer, K.; Yagci, Y.; Moszner, N. Photoinitiated bulk and emulsion polymerization of styrene – evidence for photo-controlled radical polymerization. *Macromolecules* **2011**, *44* (24), 9539–9549. https://doi.org/10.1021/ma2021997.

(93) Laurino, P.; Hernandez, H. F.; Bräuer, J.; Krüger, K.; Grützmacher, H.; Tauer, K.; Seeberger, P. H. Snowballing radical generation leads to ultrahigh molecular weight polymers. *Macromol. Rapid Commun.* **2012**, *33* (20), 1770–1774. https://doi.org/10.1002/marc.201200384.

(94) Le Quemener, F.; Subervie, D.; Morlet-Savary, F.; Lalevee, J.; Lansalot, M.; Bourgeat-Lami, E.; Lacote, E. Visible-light emulsion photopolymerization of styrene. *Angew. Chem. Int. Ed. Engl.* **2018**, *57* (4), 957–961. https://doi.org/10.1002/anie.201710488.

(95) Cao, Q.; Heil, T.; Kumru, B.; Antonietti, M.; Schmidt, B. V. K. J. Visible-light induced emulsion photopolymerization with carbon nitride as a stabilizer and photoinitiator. *Polym. Chem.* **2019**, *10* (39), 5315–5323. https://doi.org/10.1039/c9py01157a.

(96) Subervie, D.; Le Quéméner, F.; Canterel, R.; Dugas, P.-Y.; Boyron, O.; Lalevée, J.; Bourgeat-Lami, E.; Lansalot, M.; Lacôte, E. Visible-light emulsion photopolymerization of acrylates and methacrylates: mechanistic insights and introduction of a simplified sulfur-based photoinitiating system. *Macromolecules* **2021**, *54* (5), 2124–2133. https://doi.org/10.1021/acs.macromol.0c01692.

(97) Tang, P. L.; Sudol, E. D.; Adams, M. E.; Silebi, C. A.; El-Aasser, M. S. Miniemulsion polymerization. in *polymer latexes*; ACS Symposium Series; American Chemical Society, 1992; Vol. 492, pp 72–98. https://doi.org/10.1021/bk-1992-0492.ch006.

(98) Asua, J. M. Miniemulsion polymerization. *Prog. Polym. Sci.* **2002**, *27* (7), 1283–1346. https://doi.org/10.1016/S0079-6700(02)00010-2.

(99) Cheng, S.; Guo, Y.; Zetterlund, P. B. Miniemulsion polymerization based on low energy emulsification with preservation of initial droplet identity. *Macromolecules* **2010**, *43* (19), 7905–7907. https://doi.org/10.1021/ma101574x.

(100) Boscán, F.; Barandiaran, M. J.; Paulis, M. From miniemulsion to nanoemulsion polymerization of superhydrophobic monomers through low energy phase inversion temperature. *J. Ind. Eng. Chem.* **2018**, *58*, 1–8. https://doi.org/10.1016/j.jiec.2017.08.052.

(101) Nauman, N.; Zaquen, N.; Junkers, T.; Boyer, C.; Zetterlund, P. B. Particle size control in miniemulsion polymerization via membrane emulsification. *Macromolecules* **2019**, *52* (12), 4492–4499. https://doi.org/10.1021/acs.macromol.9b00447.

(102) Zetterlund, P. B.; Thickett, S. C.; Perrier, S.; Bourgeat-Lami, E.; Lansalot, M. Controlled/living radical polymerization in dispersed systems: an update. *Chem. Rev.* **2015**, *115* (18), 9745–9800. https://doi.org/10.1021/cr500625k.

(103) Asua, J. M.; Rodriguez, V. S.; Silebi, C. A.; El-Aasser, M. S. Miniemulsion copolymerization of styrene-methyl methacrylate: effect of transport phenomena. *Makromol. Chem. Macromol. Symp.* **1990**, *35–36* (1), 59–85. https://doi.org/10.1002/masy.19900350107.

(104) Chern, C. S.; Chen, T. J.; Liou, Y. C. Miniemulsion polymerization of styrene in the presence of a water-insoluble blue dye. *Polymer* **1998**, *39* (16), 3767–3777. https://doi.org/10.1016/s0032-3861(97)10347-0.

(105) Li, J.; Fan, J.; Cao, R.; Zhang, Z.; Du, J.; Peng, X. Encapsulated dye/polymer nanoparticles prepared via miniemulsion polymerization for inkjet printing. *ACS Omega* **2018**, *3* (7), 7380–7387. https://doi.org/10.1021/acsomega.8b01151.

(106) Freire, N. F.; Feuser, P. E.; da Silva Abel, J.; Machado-de-Ávila, R. A.; Lopes Fialho, R.; Cabral Albuquerque, E.; Sayer, C.; Hermes de Araújo, P. H. Zinc phthalocyanine encapsulation via thiol-ene miniemulsion polymerization and in vitro photoxicity studies. *Int. J. Polym. Mater. Polym. Biomater.* **2020**, 1–10. https://doi.org/10.1080/00914037.2020.1838517.

(107) Volz, M.; Ziener, U.; Salz, U.; Zimmermann, J.; Landfester, K. Preparation of protected photoinitiator nanodepots by the miniemulsion process. *Colloid Polym. Sci.* **2007**, *285* (6), 687–692. https://doi.org/10.1007/s00396-006-1591-7.

(108) Santos, P. C. M.; Machado, T. O.; Santin, J. V. C.; Feuser, P. E.; Córneo, E. S.; Machado-de-Ávila, R. A.; Sayer, C.; Araújo, P. H. H. Superparamagnetic biobased poly(thioether-ester) via thiol-ene polymerization in miniemulsion for hyperthermia. *J. Appl. Polym. Sci.* **2020**. https://doi.org/10.1002/app.49741.

(109) Landfester, K. Miniemulsion polymerization and the structure of polymer and hybrid nanoparticles. *Angew. Chem. Int. Ed. Engl.* **2009**, *48* (25), 4488–4507. https://doi.org/10.1002/anie.200900723.

(110) Hu, J.; Chen, M.; Wu, L. Organic-inorganic nanocomposites synthesized via miniemulsion polymerization. *Polym Chem* **2011**, *2* (4), 760–772. https://doi.org/10.1039/c0py00284d.

(111) Tiarks, F.; Landfester, K.; Antonietti, M. Preparation of polymeric nanocapsules by miniemulsion polymerization. *Langmuir* **2001**, *17* (3), 908–918. https://doi.org/10.1021/la001276n.

(112) Zhou, J.; Cui, Y.; Yao, H.; Ma, J.; Ren, H. Nanocapsules containing binary phase change material obtained via miniemulsion polymerization with reactive emulsifier: synthesis, characterization, and application in fabric finishing. *Polym. Eng. Sci.* **2019**, *59* (s2), E42–E51. https://doi.org/10.1002/pen.24951.

(113) Jung, K.; Xu, J.; Zetterlund, P. B.; Boyer, C. Visible-light-regulated controlled/living radical polymerization in miniemulsion. *ACS Macro Lett.* **2015**, *4* (10), 1139–1143. https://doi.org/10.1021/acsmacrolett.5b00576.

(114) Zaborniak, I.; Chmielarz, P. Temporally controlled ultrasonication-mediated atom transfer radical polymerization in miniemulsion. *Macromol. Chem. Phys.* **2019**, *220* (17). https://doi.org/10.1002/macp.201900285.

(115) Liu, X.; Jing, Y.; Bai, Y. Controlled/living photopolymerization of methyl methacrylate in miniemulsion mediated by HTEMPO. *Front. Chem. China* **2008**, *3* (1), 41–46. https://doi.org/10.1007/s11458-008-0021-4.

(116) Jung, K.; Boyer, C.; Zetterlund, P. B. RAFT Iniferter polymerization in miniemulsion using visible light. *Polym. Chem.* **2017**, *8* (27), 3965–3970. https://doi.org/10.1039/c7py00939a.

(117) Tonnar, J.; Pouget, E.; Lacroix-Desmazes, P.; Boutevin, B. Synthesis of poly(vinyl acetate)-block-poly(dimethylsiloxane)-block-poly(vinyl acetate) copolymers by iodine transfer photopolymerization in miniemulsion. *Macromol. Symp.* **2009**, *281* (1), 20–30. https://doi.org/10.1002/masy.200950703.

(118) Photo-initiated miniemulsion polymerization as a route to the synthesis of gold nanoparticle encapsulated latexes. *Polymer* **2010**, *51* (10), 2119–2124. https://doi.org/10.1016/j.polymer.2010.03.019.

(119) Dou, J.; Zhang, Q.; Jian, L.; Gu, J. Magnetic nanoparticles encapsulated latexes prepared with photo-initiated miniemulsion polymerization. *Colloid Polym. Sci.* **2010**, *288* (18), 1751–1756. https://doi.org/10.1007/s00396-010-2310-y.

(120) Chemtob, A.; Kunstler, B.; Croutxé-Barghorn, C.; Fouchard, S. Photoinduced miniemulsion polymerization. *Colloid Polym. Sci.* **2010**, *288* (5), 579–587. https://doi.org/10.1007/s00396-010-2190-1.

(121) Hoijemberg, P. A.; Chemtob, A.; Croutxé-Barghorn, C.; Poly, J.; Braun, A. M. Radical photopolymerization in miniemulsions. fundamental investigations and technical development. *Macromolecules* **2011**, *44* (22), 8727–8738. https://doi.org/10.1021/ma201753d.

(122) Hoijemberg, P. A.; Chemtob, A.; Croutxé-Barghorn, C. Two routes towards photoinitiator-free photopolymerization in miniemulsion: acrylate self-initiation and photoactive surfactant. *Macromol. Chem. Phys.* **2011**, *212* (22), 2417–2422. https://doi.org/10.1002/macp.201100343.

(123) Daniloska, V.; Tomovska, R.; Asua, J. M. Hybrid miniemulsion photopolymerization in a continuous tubular reactor—a way to expand the characteristics of polyurethane/acrylics. *Chem. Eng. J.* **2012**, *184*, 308–314. https://doi.org/10.1016/j.cej.2012.01.040.

(124) Daniloska, V.; Tomovska, R.; Asua, J. M. Designing tubular reactors to avoid clogging in high solids miniemulsion photopolymerization. *Chem. Eng. J.* **2013**, *222*, 136–141. https://doi.org/10.1016/j.cej.2013.02.015.

(125) Jasinski, F.; Lobry, E.; Chemtob, A.; Croutxé-Barghorn, C.; Criqui, A. Photopolymerizable monomer miniemulsions: why does droplet size matter? *Macromol. Chem. Phys.* **2013**, *214* (15), 1669–1676. https://doi.org/10.1002/macp.201300278.

(126) Tomovska, R.; de la Cal, J. C.; Asua, J. M. Miniemulsion photo-copolymerization of styrene/butyl acrylate in a continuous tubular reactor. *Ind. Eng. Chem. Res.* **2013**, *53* (18), 7313–7320. https://doi.org/10.1021/ie402779y.

(127) Lobry, E.; Jasinski, F.; Penconi, M.; Chemtob, A.; Ley, C.; Croutxé-Barghorn, C.; Oliveros, E.; Braun, A. M.; Criqui, A. Absorption and scattering in concentrated monomer miniemulsions: static and dynamic investigations. *Macromol. Chem. Phys.* **2014**, *215* (12), 1201–1211. https://doi.org/10.1002/macp.201400072.

(128) Lobry, E.; Jasinski, F.; Penconi, M.; Chemtob, A.; Croutxé-Barghorn, C.; Oliveros, E.; Braun, A. M.; Criqui, A. Continuous-flow synthesis of polymer nanoparticles in a microreactor via miniemulsion photopolymerization. *RSC Adv.* **2014**, *4* (82), 43756–43759. https://doi.org/10.1039/C4RA06814A.

(129) Daniloska, V.; Carretero, P.; Tomovska, R.; Asua, J. M. High performance pressure sensitive adhesives by miniemulsion photopolymerization in a continuous tubular reactor. *Polymer* **2014**, *55* (20), 5050–5056. https://doi.org/10.1016/j.polymer.2014.08.038.

(130) Roose, P.; Berlier, M.; De Doncker, P.; Baurant, J.-N.; Walters, P. UV-nanoparticles: photopolymerized polymer colloids from aqueous dispersions of acrylated oligomers. *Prog. Org. Coat.* **2014**, *77* (10), 1569–1576. https://doi.org/10.1016/j.porgcoat.2013.11.031.

(131) Jasinski, F.; Rannee, A.; Schweitzer, J.; Fischer, D.; Lobry, E.; Croutxe-Barghorn, C.; Schmutz, M.; Le Nouen, D.; Criqui, A.; Chemtob, A. Thiol-ene linear step-growth photopolymerization in miniemulsion: fast rates, redox-responsive particles, and semicrystalline films. *Macromolecules* **2016**, *49* (4), 1143–1153. https://doi.org/10.1021/acs.macromol.5b02512.

(132) Chemtob, A.; Lobry, E.; Rannée, A.; Jasinski, F.; Penconi, M.; Oliveros, E.; Braun, A. M.; Criqui, A. Flash latex production in a continuous helical photoreactor: releasing the brake pedal on acrylate chain radical polymerization. *Macromol. React. Eng.* **2016**, *10* (3), 261–268. https://doi.org/10.1002/mren.201500060.

(133) Chemtob, A.; Rannée, A.; Chalan, L.; Fischer, D.; Bistac, S. Continuous flow reactor for miniemulsion chain photopolymerization: understanding plugging issue. *Eur. Polym. J.* **2016**, *80*, 247–255. https://doi.org/10.1016/j.eurpolymj.2016.03.038.

(134) Saadé, J.; Bordes, C.; Raffin, G.; Hangouët, M.; Marote, P.; Faure, K. Response surface optimization of miniemulsion: application to uv synthesis of hexyl acrylate nanoparticles. *Colloid Polym. Sci.* **2016**, *294* (1), 27–36. https://doi.org/10.1007/s00396-015-3778-2.

(135) Radtke, C. P.; Delbé, M.; Wörner, M.; Hubbuch, J. Photoinitiated miniemulsion polymerization in microfluidic chips on automated liquid handling stations: proof of concept. *Eng. Life Sci.* **2016**, *16* (6), 505–514.

(136) Roose, P.; Berlier, M.; Lazzaroni, R.; Leclère, P. Dispersion photopolymerization of acrylated oligomers using a flexible continuous reactor. *Macromol. React. Eng.* **2016**, *10* (5), 502–509. https://doi.org/10.1002/mren.201500078.

(137) Pichavant, L.; Lacroix-Desmazes, P.; Chemtob, A.; Pinaud, J.; Héroguez, V. Photolatent ring-opening metathesis polymerization in miniemulsion: a powerful approach to produce polynorbornene latexes. *Polym. Chem.* **2018**, *9* (46), 5491–5498. https://doi.org/10.1039/c8py01011k.

(138) Artusio, F.; Bazzano, M.; Pisano, R.; Coulon, P.-E.; Rizza, G.; Schiller, T.; Sangermano, M. Polymeric nanocapsules via interfacial cationic photopolymerization in miniemulsion. *Polymer* **2018**, *139*, 155–162. https://doi.org/10.1016/j.polymer.2018.02.019.

(139) Wang, Y.; Dadashi-Silab, S.; Matyjaszewski, K. Photoinduced miniemulsion atom transfer radical polymerization. *ACS Macro Lett.* **2018**, *7* (6), 720–725. https://doi.org/10.1021/acsmacrolett.8b00371.

(140) Pichavant, L.; Lacroix-Desmazes, P.; Chemtob, A.; Pinaud, J.; Héroguez, V. Polynorbornene latex synthesis by uv-triggered ring-opening metathesis polymerization in miniemulsion. *Polymer* **2020**, *190*. https://doi.org/10.1016/j.polymer.2020.122200.

(141) Nauman, N.; Zaquen, N.; Boyer, C.; Zetterlund, P. B. Miniemulsion photopolymerization in a continuous tubular reactor: particle size control via membrane emulsification. *Polym. Chem.* **2020**. https://doi.org/10.1039/d0py00654h.

(142) Abd El-Mageed, A. I. A.; Essawy, H. A.; Dyab, A. K. F. Dipolar particles via photopolymerization of 1,6-hexanediol diacrylate miniemulsion template tailored with oppositely-charged polymerizable surfactants. *J. Mol. Struct.* **2021**, *1246*, 131197. https://doi.org/10.1016/j.molstruc.2021.131197.

(143) Infante Teixeira, L.; Landfester, K.; Thérien-Aubin, H. Selective oxidation of polysulfide latexes to produce polysulfoxide and polysulfone in a waterborne environment. *Macromolecules* **2021**, *54* (8), 3659–3667. https://doi.org/10.1021/acs.macromol.1c00382.

(144) Denes, F.; Pichowicz, M.; Povie, G.; Renaud, P. Thiyl radicals in organic synthesis. *Chem. Rev.* **2014**, *114* (5), 2587–2693. https://doi.org/10.1021/cr400441m.

(145) Moon Kim, B.; Sharpless, K. B. Heterogeneous catalytic asymmetric dihydroxylation: use of a polymer-bound alkaloid. *Tetrahedron Lett.* **1990**, *31* (21), 3003–3006. https://doi.org/10.1016/S0040-4039(00)89009-7.

(146) Wu, J.-T.; Huang, C.-H.; Liang, W.-C.; Wu, Y.-L.; Yu, J.; Chen, H.-Y. Reactive polymer coatings: a general route to thiol-ene and thiol-yne click reactions. *Macromol. Rapid Commun.* **2012**, *33* (10), 922–927. https://doi.org/10.1002/marc.201200011.

(147) Dondoni, A. The emergence of thiol–ene coupling as a click process for materials and bioorganic chemistry. *Angew. Chem. Int. Ed.* **2008**, *47* (47), 8995–8997. https://doi.org/10.1002/anie.200802516.

(148) Floyd, N.; Vijayakrishnan, B.; Koeppe, J. R.; Davis, B. G. Thiyl glycosylation of olefinic proteins: s-linked glycoconjugate synthesis. *Angew. Chem. Int. Ed.* **2009**, *48* (42), 7798–7802. https://doi.org/10.1002/anie.200903135.

(149) Dondoni, A.; Marra, A. Recent applications of thiol –ene coupling as a click process for glycoconjugation. *Chem. Soc. Rev.* **2012**, *41* (2), 573–586. https://doi.org/10.1039/C1CS15157F.

(150) Aimetti, A. A.; Machen, A. J.; Anseth, K. S. Poly(Ethylene Glycol) hydrogels formed by thiol-ene photopolymerization for enzyme-responsive protein delivery. *Biomaterials* **2009**, *30* (30), 6048–6054. https://doi.org/10.1016/j.biomaterials.2009.07.043.

(151) Quoc Le, C. M.; Schmutz, M.; Chemtob, A. Ab initio batch emulsion thiol–ene photopolymerization. *Macromolecules* **2020**, *53* (7), 2369–2379. https://doi.org/10.1021/acs.macromol.0c00265.

(152) Killops, K. L.; Campos, L. M.; Hawker, C. J. Robust, efficient, and orthogonal synthesis of dendrimers via thiol-ene "click" chemistry. *J. Am. Chem. Soc.* **2008**, *130* (15), 5062–5064. https://doi.org/10.1021/ja8006325.

(153) Cramer, N. B.; Bowman, C. N. Thiol-ene chemistry. In *Chemoselective and Bioorthogonal Ligation Reactions*; Algar, W. R., Dawson, P. E., Medintz, I. L., Eds.; Wiley-VCH: Weinheim, Germany, 2017; pp 117–145. https://doi.org/10.1002/9783527683451.ch5.

(154) Plessis, C.; Arzamendi, G.; Leiza, J. R.; Alberdi, J. M.; Schoonbrood, H. a. S.; Charmot, D.; Asua, J. M. Seeded semibatch emulsion polymerization of butyl acrylate: effect of the chain-transfer agent on the kinetics and structural properties. *J. Polym. Sci. Part Polym. Chem.* **2001**, *39* (7), 1106–1119.

(155) Fernandes, M. M.; Gomes, A. C.; Vasconcelos, A.; Munteanu, F.-D.; Tzanov, T.; Gonçalves, M. S. T.; End, N.; Schoening, K.-U.; Guebitz, G. M.; Cavaco-Paulo, A. Protein disulphide isomerase-assisted functionalization of keratin-based matrices. *Appl. Microbiol. Biotechnol.* **2011**, *90* (4), 1311–1321. https://doi.org/10.1007/s00253-011-3194-6.

(156) Yang, G.; Kristufek, S. L.; Link, L. A.; Wooley, K. L.; Robertson, M. L. Synthesis and physical properties of thiol-ene networks utilizing plant-derived phenolic acids. *Macromolecules* **2015**, *48* (23), 8418–8427. https://doi.org/10.1021/acs.macromol.5b01796.

(157) Yang, Z.; Wicks, D. A.; Hoyle, C. E.; Pu, H.; Yuan, J.; Wan, D.; Liu, Y. Newly UV-curable polyurethane coatings prepared by multifunctional thiol- and ene-terminated polyurethane aqueous dispersions mixtures: preparation and characterization. *Polymer* **2009**, *50* (7), 1717–1722. https://doi.org/10.1016/j.polymer.2008.12.018.

(158) Carioscia, J. A.; Schneidewind, L.; O'Brien, C.; Ely, R.; Feeser, C.; Cramer, N.; Bowman, C. N. Thiol–norbornene materials: approaches to develop high Tg thiol–ene polymers. *J. Polym. Sci. Part Polym. Chem.* **2007**, *45* (23), 5686–5696. https://doi.org/10.1002/pola.22318.

(159) Bagheri, A.; Jin, J. Y. Photopolymerization in 3D printing. *Acs Appl. Polym. Mater.* **2019**, *1* (4), 593–611. https://doi.org/10.1021/acsapm.8b00165.

(160) Belbakra, Z.; Cherkaoui, Z. M.; Allonas, X. Photocurable polythiol based (meth)acrylate resins stabilization: new powerful stabilizers and stabilization systems. *Polym. Degrad. Stab.* **2014**, *110*, 298–307. https://doi.org/10.1016/j.polymdegradstab.2014.09.012.

(161) Odian, G. Radical chain polymerization. in *principles of polymerization*; John Wiley & Sons: Hoboken, USA, 2004. https://doi.org/10.1002/047147875X.

(162) Khuong, K. S.; Jones, W. H.; Pryor, W. A.; Houk, K. N. The mechanism of the self-initiated thermal polymerization of styrene. theoretical solution of a classic problem. *J. Am. Chem. Soc.* **2005**, *127* (4), 1265–1277. https://doi.org/10.1021/ja0448667.

(163) Lingnau, J.; Stickler, M.; Meyerhoff, G. The spontaneous polymerization of methyl methacrylate-IV: formation of cyclic dimers and linear trimers. *Eur. Polym. J.* **1980**, *16* (8), 785–791. https://doi.org/10.1016/0014-3057(80)90050-6.

(164) Rzaev, Z. M. O. Complex-radical alternating copolymerization. *prog. polym. sci.* **2000**, *25* (2), 163–217. https://doi.org/10.1016/S0079-6700(99)00027-1.

(165) Chen, L.; Wu, Q.; Wei, G.; Liu, R.; Li, Z. Highly stable thiol-ene systems: from their structure-property relationship to DLP 3D printing. *J. Mater. Chem. C* **2018**, *6* (43), 11561–11568. https://doi.org/10.1039/c8tc03389g.

(166) Sensfuss, S.; Friedrich, M.; Klemm, E. Investigations on thiol/en-polymerization - electron-spin-resonance spectroscopic proof of spontaneous radical formation. *Makromol. Chem. Macromol. Chem. Phys.* **1991**, *192* (12), 2895–2900.

(167) Klemm, E.; Sensfuß, S. Untersuchungen zum selbstinitiierungs-mechanismus der thiol/en-polymerisation. *Makromol. Chem.* **1991**, *192* (1), 159–164. https://doi.org/10.1002/macp.1991.021920114.

(168) Bagiyan, G. A.; Koroleva, I. K.; Soroka, N. V.; Ufimtsev, A. V. Oxidation of thiol compounds by molecular oxygen in aqueous solutions. *Russ. Chem. Bull.* **2003**, *52* (5), 1135–1141. https://doi.org/10.1023/A:1024761324710.

(169) Szmant, H. H.; Mata, A. J.; Namis, A. J.; Panthananickal, A. M. The thiol-olefin co-oxidation (TOCO) reaction—IV: temperature effects on product distribution in the TOCO reaction of indene and aromatic thiols. *Tetrahedron* **1976**, *32* (22), 2665–2680. https://doi.org/10.1016/0040-4020(76)80104-4.

(170) Pryor, W. A. Radical production from the interaction of closed-shell molecules. In *Organic Free Radicals*; ACS Symposium Series; American Chemical Society, 1978; Vol. 69, pp 33–62. https://doi.org/10.1021/bk-1978-0069.ch003.

(171) Pryor, W. A.; Coco, J. H.; Daly, W. H.; Houk, K. N. Radical generation from polymolecular reactions of closed shell molecules. Molecule-Assisted Homolysis (MAH). hydrogen atom transfer from a Diels-Alder adduct to an alkene. *J. Am. Chem. Soc.* **1974**, *96* (17), 5591–5593. https://doi.org/10.1021/ja00824a058.

(172) Beare, K. D.; Coote, M. L. What influences barrier heights in hydrogen abstraction from thiols by carbon-centered radicals? A Curve-Crossing Study. *J. Phys. Chem. A* **2004**, *108* (35), 7211–7221. https://doi.org/10.1021/jp048092s.

(173) D'Souza, V. T.; Iyer, V. K.; Szmant, H. H. Thiol-olefin cooxidation (TOCO) reaction. 8. solvent effects in the oxidation of some thiols with molecular oxygen. *J. Org. Chem.* **1987**, *52* (9), 1725–1728. https://doi.org/10.1021/jo00385a015.

(174) D'Souza, V. T.; Nanjundiah, R.; Baeza H., J.; Szmant, H. H. thiol-olefin cooxidation (TOCO) reaction. 7. a proton nmr study of thiol solvation. *J. Org. Chem.* **1987**, *52* (9), 1720–1725. https://doi.org/10.1021/jo00385a014.

(175) D'Souza, V. T.; Nanjundiah, R.; Baeza, H. J.; Szmant, H. H. Thiol-olefin cooxidation (TOCO) reaction. 9. a self-consistent mechanism under nonradical-inducing conditions. *J. Org. Chem.* **1987**, *52* (9), 1729–1740. https://doi.org/10.1021/jo00385a016.

(176) Voronkov, M. G.; Deryagina, E. N. Thermal reactions of thiyl radicals. *Russ. Chem. Rev.* **1990**, *59* (8), 778. https://doi.org/10.1070/RC1990v059n08ABEH003554.

(177) Ito, O.; Matsuda, M. Kinetic study for spin-trapping reactions of thiyl radicals with nitroso compounds. *J. Am. Chem. Soc.* **1983**, *105* (7), 1937–1940. https://doi.org/10.1021/ja00345a044.

(178) Stoyanovsky, D. A.; Maeda, A.; Kagan, V. E. Assessments of thiyl radicals in biosystems: difficulties and new applications. *Anal. Chem.* **2011**, *83* (17), 6432–6438. https://doi.org/10.1021/ac200418s.

(179) Polovyanenko, D. N.; Plyusnin, V. F.; Reznikov, V. A.; Khramtsov, V. V.; Bagryanskaya, E. G. Mechanistic studies of the reactions of nitrone spin trap PBN with glutathiyl radical. *J. Phys. Chem. B* **2008**, *112* (15), 4841–4847. https://doi.org/10.1021/jp711548x.

(180) Fava, A.; Iliceto, A.; Camera, E. Kinetics of the thiol-disulfide exchange. *J. Am. Chem. Soc.* **1957**, *79* (4), 833–838. https://doi.org/10.1021/ja01561a014.

(181) McCourt, R. O.; Scanlan, E. M. Atmospheric oxygen mediated radical hydrothiolation of alkenes. *Chem. – Eur. J.* **2020**, *26* (68), 15804–15810. https://doi.org/10.1002/chem.202002542.

(182) Sandhiya, L.; Jangra, H.; Zipse, H. Molecule-Induced Radical Formation (MIRF) Reactions—a reappraisal. *Angew. Chem. Int. Ed.* **2020**, *59* (16), 6318–6329. https://doi.org/10.1002/anie.201912382.

(183) Biermann, U.; Klaassen, G.; Koch, R.; Metzger, J. O. Alkene assisted homolysis of the Si-H, Ge-H, and Sn-H bond: new examples of Molecule Assisted Homolysis (MAH). *Eur. J. Org. Chem.* **2019**, *2019* (22), 3599–3604. https://doi.org/10.1002/ejoc.201900363.

(184) Biermann, U.; Metzger, J. O. Regioselectivity of radical addition of thiols to 1-alkenes. *Eur. J. Org. Chem.* **2018**, *2018* (6), 730–734. https://doi.org/10.1002/ejoc.201701692.

(185) Pryor, W. A.; Kurz, M. E. On the mechanism of the reaction of ozone with tert-butyl hydroperoxide: 1, 3-dipolar insertion, electron-transfer, or molecule-assisted homolysis. *Tetrahedron Lett.* **1978**, *19* (8), 697–700.

(186) Nuyken, O.; Völkel, T.; Pöhlmann, T. Telechelics via addition of dithiols onto alkadienes, 1. radical mechanism. *Makromol. Chem.* **1991**, *192* (9), 1959–1968. https://doi.org/10.1002/macp.1991.021920906.

(187) Biermann, U.; Butte, W.; Koch, R.; Fokou, P. A.; Türünç, O.; Meier, M. A. R.; Metzger, J. O. Initiation of radical chain reactions of thiol compounds and alkenes without any added initiator: thiol-catalyzed cis/trans isomerization of methyl oleate. *Chem. – Eur. J.* **2012**, *18* (26), 8201–8207. https://doi.org/10.1002/chem.201103252.

(188) Northrop, B. H.; Coffey, R. N. Thiol–ene click chemistry: computational and kinetic analysis of the influence of alkene functionality. *J. Am. Chem. Soc.* **2012**, *134* (33), 13804–13817. https://doi.org/10.1021/ja305441d.

(189) Schwalm, R. Chapter 2 - The UV curing process. In *UV Coatings*; Elsevier: Amsterdam, 2007; pp 19–61. https://doi.org/10.1016/B978-044452979-4/50002-0.

(190) Zhang, Y.; Liu, S.; Li, T.; Zhang, L.; Azhar, U.; Ma, J.; Zhai, C.; Zong, C.; Zhang, S. Cytocompatible and non-fouling zwitterionic hyaluronic acid-based hydrogels using thiol-ene "click" chemistry for cell encapsulation. *Carbohydr. Polym.* **2020**, *236*, 116021. https://doi.org/10.1016/j.carbpol.2020.116021.

(191) Fu, W.; Wang, L.; He, J. Evaluation of mechanical properties and shrinkage stress of thiol-ene-methacrylate dental composites with synthesized fluorinated allyl ether. *J. Mech. Behav. Biomed. Mater.* **2019**, *95*, 53–59. https://doi.org/10.1016/j.jmbbm.2019.03.027.

(192) Javadi, A.; Cobaj, A.; Soucek, M. D. Commercial waterborne coatings. in *handbook of waterborne coatings*; Elsevier, 2020; pp 303–344. https://doi.org/10.1016/B978-0-12-814201-1.00012-3.

(193) Deubel, F.; Bretzler, V.; Holzner, R.; Helbich, T.; Nuyken, O.; Rieger, B.; Jordan, R. Polythioethers by thiol-ene click polyaddition of α,ω-alkylene thiols. *Macromol. Rapid Commun.* **2013**, *34* (12), 1020–1025. https://doi.org/10.1002/marc.201300265.

(194) Amato, D. V.; Amato, D. N.; Flynt, A. S.; Patton, D. L. Functional, sub-100 nm polymer nanoparticles via thiol–ene miniemulsion photopolymerization. *Polym. Chem.* **2015**, *6* (31), 5625–5632. https://doi.org/10.1039/C4PY01449A.

(195) Taghavikish, M.; Subianto, S.; Dutta, N. K.; de Campo, L.; Mata, J. P.; Rehm, C.; Choudhury, N. R. Polymeric ionic liquid nanoparticle emulsions as a corrosion inhibitor in anticorrosion coatings. *ACS Omega* **2016**, *1* (1), 29–40.

(196) Meneses, A. C. de; Machado, T. O.; Sayer, C.; Araújo, P. H. H.; Oliveira, D. de. Development of antioxidant poly(thioether-ester) nanoparticles. *Braz. J. Chem. Eng.* **2018**, *35* (2), 691–698. https://doi.org/10.1590/0104-6632.20180352s20160605.

(197) de Meneses, A. C.; dos Santos, P. C. M.; Machado, T. O.; Sayer, C.; de Oliveira, D.; Hermes de Araújo, P. H. Poly(thioether-ester) nanoparticles entrapping clove oil for antioxidant activity improvement. *J. Polym. Res.* **2017**, *24* (11), 202. https://doi.org/10.1007/s10965-017-1353-x.

(198) Machado, T. O.; Cardoso, P. B.; Feuser, P. E.; Sayer, C.; Araújo, P. H. Thiol-ene miniemulsion polymerization of a biobased monomer for biomedical applications. *Colloids Surf. B Biointerfaces* **2017**, *159*, 509–517.

(199) Cardoso, P. B.; Machado, T. O.; Feuser, P. E.; Sayer, C.; Meier, M. A.; Araújo, P. H. Biocompatible polymeric nanoparticles from castor oil derivatives via thiol-ene miniemulsion polymerization. *Eur. J. Lipid Sci. Technol.* **2018**, *120* (1), 1700212.

(200) Hoelscher, F.; Machado, T. O.; de Oliveira, D.; Hermes de Araújo, P. H.; Sayer, C. Enzymatically catalyzed degradation of poly (thioether-ester) nanoparticles. *Polym. Degrad. Stab.* **2018**, *156*, 211–217. https://doi.org/10.1016/j.polymdegradstab.2018.09.007.

(201) Santos, P. C. M.; Machado, T. O.; Santin, J. V. C.; Feuser, P. E.; Córneo, E. S.; Machado-de-Ávila, R. A.; Sayer, C.; Araújo, P. H. H. Superparamagnetic biobased poly(thioether-ester) via thiol-ene polymerization in miniemulsion for hyperthermia. *J. Appl. Polym. Sci.* **2021**, *138* (4), 49741. https://doi.org/10.1002/app.49741.

(202) Jiang, K.; Liu, Y.; Yan, Y.; Wang, S.; Liu, L.; Yang, W. Combined chain- and step-growth dispersion polymerization toward pst particles with soft, clickable patches. *Polym. Chem.* **2017**, *8* (8), 1404–1416. https://doi.org/10.1039/C6PY02094A.

(203) Alimohammadi, F.; Wang, C.; Durham, O. Z.; Norton, H. R.; Bowman, C. N.; Shipp, D. A. Radical mediated thiol-ene/yne dispersion polymerizations. *Polymer* **2016**, *105*, 180–186.

(204) Durham, O. Z.; Chapman, D. V.; Krishnan, S.; Shipp, D. A. Radical mediated thiol-ene emulsion polymerizations. *Macromolecules* **2017**, *50* (3), 775–783.

(205) Liu, D.; Yu, B.; Jiang, X.; Yin, J. Responsive hybrid microcapsules by the one-step interfacial thiol–ene photopolymerization. *Langmuir* **2013**, *29* (17), 5307–5314. https://doi.org/10.1021/la400098c.

(206) Durham, O. Z.; Shipp, D. A. Suspension "click" polymerizations: thiol-ene polymer particles prepared with natural gum stabilizers. *Colloid Polym. Sci.* **2015**, *293* (8), 2385–2394.

(207) Cassidy, K. J.; Durham, O. Z.; Shipp, D. A. Composite particles from pickering-stabilized radical mediated thiol-ene suspension polymerizations. *Macromol. React. Eng.* **2019**, *13* (2), 1800075. https://doi.org/10.1002/mren.201800075.

(208) Muhsir, P.; Çakmakçi, E.; Demir, S.; Ogan, A. Amine functional magnetic nanoparticles via waterborne thiol–ene suspension photopolymerization for antibody immobilization. *Colloids Surf. B Biointerfaces* **2018**, *170*, 122–128. https://doi.org/10.1016/j.colsurfb.2018.05.062.

(209) Asua, J. M. challenges in polymerization in dispersed media. in *polymer reaction engineering of dispersed systems: volume ii*; Pauer, W., Ed.; Advances in Polymer Science; Springer International Publishing: Cham, 2018; pp 1–22. https://doi.org/10.1007/12_2017_21.

(210) Lowe, A. B. Thiol-ene "click" reactions and recent applications in polymer and materials synthesis: a first update. *Polym Chem* **2014**, *5* (17), 4820–4870. https://doi.org/10.1039/c4py00339j.

(211) Scott, P. J.; Kasprzak, C. R.; Feller, K. D.; Meenakshisundaram, V.; Williams, C. B.; Long, T. E. Light and latex: advances in the photochemistry of polymer colloids. *Polym. Chem.* **2020**, *11* (21), 3498–3524. https://doi.org/10.1039/D0PY00349B.

(212) Schork, F. J.; Luo, Y.; Smulders, W.; Russum, J. P.; Butté, A.; Fontenot, K. Miniemulsion polymerization. in *polymer particles*; Springer, 2005; pp 129–255.

(213) Chern, C. S.; Liou, Y. C.; Chen, T. J. Particle nucleation loci in styrene miniemulsion polymerization using alkyl methacrylates as the reactive cosurfactant. *Macromol. Chem. Phys.* **1998**, *199* (7), 1315–1322. https://doi.org/10.1002/(SICI)1521-3935(19980701)199:7<1315::AID-MACP1315>3.0.CO;2-9.

(214) Luo, Y.; Schork, F. J. Emulsion and miniemulsion polymerizations with an oil-soluble initiator in the presence and absence of an aqueous-phase radical scavenger. *J. Polym. Sci. Part Polym. Chem.* **2002**, *40* (19), 3200–3211. https://doi.org/10.1002/pola.10408.

(215) Rodríguez, R.; Barandiaran, M. J.; Asua, J. M. Particle nucleation in high solids miniemulsion polymerization. *Macromolecules* **2007**, *40* (16), 5735–5742. https://doi.org/10.1021/ma070525c.

(216) Odian, G. Step polymerization. in *principles of polymerization*; John Wiley & Sons, Ltd, 2004; pp 39–197. https://doi.org/10.1002/047147875X.ch2.

(217) Hanus, L. H.; Ploehn, H. J. Conversion of intensity-averaged photon correlation spectroscopy measurements to number-averaged particle size distributions. 1. theoretical development. *Langmuir* **1999**, *15* (9), 3091–3100. https://doi.org/10.1021/la980958w.

(218) Mengual, O.; Meunier, G.; Cayré, I.; Puech, K.; Snabre, P. Turbiscan MA 2000: multiple light scattering measurement for concentrated emulsion and suspension instability analysis. *Talanta* **1999**, *50* (2), 445–456. https://doi.org/10.1016/S0039-9140(99)00129-0.

(219) Cramer, N. B.; Scott, J. P.; Bowman, C. N. Photopolymerizations of thiol-ene polymers without photoinitiators. *Macromolecules* **2002**, *35* (14), 5361–5365. https://doi.org/10.1021/ma0200672.

(220) Sensfuß, S.; Friedrich, M.; Klemm, E. Untersuchungen Zur thiol/en-polymerisation: elektronenspinresonanzspektroskopischer nachweis spontaner radikalbildung. *Makromol. Chem.* **1991**, *192* (12), 2895–2900. https://doi.org/10.1002/macp.1991.021921205.

(221) Manea, M.; Chemtob, A.; Paulis, M.; de la Cal, J. C.; Barandiaran, M. J.; Asua, J. M. Miniemulsification in high-pressure homogenizers. *AICHE J.* **2008**, *54* (1), 289–297. https://doi.org/10.1002/aic.11367.

(222) Bhanvase, B. A.; Pinjari, D. V.; Sonawane, S. H.; Gogate, P. R.; Pandit, A. B. Analysis of semibatch emulsion polymerization: role of ultrasound and initiator. *Ultrason. Sonochem.* **2012**, *19* (1), 97–103. https://doi.org/10.1016/j.ultsonch.2011.05.016.

(223) Teo, B. M.; Prescott, S. W.; Ashokkumar, M.; Grieser, F. Ultrasound initiated miniemulsion polymerization of methacrylate monomers. *Ultrason. Sonochem.* **2008**, *15* (1), 89–94. https://doi.org/10.1016/j.ultsonch.2007.01.009.

(224) Miller, C. M.; Blythe, P. J.; Sudol, E. D.; Silebi, C. A.; El-Aasser, M. S. Effect of the presence of polymer in miniemulsion droplets on the kinetics of polymerization. *J. Polym. Sci. Part Polym. Chem.* **1994**, *32* (12), 2365–2376. https://doi.org/10.1002/pola.1994.080321217.

(225) Poggi, E.; Gohy, J.-F. Janus particles: from synthesis to application. *Colloid Polym. Sci.* **2017**, *295* (11), 2083–2108. https://doi.org/10.1007/s00396-017-4192-8.

(226) Hu, S.-H.; Gao, X. Nanocomposites with spatially separated functionalities for combined imaging and magnetolytic therapy. *J. Am. Chem. Soc.* **2010**, *132* (21), 7234–7237. https://doi.org/10.1021/ja102489q.

(227) Renz, P.; Kokkinopoulou, M.; Landfester, K.; Lieberwirth, I. Imaging of polymeric nanoparticles: hard challenge for soft objects. *Macromol. Chem. Phys.* **2016**, *217* (17), 1879–1885. https://doi.org/10.1002/macp.201600246.

(228) Franken, L. E.; Boekema, E. J.; Stuart, M. C. A. Transmission electron microscopy as a tool for the characterization of soft materials: application and interpretation. *Adv. Sci.* **2017**, *4* (5), 1600476. https://doi.org/10.1002/advs.201600476.

(229) Scarff, C. A.; Fuller, M. J. G.; Thompson, R. F.; Iadaza, M. G. Variations on negative stain electron microscopy methods: tools for tackling challenging systems. *J. Vis. Exp.* **2018**, No. 132. https://doi.org/10.3791/57199.

(230) *Chemistry and technology of emulsion polymerisation*; van Herk, A. M., Ed.; John Wiley & Sons Ltd: Oxford, UK, 2013. https://doi.org/10.1002/9781118638521.

(231) Gilbert, R. G. *Emulsion polymerization: a mechanistic approach*; Academic Press, 1995.

(232) Antonietti, M.; Tauer, K. 90 Years of polymer latexes and heterophase polymerization: more vital than ever. *Macromol. Chem. Phys.* **2003**, *204* (2), 207–219.

(233) Sajjadi, S.; Brooks, B. W. Butyl acrylate batch emulsion polymerization in the presence of sodium lauryl sulphate and potassium persulphate. *J. Polym. Sci. Part Polym. Chem.* **1999**, *37* (21), 3957–3972. https://doi.org/10.1002/(SICI)1099-0518(19991101)37:21<3957::AID-POLA11>3.0.CO;2-Q.

(234) Thickett, S. C.; Gilbert, R. G. Emulsion polymerization: state of the art in kinetics and mechanisms. *Polymer* **2007**, *48* (24), 6965–6991. https://doi.org/10.1016/j.polymer.2007.09.031.

(235) Asua, J. M. Emulsion polymerization: from fundamental mechanisms to process developments. *J. Polym. Sci. Part Polym. Chem.* **2004**, *42* (5), 1025–1041. https://doi.org/10.1002/pola.11096.

(236) Jönsson, J. B.; Müllner, M.; Piculell, L.; Karlsson, O. J. Emulsion condensation polymerization in dispersed aqueous media. interfacial reactions and nanoparticle formation. *Macromolecules* **2013**, *46* (22), 9104–9113. https://doi.org/10.1021/ma401799g.

(237) Sousa, A. F.; Silvestre, A. J. D.; Gandini, A.; Neto, C. P. Synthesis of aliphatic suberin-like polyesters by ecofriendly catalytic systems. *High Perform. Polym.* **2012**, *24* (1), 4–8. https://doi.org/10.1177/0954008311431114.

(238) Baile, M.; Chou, Y. J.; Saam, J. C. Direct polyesterifcation in aqueous emulsion. *Polym. Bull.* **1990**, *23* (3), 251–257. https://doi.org/10.1007/BF01032438.

(239) Saam, J. C.; Huebner, D. J. Condensation polymerization of oligomeric polydimethylsiloxanols in aqueous emulsion. *J. Polym. Sci. Polym. Chem. Ed.* **1982**, *20* (12), 3351–3368. https://doi.org/10.1002/pol.1982.170201209.

(240) Takasu, A.; Takemoto, A.; Hirabayashi, T. Polycondensation of dicarboxylic acids and diols in water catalyzed by surfactant-combined catalysts and successive chain extension. *Biomacromolecules* **2006**, *7* (1), 6–9.

(241) Billiet, L.; Fournier, D.; Du Prez, F. Step-growth polymerization and 'click' chemistry: the oldest polymers rejuvenated. *Polymer* **2009**, *50* (16), 3877–3886. https://doi.org/10.1016/j.polymer.2009.06.034.

(242) Landfester, K.; Tiarks, F.; Hentze, H. P.; Antonietti, M. Polyaddition in miniemulsions: a new route to polymer dispersions. *Macromol. Chem. Phys.* **2000**, *201* (1), 1–5. https://doi.org/10.1002/(SICI)1521-3935(20000101)201:1<1::AID-MACP1>3.0.CO;2-N.

(243) Barrere, M.; Landfester, K. High molecular weight polyurethane and polymer hybrid particles in aqueous miniemulsion. *Macromolecules* **2003**, *36* (14), 5119–5125. https://doi.org/10.1021/ma025981+.

(244) Barrère, M.; Landfester, K. Polyester synthesis in aqueous miniemulsion. *Polymer* **2003**, *44* (10), 2833–2841. https://doi.org/10.1016/S0032-3861(03)00151-4.

(245) Landfester, K.; Pawelzik, U.; Antonietti, M. Polydimethylsiloxane latexes and copolymers by polymerization and polyaddition in miniemulsion. *Polymer* **2005**, *46* (23), 9892–9898. https://doi.org/10.1016/j.polymer.2005.07.080.

(246) Paulis, M.; Asua, J. M. Knowledge-based production of waterborne hybrid polymer materials. *Macromol. React. Eng.* **2016**, *10* (1), 8–21. https://doi.org/10.1002/mren.201500042.

(247) Asua, J. M. Challenges for industrialization of miniemulsion polymerization. *Prog. Polym. Sci.* **2014**, *39* (10), 1797–1826. https://doi.org/10.1016/j.progpolymsci.2014.02.009.

(248) Zhou, X.; Li, Y.; Fang, C.; Li, S.; Cheng, Y.; Lei, W.; Meng, X. Recent advances in synthesis of waterborne polyurethane and their application in water-based ink: A Review. *J. Mater. Sci. Technol.* **2015**, *31* (7), 708–722. https://doi.org/10.1016/j.jmst.2015.03.002.

(249) Choi, K. Y.; McAuley, K. B. Step-growth polymerization. in *polymer reaction engineering*; John Wiley & Sons, Ltd, 2008; pp 273–314. https://doi.org/10.1002/9780470692134.ch7.

(250) Wang, S.; Daniels, E. S.; Sudol, E. D.; Klein, A.; El-Aasser, M. S. Isothermal emulsion polymerization of n-butyl methacrylate with kps and redox initiators: kinetic study at different surfactant/initiator concentrations and reaction temperature. *J. Appl. Polym. Sci.* **2016**, *133* (7), 1–8. https://doi.org/10.1002/app.43037.

(251) Rocha-Botello, G.; Olvera-Guillen, R.; Herrera-Ordonez, J.; Cruz-Soto, M.; Victoria-Valenzuela, D. Unexpected secondary nucleation in poly(vinyl acetate) nanoparticle synthesis by ab initio batch emulsion polymerization using poly(vinyl alcohol) as surfactant. *Macromol. React. Eng.* **2019**, *13* (5). https://doi.org/10.1002/mren.201900024.

(252) Renz, P.; Kokkinopoulou, M.; Landfester, K.; Lieberwirth, I. Imaging of polymeric nanoparticles: hard challenge for soft objects. *Macromol. Chem. Phys.* **2016**, *217* (17), 1879–1885.

(253) Elizalde, O.; Leal, G. P.; Leiza, J. R. Particle size distribution measurements of polymeric dispersions: a comparative study. *Part. Part. Syst. Charact.* **2000**, *17* (5–6), 236–243. https://doi.org/10.1002/1521-4117(200012)17:5/6<236::AID-PPSC236>3.0.CO;2-0.

(254) Piradashvili, K.; Alexandrino, E. M.; Wurm, F. R.; Landfester, K. Reactions and polymerizations at the liquid–liquid interface. *Chem. Rev.* **2016**, *116* (4), 2141–2169. https://doi.org/10.1021/acs.chemrev.5b00567.

(255) Song, Y.; Fan, J.-B.; Wang, S. Recent progress in interfacial polymerization. *Mater. Chem. Front.* **2017**, *1* (6), 1028–1040. https://doi.org/10.1039/C6QM00325G.

(256) Nagarjuna, R.; Saifullah, M. S. M.; Ganesan, R. Oxygen insensitive thiol-ene photo-click chemistry for direct imprint lithography of oxides. *RSC Adv.* **2018**, *8* (21), 11403–11411. https://doi.org/10.1039/c8ra01688g.

(257) Ai, Z.; Deng, R.; Zhou, Q.; Liao, S.; Zhang, H. High solid content latex: preparation methods and application. *Adv. Colloid Interface Sci.* **2010**, *159* (1), 45–59. https://doi.org/10.1016/j.cis.2010.05.003.

(258) Krishnan, S.; Klein, A.; El-Aasser, M. S.; Sudol, E. D. Effect of surfactant concentration on particle nucleation in emulsion polymerization ofn-butyl methacrylate. *Macromolecules* **2003**, *36* (9), 3152–3159. https://doi.org/10.1021/ma021120p.

(259) Sütterlin, N.; Kurth, H.-J.; Markert, G. Ein beitrag zur teilchenbildung bei der emulsionspolymerisation von acrylsäure- und methacrylsäureestern. *Makromol. Chem.* **1976**, *177* (5), 1549–1565. https://doi.org/10.1002/macp.1976.021770523.

(260) Sütterlin, N. Influence of monomer polarity on particle formation in emulsion polymerization. in *polymer colloids II*; Springer, 1980; pp 583–597.

(261) Van Der Hoff, B. M. E. Kinetics of emulsion polymerization. in *polymerization and polycondensation processes*; Advances in Chemistry; American Chemical Society, 1962; Vol. 34, pp 6–31.

(262) Cook, W. D.; Chen, F.; Pattison, D. W.; Hopson, P.; Beaujon, M. Thermal polymerization of thiol–ene network-forming systems. *Polym. Int.* **2007**, *56* (12), 1572–1579. https://doi.org/10.1002/pi.2314.

(263) Cramer, N. B.; Bowman, C. N. Kinetics of thiol-ene and thiol-acrylate photopolymerizations with real-time fourier transform infrared. *J. Polym. Sci. Part Polym. Chem.* **2001**, *39* (19), 3311–3319. https://doi.org/10.1002/pola.1314.

(264) Tyson, E. L.; Ament, M. S.; Yoon, T. P. Transition metal photoredox catalysis of radical thiol-ene reactions. *J Org Chem* **2013**, *78* (5), 2046–2050. https://doi.org/10.1021/jo3020825.

(265) Tyson, E. L.; Niemeyer, Z. L.; Yoon, T. P. Redox mediators in visible light photocatalysis: photocatalytic radical thiol-ene additions. *J Org Chem* **2014**, *79* (3), 1427–1436. https://doi.org/10.1021/jo500031g.

(266) Keylor, M. H.; Park, J. E.; Wallentin, C.-J.; Stephenson, C. R. J. Photocatalytic initiation of thiol–ene reactions: synthesis of thiomorpholin-3-ones. *Tetrahedron* **2014**, *70* (27), 4264–4269. https://doi.org/10.1016/j.tet.2014.03.041.

(267) Guerrero-Corella, A.; Maria Martinez-Gualda, A.; Ahmadi, F.; Ming, E.; Fraile, A.; Aleman, J. Thiol-ene/oxidation tandem reaction under visible light photocatalysis: synthesis of alkyl sulfoxides. *Chem Commun Camb* **2017**, *53* (75), 10463–10466. https://doi.org/10.1039/c7cc05672a.

(268) Bhat, V. T.; Duspara, P. A.; Seo, S.; Abu Bakar, N. S.; Greaney, M. F. Visible light promoted thiol-ene reactions using titanium dioxide. *Chem Commun Camb* **2015**, *51* (21), 4383–4385. https://doi.org/10.1039/c4cc09987g.

(269) Fadeyi, O. O.; Mousseau, J. J.; Feng, Y.; Allais, C.; Nuhant, P.; Chen, M. Z.; Pierce, B.; Robinson, R. Visible-light-driven photocatalytic initiation of radical thiol–ene reactions using bismuth oxide. *Org. Lett.* **2015**, *17* (23), 5756–5759. https://doi.org/10.1021/acs.orglett.5b03184.

(270) Zhao, G.; Kaur, S.; Wang, T. Visible-light-mediated thiol-ene reactions through organic photoredox catalysis. *Org Lett* **2017**, *19* (12), 3291–3294. https://doi.org/10.1021/acs.orglett.7b01441.

(271) Levin, V. V.; Dilman, A. D. Visible-light-mediated organocatalyzed thiol–ene reaction initiated by a proton-coupled electron transfer. *J. Org. Chem.* **2019**, *84* (12), 8337–8343. https://doi.org/10.1021/acs.joc.9b01331.

(272) Kaur, S.; Zhao, G.; Busch, E.; Wang, T. Metal-free photocatalytic thiol–ene/thiol–yne reactions. *Org. Biomol. Chem.* **2019**, *17* (7), 1955–1961. https://doi.org/10.1039/C8OB02313A.

(273) DeForest, C. A.; Anseth, K. S. Cytocompatible Click-based hydrogels with dynamically tunable properties through orthogonal photoconjugation and photocleavage reactions. *Nat. Chem.* **2011**, *3* (12), 925–931. https://doi.org/10.1038/nchem.1174.

(274) DeForest, C. A.; Anseth, K. S. Photoreversible patterning of biomolecules within click-based hydrogels. *Angew. Chem. Int. Ed.* **2012**, *51* (8), 1816–1819. https://doi.org/10.1002/anie.201106463.

(275) Shih, H.; Lin, C. C. Visible-light-mediated thiol-ene hydrogelation using eosin-y as the only photoinitiator. *Macromol Rapid Commun* **2013**, *34* (3), 269–273. https://doi.org/10.1002/marc.201200605.

(276) Shih, H.; Fraser, A. K.; Lin, C. C. Interfacial thiol-ene photoclick reactions for forming multilayer hydrogels. *ACS Appl Mater Interfaces* **2013**, *5* (5), 1673–1680. https://doi.org/10.1021/am302690t.

(277) Singh, M.; Yadav, A. K.; Yadav, L. D. S.; Singh, R. K. P. Visible-light-activated selective synthesis of sulfoxides via thiol-ene/oxidation reaction cascade. *Tetrahedron Lett.* **2018**, *59* (5), 450–453. https://doi.org/10.1016/j.tetlet.2017.12.066.

(278) Limnios, D.; Kokotos, C. G. Photoinitiated thiol-ene "click" reaction: an organocatalytic alternative. *Adv. Synth. Catal.* **2017**, *359* (2), 323–328. https://doi.org/10.1002/adsc.201600977.

(279) Ma, W.; Chen, D.; Liu, L.; Ma, Y.; Wang, L.; Zhao, C.; Yang, W. Visible light-induced thiol-ene reaction: a new strategy to prepare α,ω-dithiol and α,ω-divinyl telechelic polythiolether oligomers. *J. Polym. Sci. Part Polym. Chem.* **2016**, *54* (6), 740–749. https://doi.org/10.1002/pola.27906.

(280) Wang, Y.; Zhang, X.; Ma, Y.; Chen, D.; Zhao, C.; Yang, W. Polythioethers with controlled α,ω-end groups prepared by visible light induced thiol–ene click polymerization of dithiol and divinyl ether with 4-(N,N -diphenylamino)benzaldehyde as organocatalyst. *Macromol. Chem. Phys.* **2020**, *221* (6). https://doi.org/10.1002/macp.201900557.

(281) Xu, J.; Boyer, C. Visible Light Photocatalytic Thiol-Ene Reaction: An elegant approach for fast polymer post-functionalization and step-growth polymerization. *Macromolecules* **2015**, *48* (3), 520–529. https://doi.org/10.1021/ma502460t.

(282) Allegrezza, M. L.; Thompson, A. M.; Kloster, A. J.; Konkolewicz, D. Photocatalyzed thiol–alkene coupling: mechanistic study and polymer synthesis. *J. Polym. Sci. Part Polym. Chem.* **2019**, *57* (18), 1931–1937. https://doi.org/10.1002/pola.29319.

(283) Skubi, K. L.; Blum, T. R.; Yoon, T. P. Dual catalysis strategies in photochemical synthesis. *Chem. Rev.* **2016**, *116* (17), 10035–10074. https://doi.org/10.1021/acs.chemrev.6b00018.

(284) Majek, M.; Jacobi von Wangelin, A. Mechanistic perspectives on organic photoredox catalysis for aromatic substitutions. *Acc Chem Res* **2016**, *49* (10), 2316–2327. https://doi.org/10.1021/acs.accounts.6b00293.

(285) Moly, K. A.; Radusch, H. J.; Androsh, R.; Bhagawan, S. S.; Thomas, S. Nonisothermal crystallisation, melting behavior and wide angle x-ray scattering investigations on linear low density polyethylene (LLDPE)/ethylene vinyl acetate (EVA) blends: effects of compatibilisation and dynamic crosslinking. *Eur. Polym. J.* **2005**, *41* (6), 1410–1419.

(286) Li, M. Y.; Cline, C. S.; Koker, E. B.; Carmichael, H. H.; Chignell, C. F.; Bilski, P. Quenching of singlet molecular oxygen ($^1O_2$) by azide anion in solvent mixtures. *Photochem. Photobiol.* **2001**, *74* (6), 760–764. https://doi.org/10.1562/0031-8655(2001)0740760QOSMOO2.0.CO2.

(287) Aguirre-Soto, A.; Kaastrup, K.; Kim, S.; Ugo-Beke, K.; Sikes, H. D. Excitation of metastable intermediates in organic photoredox catalysis: z-scheme approach decreases catalyst inactivation. *ACS Catal.* **2018**, *8* (7), 6394–6400. https://doi.org/10.1021/acscatal.8b00857.

(288) Cismesia, M. A.; Yoon, T. P. Characterizing chain processes in visible light photoredox catalysis. *Chem. Sci.* **2015**, *6* (10), 5426–5434. https://doi.org/10.1039/C5SC02185E.

(289) Crisenza, G. E. M.; Mazzarella, D.; Melchiorre, P. Synthetic methods driven by the photoactivity of electron donor-acceptor complexes. *J Am Chem Soc* **2020**, *142* (12), 5461–5476. https://doi.org/10.1021/jacs.0c01416.

(290) Kim, D.; Scranton, A. B.; Stansbury, J. W. Analysis of association constant for ground state dye-electron acceptor complex of photoinitiator systems and the association constant effect on the kinetics of visible-light-induced polymerizations. *J Polym Sci Polym Chem* **2009**, *47* (5), 1429–1439. https://doi.org/10.1002/pola.23252.

(291) Childress, K. K.; Alim, M. D.; Mavila, S.; Martinez, V.; Ding, Y.; Bowman, C. N.; Stansbury, J. W. Systematic modulation and structure–property relationships in photopolymerizable thermoplastics. *ACS Appl. Polym. Mater.* **2021**, *3* (2), 1171–1181. https://doi.org/10.1021/acsapm.0c01393.

(292) Sarapas, J. M.; Tew, G. N. Poly(Ether–Thioethers) by Thiol–ene click and their oxidized analogues as lithium polymer electrolytes. *Macromolecules* **2016**, *49* (4), 1154–1162. https://doi.org/10.1021/acs.macromol.5b02513.

(293) Sarapas, J. M.; Tew, G. N. Thiol-ene step-growth as a versatile route to functional polymers. *Angew. Chem. Int. Ed. Engl.* **2016**, *55* (51), 15860–15863. https://doi.org/10.1002/anie.201609023.

(294) Brubaker, C. E.; Velluto, D.; Demurtas, D.; Phelps, E. A.; Hubbell, J. A. Crystalline oligo(ethylene sulfide) domains define highly stable supramolecular block copolymer assemblies. *ACS Nano* **2015**, *9* (7), 6872–6881. https://doi.org/10.1021/acsnano.5b02937.

(295) Takahashi, Y.; Tadokoro, H.; Chatani, Y. Structure of polyethylene sulfide. *J. Macromol. Sci. Part B Phys.* **1968**, *2* (2), 361–367.

(296) Banetta, L.; Storti, G.; Hoggard, G.; Simpson, G.; Zaccone, A. Predictive model of polymer reaction kinetics and coagulation behavior in seeded emulsion co- and ter-polymerizations. *Polym. Chem.* **2020**, *11* (41), 6599–6615. https://doi.org/10.1039/d0py01138j.

(297) Sajjadi, S.; Yianneskis, M. Semibatch emulsion polymerization of methyl methacrylate with a neat monomer feed. *Polym. React. Eng.* **2003**, *11* (4), 715–736. https://doi.org/10.1081/pre-120026371.

(298) Ocepek, M.; Zhong, W.; Meng, L.; Soucek, M. D. Influence of hydrophobic monomers on secondary nucleation of hydroxyl-functionalized latexes. *J. Polym. Sci. Part Polym. Chem.* **2017**, *55* (13), 2190–2202. https://doi.org/10.1002/pola.28604.

(299) Morrison, B. R.; Maxwell, I. A.; Gilbert, R. G.; Napper, D. H. Testing nucleation models for emulsion-polymerization systems. In *polymer latexes: preparation, characterization, and applications*; 1992; pp 28–44.